



UCGE Reports

Number 20297

Department of Geomatics Engineering

**Development and Testing of an L1 Combined GPS-Galileo
Software Receiver**

(URL: <http://www.geomatics.ucalgary.ca/graduatetheses>)

by

Florence Macchi

January 2010



UNIVERSITY OF CALGARY

DEVELOPMENT AND TESTING OF AN L1 COMBINED GPS-GALILEO
SOFTWARE RECEIVER

by

FLORENCE MACCHI

A THESIS

SUBMITTED TO THE FACULTY OF GRADUATE STUDIES
IN PARTIAL FULFILMENT OF THE REQUIREMENTS FOR THE
DEGREE OF DOCTOR OF PHILOSOPHY

DEPARTMENT OF GEOMATICS ENGINEERING

CALGARY, ALBERTA

JANUARY, 2010

© Florence Macchi 2010

Abstract

The GPS L1 signal is being augmented by L1C and the European GNSS Galileo is under development. The GPS L1C and Galileo L1 signals use a common design and in particular a MBOC modulation. This dissertation investigates combined acquisition and tracking algorithms for GPS and Galileo signals in the L1 band.

Since these signals are not yet being broadcast, a software signal simulator able to simulate GPS L1 C/A, GPS L1C (pilot and data channels) and Galileo L1 (pilot and data channels) is first developed. The simulator is able to simulate white noise, different types of interference and various types of receiver oscillators. A new oscillator model was developed for the latter.

In term of signal acquisition, different algorithms are developed to take advantage of these new signals. Each algorithm is characterized using real data and from a statistical point of view with a focus on the false alarm and detection probabilities and the mean acquisition time. Techniques using 16 ms of incoming signal show 2-6 dB higher deflection coefficients compared to using only 8 ms of signal, but also require a higher computational load and thus the choice of the algorithm should depend on the receiver's operating conditions. An acquisition that combines the different signals (GPS L1 C/A and L1C or Galileo) is also developed and tested using the aforementioned software simulator. The combined acquisition succeeds to acquire the signal at low C/N_0 , whereas the acquisition using the L1C data channel only fails.

For tracking, a method to combine different signals (GPS L1 C/A and L1C or Galileo) before the discriminator is developed. This method shows better performance than the traditional tracking using only one signal. Then, a method for simultaneous tracking of the GPS L1 C/A and L1C signals using a Kalman filter approach is developed and found to be preferred over traditional methods. A novel Kalman filter capable of combining and simultaneously tracking the L1 C/A and L1C signal is introduced. Testing with the software signal simulator showed that this approach improves performance of tracking in terms of accuracy and sensitivity compared to the C/A-only Kalman filter and the traditional tracking in various dynamic modes, with and without oscillator errors and at low and high signal power.

Acknowledgements

I would like to thank the people who helped me and supported me in many ways the last few years. More specifically, I would like to thank:

- My husband, **Cyrille Gernot**. You helped me and supported me during our whole time in Calgary, where you are my only family. I love you more every day and I would have never succeeded without you.
- My supervisors, **G rard Lachapelle and Mark Petovello**. Thank you for your guidance, useful advices and financial support during the last three years. You have permitted me to learn a lot.
- **Ma famille**. Je remercie mes parents pour m'avoir soutenue toute ma vie, quels que soient mes choix et pour avoir toujours cru en moi. Sans vous, je n'en serais jamais arriv e l .
- All the **PLAN Group members** for the great working environment. More specifically, I would like to thank for their help and their friendship **C cile Mongr dien, Julien Courtois, Nadia Sokolova, Aleksandar Knezevic, Aiden Morrison** as well as Kyle O'Keefe, Jared Bancroft, Kannan Muthuraman and Richard Ong.

Table of Contents

Abstract	iii
Acknowledgements	v
Table of Contents	vi
List of Tables	ix
List of Figures and Illustrations	x
List of Symbols, Abbreviations and Nomenclature	xv
CHAPTER ONE: INTRODUCTION	1
1.1 Background	2
1.2 Previous research and motivation	7
1.3 Objectives	16
1.4 Thesis outline	19
CHAPTER TWO: GPS L1 C/A AND L1C SIGNAL STRUCTURE	21
2.1 Brief History and GPS L1 C/A Signal Structure	21
2.1.1 Brief History of GPS and Creation of the GPS L1 C/A Signal	22
2.1.2 Structure of the GPS L1 C/A Signal	24
2.1.3 Correlation properties of GPS L1 C/A	32
2.2 GPS L1C	37
2.2.1 From GPS L1 C/A to GPS L1C: Overview of the GPS Modernization	38
2.2.2 Structure of the GPS L1C Signal	42
2.2.3 Correlation properties of GPS L1C	52
2.3 Improvements brought by GPS L1C compared to GPS L1 C/A	57
CHAPTER THREE: GALILEO L1 SIGNAL	62
3.1 Brief History of the Galileo System and Forecast Deployment of the Galileo Constellation	62
3.2 Structure of the Open Service Galileo L1 Signal	70
3.3 Galileo L1 Signal Model	78
3.4 Cross Correlation Properties of the Galileo L1 Open Service Signal	81
CHAPTER FOUR: GPS AND GALILEO L1 SOFTWARE SIGNAL SIMULATOR	86
4.1 Overview of the software signal simulator structure	90
4.1.1 Initialization phase	94
4.1.2 Cubic spline interpolation	95
4.1.3 Generation of the navigation message	100
4.1.4 Generation of the signal broadcast by one satellite	102
4.1.5 Generation of the samples of the signal at the front-end level	106
4.2 Generation of interference	107
4.2.1 Continuous Wave (CW) Interference	108
4.2.2 Narrowband interference	110
4.3 Oscillator model	110
4.3.1 Model in the Continuous Domain	111
4.3.2 Transformation in the Discrete Domain	120

4.3.3 Simulation of the oscillator error.....	122
CHAPTER FIVE: DEVELOPMENT, TESTING AND STATISTICAL ANALYSIS OF INDEPENDENT GPS AND GALILEO L1 ACQUISITION ALGORITHMS	
5.1 Acquisition methods for GPS L1C and Galileo L1	125
5.1.1 Test procedure	126
5.1.2 Methods of acquisition of the Galileo L1 pilot and data channels	128
5.1.2.1 First and second methods of acquisition.....	131
5.1.2.2 Third method of acquisition.....	134
5.1.2.3 Fourth method.....	136
5.1.3 Results of the acquisition methods using real data and comparison	140
5.1.4 Statistical analysis	151
5.1.4.1 Data channel over 8 ms (Method D1).....	151
5.1.4.2 Data channel over 16 ms (Method D2).....	154
5.1.4.3 Pilot channel over 16 ms (Method P1)	155
5.1.4.4 Pilot channel over 8 ms (Method P2)	156
5.1.4.5 ROC Curves.....	157
5.1.4.6 Mean acquisition time.....	158
5.2 Acquisition algorithm to combine GPS L1 C/A with GPS L1C (data and pilot channels)	163
5.2.1 Method of acquisition.....	163
5.2.2 Results using the software signal simulator	168
CHAPTER SIX: DEVELOPMENT, IMPLEMENTATION AND TESTING OF COMBINED TRACKING FOR GPS AND GALILEO L1 SIGNALS	
6.1 Traditional tracking method.....	173
6.2 Combined GPS L1 C/A and GPS L1C (data and pilot channels) tracking.....	178
6.2.1 Method of tracking	178
6.2.2 Results using the software signal simulator	181
6.3 Kalman filter for tracking	187
6.3.1 Traditional Kalman filter for GPS L1 C/A only tracking.....	187
6.3.2 Kalman filter to simultaneously combine GPS L1 C/A with GPS L1C (data and pilot channels)	193
6.3.3 Results and comparison of the performance of the Kalman filters with the traditional tracking	198
6.3.3.1 Tests in static mode.....	199
6.3.3.2 Tests in dynamic mode	207
CHAPTER SEVEN: CONCLUSIONS AND RECOMMENDATIONS FOR FUTURE WORK.....	
7.1 Conclusions.....	214
7.1.1 Signal Software Simulator.....	214
7.1.2 Acquisition algorithms	215
7.1.3 Tracking algorithms.....	216
7.2 Recommendations for future work	217
7.2.1 Use of Real Data.....	218

7.2.2 Acquisition	218
7.2.3 Tracking.....	218
7.2.4 Position solution	219
APPENDIX A: COMPUTATION OF THE SATELLITE VELOCITY USING THE EPHEMERIS PARAMETERS	229
APPENDIX B: GENETIC ALGORITHM PRINCIPLE	234
APPENDIX C: IMPACT OF THE APPROXIMATION OF THE MBOC BY A BOC(1,1) ON ACQUISITION PERFORMANCE.....	237
APPENDIX D: IMPLEMENTATION OF A KALMAN FILTER FOR GPS L1 C/A AND L1C (DATA AND PILOT) SIGNAL TRACKING.....	258

List of Tables

<i>Table 2-1: Modulation tradeoff for BPSK, BOC(1,1) and TMBOC modulations (from Betz et al 2006)</i>	60
<i>Table 4-1: Sources and services of interference v/s harmonics (from Landry & Renard 1997)</i>	108
<i>Table 4-2: Parameters for the Allan variance of several oscillators (from Winkel 2003)</i>	112
<i>Table 5-1: GPS L1 C/A – L1C Simulation parameters</i>	169
<i>Table 6-1: Summary of Traditional Tracking Parameters</i>	177
<i>Table 6-2: Simulation parameters</i>	182
<i>Table 6-3: Numerical values of the covariance matrix</i>	191
<i>Table 6-4: Simulation parameters</i>	200
<i>Table 6-5: Simulation parameters</i>	208
<i>Table C-1: Tracking parameters</i>	239
<i>Table C-2: CW interference simulation parameters</i>	240
<i>Table C-3: Simulation parameters for narrowband interference at 1 MHz</i>	246
<i>Table C-4: Simulation parameters for narrow band interference at 6 MHz</i>	247

List of Figures and Illustrations

<i>Figure 1-1: GPS modernization (from Crews 2008)</i>	5
<i>Figure 2-1: GPS L1 C/A code generation¹</i>	25
<i>Figure 2-2: Autocorrelation of the GPS L1 C/A code (top) and detail of the main peak (bottom).....</i>	27
<i>Figure 2-3: Normalized PSD (Power spectral density) of the GPS L1 C/A signal</i>	29
<i>Figure 2-4: Cumulative probability for the cross correlation of PRNs 1 and 2 of the GPS L1 C/A codes</i>	33
<i>Figure 2-5: Cumulative probability for the cross correlation of PRNs 1 and 2 of the GPS L1 C/A codes with synchronous sampling (red), asynchronous sampling (cyan) and without sampling (blue)</i>	35
<i>Figure 2-6: Cumulative probability for the cross correlation of PRNs 1 and 2 of the GPS L1 C/A codes with different relative Doppler offsets</i>	37
<i>Figure 2-7: GPS modernization (from Crews 2008)</i>	38
<i>Figure 2-8: Improvements brought by the GPS modernization (from Cabler 2003)</i>	41
<i>Figure 2-9: Generation of the LIC primary codes</i>	43
<i>Figure 2-10: BOC(1,1) modulation</i>	45
<i>Figure 2-11: TMBOC modulation</i>	45
<i>Figure 2-12: Autocorrelation of the GPS LIC code (left column) and detail of the peak (right column) for the spreading code only (top figures), data channel modulated by BOC (middle figures) and the pilot channel modulated by TMBOC (bottom figures).....</i>	46
<i>Figure 2-13: Normalized PSD of the LIC data channel (top left), LIC pilot channel (top right) and the complete LIC signal (bottom)</i>	50
<i>Figure 2-14: Cumulative probability for the cross correlation of PRNs 1 and 2 of the GPS LIC pilot and data codes</i>	53
<i>Figure 2-15: Cumulative probability for the cross correlation of PRNs 1 and 2 of the GPS LIC pilot codes (top) and the data codes (bottom) with asynchronous sampling (15 MHz) in black, and without sampling in red.....</i>	54

<i>Figure 2-16: Cumulative probability for the cross correlation of PRNs 1 and 2 of the GPS L1C codes for the data channel (top) and the pilot channel (bottom) with different relative Doppler offsets</i>	<i>56</i>
<i>Figure 3-1: GIOVE-B satellite in its test facility (from ESA website).....</i>	<i>65</i>
<i>Figure 3-2: Galileo constellation (from ESA website)</i>	<i>67</i>
<i>Figure 3-3: Galileo and GPS frequency plan.....</i>	<i>69</i>
<i>Figure 3-4: Power Spectral densities of the Galileo signals</i>	<i>70</i>
<i>Figure 3-5: Tiered code generation (from GIOVE-A SIS ICD 2007)</i>	<i>72</i>
<i>Figure 3-6: CBOC modulation on the data channel (on the left) and the pilot channel (on the right) (from Floc'H & Soellner 2007)</i>	<i>74</i>
<i>Figure 3-7: Galileo L1 power spectrum (from Avila-Rodriguez et al 2007).....</i>	<i>75</i>
<i>Figure 3-8: Example of autocorrelation of the GIOVE-A codes for the data channel (on top left) and for the pilot channel (on bottom left) and their detail (on the right)</i>	<i>77</i>
<i>Figure 3-9: Example of autocorrelation of the Galileo codes for the data channel (on the left) and its detail (on the right)</i>	<i>78</i>
<i>Figure 3-10: Cumulative probability for the pilot and data channels of Galileo L1</i>	<i>82</i>
<i>Figure 3-11: Cumulative probability for the Galileo L1-C pilot code with and without sampling</i>	<i>83</i>
<i>Figure 3-12: Cumulative probability for the Galileo L1-B channel for various Doppler offsets ranging from 0 to 1000 Hz</i>	<i>84</i>
<i>Figure 4-1: Signal simulated by the software signal simulator.....</i>	<i>89</i>
<i>Figure 4-2: Top level architecture diagram of software signal simulator</i>	<i>91</i>
<i>Figure 4-3: Flow Diagram of software signal simulator.....</i>	<i>93</i>
<i>Figure 4-4: Error in the X, Y and Z axis for a static receiver using a cubic spline with an interval of 10, 30, 60 and 300 seconds</i>	<i>100</i>
<i>Figure 4-5: Flow chart of the signal generation</i>	<i>103</i>
<i>Figure 4-6: Potential TV interference (from Landry & Renard 1997).....</i>	<i>109</i>
<i>Figure 4-7: Cost function of the genetic algorithm</i>	<i>117</i>

<i>Figure 4-8: Theoretical Allan standard deviation and simulated Allan standard deviation for the OCXO and Rubidium oscillators</i>	123
<i>Figure 5-1: GIOVE-A data collection set-up</i>	127
<i>Figure 5-2: Parallel code phase search acquisition scheme</i>	129
<i>Figure 5-3: Illustration of the zero padding technique</i>	133
<i>Figure 5-4: Illustration of the technique of correlation over 16 ms for the data channel (method D2)</i>	136
<i>Figure 5-5: Illustration of the technique of correlation over 8 ms for the pilot channel (method P2)</i>	139
<i>Figure 5-6: Acquisition of the data channel using 8 ms of incoming signal (method D1)</i>	141
<i>Figure 5-7: Results of the acquisition for the data channel using 8 ms of incoming signal (method D1)</i>	143
<i>Figure 5-8: Results of the acquisition for the data channel using 16 ms of incoming signal (method D2)</i>	143
<i>Figure 5-9: Results of the acquisition for the pilot channel using 8 ms of incoming signal (method P2)</i>	144
<i>Figure 5-10: Results of the acquisition for the pilot channel using 16 ms of incoming signal (method P1)</i>	145
<i>Figure 5-11: Detail of the BOC correlation for real data (on the top) and for simulated data (on the bottom)</i>	147
<i>Figure 5-12: Comparison of the sensitivity of the four acquisition methods</i>	149
<i>Figure 5-13: ROC Curves for the four acquisition methods. The lower plot shows the upper left portion of the top plot in more detail. Note that, on the top figure, the ROC curves corresponding to the methods D2 and P1 are overlaid.</i>	158
<i>Figure 5-14: Acquisition bloc diagram</i>	160
<i>Figure 5-15: Mean acquisition time in function of the penalty time</i>	162
<i>Figure 5-16: Combined GPS L1 C/A – L1C acquisition scheme</i>	163
<i>Figure 5-17: Results of the combined acquisition with a C/N_0 of 45 dB-Hz</i>	170
<i>Figure 5-18: Results of the combined acquisition with a C/N_0 of 32 dB-Hz</i>	171

<i>Figure 5-19: Acquisition of the LIC data channel alone for a C/N_0 of 32 dB-Hz</i>	172
<i>Figure 6-1: Scheme of a PLL (Phase Lock Loop)</i>	175
<i>Figure 6-2: Scheme of a DLL (Delay Lock Loop)</i>	175
<i>Figure 6-3: Scheme of the combined tracking method</i>	179
<i>Figure 6-4: Doppler (on top) and PLI (on the bottom) for the combined tracking and the LIC data channel only tracking - First simulation</i>	184
<i>Figure 6-5: Doppler (on top) and PLI (on the bottom) for the combined tracking - First and second simulations</i>	185
<i>Figure 6-6: Doppler (on top) and PLI (on the bottom) for the combined tracking and the LIC data channel only tracking - Third simulation</i>	186
<i>Figure 6-7: Model of the autocorrelation function of LIC (on the right) and its derivative (on the left)</i>	196
<i>Figure 6-8: Doppler and error in Doppler for the first static test for the three tracking methods</i>	201
<i>Figure 6-9: Code delay error for the first test for the three tracking methods</i>	202
<i>Figure 6-10: PLI for the first test for the three tracking methods</i>	203
<i>Figure 6-11: Doppler and Doppler error for the second static test (top figures), code delay error (bottom left figure) and PLI (bottom right figure)</i>	204
<i>Figure 6-12: Doppler and Doppler error for the third static test (top figures), code delay error (bottom left figure) and PLI (bottom right figure)</i>	206
<i>Figure 6-13: Doppler and Doppler error for the first dynamic test (top figures), code delay error (bottom left figure) and PLI (bottom right figure)</i>	210
<i>Figure 6-14: Doppler and Doppler error for the second dynamic test (top figures), code delay error (bottom left figure) and PLI (bottom right figure)</i>	211
<i>Figure 6-15: Doppler and Doppler error for the third dynamic test (top figures), detail of the Doppler error (middle figure) and code delay error (bottom left figure) and PLI (bottom right figure)</i>	213
<i>Figure C-1: Test procedure</i>	238
<i>Figure C-2: Deflection coefficient as a function of the interference power for a CW interference (on top) and Power of the CW interference over time (at the bottom)</i>	242
<i>Figure C-3: C/N_0 as a function of the interference power for CW interference</i>	244

<i>Figure C-4: Phase lock indicator (PLI) for CBOC and BOC for CW interference</i>	244
<i>Figure C-5: Doppler in function of time for CBOC and BOC modulations in presence of CW interference (on top) and Power of the CW interference over time (at the bottom)</i>	245
<i>Figure C-6: Magnitude response of the band pass filter centered at 1 MHz from the IF</i>	248
<i>Figure C-7: Magnitude response of the band pass filter centered at 6 MHz from the IF</i>	248
<i>Figure C-8: Deflection coefficient as a function of the interference power for a narrow band interference at 1 MHz.....</i>	250
<i>Figure C-9: Improvement in the deflection coefficient of the CBOC compared to the BOC for a narrowband interference at 1 MHz (on top) and interference power over time (at the bottom).....</i>	251
<i>Figure C-10: C/N_0 as a function of the interference power for narrowband interference centered at 1 MHz.....</i>	251
<i>Figure C-11: Phase lock indicator for the BOC(1,1) and CBOC in the presence of narrowband interference at 1 MHz (on top) and Interference power over time (at the bottom).....</i>	252
<i>Figure C-12: Deflection coefficient as a function of the interference power for a narrowband interference at 6 MHz.....</i>	253
<i>Figure C-13: Difference between the deflection coefficients of the CBOC and BOC for narrowband interference at 6 MHz.....</i>	254
<i>Figure C-14: C/N_0 as a function of the interference power for narrowband interference centered at 6 MHz.....</i>	254
<i>Figure C-15: Doppler as a function of the interference power for narrow band interference centered at 6 MHz.....</i>	255
<i>Figure C-16: Multipath envelope for BOC(1,1) in blue and CBOC in red.....</i>	257
<i>Figure C-17: Multipath envelope for NELP processing, 24 MHz bandwidth and 0.05 chip early-late spacing (from Hein 2006).....</i>	257

List of Symbols, Abbreviations and Nomenclature

Symbol	Definition
A	Signal amplitude
$A_{C/A}$	Amplitude of the GPS L1 C/A signal
C_{ic}	Amplitude of cosine correction to inclination angle
C_{is}	Amplitude of sine correction to inclination angle
C_{rc}	Amplitude of cosine correction to orbital radius
C_{rs}	Amplitude of sine correction to orbital radius
C_{uc}	Amplitude of cosine correction to argument of latitude
C_{us}	Amplitude of sine correction to argument of latitude
$\frac{C}{N_0}$	Signal to noise ratio for GPS L1 C/A
C_{v_k}	Covariance matrix associated with the measurement model
E_k	Eccentric anomaly at time T_k
$E(T / H_0)$	Mean of the noise
$E(T / H_1)$	Mean value of the main peak
F	Fourier transform
F_C	Cost function
$G_{BOC(1,1)}$	Normalized PSD of the BOC(1,1) modulation
$G_{BOC(6,1)}$	Normalized PSD of the BOC(6,1) modulation
$G_{C/A}$	Normalized PSD of the GPS L1 C/A ranging code
G_{L1C}	Normalized PSD of the GPS L1C signal
G_{L1CD}	Normalized PSD of the GPS L1C data channel
G_{L1CP}	Normalized PSD of the GPS L1C pilot channel
H	Transfer function to transform white noise into oscillator noise
H_k	Design matrix
I	In-phase component
I_0	Modified Bessel function of the first kind
I_E	Output of the early correlator of the in-phase component
I_L	Output of the late correlator of the in-phase component
I_P	Output of the prompt correlator of the in-phase component
K	Kalman gain matrix
L	Legendre sequence
$L1C_0$	Secondary code on the pilot channel
M_0	Mean anomaly at the reference time of the ephemeris

M_k	Mean anomaly at time T_k
$N(\mu, \sigma^2)$	Gaussian of mean μ and variance σ^2
P	Covariance matrix of the state vector
$P_{C/A}$	Received power for L1 C/A
P_{DET}	Global probability of detection
P_{det}	Probability of detection for one cell
P_{FA}	Global probability of false alarm
P_{fa}	Probability of false alarm for one cell
P_{L1-B}	Received power on the Galileo L1 data channel
P_{L1-C}	Received power on the Galileo L1 pilot channel
P_{L1CD}	Received power on the GPS L1C data channel
P_{L1CP}	Received power on the GPS L1C pilot channel
$P_{rx}(t)$	Receiver position
$P_{sat}(t)$	Satellite position
Q	Process noise of the covariance matrix associated with the dynamic model
Q_E	Output of the early correlator of the in-quadrature component
Q_L	Output of the late correlator of the in-quadrature component
Q_P	Output of the prompt correlator of the in-quadrature component
Q_K	Marcum Q-function
\tilde{R}	Autocorrelation function
\vec{R}	Satellite position in the ECEF frame
$R_{N,C/A}$	Normalized autocorrelation function of C/A
$R_{N,BOC(1,1)}$	Normalized BOC(1,1) autocorrelation function
$R_{S,L1-B}$	Subcarrier frequency of L1-B (used in the BOC modulation)
$R_{S,L1-C}$	Subcarrier frequency of L1-C (used in the BOC modulation)
S	Spectral density
T	Coherent integration time interval
T_C	Ranging code chip duration
T_d	Time to acquire the signal
T_k	Difference between the current time and the reference time of the ephemeris
T_{oe}	Reference time of ephemeris
T_p	Penalty time
\vec{V}	Satellite velocity in the ECEF frame
W	Weil code
$X_{C/A}$	Distribution of L1 C/A

X_{L1CD}	Distribution of L1C data channel
X_{L1CP}	Distribution of L1C pilot channel
X_p	In plane x position at time T_k
Y_p	In plane y position at time T_k
X_s	ECEF x-coordinate at time T_k
Y_s	ECEF y-coordinate at time T_k
Z_s	ECEF z-coordinate at time T_k
c	Speed of light
$c_{C/A}$	C/A ranging code
c_D	Code Doppler
c_{delay}	Code delay
c_{L1-B}	Galileo L1 ranging code on the data channel
$c_{L1-B,[i]_{L1-B}}$	Galileo ranging code of the L1-B component
c_{L1-C}	Galileo L1 ranging code on the pilot channel
$c_{L1-C,[i]_{L1-C}}$	Galileo ranging code of the L1-C component
c_{L1CD}	L1C ranging code on the data channel
c_{L1CP}	L1C ranging code on the pilot channel
c_{sec}	Secondary code on the Galileo pilot channel
d	Deflection coefficient
$d_{C/A}$	L1 C/A data bit of the binary NRZ navigation message
$\frac{di}{dt}$	Rate of change of inclination angle
d_{L1-B}	Data bit of the binary NRZ navigation message of the Galileo L1 data channel
$d_{L1-B,[i]_{d_{L1-B}}}$	Galileo L1 navigation message
d_{L1C}	Data bit of the binary NRZ navigation message on the L1C data channel
e	Eccentricity
f	Intermediate frequency
f_0	Desired frequency
f_C	Chipping rate
f_D	Doppler frequency due to the user and satellite motion
f_{Dtotal}	Doppler frequency due to the satellite and user motion plus the Doppler shift due to atmospheric and clock errors
f_{iono}	Doppler shift and due to the ionosphere

f_{L1}	GPS L1 central frequency
f_{time}	Doppler shift due to the oscillator variations
f_{Trop}	Doppler shift due to the troposphere
f_s	Sampling frequency
$h(x,k)$	Function which express z_k as function of x_k
h_i	h parameters of the oscillator
i	Interference
i_0	Inclination angle at the reference time of ephemeris
i_k	Corrected radius at time T_k
n	Corrected mean motion
p	Variable in Laplace domain
$rect_{T_c}(t)$	“rectangle” function (defined to equal to one between 0 and T_c and 0 elsewhere)
$s_{C/A}$	C/A signal
$sc_{BOC(1,1)}$	the BOC(1,1) subcarrier
$sc_{BOC(6,1)}$	BOC(6,1) subcarrier
sc_{CBOC}	Subcarrier CBOC modulation
$sc_{CBOC_Data}(t)$	CBOC subcarrier of the data channel
$sc_{CBOC_Pilot}(t)$	CBOC subcarrier of the pilot channel
s_{L1}	Galileo L1 OS signal
s_{L1-B}	Galileo L1-B signals
s_{L1-C}	Galileo L1-C signals
s_{L1C}	GPS L1C signal
t_{GPS}	GPS time
$t_{Galileo}$	Galileo time
$t_{CubicSpline}$	Cubic spline interval
$t_{transit}$	Transit time
$tri\left(\frac{x}{y}\right)$	unit triangular function of width $2y$ centered at 0
t_{rx}	Receiver time
t_{sat}	Satellite time
u_k	Corrected argument of latitude at time T_k
$\text{var}(T/H_0)$	Variance of the noise
v_k	Noise associated with the measurement model
v_k	True anomaly at time T_k
v_r	Relative velocity satellite-receiver projected on the satellite-receiver vector

v_{rx}	Receiver speed
v_{sat}	Satellite speed
w	Weil index
$w(t)$	Noise approximated as Gaussian with zero mean
w_e	Rotation rate of the Earth
x_k	State vector at epoch k
\hat{x}_k	Estimated State vector at epoch k
y	Ratio of the frequency errors normalized by the desired frequency
z_k	Real values of the measurements at epoch k
\hat{z}_k	Estimated values of the measurements at epoch k
α_D	Scale factor to account for the difference in transmitted power of the L1C data channel
α_P	Scale factor to account for the difference in transmitted power of the L1C pilot channel
β	Threshold
χ_2^2	Chi Square with 2 degrees of freedom
$\Delta\phi_{iono}$	Phase variation due to the ionosphere
$\Delta\phi_{time}$	Phase variation due to the oscillator variations
$\Delta\phi_{Trop}$	Phase variation due to the troposphere
Δt_{Iono}	Ionospheric delay
Δt_{Trop}	Tropospheric delay
δf_0	Error in the local carrier frequency at the beginning of the integration interval
$\delta\phi_k$	Argument of latitude correction at time T_k
$\delta\phi$	Average error in the local carrier phase over the integration interval
$\delta\phi_0$	Error in the local carrier phase at the beginning of the integration interval
δR_k	Radius correction at time T_k
δx_k	Perturbed state vector
δz_k	Measurement misclosure
Δ	Spacing between the prompt and the early/late correlators
\mathcal{E}	White noise of unit variance and zero mean
λ	Non-centrality parameter
$\mu_{C/A}$	Size of the correlation peak of the L1 C/A channel
μ_{L1CD}	Size of the correlation peak of the L1C data channel
μ_{L1CP}	Size of the correlation peak of the L1C pilot channel
Ω	Argument of perigee at the reference time of the ephemeris

Ω_0	Longitude of the ascending node (at weekly epoch)
Ω_e	Rate of Earth rotation
Ω_k	Corrected longitude of node at time T_k
$\dot{\Omega}$	Rate of change of longitude of the ascending node
Φ	Transition matrix
$\phi_{C/A}$	Initial L1 C/A phase in radians
ϕ_k	Argument of latitude at time T_k
ϕ_{L1}	Initial Galileo L1 phase in radians
ϕ_{L1C}	Initial GPS L1C phase in radians
ρ	Geometric distance between the satellite and the receiver
σ	Noise variance
$\sigma_{C/A}^2$	Variance of the noise associated with the L1 C/A channel
σ_{L1}^2	Variance of the noise associated with the GPS L1 signal
σ_{L1C}^2	Variance of the noise associated with the L1C signal
σ_{L1CD}^2	Variance of the noise associated with the L1C data channel
σ_{L1CP}^2	Variance of the noise associated with the L1C pilot channel
σ_n^2	Noise variance at the correlator output
τ	Mean acquisition time
$\tau_{C/A}$	Time delay for L1 C/A due to the propagation between the satellite and the receiver including the time delay created by the atmosphere
τ_{L1}	Galileo time delay due to the propagation between the satellite and the receiver including the delay induced by the atmospheric clock delays
τ_{L1C}	Time delay for GPS L1C due to the propagation between the satellite and the receiver including the atmosphere clock delays

Acronym	Definition
AGPS	Aided GPS
AltBOC	Alternative BOC
ARNS	Aeronautical Radio Navigation Services
BER	Bit Error Rate
BOC	Binary Offset Carrier
BPSK	Binary Phase Shift Keying
C/A	Coarse Acquisition
CASM	Coherent Adaptive Subcarrier Modulation
CBOC	Composite BOC
CDMA	Code Division Multiple Access
CRC	Cyclic Redundancy Check
CS	Commercial Service
CW	Continuous Wave
DLL	Delay Lock Loop
DME	Distance Measuring Equipment
DoD	Department of Defense
DS-SS	Sequence-Spread Spectrum
EC	European Commission
ESA	European Space Agency
EU	European Union
FEC	Forward Error Correction
FFT	Fast Fourier Transform
FFT	Fast Fourier Transform
FLL	Frequency Lock Loop
FM	Frequency Modulation
GIOVE-A	Galileo In-Orbit Validation Element
GNSS	Global Navigation Satellite System
GPS	Global Positioning System
I/NAV	Integrity NAVigation message type
ICAO	International Civil Aviation Organization
IF	Intermediate Frequency
IFG2Sim™	Intermediate Frequency GPS and Galileo Simulator
KF	Kalman filter
L1C _D	GPS L1C data channel
L1C _P	GPS L1C pilot channel
LFSR	Linear Feedback Shift Register
MBOC	Multiplexed Binary Offset Carrier
NASA	National Aeronautics and Space Administration
NATO	North Atlantic Treaty Organization
NELP	Noncoherent Early-Late Processing
NRZ	Non-Return to Zero
OS	Open Service
PLI	Phase Lock Indicator
PLL	Phase Lock Loop

PRN	Pseudo-Random Noise
PRS	Public Regulated Service
PSD	Power Spectral Density
QPSK	Quadrature Phase Shift Keying
RHCP	Right Hand Circular Polarized
RNSS	Radio Navigation Satellite Services
ROC	Receiver Operating Characteristic
SAR	Search And Rescue
SBAS	Satellite-Based Augmentation System
SNR	Signal to Noise Ratio
SoL	Safety of Life
sps	Symbols per second
TACAN	TACTical Air Navigation
TEC	Total Electron Content
TMBOC	Time Multiplexed Binary Offset Carrier
TOW	Time of Week
TV	Television
UHF	Ultra High Frequency
US	United States
USA	United States of America
VHF	Very High Frequency

Chapter One: INTRODUCTION

The current *Global Positioning System* (GPS) has been widely studied since its creation. Nevertheless, with the recent or upcoming availability of several new signals from GPS, Galileo, GLONASS and Compass, the beginning of a new era in the field of GNSS has arrived. The recent development and launching of the two first Galileo satellites GIOVE-A and GIOVE-B, part of the Galileo System Test Bed, as well as the future modernization of GPS, are the start of this new age. Therefore, with such an improvement in the number of signals available to the user and the geometry offered by the combination of the various constellations and signals, the current capabilities of Global Navigation Satellite System (GNSS) receivers will increase. At the same time however, the receiver implementation will also become more complex. To this end, new techniques of acquisition and tracking as well as new algorithms need to be developed to handle these new signals.

For instance, in the GPS L1 frequency band, many signals will be available in the next decade: L1 C/A and L1C for GPS, and L1-B and L1-C for Galileo (GPS ICD 200D 2004, OS SIS ICD Draft 0 2006, OS SIS ICD Draft 1 2008). Concerning Galileo, only the two test satellites GIOVE-A and GIOVE-B have been launched for the moment and the full constellation should be deployed by 2013 (European Space Agency website). In the case of GPS, the L1C signal will not be transmitted before 2011 (Cameron 2007), but because of its structure, it will improve the accuracy and reliability of the current GPS L1 signal. The combination of these two Global Navigation Satellite Systems (GNSS) will allow an

improvement of the geometry and an increase in reliability for the user (Lachapelle 2001).

This thesis focuses on the acquisition and tracking of GPS and Galileo L1 signals, and introduces new techniques allowing to combine the signals from the same satellite at the acquisition and tracking levels, as well as taking advantage of the properties of these signals. Particular attention is given to combining the signals in acquisition and tracking under challenging conditions (low signal power, high dynamics, etc).

1.1 Background

GPS was the first modern operational GNSS available. However, a lot of new GNSS systems are today under development and four GNSS systems should be operational in the next decade. To address the ever increasing demands of the user in terms of availability, accuracy and reliability, these systems will bring new enhancements, especially with respect to signal structures and modulations.

GPS allows users everywhere on Earth to know their position, velocity and time independent of the weather and at any time. The system is based on a very accurate time provided by an extremely stable timing system composed of synchronized atomic clocks on board of the satellites with a very accurate reference timing system located on the ground. This very precise time is used to determine the transit time which corresponds to the time taken by the signal to travel from the satellite to the user. Thus, using four

satellites, four transit times can be determined. Moreover, the orbits of the satellites are transmitted in the navigation message and allow the user to compute the position of the satellite, thus allowing the user to compute their position in 3D and the time. In a common receiver, two different ways can be used to determine the position: determination of the pseudoranges (distance deduced from the transit time) or use of the carrier phase measurements. The latter measurements provide more accurate position because of their lower multipath error, but to be useful, an ambiguity needs to be determined and the measurements have to be integrated over time (Cannon 2005).

The position solution given by GPS includes errors due to the receiver, the satellite and the environment between the satellite and the receiver (Kaplan 2006). Indeed, the oscillators of the receiver and satellites are not perfect and induce clock errors (Kaplan 2006). The orbit of the satellite is not known perfectly even with the correction parameters and creates an orbital error (Kaplan 2006). In fact, due to the attraction of other planets and the non-uniform gravity of the Earth which are not completely taken into account, an error remains in the position of the satellite and can generate an error in the user position. Due to the ionosphere and troposphere, the signal does not travel in a straight line from the satellite to the receiver at the speed of the light but is delayed and curved (Skone 2007) and therefore induces an error in the measurement of the pseudorange (distance between the satellite and the receiver including the effect of an unknown receiver clock offset). Finally, ambient noise as well as the environment (multipath and interference) adds errors (Lachapelle 2006).

It is less expensive and most common to use a stand-alone receiver (without any aiding) for civil applications but the resulting position accuracy is on the order of one metre in the best case. Due to the very low received power (the minimum expected power of GPS L1 C/A is -158.5 dBW (GPS ICD 200D 2004)), GPS signals are very sensitive to signal degradation due to the environment (trees, urban environment, indoor, etc.) or interference. Therefore, a modernization of the GPS system is currently under development, which will result in improved performance of stand-alone receivers.

The first version of GPS has been fully operational since 1995 and contains only one public signal, namely L1 C/A. The modernization of the GPS system is being realized in three main phases as presented in Figure 1-1 (Crews 2008). Although improvements are being made in terms of the military codes, the focus here is on the civil signals. To this end, relative to the current “legacy” satellites, the Block IIR-M will be implemented first. It corresponds to an augmentation of the L2 frequency (1227.6 MHz) with the insertion of a new civilian signal L2C. The L2C signal contains two open service channels time multiplexed together; one pilot channel (without a navigation message) and one data channel (with a navigation message). At the time of writing, there are already six Block IIR-M satellites in operation. Following the Block IIR-M satellites, the Block IIF satellites will also broadcast a new civilian signal at the L5 centre frequency 1176.45 MHz. The first satellite to broadcast this signal is actually a modified Block IIR-M and has been launched in March 2009. The L5 signal also contains data and pilot channels, and is transmitted at a faster chipping rate and at higher power than the GPS L1 and L2 signals. This signal should improve the position accuracy and be more robust to

interference due to its wider bandwidth (Mongrédien et al 2007). Finally, the L1 signal will be augmented by the L1C signal in the Block III satellites.

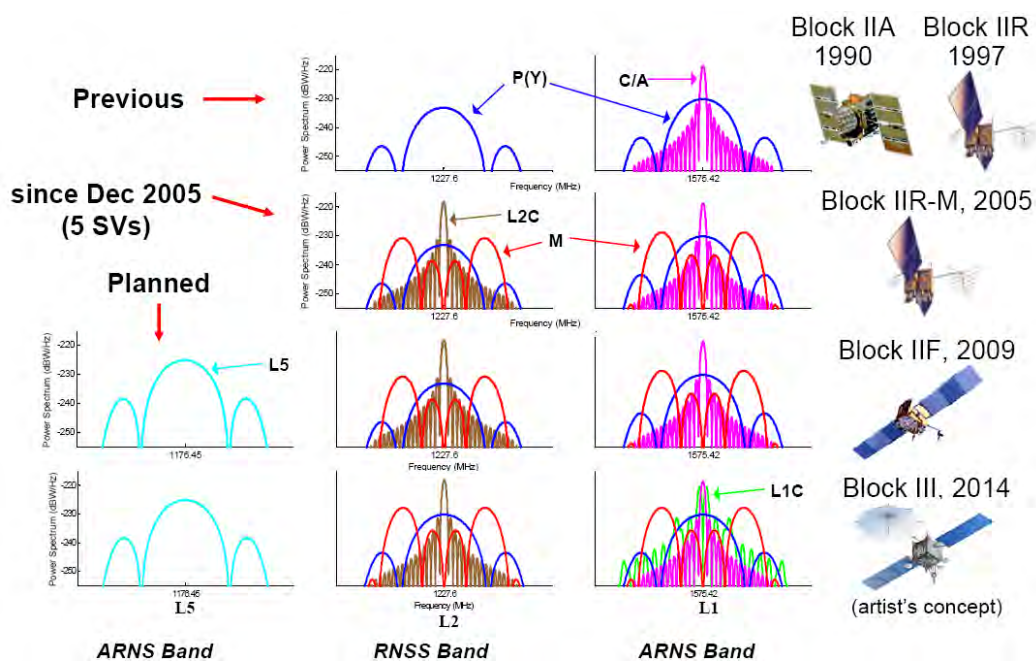


Figure 1-1: GPS modernization (from Crews 2008)

The deployment of this new signal is forecast for 2013, but the U.S. Air Force hopes to finish the development by 2011 (Cameron 2007).

Concerning Galileo, the European Commission (EC) and the European Space Agency (ESA) have been collaborating to create the first European global navigation system. This new constellation named Galileo will be mainly civilian and commercial - except for the PRS (Public Regulated Service) which is reserved for public authorities - and will be inter-operable with GPS and GLONASS, the American and Russian GNSSs.

The first Galileo satellite, GIOVE-A was launched on 28 December 2005 and is being used to test satellite equipment and the ground stations and to secure the Galileo frequencies with the International Telecommunications Union. The second test satellite GIOVE-B was launched on 30 April 2008 to continue the tests and incorporate some improvements such as the new navigation message and modulation formats.

Four operational satellites should then be launched to validate the Galileo concept, and once this phase is complete, the full constellation will be deployed. When the deployment is complete, the constellation will contain 27 operational satellites plus 3 active spares (Benedicto et al 2000) divided in three orbital planes and transmitting at three frequencies for civilian and commercial use (no military signal).

The Galileo L1 and the GPS L1C signals have several advantages compared to the currently transmitted L1 C/A signal, including (Hudnut 2005, Hein et al 2006):

- The power is split between a data and pilot channel, which allows a better tracking and permits the elimination of half-cycle ambiguities
- The spreading codes are longer and thus are more resistant to narrow band interference and have lower cross correlation properties
- The navigation message will be improved, especially in terms of coding (detection and correction of miss detected data bits)
- The data and pilot channel have the same spreading code period and thus can be combined in acquisition and tracking
- MBOC (Multiplexed Binary Offset Carrier) modulation which improves signal tracking performance especially in presence of multipath

1.2 Previous research and motivation of this thesis

In this section, previous research relevant to the work done in this thesis is presented.

Then, the motivations of this work are introduced.

A GPS receiver can be divided in four main parts (Raquet 2006):

1. The Front-end: Down conversion of the signal from the received carrier frequency to an intermediate frequency and sampling of the IF signal.
2. Acquisition: Process a 3D Space search to find the code delay and the Doppler frequency. This search is done for all PRNs (Pseudo-Random Noise).
3. Tracking: Once the signal is acquired, the changes in Doppler and code delay are monitored through the signal tracking process.
4. Computation of a position: Once the signal is tracked, the bits of the navigation message can be decoded and used to compute the position of the satellite.

The three last parts can be implemented in software and are discussed in more detail below.

Acquisition

As mentioned before, the goal of the acquisition process is to determine the code delay and the Doppler of the signal for each visible satellite.

Once the signal is received, down converted and sampled by the Front-end, a search is done on all PRNs to find the visible satellites and the corresponding code delays and

Doppler effects. To do so, the incoming signal is multiplied by a locally generated carrier (corresponding to the approximate received signal frequency) and a local replica of the spreading code (Van Nee & Coenen 1991). This search is completed for all possible code delays (1023 chips in the case of GPS L1 C/A) and over a typical Doppler range between -5000 Hz and +5000 Hz. In the case of a software receiver, these multiplications are in general realized in the frequency domain using an FFT (Fast Fourier Transform) (Akopian 2005).

In the case of coherent acquisition, the increment in the locally generated Doppler depends on the acquisition time: the longer the acquisition time, the smaller should be the size of the frequency bin (Raquet 2006). Thus, one has to keep in mind that in the case of weak signals (indoor, urban canyon, foliage, etc.), the acquisition time needs to be increased in order to acquire the signal but the processing time increases quickly due to the size of the vectors of samples to correlate and the number of frequency bins. Indeed, when the acquisition time is increased, the number of frequency bins needs to be increased to acquire the signal (if the size of the frequency bin is not decreased the error in frequency can destroy the correlation). However, it is possible to use a non-coherent correlation (addition of the correlator outputs squared) in order to acquire lower power signals. This way, the size of the frequency bin does not need to be changed but the performance is not as good in terms of SNR (Signal to Noise Ratio) as with coherent integration due to the increase of the noise (since the correlations are squared before being added). However, it is possible to combine a non-coherent or a differential

technique with a coherent integration. These techniques permit to acquire signals attenuated by as much as 20 dB (MacGougan 2003, Shanmugam et al 2005).

Concerning the GPS L1 C/A signal, the correlation can be realized using 1 to 10 ms (i.e. 1 to 10 spreading code periods) of incoming signal without the correlation being affected by the change in the sign of the data bit (since the data bit sign can change every 20 ms). Indeed, if one integrates over 10 ms and a data bit sign change occurs, one just needs to take the next 10 ms. Nevertheless, if one considers the case of Galileo L1 (see Chapter 3), the spreading code period of the data channel is 4 ms and the data bit sign can change every 4 ms, thus every spreading code period. Due to this possible change in sign, a destructive combination can occur over longer coherent integration times, leading to degraded acquisition performance or a total destruction of the correlation. The same problem is encountered in the case of the pilot channel of Galileo L1 where the secondary code plays the same role as the navigation data message (which is actually absent from the signal): the sign of the secondary bit can change each time the spreading code repeats. Again, the same situation occurs for the pilot and data channels of the GPS L1C signal. The same problem also occurs for GPS L5, and the Zero Padding technique is applied to these signals to acquire the signal using a parallel code phase search acquisition (Mongredien 2008, Yang 2004), or using an optimal detector (Hegarty et al 2003, Hegarty 2006). This later method has been applied to Galileo. Moreover, other methods have been created using this method as a basis in Macchi & Petovello (2007) to realize the acquisition using different length of incoming signal.

The modulations of GPS L1C and Galileo L1 include BOC (Binary Offset Carrier) and TMBOC (Time Multiplexed Binary Offset Carrier) modulations. Thus, the shape of the autocorrelation (see Chapter 2) is no longer a unique peak at the code delay, but contains side peaks (Borio et al 2006, Mattos 2005, Mattos 2006). For example, for a BOC(1,1), the correlation includes one main peak at the code delay and two side peaks with half the power of the main peak on each side. In case of weak signals, the acquisition performance can be degraded due to these peaks. Some prefiltering techniques have been developed to change the shape of the autocorrelation function (removal of the side peaks) and improve the sensitivity and reliability of the acquisition (Yang 2007).

In general, acquisition performance is completely determined by the following parameters:

- Probability of detection: probability of correctly determining the presence of the signal and estimating the right Doppler shift and code delay
- Probability of false alarm: Probability to wrongly declaring the signal present
- Mean time of acquisition: time required to correctly detect the signal. Note that to correctly estimate the effect of the acquisition time, its distribution would need to be determined.

The plot of the probability of detection versus the probability of false alarm is generally called ROC (Receiver Operating Characteristic) and completely characterizes from a statistical point of view the detection performance (DiFranco & Rubin 2004). However, even if the information carried by the ROC is complete (see Chapter 5 for more detail on this), the deflection coefficient (defined in Chapter 5) is often used instead because of its

simplicity of computation and its more intuitive information. Indeed, the deflection coefficient is an estimation of the post correlation SNR and allows comparisons between different acquisition sensitivities if they have the same distribution (Kay 1993).

In the literature, different methods of acquisition have been developed and their performance has been statistically determined. These techniques can be divided in three main categories (Shanmugam 2008): coherent and non coherent integration due to the deep analogy between the radar detection and signal acquisition (Marcum 1960, Shnidman 1989, Shnidman 1995), differentially coherent (Àvila Rodriguez 2004, Àvila Rodriguez 2005) or a combination of these.

Tracking

Once the signal is acquired, the Doppler and code delay of each satellite have to be tracked over time. In most receivers, the goal of the tracking is to keep all the power in the in phase component, which allows the decoding of the bits of the navigation message. However, some receivers use only a frequency loop (and then have a phase offset between the incoming signal and the local replica), or detect changes in the navigation data bit sign and use this to extract the navigation data.

During tracking, two coupled loops are used to follow the carrier phase (or the frequency) and the code delay. A PLL (Phase Lock Loop) or FLL (Frequency Lock Loop) or a combination of both is used to follow the changes in the carrier phase. A DLL (Delay Lock Loop) is used to follow the code delay. The incoming signal is multiplied by a

locally generated carrier and spreading code, then discriminators are computed for both loops; they are then filtered to deduce the correction to apply to the code delay and Doppler (and code Doppler). Further details can be found in Van Dierendonck (1996), Kaplan (2006), and Peterson et al (1995). On all the signals considered here, there is a sign ambiguity due to the navigation message or the secondary code. Due to this ambiguity, it is necessary to use a Costas loop (insensitive to 180° phase shift). Nevertheless, the secondary code is known, and once the receiver determines its location within the code, it is possible to implement a pure lock loop on the pilot channel which allows the PLL to track signals up to 6 dB lower (Kaplan 2006, Tran & Hegarty 2002, Julien 2005).

The accuracy of a tracking loop depends on its ability to follow the sources of errors: thermal noise, multipath, interference and user dynamics mainly. The DLL is more affected by noise and multipath, whereas the interferences can affect all the loops. The spreading code used to modulate the signal has a large influence on the impact of these errors on the tracking. For example, a higher chipping rate and a longer spreading code period can reduce the impact of these errors (Braasch 1997, Betz 2002, Tran 2004). From these observations, one can deduce that L1C GPS and L1 Galileo signals should be less affected by these errors than GPS L1 C/A due to the length of the spreading codes.

In the case of a BOC modulation, the autocorrelation function contains a main peak that is sharper than the one of a BPSK modulation and reduces the noise (Betz 2002). However the side peaks can create an ambiguity and can be wrongly tracked instead of

the main one, leading to degraded tracking performance. Some research has been done on discriminators to avoid the tracking of these side peaks (Julien 2005). One of the first commercial receivers able to track on Galileo L1 and E5a was developed by NovAtel, namely the 15a model (Gerein et al 2004). Some tracking techniques which can significantly simplify the receiver architecture of future GPS/Galileo L1 receivers have been developed in Julien et al (2007). These techniques take into consideration a pure BOC(1,1) (see Chapter 2) but are easily adaptable to TMBOC signals (consideration of the BOC(6,1) as well as explained in Appendix C) depending on the type of receiver implemented. Indeed, depending on the tracking accuracy desired, the TMBOC can be considered as a BOC(1,1) for complexity reasons (Floc'H & Soellner 2007).

Data demodulation

The data rate on GPS L1 C/A is 50 symbols per second (sps), but it will be 100 sps on GPS L1C and 250 sps on Galileo L1. Thus, the navigation message can be acquired faster on these new signals. However, since the data rate is much higher, if the same techniques as for GPS L1 C/A were kept to code the navigation message, the error rate would increase significantly. Therefore, other techniques (FEC, CRC and interleaving) have been implemented to not increase the error rate and acquire the entire navigation message (and thus obtain a position) faster (GPS ICD 800 2007).

The two major improvements in terms of data modulation of GPS L1C and Galileo L1 as compared to GPS L1 C/A are the following:

- FEC (Forward Error Correction): Method used to code bits of the navigation message in order to have a better BER (Bit Error Rate). This method increases the symbol rate for the same data rate (Bastide et al 2002)
- Pilot (dataless channel): The GPS L1C signal and Galileo L1 are each composed of two channels, a pilot channel which does not contain any navigation message (only a spreading code) and a data channel. The pilot channel can improve the tracking performance. Indeed, once the position within the secondary code is known, there is no longer a sign ambiguity and thus integration time can be increased. This allows for tracking of weaker signals. Moreover, as mentioned before, the Costas loop used currently in the PLLs are no longer necessary and can be replaced by a pure lock loop. This way, the minimum necessary phase tracking threshold can be reduced by up to 6 dB (Tran & Hegarty 2002).

These two improvements lead to a more accurate tracking and thus an improvement in the precision and accuracy (if the ionosphere error is removed) of the position.

Specific techniques

As mentioned earlier, the acquisition and tracking processes are affected by errors. The amplitude of these errors as well as their impact on acquisition and tracking performance depend on the structure of the signal and the techniques used. In this research, the main points of interest are weak signal conditions, high dynamic and oscillator errors.

The new signals, especially the BOC and TMBOC modulations, allow the development of new techniques or the adaption of already existing techniques in order to mitigate

errors or to acquire and track weaker signals. For example, new discriminators have been implemented in Julien (2005) to reject the side peaks of the BOC modulation and thus improving the tracking performance. Several correlators can be combined as well to mitigate multipath (Pany et al 2005). Formal expressions of the different possible offset carrier modulations, their main properties and their adaptation to the tracking architectures are proposed and discussed by Ries et al (2003). These expressions are presented in the later in terms of complexity for the BOC modulation in order to mitigate multipath. In Nunes et al (2005), a new multipath mitigation technique is proposed for the BOC modulation and the performance is compared with the narrow correlator and the double-delta (HRC) solutions. To reject multipath, a family of waveforms has been created by Avellone et al (2007). These waveforms are used as the local code in the classical early minus late code tracking scheme and are focused on the BOC modulations.

Interference sources on the L1 band have been listed by Landry & Renard (1997). New methods can be studied to take advantage of all the signals in the L1 band to reject and detect these interference sources.

In order to improve tracking performance and reduce the effect of the errors described above, Kalman filter based tracking loops have been implemented by Psiaki & Jung (2002), Ziedan & Garrison (2004), Petovello (2006), and Mongrédien (2008). There are two main advantages to using a Kalman filter for tracking. The first one is an adaptive bandwidth filtering through the Kalman gain (the Kalman gain is computed at each iteration), which weighs the measurements depending on their reliability. Moreover, the

Kalman filter uses all prior information to perform an update, so it will have a better behavior in case of dynamics.

1.3 Objectives

With GPS and Galileo, the L1 band will, in the next decade, contain three signals, two of them divided in two channels. All these signals have different properties and thus different advantages and disadvantages. Moreover, the L1 band has several advantages compared to other frequencies: the most number of signals are in this band, it should be the frequency band the less affected by interference since it has been designed for use only by satellite navigation signals (Kaplan 2006). Finally, as most of the commercial receivers are for the moment designed to track only L1 signals, related research has a direct impact on industry.

The objectives of this thesis are as follows:

1. Develop a complete GPS and Galileo L1 signal simulator in software, including simulated interference and oscillator errors. The simulation of interference sources is used to assess the impact of the approximation of the CBOC by a BOC(1,1) on tracking and acquisition sensitivity (see Appendix C). The oscillator error is simulated in order to study the impact of the receiver oscillator on the performance of the Kalman filter.
2. Develop acquisition algorithms adapted to the new GPS and Galileo L1 signals using different lengths of incoming signals and completely assess their statistical

performance. This includes investigating the possible benefits of trying to acquire multiple signals simultaneously (e.g., data and pilot) in order to improve performance.

3. Develop combined tracking methods to take advantage of all the signals transmitted on the L1 frequency for both GPS and Galileo. The presence of L1-B and L1-C for Galileo and L1C pilot, L1C data and legacy L1 C/A for GPS offers numerous possibilities in terms of combination.
4. Investigate the combination of all signals from one system through a Kalman filter at the tracking level. From a traditional Kalman filter model able to track a single signal, a Kalman filter able to simultaneously combine the signal is to be developed and tested under a wide range of conditions.

New acquisition and tracking techniques adapted to each of these signals are presented. Then these signals are combined at different stages in the receiver to reduce the errors and improve the accuracy of the acquisition and tracking. The novelties brought by this thesis are as follows:

1. Implementation of a new oscillator model
2. Implementation of a Kalman filter for combining several signals for tracking
3. Implementation of new acquisition algorithms adapted to the Galileo L1 and GPS L1C signals and complete derivation of their statistical performance
4. Implementation of a combined acquisition technique
5. Implementation of a combined tracking technique

All algorithms have been developed first in Matlab to test more easily the different algorithms and parameters, except the software signal simulator which has been implemented in the C language to decrease as much as possible the processing time. In order to be familiar with all the steps in signal simulation as well as signal acquisition and tracking, the author decided to not use any previous software as a starting point.

All the algorithms for Galileo L1 and GPS L1 C/A have been tested using a real data mode of operation. However, in the case of Galileo, only two test satellites are broadcasting the signal (which is slightly different from the future signal), so only the algorithms using the currently broadcast signals can be tested using real data. Therefore, the algorithms developed have also been tested using the currently broadcast signals, and at the end the future signals are simulated. However, in the case of GPS L1C, since there is no satellite yet broadcasting the signals, the only method to test the algorithms was to implement a software signal simulator. The simulator has been implemented for all GPS and Galileo signals of the L1 band for two reasons, namely to test the algorithms using all the signals, and to validate it as a tool using real signals.

All the algorithms presented in this thesis can be applied alone or in combination with other techniques in order to improve the acquisition and tracking sensitivity and can be used for numerous precise applications such as surveying. However, the error due to the ionosphere has to be corrected separately since here only one frequency is used (and the ionosphere error is frequency dependent, Skone 2007).

1.4 Thesis outline

The structure of the subsequent chapters is described below.

Chapter 2 gives an overview of the GPS L1 C/A signal as well as the GPS modernized L1C. This chapter includes an historical review of the GPS modernization program. Then, it describes the characteristics of the GPS L1 signals and their impact on acquisition and tracking.

In Chapter 3, the structure of the Galileo L1 OS (Open Service) signal (according to OS SIS ICD Draft 0 2006 and Draft 1 2008) is given in detail including its main properties and its impact on acquisition and tracking performance.

Chapter 4 shows the structure of the implemented signal software simulator, including its architecture and characteristics. The models used to simulate the various errors of interest such as interference and oscillator errors are explained in detail.

In Chapter 5, new acquisition algorithms are proposed to improve acquisition performance. These algorithms are tested using real and simulated data under various scenarios. Their performance is also evaluated and compared statistically.

Chapter 6 proposes tracking algorithms to track separately or to combine the signals broadcast at the same frequency in a Kalman filter. The performance is evaluated under various scenarios using real and simulated data.

Finally, Chapter 7 draws conclusions and makes recommendations for future work.

Chapter Two: GPS L1 C/A AND L1C SIGNAL STRUCTURE

This chapter begins with a description of the current GPS signal broadcast on L1, namely the GPS Coarse/Acquisition (C/A) signal. Since this thesis focuses on acquisition and tracking techniques, particular emphasis is given to the structure of this signal and its main properties and characteristics. More information about GPS and its applications can be found in Parkinson (1996), Tsui (2005), Kaplan (2006), Misra & Enge (2006). The GPS L1 C/A signal was designed in the 1960s to help in the acquisition of the military signals. The C/A signal is presented as well as the signal model, the limitations in acquisition and tracking performance due to its design. Then, the different steps of the GPS modernization are introduced. Finally, the future GPS L1C signal structure is described in detail, including the differences with GPS L1 C/A, its main properties and their impact on acquisition and tracking performance.

2.1 Brief History and GPS L1 C/A Signal Structure

It is important to keep in mind that this signal has not been designed to be used for precise civilian applications. Therefore, its performance depends highly on the environment since it is subject to many errors as explained in the following paragraphs.

2.1.1 Brief History of GPS and Creation of the GPS L1 C/A Signal

The project for the development of the NAVSTAR (Navigation System for Timing and Ranging) system, commonly called GPS (Global Positioning System), was started in 1973. At the beginning, the primary use of the system was supposed to be for military applications (Parkinson 1996). The first generation of GPS was designed from a simple idea, called multi-lateration: measure the distance between satellites (with well-known positions) and the user to retrieve the position of the user. The GPS signal was designed with the following main properties in mind (Spilker 2007):

- Resistance to intra-system interference i.e. multiple access capability
- Resistance to a certain level of multipath interference (such as reflection by a building, foliage, etc.)
- Resistance to reasonable levels of unintentional or intentional interference such as jamming or spoofing

The key techniques used to fulfill these requirements are:

- The Direct Sequence-Spread Spectrum (DS-SS) technique used to spread the navigation message on the ranging code
- The Code Division Multiple Access (CDMA) technique used to differentiate the signals from different satellites at the same frequency and spread the spectrum

Using the above techniques, each satellite has its own ranging code which spreads the spectrum over a large bandwidth (and therefore is more resistant to interference). Due to the free space loss over the distance from the satellite to the receiver, the aforementioned spread spectrum of the received signal is buried under the noise level, and despread

allows for signal recovery. Furthermore, it allows the distance between the satellite and the receiver to be determined using the correlation properties of this ranging code. Then, the navigation message, containing the data necessary to compute the satellite position, is added to this ranging code at a lower data rate.

In the first generation of GPS signals, three signals were designed and broadcast at two frequencies. First, two signals with restricted access were broadcast at two different carrier frequencies: L1 at 1575.42 MHz and L2 at 1227.6 MHz. These two signals have good performance due to their very long ranging codes and their high chipping rate. With two available frequencies, the error introduced by the ionosphere can be removed, and the signal is more resistant to interference because of frequency diversity. The codes used are called Precise (P) ranging codes and are encrypted by a classified Y code, accessible for military operations. Then, a third signal was designed with lower performance (in terms of acquisition and tracking accuracy) but allowing a faster acquisition. This signal is called the C/A (Coarse Acquisition) signal and is transmitted at the L1 frequency as well and is publicly available (not encrypted). The length of the ranging code is much shorter than that of the military code and is transmitted at a chipping rate ten times lower. Therefore, using the fast acquisition of this signal, the military signal can be acquired allowing a faster but still as accurate position. Even if created at the beginning for military applications, this signal has been left freely available to users.

2.1.2 Structure of the GPS L1 C/A Signal

In the following section, except otherwise specified, all the descriptions concerning the structure of the GPS L1 C/A signal are from IS-GPS-200 Revision D (2004).

The GPS L1 C/A signal is Right Hand Circular Polarized (RHCP) and is received at a minimum power of -158.5 dBW. It is transmitted at the central frequency of 1575.42 MHz, which corresponds to a wavelength of approximately 19 cm. The carrier being modulated by the spreading code transmitted at 1.023 MHz using a Binary Phase Shift Keying (BPSK), the minimum bandwidth required is of 2.046 MHz in order to include the whole power of the main lobe (see later for more details on the power spectral density). As mentioned before, the L1 C/A signal is composed of:

- A navigation message, including precise orbital parameters for the satellite, called ephemeris parameters and approximate orbital parameters for the entire constellation called almanac parameters.
- A spreading code called Pseudo-Random Noise (PRN) code, using rectangular Non-Return to Zero (NRZ) symbols.
- A carrier modulated by the summation of the spreading code and the navigation message.

The navigation message is transmitted at a data rate of 50 Hz. This low data rate permits to have an acceptable Bit Error Rate (BER) at most common Signal-to-Noise Ratios (SNR) (Van Dierendonck 1996) without using specific techniques such as Forward Error Correction (FEC) as in the next GNSS generation.

The spreading codes called PRN are generated using LFSRs (Linear Feedback Shift Register). The generation of the PRN codes for GPS L1 C/A is shown in Figure 2-1. All the codes are generated using the same set of two LFSR and the same initialization sequence, and only the taps used for the output of the second LFSR change as a function of the PRN number. The codes generated are called Gold codes: their main property is a good correlation product and a low cross correlation product. They contain 1023 chips transmitted at the chipping rate of 1.023 Mchips/s, and thus one spreading code period lasts 1 ms. As its name indicates, the spreading code is used to spread the signal in frequency, to be more robust to interference (Parkinson 1996).

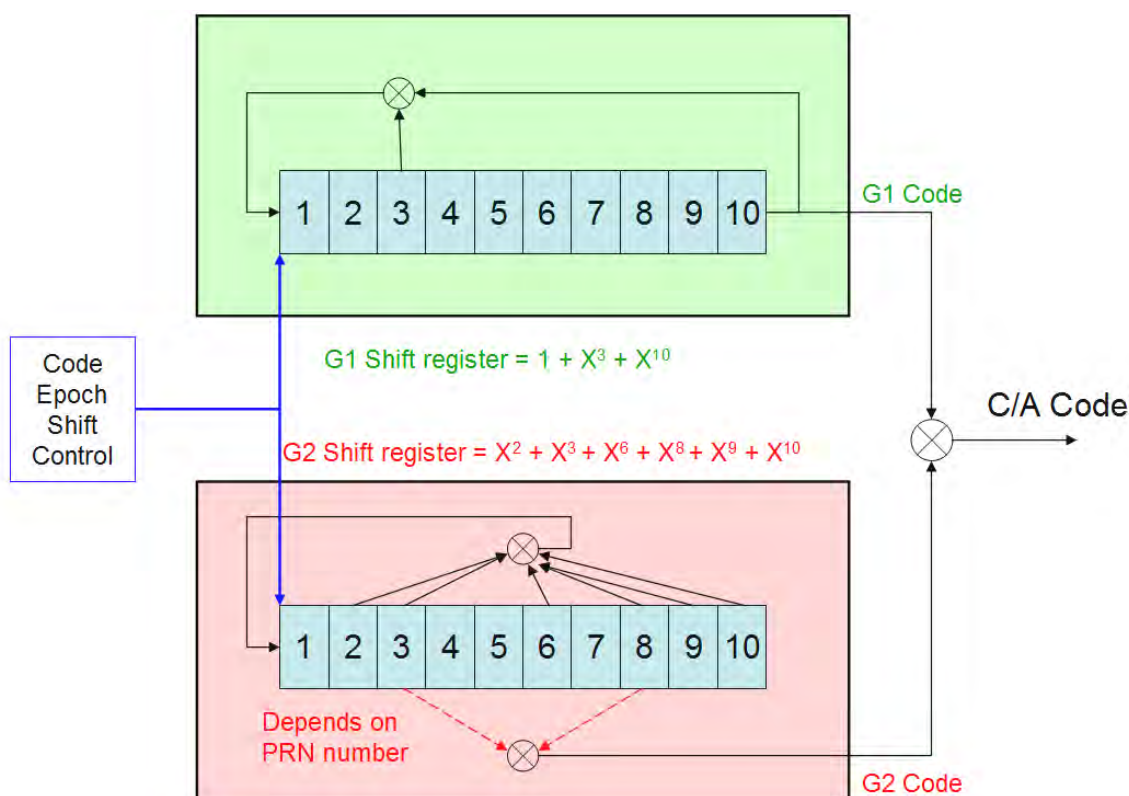


Figure 2-1: GPS L1 C/A code generation

One critical property of the PRN code is the shape of the autocorrelation function. Indeed, the shape of the autocorrelation is important for the tracking performance as explained in Spilker (1996) as well as the cross-correlation properties, i.e. the correlation between different PRN codes. In fact, the cross-correlation products have to be as small as possible to reduce intra-system interference. An example of autocorrelation with a zoom on the main peak is shown in Figure 2-2 for PRN 1 and a code delay of 500 chips.

The normalized autocorrelation function can be approximated by the following equation (Holmes 1982):

$$R_{N,C/A}(x) = \begin{cases} 1-|x| & \text{if } |x| < 1 \text{ chip} \\ 0 & \text{if } |x| > 1 \text{ chip} \end{cases} \quad (2.1)$$

As shown in Figure 2-2, this approximation fits well the reality. Indeed, the side peaks can be neglected most of the time except in specific situations for the acquisition (these specific cases will be explained later). The cross correlation properties of the GPS L1 C/A ranging codes are described in the next section.

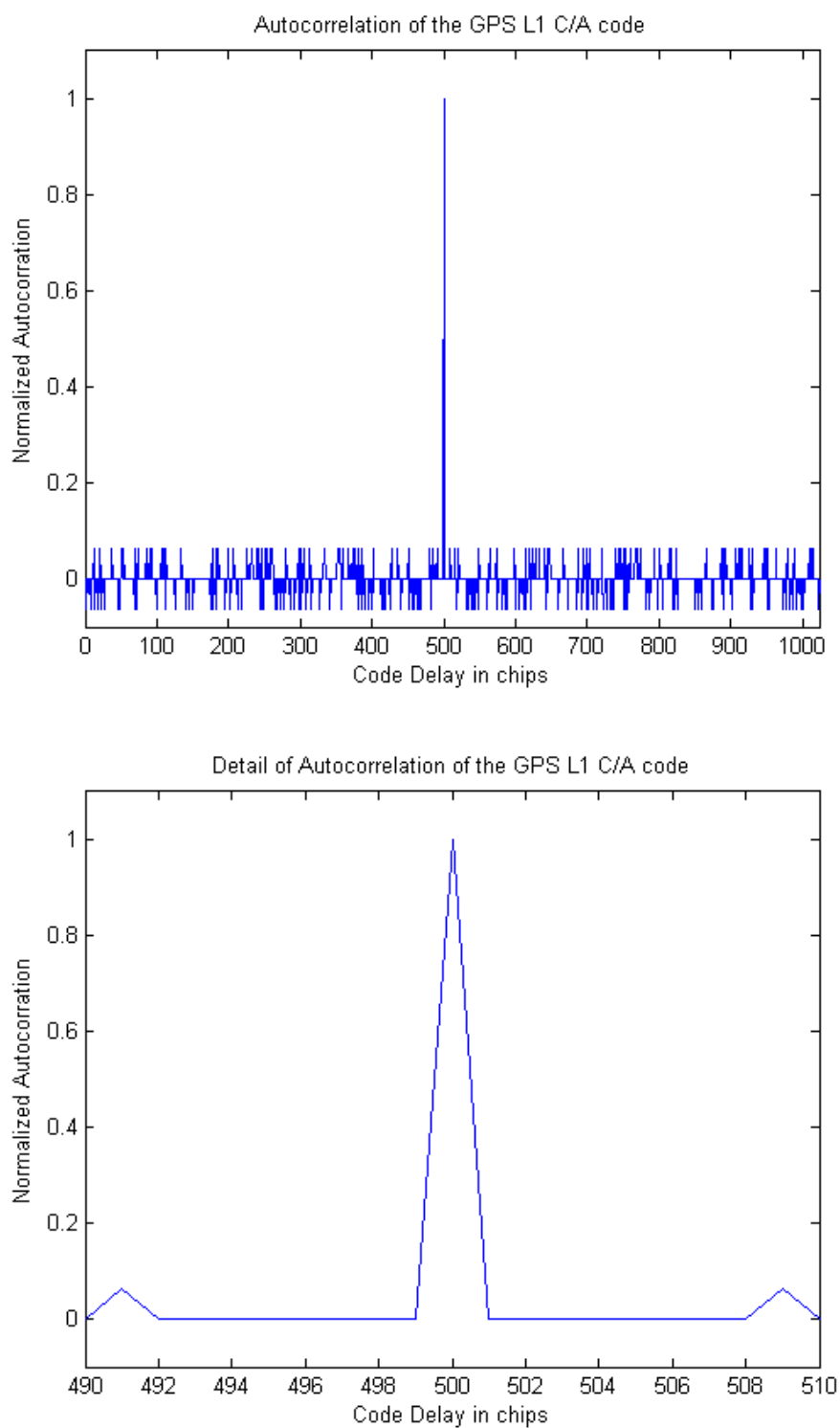


Figure 2-2: Autocorrelation of the GPS L1 C/A code (top) and detail of the main peak (bottom)

The Power Spectral Density (PSD) of the GPS L1 C/A signal can be derived by computing the Fourier transform of the autocorrelation function of the GPS L1 C/A signal. This PSD can be approximated by a sinc envelope as demonstrated by Julien et al (2005). This sinc envelope corresponds to the PSD of the BPSK subcarrier alone, and the spectral lines of the PSD are separated by the ratio between the chipping rate and the length of the ranging code period, that is to say 1 kHz in the case of GPS L1 C/A (Julien 2005). The normalized GPS L1 C/A envelope can therefore be expressed as:

$$G_{C/A}(f) = T_c \left(\frac{\sin\left(\pi \frac{f}{f_c}\right)}{\pi \frac{f}{f_c}} \right)^2 \quad (2.2)$$

where $G_{C/A}$ is the normalized PSD of the GPS L1 C/A ranging code

f_c is the GPS L1 C/A chipping rate

$T_c = \frac{1}{f_c}$ is the GPS L1 C/A ranging code chip duration.

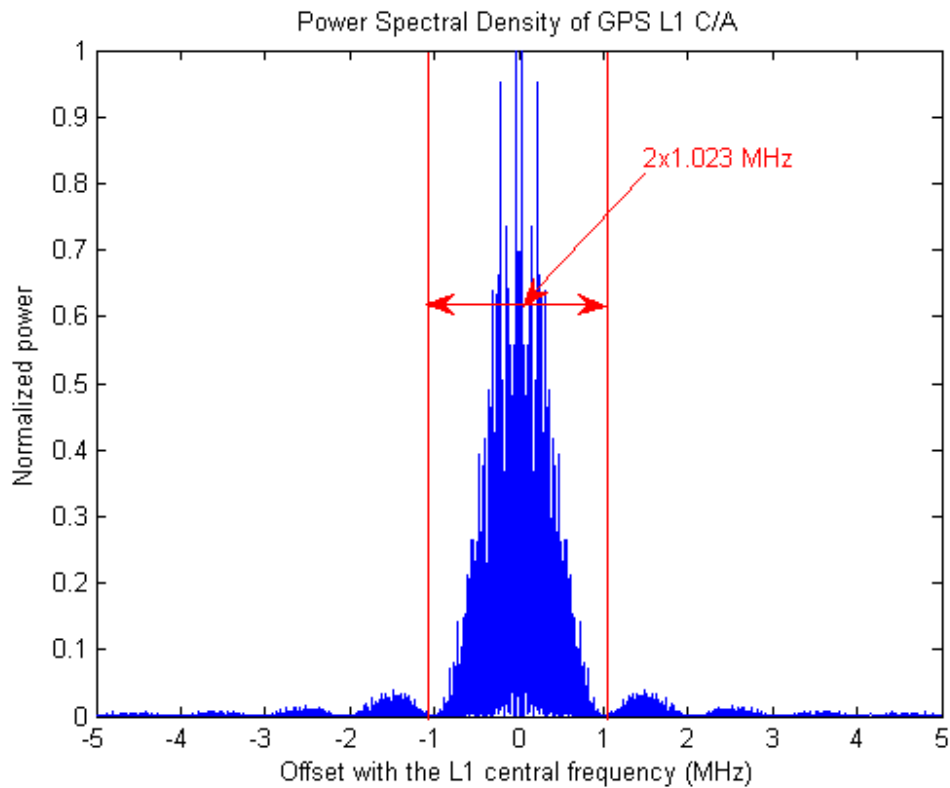


Figure 2-3: Normalized PSD (Power spectral density) of the GPS L1 C/A signal

The normalized PSD of the GPS L1 C/A signal is shown in Figure 2-3. As mentioned before, the received GPS signal is at low power (-158.5 dBW) and is therefore under the level of white noise (around -205 dBW/Hz under normal conditions, Van Dierendonck 1997). This was done to avoid interference with the signals in the same frequency band and for power requirements at the satellite level. Therefore, the GPS L1 C/A signal cannot be detected directly, for example using a power spectrum analyzer because only white noise will be seen. However, the signal can be detected using other techniques such as correlation (see Chapter 4 and sequel).

At the receiver level, and taking into account the propagation time, the GPS L1 C/A signal transmitted by one satellite can be expressed as followed:

$$s_{C/A}(t_{GPS}) = \sqrt{2 \cdot P_{C/A}(t_{GPS})} \cdot d_{C/A}(t_{GPS} - \tau_{C/A}(t_{GPS})) \cdot c_{C/A}(t_{GPS} - \tau_{C/A}(t_{GPS})) \cdot \cos(2 \cdot \pi \cdot (f_{L1} + f_{Dtotal}) \cdot t_{GPS} + \phi_{C/A}) + w(t_{GPS}) \quad (2.3)$$

where $s_{C/A}$ is the C/A signal

t_{GPS} is the GPS time

$\tau_{C/A}$ is the time delay due to the propagation between the satellite and the receiver including the time delay created by the atmosphere

$P_{C/A}$ is the received power

$d_{C/A}$ is the data bit of the binary NRZ navigation message

$c_{C/A}$ is the C/A ranging code

f_{L1} is the GPS L1 central frequency (1575.42 MHz)

f_{Dtotal} is the Doppler frequency due to the satellite and user motion plus the Doppler shift due to atmospheric and clock errors

$\phi_{C/A}$ is the initial L1 C/A phase in radians

$w(t)$ is the noise approximated as Gaussian with zero mean.

In the above equation, the code delay $\tau_{C/A}$ can be written as:

$$\tau_{C/A} = \frac{\rho}{c} + (t_{rx} - t_{sat}) + \Delta t_{iono} + \Delta t_{trop} \quad (2.4)$$

and the carrier phase delay ϕ in radians varying over time can be expressed as:

$$\phi = 2 \cdot \pi \cdot \int_0^t f_{Dtotal} \quad (2.5)$$

with ρ the geometric distance between the satellite and the receiver

c the speed of light

t_{rx} the receiver time

t_{sat} the satellite time

Δt_{Iono} the ionospheric delay

Δt_{Trop} the tropospheric delay.

The total Doppler frequency f_{Dtotal} can then be expressed as:

$$f_{Dtotal} = f_D + f_{Iono} + f_{Trop} + f_{time} \quad (2.6)$$

$$f_{Dtotal} = \frac{\|v_{sat} - v_{rx}\|}{c} \cdot f_{L1} + \frac{1}{2\pi} \cdot \left[\frac{d\Delta\phi_{Trop}}{dt} + \frac{d\Delta\phi_{Iono}}{dt} + \frac{d\Delta\phi_{time}}{dt} \right] \quad (2.7)$$

with v_{rx} and v_{sat} the speed of the receiver and the satellite respectively projected on the satellite-receiver axis

f_D the Doppler frequency due to the user and satellite motion, expressed as a function v_{rx} and v_{sat}

f_{Iono} and $\Delta\phi_{Iono}$ the respective Doppler shift and phase variation due to the ionosphere (signal path and TEC – Total Electron Content – variations)

f_{Trop} and $\Delta\phi_{Trop}$ the respective Doppler shift and phase variation due to the troposphere (tropospheric conditions and signal path variations)

f_{time} and $\Delta\phi_{time}$ the respective Doppler shift and phase variation due to the oscillator variations.

The effect of the ionosphere on the code has the same magnitude as the one on the phase. However, the code is delayed whereas the phase is advanced.

Finally, the carrier phase delay can be expressed as:

$$\phi = \phi_{C/A} + \frac{\|v_{sat} - v_{rx}\|}{c} \cdot 2 \cdot \pi \cdot f_{L1} \cdot t + \Delta\phi_{Trop} + \Delta\phi_{Iono} + \Delta\phi_{time} \quad (2.8)$$

2.1.3 Correlation properties of GPS L1 C/A

Another important property of the codes is the cross correlation performance. First, the cross correlation protection of the GPS L1 C/A codes will be computed. Then, the cross correlation performance will be studied considering various Doppler offsets and a range of relative powers. All the following is based on the methods shown by Qaisar & Dempster (2007).

First, the correlation protection between all the codes is computed. To achieve this, all the codes are correlated between each other and the maximum power for each cross correlation is differenced with the autocorrelation power. For the GPS L1 C/A codes, the correlation protection found is about 23.94 dB, which is in accordance with the 24 dB given in the IS-GPS-200 Revision D (2004). More specifically, if one looks at the cross correlation of the PRN codes 1 and 2, about 30 % of the cross correlation output offers a protection around 24 dB and 70 % around 60 dB compared to the autocorrelation, as

shown in Figure 2-4. Similar results can be found for all other cross correlation products (Dempster 2006).

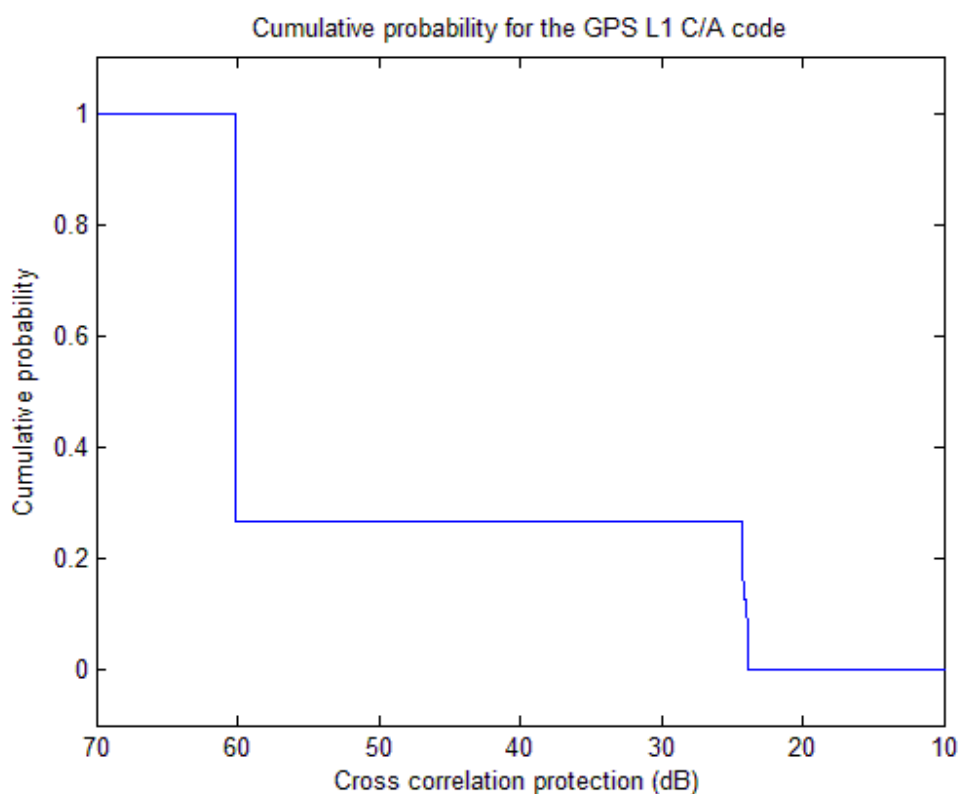


Figure 2-4: Cumulative probability for the cross correlation of PRNs 1 and 2 of the GPS L1 C/A codes

In the previous case, the cross correlation protection was computed using only the cross correlation of two codes, i.e. without sampling and without modulating the carrier. In the second case, sampling is added to the two PRNs codes and the same procedure is realized. First, synchronous sampling is considered (ten times the chipping rate in this case), namely the sampling rate is a multiple of the chipping rate i.e. there is an entire number of samples in one chip. Then, an asynchronous sampling is simulated (a sampling rate of 10 MHz is simulated here), i.e. the sampling rate is not a multiple of the chipping

rate that is to say that there is not the same number of samples of each chip. The results with sampling are presented in Figure 2-5. As can be seen, the results with and without sampling give the same cross correlation protection of about 24 dB. Even though the minimum cross correlation protection remains the same in all cases, the sampling degrades the overall cross correlation properties of the codes. Moreover, the asynchronous sampling gives worse performance than the synchronous one in 50 % of the cases. However, the performance in the case of the sampling are dependent on the sampling rate chosen (here the values of synchronous and asynchronous sampling have been chosen to be of the same order of magnitude to allow a comparison). Considering asynchronous sampling, when the sampling rate is increased, the curves are smoother and closer to the synchronous case.

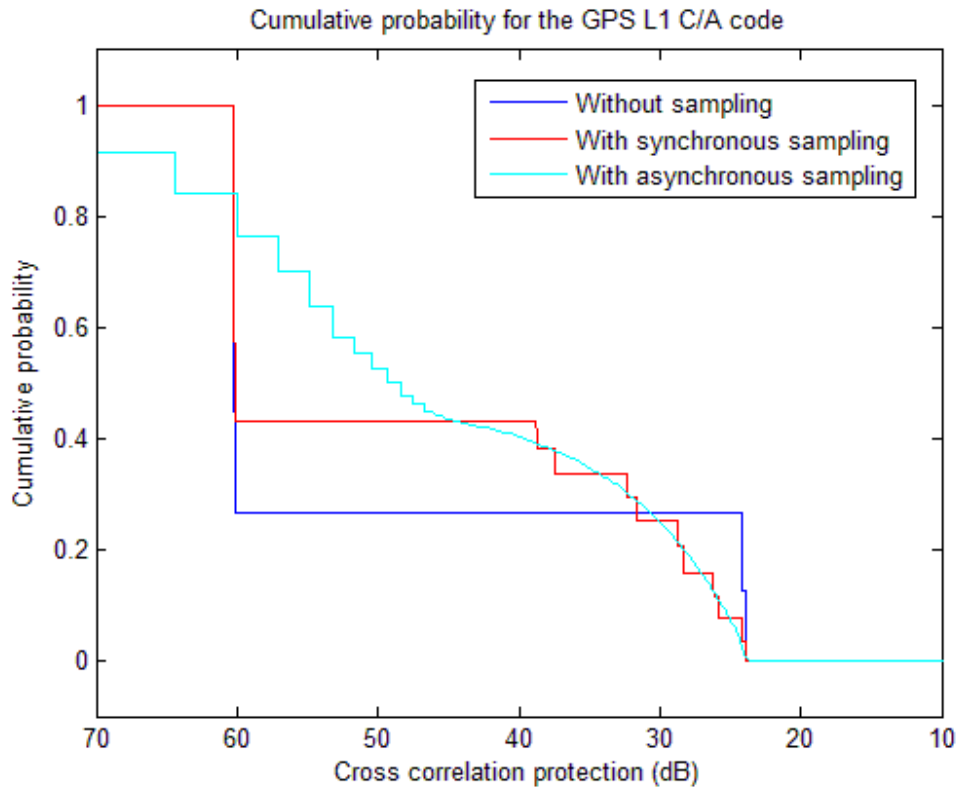


Figure 2-5: Cumulative probability for the cross correlation of PRNs 1 and 2 of the GPS L1 C/A codes with synchronous sampling (red), asynchronous sampling (cyan) and without sampling (blue)

Finally, the carrier is added to the simulated codes and the impact of the Doppler difference on the cross correlation protection is studied. The range of Doppler offset considered goes from 0 to 1000 Hz and the results are shown in Figure 2-6. All these results have been obtained using a synchronous sampling to remove the effects other than the Doppler on the cross correlation performance, and the code Doppler and Doppler have been simulated on the signals.

First, the results obtained in the case of no Doppler offset are exactly the same as the ones in Figure 2-5. This was to be expected since the carrier wave is completely removed before the correlation and therefore the results are the same as without a carrier. In all the cases, the minimum cross correlation protection is still about 24 dB, the same as in the previous cases. Finally, when the Doppler offset between the two codes increases, the performance is slightly better for a cross correlation protection under 30 dB but it is worse above 30 dB. As expected, larger cross correlation values are observed at multiples of 1 kHz. All these results have been obtained using the cross correlation of PRNs 1 and 2 but similar results can be obtained with other PRNs. All the simulations were performed using Matlab.

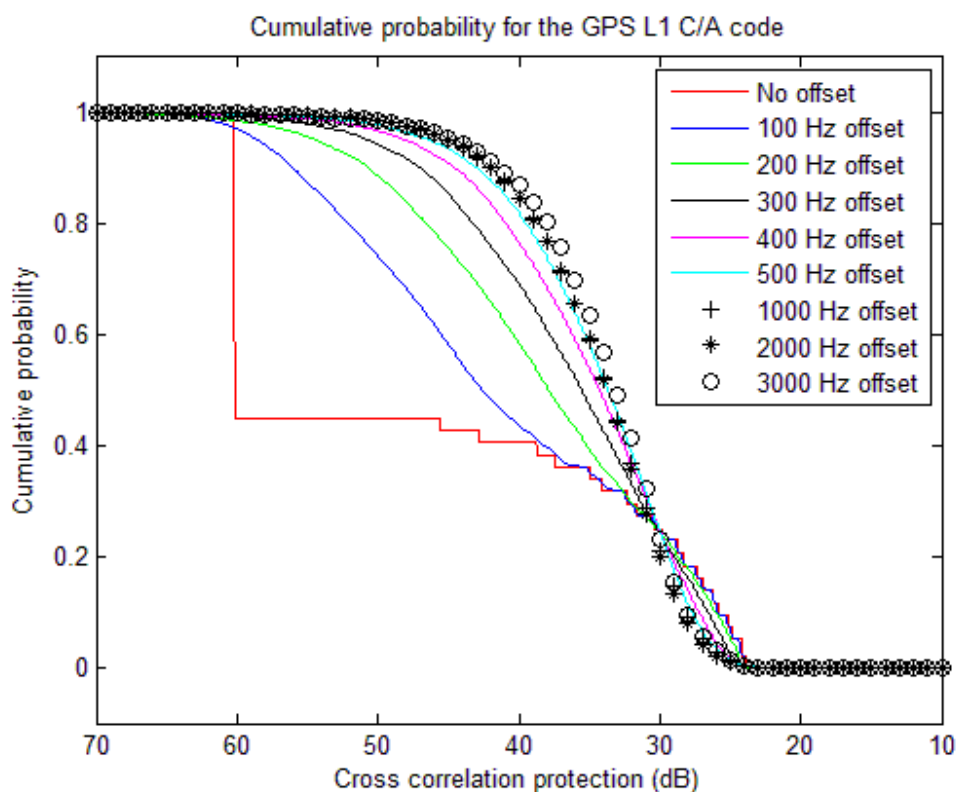


Figure 2-6: Cumulative probability for the cross correlation of PRNs 1 and 2 of the GPS L1 C/A codes with different relative Doppler offsets

2.2 GPS L1C

As mentioned earlier, the GPS L1 C/A signal was the first publicly available signal and the system has been fully operational from 1995¹. However, with the increased demand in accuracy and reliability by the users and the development or modernization of other GNSS (Global Navigation Satellites Systems), the US government decided to modernize GPS as well. One of the elements of this modernization is the creation of a new GPS signal at the L1 central frequency: the L1C signal. In this section, a brief overview of the

steps of the modernization of GPS is introduced, then the structure of the GPS L1C signal is described and finally the advantages and innovations brought by this signal compared to L1 C/A are shown.

2.2.1 From GPS L1 C/A to GPS L1C: Overview of the GPS Modernization

The modernization is realized in three main phases as presented in Figure 2-7 (Crews 2008). Although improvements are made in terms of the military codes, the focus here is on the civil signals.

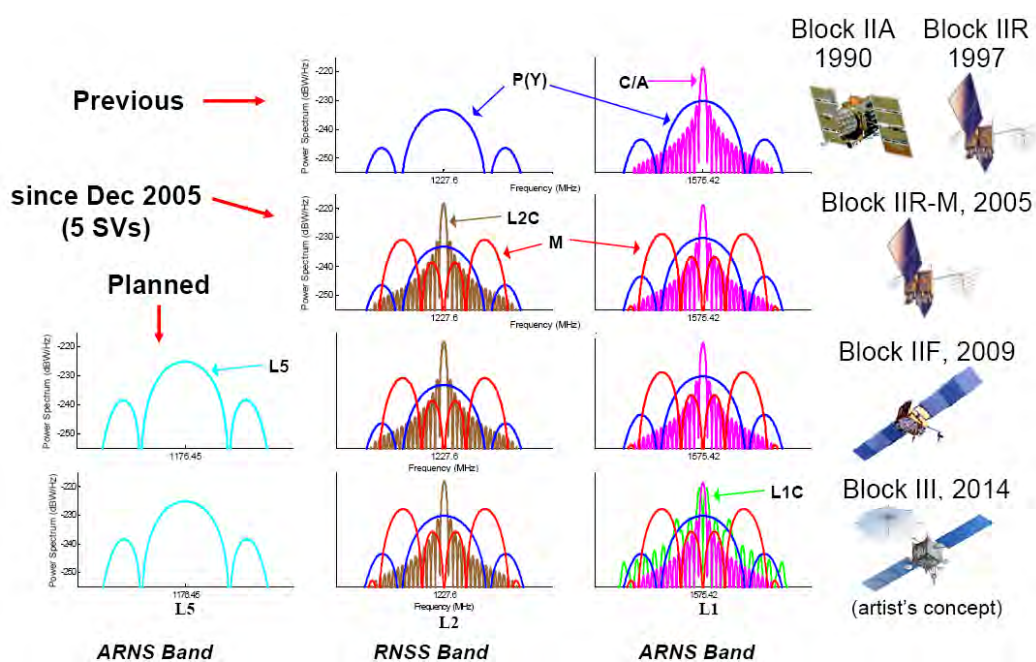


Figure 2-7: GPS modernization (from Crews 2008)

To this end, relative to the current “legacy” satellites, the Block IIR-M is implemented first. The Block IIR-M corresponds to an augmentation of the L2 frequency (1227.6 MHz) with the insertion of a new civilian signal L2C. The L2C signal contains two open service channels time multiplexed together; one pilot channel (without navigation message) and one data channel (with navigation message). Today, there are six GPS satellites able to transmit the L2C signal¹. The L2C signal was designed to improve position accuracy and reliability and to provide a signal easier to track thanks to the pilot channel. Moreover, the L2C signal brings other several advantages compared to L1 C/A alone, namely:

- Presence of a pilot and a data channel: the pilot channel can be used to perform a longer integration in case of weak signals
- In case of interference in the L1 band degrading the performance of the L1 C/A signal, the L2C signal can be used to compute a position
- With two signals coming from the same satellite at different frequencies, it is now possible to remove most of the ionospheric effect (since it is dependent on the frequency) without using augmented systems such as SBAS (Satellite-Based Augmentation System) or a model which gives only an approximation of the ionospheric error.

Following the Block IIR-M satellites, the Block IIF satellites will also broadcast a new civilian signal at the L5 central frequency 1176.45 MHz. The first satellite to broadcast this signal is actually a modified Block IIR-M launched on March 24, 2009. The L5 signal also contains data and pilot channels, the codes are 10 times longer than on L1 C/A

and are transmitted at a faster chipping rate (10 times faster) and at higher power (3 dB). This signal should improve the position accuracy and be more robust to interference due to the wider bandwidth (Mongrédien 2008). Moreover, the increased chipping rate allows better performance in terms of multipath mitigation. Besides, the addition of a third publicly available frequency has several advantages:

- In case of intentional or unintentional interference, it is almost impossible (or very expensive) to jam the entire frequency band from L1 to L5
- With three signals available, the accuracy and reliability of the position is improved (Kaplan, 2006)
- Each signal has been designed with different advantages and therefore different applications (civil aviation for example in the case of GPS L5).

The forecast improvement brought by the different steps of the GPS modernization are shown in Figure 2-8 (Cabler 2003) in terms of 1 sigma error in the pseudorange measurement. In this figure, “today” corresponds to 2003.

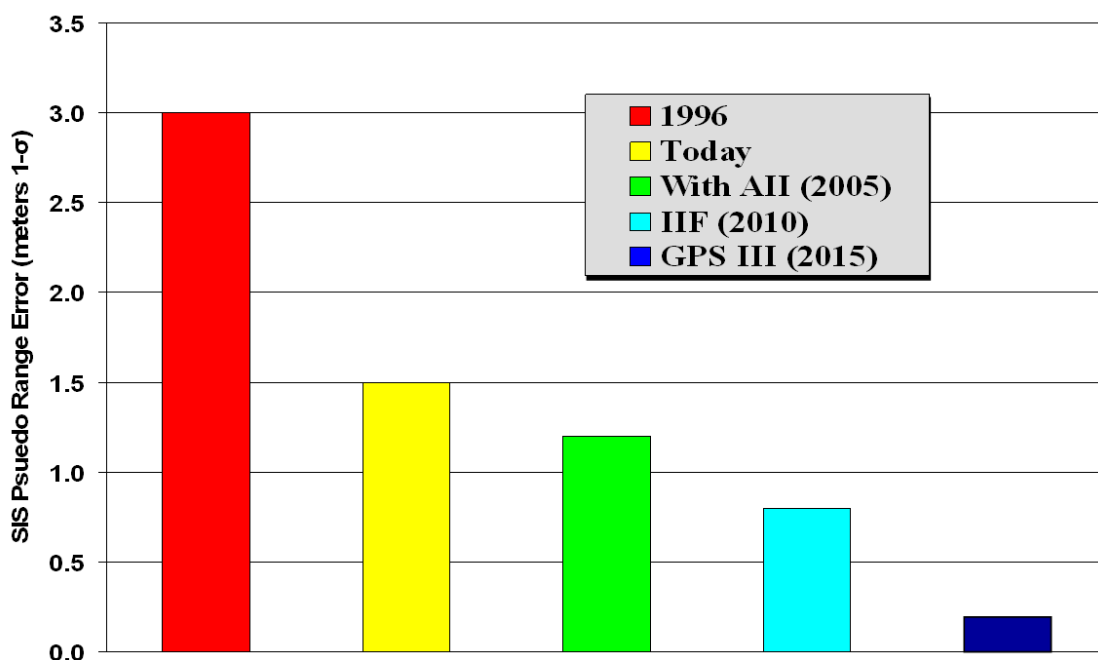


Figure 2-8: Improvements brought by the GPS modernization (from Cabler 2003)

Finally, the L1 signal will be augmented by the L1C signal in the Block III satellites. The L1C signals will also contain a pilot and data channel. However, the broadcasting of this signal is not scheduled before 2013, but the US Air Force still hopes that the satellites will be ready by 2011 (Cameron 2007). The structure and properties of the GPS L1C signal are described in detail in the following sections. The GPS L1C signal has been designed to avoid inter-system interference with the Galileo signals and to allow compatibility of the two systems.

2.2.2 Structure of the GPS L1C Signal

Unless otherwise specified, all the descriptions below concerning the structure of the GPS L1C signal are from IS-GPS-800 (2007).

The GPS L1C signal is transmitted at the same central frequency as GPS L1 C/A (1575.42 MHz), with a nominal minimum received power 1.5 dB above L1 C/A, namely -157 dBW. It is composed of two channels: a pilot (dataless) channel (denoted L1C_P) and a data channel (denoted L1C_D) transmitted in phase quadrature. The pilot channel includes a spreading code and an overlay, or secondary code, denoted as L1C_O. The overlay code is generated using a LFSR. It is transmitted at 100 bits/s and contains 1800 bits, thus it lasts 18 s. The overlay code is unique for each PRN. The data channel includes a spreading code and a navigation message. The spreading codes of the pilot and data channels are time synchronized. The spreading codes are broadcast at the same chipping rate as on L1 C/A, i.e. 1.023 Mchips/s. Both on the pilot and data channels, the spreading codes last 10 ms, therefore, they contain 10,230 chips. Their generation is described next.

The generation of the L1C spreading codes is as follows:

- First, a Legendre sequence of 10,223 chips is created (7 chips less than the 10,230 chips for the complete spreading code). The bit t of the Legendre sequence is equal to one if there exists an integer x such that t is congruent to x^2 modulo 10,223.
- Then, a Weil code, W , is generated using a pre-defined Weil index, w . The Weil index is specific to the PRN and the channel (i.e., data or pilot) considered.

- Next, the Legendre sequence generated in step 1 is shifted by this Weil index and added to the non-shifted Legendre sequence (modulo 2) as follows

$$W(t;w) = L(t) \oplus [L(t+w) \bmod 10230] \tag{2.9}$$

- Finally, a 7-chip expansion sequence is then inserted to obtain a code of 10,230 chips. The insertion sequence is common for all the satellites and the channels, and only its insertion point, p , is specific to the satellite and the channel. The final sequence, $L1C(t)$ can therefore be written as:

$$L1C(t) = \begin{cases} W(t;w) & ; 0 \leq t \leq p-2 \\ ExpansionSequence & ; p-1 \leq t \leq p+5 \\ W(t-7;w) & ; p+6 \leq t \leq 10229 \end{cases} \tag{2.10}$$

The generation of the spreading codes for L1C is summarized in Figure 2-9.

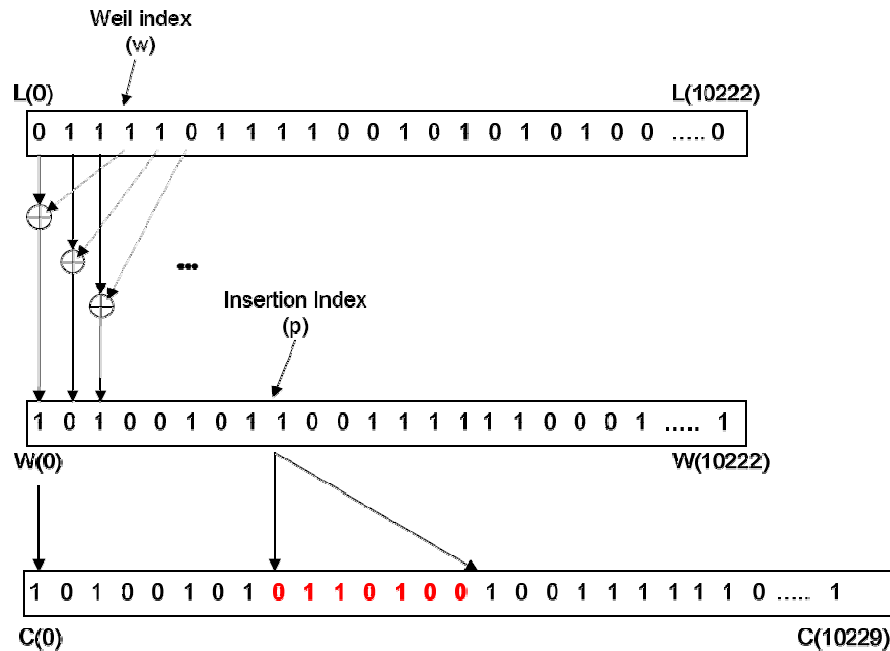


Figure 2-9: Generation of the L1C primary codes

The modulation on $L1C_D$ (data channel) is a BOC (1,1) modulation (Binary Offset Carrier) and as one will see in Chapter 3 the same on Galileo L1. A BOC signal is created by modulating a sine wave carrier with the product of the PRN spreading code and the sign of the sine of the subcarrier as shown in Figure 2-10. Due to this modulation, the spectrum of the signal is split in two symmetrical components with no remaining power at the central frequency. The two main lobes are centered at ± 1.023 MHz from the central frequency, thus a bandwidth of 4.092 MHz is needed to keep most of the power. The modulation on $L1C_P$ (pilot channel) is a TMBOC (Time Multiplexed BOC as illustrated in Figure 2-11), which consists of some chips modulated using a BOC (1,1) and others using a BOC(6,1). The first parameter of the BOC is the ratio between the subcarrier frequency and the reference frequency and the second parameter is the ratio between the spreading code frequency and the reference frequency. When BOC(6,1) is used, the number of chips (and correspondingly the chipping rate) is multiplied by 6 compared to the BOC(1,1) for a given time interval equivalent to one chip of the original ranging code. This increased chipping rate has the effect of requiring an increased sampling frequency to have all the information (because the minimum necessary bandwidth is now 14.322 MHz).

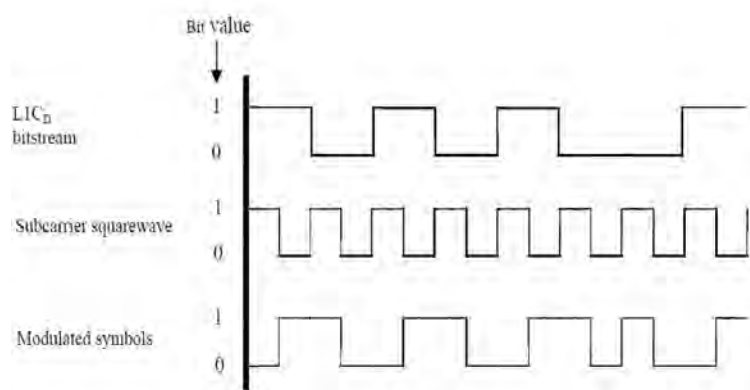


Figure 2-10: BOC(1,1) modulation

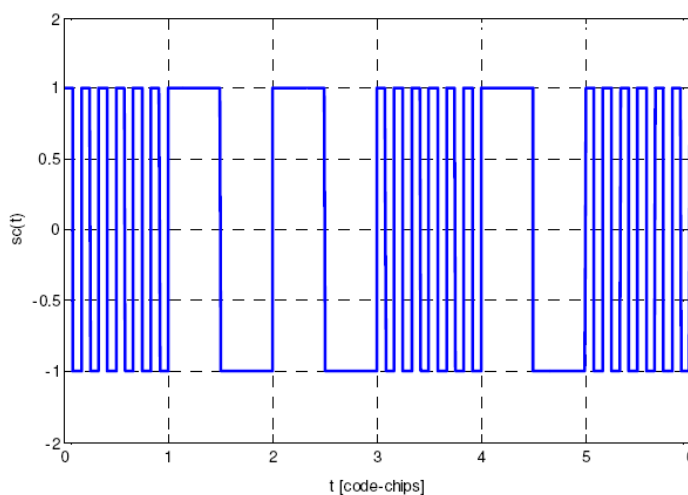


Figure 2-11: TMBOC modulation

As mentioned in the previous section, one critical property of the PRN code is the shape of the autocorrelation function. An example of normalized autocorrelation of the data and pilot channels of the L1C signal is given in Figure 2-12 for PRN 1 and a code delay of 5200 chips.

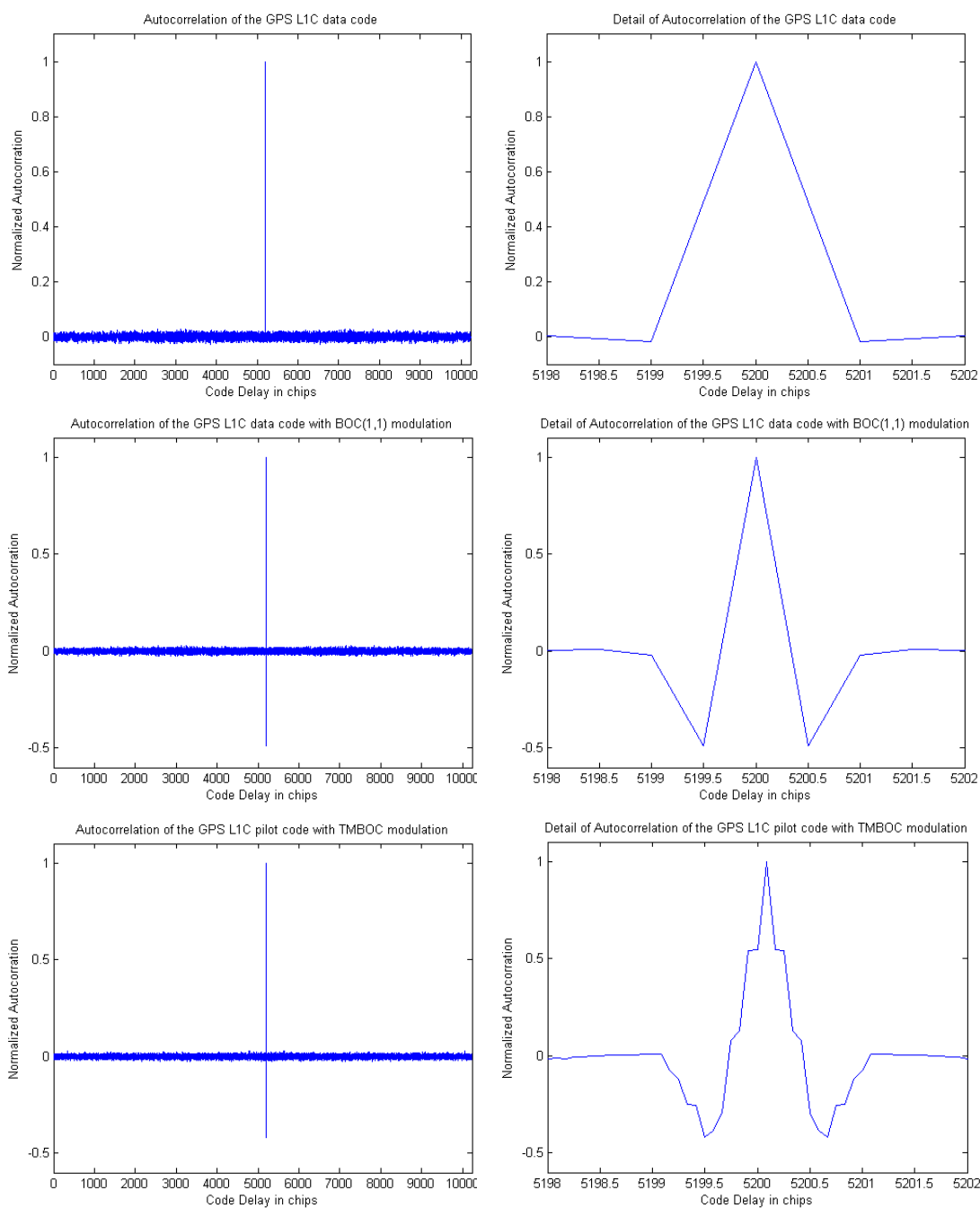


Figure 2-12: Autocorrelation of the GPS L1C code (left column) and detail of the peak (right column) for the spreading code only (top figures), data channel modulated by BOC (middle figures) and the pilot channel modulated by TMBOC (bottom figures)

In this figure, the autocorrelation of the spreading code only (with only the BPSK subcarrier and not the BOC(1,1) subcarrier modulation) is first shown on the data channel for PRN 1. The ratio between the main peak and the noise level is much higher than in the case of L1 C/A ranging codes. This was expected, due to the length of the ranging codes on L1C (10 times longer than on L1 C/A). Second, the autocorrelation of the code on the data channel including the modulation (BOC(1,1) modulation on the data channel) is shown (middle figures) for PRN 1 as well. The ratio between the main peak and the noise level remains the same, however two side peaks appear on both sides of the main peak with half the amplitude of the main peak. This is characteristic of the BOC(1,1) modulation and can become an issue for tracking if one of the side peaks is tracked instead of the main one. Finally, the autocorrelation of the pilot channel signal including the modulation (TMBOC modulation on the pilot channel) is shown on the bottom figures for the same PRN. The shape of the autocorrelation function is very similar to the one on the data channel. Indeed, the main peak looks like a distortion of the main peak of the BOC(1,1). This distortion is due to the BOC(6,1) component of the TMBOC. As shown in the figure, the main peak is sharper than that of the BOC(1,1) and will perform better in case of multipath. This will be demonstrated in Appendix C. Another advantage of the TMBOC is the spectral separation of the signals (to limit intra-system and inter-system interference). The PSD of the L1C signal is shown in the next paragraph. Other PRNs would give similar results.

The navigation message is transmitted on the data channel at 100 chips/s. The message can be broadcast at a faster chipping rate than on L1 C/A (50 chips/s). Indeed, the

navigation message of L1 C/A was not broadcast at a higher rate in order to have enough redundancy to guarantee a certain level of integrity of the extracted data bits. However, the L1C navigation message is transmitted using advanced techniques such as Cyclic Redundancy Check (CRC) and Forward Error Correction (FEC) techniques which allow the user to check the message integrity.

The Power Spectral Density (PSD) of the GPS L1C signal can be derived using the same method as for GPS L1 C/A, i.e. computing the Fourier transform of the autocorrelation function of the GPS L1C. The normalized PSD of the data channel (BOC(1,1) modulation) can be expressed as (Betz 2001):

$$G_{L1CD}(f) = T_C \left(\frac{\sin\left(\frac{\pi \cdot f}{2 \cdot f_C}\right) \cdot \sin\left(\frac{\pi \cdot f}{f_C}\right)}{\pi \cdot \frac{f}{f_C} \cdot \cos\left(\frac{\pi \cdot f}{2 \cdot f_C}\right)} \right)^2 \quad (2.11)$$

Concerning the pilot channel (TMBOC modulation), from the distribution of the signal power between the BOC(1,1) and BOC(6,1) on the pilot channel, the normalized PSD can be expressed as (Hein et al 2006):

$$G_{L1CP}(f) = \frac{29}{33} \cdot G_{BOC(1,1)} + \frac{4}{33} \cdot G_{BOC(6,1)} \quad (2.12)$$

with (Betz 2001):

$$G_{BOC(1,1)} = T_C \left(\frac{\sin\left(\frac{\pi \cdot f}{2 \cdot f_C}\right) \cdot \sin\left(\frac{\pi \cdot f}{f_C}\right)}{\pi \cdot \frac{f}{f_C} \cdot \cos\left(\frac{\pi \cdot f}{2 \cdot f_C}\right)} \right)^2 \quad (2.13)$$

$$G_{BOC(6,1)} = T_C \left(\frac{\sin\left(\frac{\pi \cdot f}{12 \cdot f_C}\right) \cdot \sin\left(\frac{\pi \cdot f}{f_C}\right)}{\pi \cdot \frac{f}{f_C} \cdot \cos\left(\frac{\pi \cdot f}{12 \cdot f_C}\right)} \right)^2 \quad (2.14)$$

Therefore, the normalized PSD of the pilot channel can be expressed as:

$$G_{L1CP}(f) = \frac{29}{33} \cdot T_C \left(\frac{\sin\left(\frac{\pi \cdot f}{2 \cdot f_C}\right) \cdot \sin\left(\frac{\pi \cdot f}{f_C}\right)}{\pi \cdot \frac{f}{f_C} \cdot \cos\left(\frac{\pi \cdot f}{2 \cdot f_C}\right)} \right)^2 + \frac{4}{33} \cdot T_C \left(\frac{\sin\left(\frac{\pi \cdot f}{12 \cdot f_C}\right) \cdot \sin\left(\frac{\pi \cdot f}{f_C}\right)}{\pi \cdot \frac{f}{f_C} \cdot \cos\left(\frac{\pi \cdot f}{12 \cdot f_C}\right)} \right)^2 \quad (2.15)$$

and from the distribution of the GPS L1C signal power between the pilot and data channel, the normalized PSD of the total L1C signal can be expressed as (Hein et al 2006):

$$G_{L1C}(f) = \frac{3}{4} \cdot G_{L1CP}(f) + \frac{1}{4} \cdot G_{L1CD}(f) \quad (2.16)$$

and therefore

$$G_{L1C}(f) = \frac{10}{11} \cdot G_{BOC(1,1)}(f) + \frac{1}{11} \cdot G_{BOC(6,1)}(f) \quad (2.17)$$

where G_{L1CD} , G_{L1CP} , G_{L1C} are the normalized PSD of the GPS L1C data channel, GPS L1C pilot channel and the complete GPS L1C respectively

$G_{BOC(1,1)}$ and $G_{BOC(6,1)}$ are the normalized PSD of a BOC(1,1) and BOC(6,1) modulations respectively

f_C is the GPS L1C chipping rate

$T_C = \frac{1}{f_C}$ is the GPS L1C ranging code chip duration

The normalized PSD of the data channel, the pilot channel and the complete L1C signal are shown in Figure 2-13.

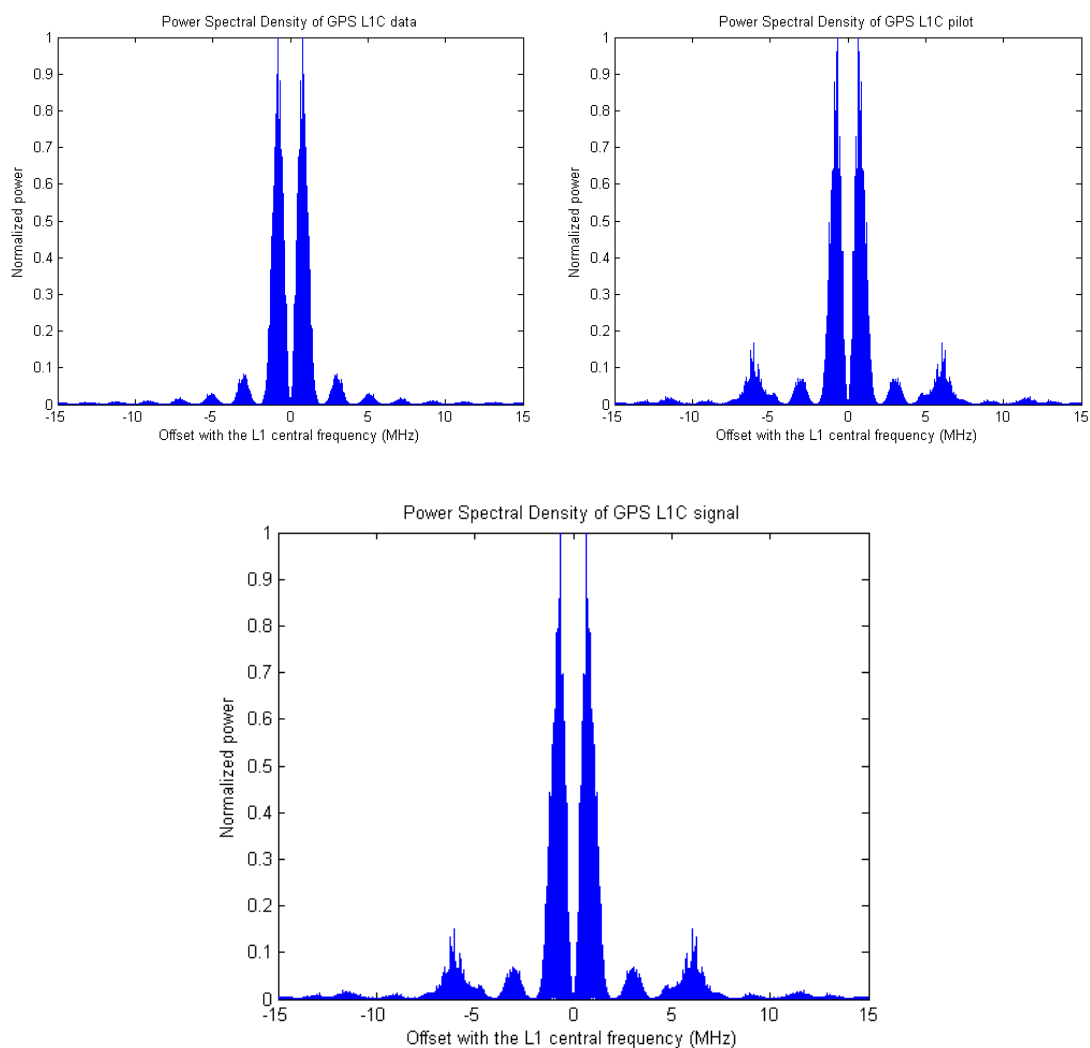


Figure 2-13: Normalized PSD of the L1C data channel (top left), L1C pilot channel (top right) and the complete L1C signal (bottom)

Similar to GPS L1 C/A, at the receiver level, and taking into account the propagation time, the GPS L1C signal transmitted by one satellite can be expressed as follows:

$$\begin{aligned}
s_{L1C}(t_{GPS}) = & \sqrt{2 \cdot P_{L1CD}(t_{GPS})} \cdot d_{L1C}(t_{GPS} - \tau_{L1C}(t_{GPS})) \cdot c_{L1CD}(t_{GPS} - \tau_{L1C}(t_{GPS})) \cdot s_{C_{BOC}}(t_{GPS} - \tau_{L1C}(t_{GPS})) \cdot \\
& \cos(2 \cdot \pi \cdot (f_{L1} + f_{Dtotal}) \cdot t_{GPS} + \varphi_{L1C}) \\
& + \sqrt{2 \cdot P_{L1CP}(t_{GPS})} \cdot L1C_0(t_{GPS} - \tau_{L1C}(t_{GPS})) \cdot c_{L1CP}(t_{GPS} - \tau_{L1C}(t_{GPS})) \cdot s_{C_{TMBOC}}(t_{GPS} - \tau_{L1C}(t_{GPS})) \cdot \\
& \sin(2 \cdot \pi \cdot (f_{L1} + f_{Dtotal}) \cdot t_{GPS} + \varphi_{L1C}) + w(t_{GPS})
\end{aligned} \tag{2.18}$$

where s_{L1C} is the L1C signal

t_{GPS} is the GPS time

τ_{L1C} is the time delay due to the propagation between the satellite and the receiver

including the atmosphere clock delays

P_{L1CD} and P_{L1CP} are the transmitted power on the pilot and data channel respectively

d_{L1C} is the data bit of the binary NRZ navigation message on the data channel

c_{L1CD} and c_{L1CP} are the L1C ranging code on the data and pilot channel respectively

$L1C_0$ is the secondary code on the pilot channel

f_{L1} is the GPS L1 central frequency (1575.42 MHz)

f_{Dtotal} is the Doppler frequency due to the satellite and user motion plus the Doppler shift due to atmospheric and clock errors

φ_{L1C} is the initial L1C phase in radians

$w(t)$ is the noise approximated as Gaussian with zero mean.

The carrier phase and code delay can be defined using the same method as for GPS L1 C/A in section 2.1.2.

2.2.3 Correlation properties of GPS L1C

As mentioned before, one of the important properties of the codes is their cross correlation performance. The same method as was used above for GPS L1 C/A is used here for GPS L1C. First, the cross correlation protection of the GPS L1C codes for the data and pilot channels (including the BOC(1,1) and TMBOC modulation respectively) is computed. Then, the cross correlation performance is studied considering various Doppler offsets. For the GPS L1C codes, the correlation protection found is about 28.5 dB for the data channel, 30.5 dB for the pilot channel (without taking into account the secondary code) and about 30.5 dB as well for the cross correlation between the pilot and data channel, which is 4.5 to 6.5 dB more than the minimal cross correlation protection of the GPS L1 C/A codes. More specifically, if one looks at the cross correlation of the PRN codes 1 and 2, in 50 % of the cases there is a protection of 45 dB or more for the L1C data channel, and 50 dB or more for the L1C pilot channel or the cross correlation between the pilot and the data channel as shown in Figure 2-14. As it can be seen in the figure, the pilot channel alone performs roughly the same as the data channel cross correlated with the pilot channel. For this figure, the PRN 1 has been chosen as an example to compute the cross correlation of the data and pilot channel. However, the performance is similar if other PRNs are considered. However, the pilot channel performs better than the data channel thanks to the TMBOC modulation. Note that the codes themselves being generated using the same algorithm, they have the same properties. Similar results can be found for all other cross correlation products. These results are in

accordance with the description of the code design requirements given by Wallner et al (2007) and Rushanan (2007).

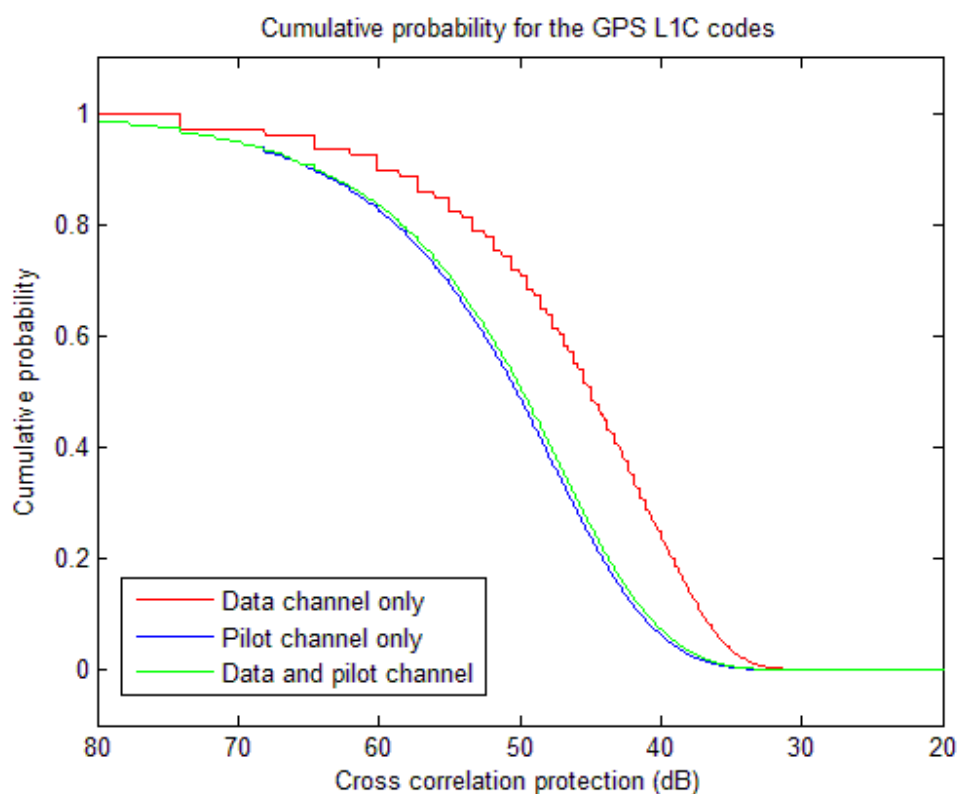


Figure 2-14: Cumulative probability for the cross correlation of PRNs 1 and 2 of the GPS L1C pilot and data codes

Now, the same process is repeated but the code is sampled. For the data channel, due to the BOC(1,1) modulation, a sampling rate of 5 MHz is necessary to keep most of the signal power. For the pilot channel, due to the TMBOC modulation, a sampling rate of 15 MHz (minimum bandwidth required to conserve the power of the two main lobes due to the TMBOC modulation) is used in this case. The results with sampling are presented in Figure 2-15. As can be seen, the results with and without sampling give slightly different results and the cross correlation protection is now about 30 dB for both the data

and pilot channels. However, the performance in the case of the sampling are again dependent on the sampling rate chosen (here the sampling rates have been chosen in accordance with the minimum bandwidth for each of the modulations and the Nyquist theorem).

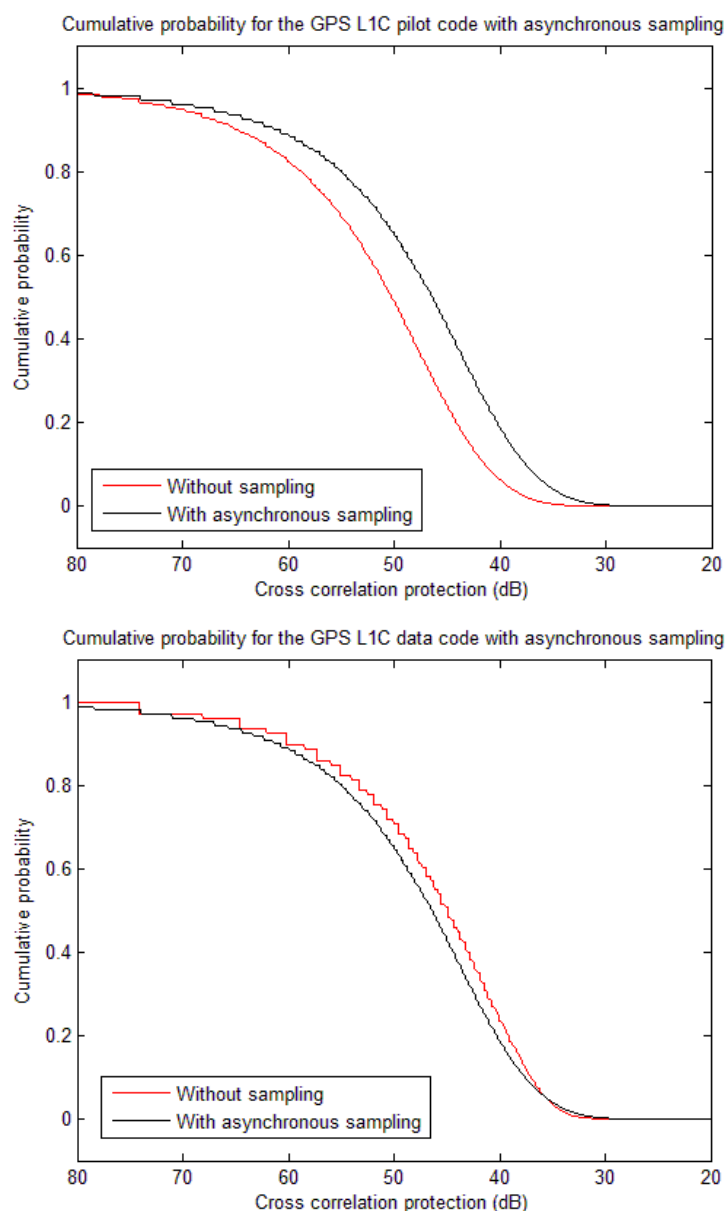


Figure 2-15: Cumulative probability for the cross correlation of PRNs 1 and 2 of the GPS L1C pilot codes (top) and the data codes (bottom) with asynchronous sampling (15 MHz) in black, and without sampling in red

Finally, the impact of the Doppler offset between two codes cross correlated is studied. The range of Doppler offset considered goes from 0 to 1000 Hz and the results for both the pilot and data channels are shown in Figure 2-16. All these results have been obtained using 5 MHz sampling rate for the data channel and 15 MHz sampling rate for the pilot channel (for the reasons explained above). Finally, both the code Doppler and carrier Doppler have been simulated.

First, the results obtained in the case of no Doppler offset are exactly the same than the ones in Figure 2-14. Again, this was to be expected since the carrier wave is completely removed before the correlation and therefore the results are the same than without a carrier. Then, in the case of the data channel, the minimum cross correlation protection is about 28 dB, therefore there is only a small degradation compared to the previous case. However, in the case of the pilot channel, the minimum protection is now about 26 dB and therefore experiences a non-negligible degradation due to the Doppler. All these results have been obtained using the cross correlation of PRNs 1 and 2 but similar results would be obtain with other PRNs. All the simulations have been done using simulation in Matlab.

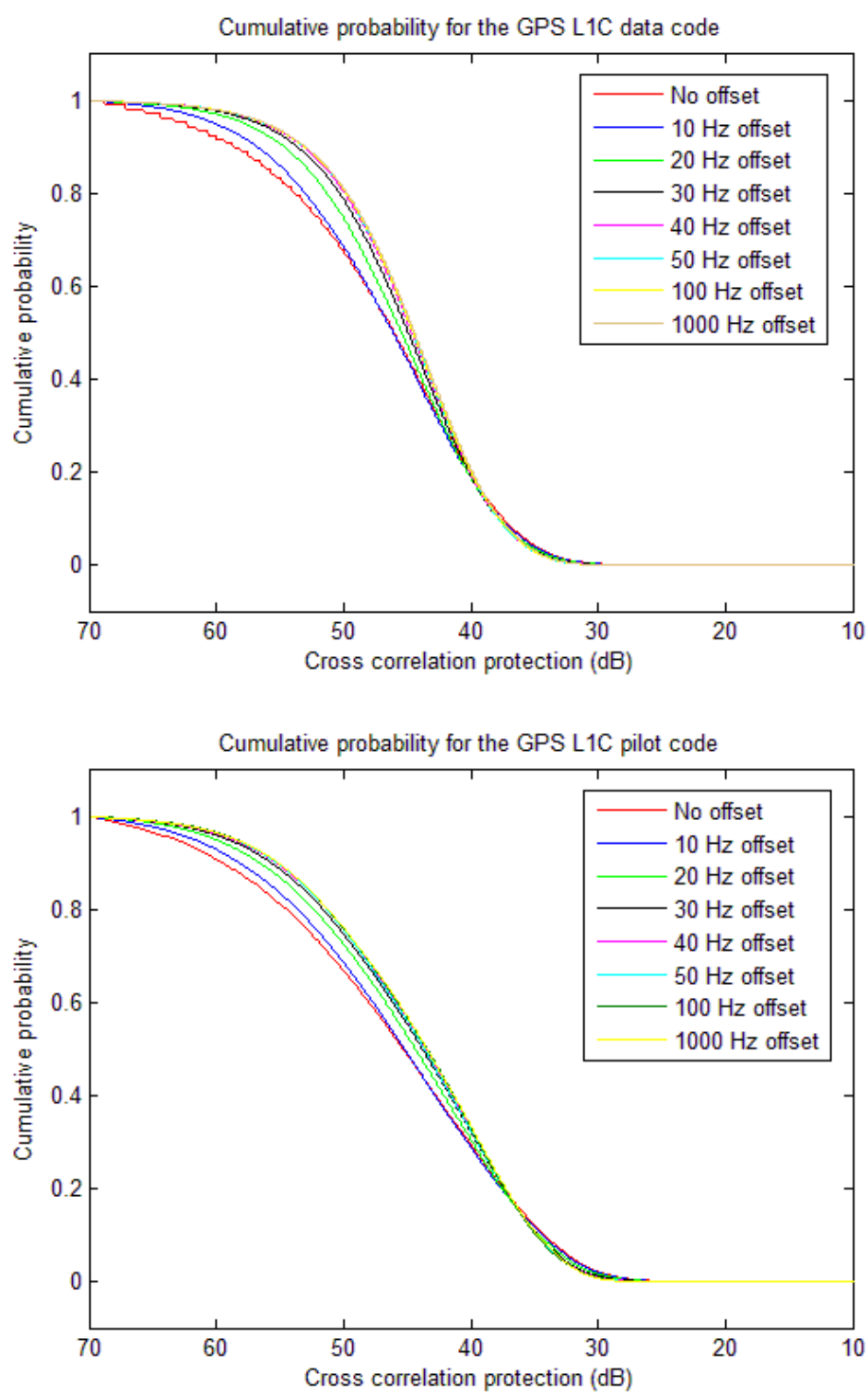


Figure 2-16: Cumulative probability for the cross correlation of PRNs 1 and 2 of the GPS L1C codes for the data channel (top) and the pilot channel (bottom) with different relative Doppler offsets

2.3 Improvements brought by GPS L1C compared to GPS L1 C/A

As mentioned before, the GPS L1 C/A signal was the first civilian signal designed and initially intended to allow for easy acquisition of the military signals. Therefore, under good signal conditions, the GPS L1 C/A will have good performance. However, it has important limitations in case of weak signals and under challenging conditions such as multipath environments or interference. Moreover, it does not have the required accuracy and/or reliability for specific applications (as surveying, plane landing, etc). In this paragraph, the improvements brought by GPS L1C compared to GPS L1 C/A are summarized and explained in light of the signal properties presented above.

First, as demonstrated in the previous section, the cross correlation protection is much higher for GPS L1C than for GPS L1 C/A in all circumstances (code only, with sampling, with Doppler shift) for the data and pilot channel. This higher minimum cross correlation protection is mainly due to the length of the primary codes. Indeed, the primary codes on L1C contain 10230 chips, which is ten times more than on L1 C/A. Moreover, the secondary code on the pilot channel increases again this cross correlation protection as explained in Mongrédien (2008) in the case of GPS L5. In good conditions, namely in open sky environments, the cross correlation protection of GPS L1 C/A is sufficient. However, under challenging conditions, such as indoor, in urban canyons or under foliage where there is a lot of multipath and the signals are weaker, this cross correlation protection can become an issue.

Another advantage of the GPS L1C signal is the presence of a pilot channel. As mentioned above, the pilot channel includes a primary and a secondary code. The secondary code has several advantages: it increases the cross correlation protection and it helps to achieve the data bit synchronization on the data channel (Julien 2005). Moreover, on GPS L1 C/A the coherent integration time was limited to 20 ms due to the bits of the navigation message which can change every 20 ms. The solutions to solve this problem were to use a non coherent integration but the performance will be degraded compared to a coherent integration or to the use of AGPS (Aided GPS), but this requires an external data link. However, the problem of data bits transitions is removed with the presence of a pilot channel: the integration time is now mainly limited by the oscillator quality and the user dynamics. Therefore, longer integration times can be achieved, which increases the sensitivity of the receiver and allows the acquisition of weaker signals. Finally, a pure PLL (Phase Lock Loop) can be used in the tracking stage instead of a Costas Loop (which are not sensitive to 180° phase shifts). More details on this last point will be presented in Chapter 5.

One other main difference between GPS L1C and L1 C/A is the modulation used. Indeed, a BOC(1,1) and TMBOC modulations are used for L1C and a BPSK for L1 C/A. The BOC(1,1) modulation presents a sharper peak than L1 C/A and the TMBOC has an autocorrelation peak again sharper as shown in Figure 2-2 and Figure 2-12. This sharper peak can offer better performance in terms of tracking: more accurate tracking especially in presence of multipath. More details concerning this are presented in Chapter 5 and Chapter 6. Another advantage of the BOC(1,1) and TMBOC modulations is a wider

spectrum: around 4 MHz and 14 MHz respectively to keep most of the signal power. This wider spectrum allows a stronger resistance to interference (see Appendix C) and limits intra and inter-system interference (see Chapter 3). Indeed, the development of GPS L1C has been done jointly with the development of Galileo L1 because the two signals share the same spectrum. This has been done to limit the inter-system interference and to allow a common receiver architecture. More details on this point are given in Chapter 3.

Finally, the structure of the navigation message has been greatly improved. Indeed, for L1 C/A, to maintain an acceptable level of reliability, the navigation message was transmitted at a rate of 50 symbols/s, and each symbol was therefore coded on 20 ranging code periods. In the case of GPS L1C, two techniques are used to insure the reliability of the decoding of the navigation message: CRC and FEC as described above.

Nevertheless, there are a few drawbacks: the wider bandwidth required due to the modulations (especially the TMBOC) can become an issue for mass market receivers. Research has been conducted herein concerning this point and is presented in Appendix C. Finally, the apparent increased chipping rate (due to the BOC(1,1) and TMBOC modulations) necessitate more processing time and this can be a problem for real time applications.

Research done in Betz et al (2006) studied some of the advantages and disadvantages of the GPS L1C signal. The conclusions of this research are reproduced in Table 2-1 (Betz et al 2006).

Table 2-1: Modulation tradeoff for BPSK, BOC(1,1) and TMBOC modulations (from Betz et al 2006)

Tradeoff Factor	BOC(1,1) compared to BPSK	TMBOC compared to BPSK
Multipath Mitigation using Early-Late Processing ¹	Same for Delays < 500 ns, Superior for Longer Delays	Superior for Excess Delays > 70 ns
Multipath Mitigation using Double Delta Processing ¹	Same for Excess Delays less than 500 ns, Inferior for Longer Delays	Same for Excess Delays < 500 ns, Inferior for Longer Delays
Multipath Mitigation Using Advanced Multipath Mitigation ¹	+4.9 dB	+7.5 dB
Early-Late Code Tracking SNR ¹	+4.9 dB	+7.5 dB
Double-Delta Code Tracking SNR ¹	Same	-0.6dB
Power for Initial Synch Processing ²	-0.4 dB	-0.9 dB
L1C Power for Narrowband Receiver	-0.4 dB	-0.9 dB
Combined L1C and C/A Code Power for Narrowband Receiver ^{2,3}	-0.2 dB	-0.4 dB
Susceptibility to Narrowband Interference ⁴	+2.7 dB	+3.2 dB
Self-Interference	+3.0 dB	+3.7 dB
Interference to C/A Code	+6.0 dB	+6.3 dB
10 ⁻⁶ Probability Pilot Autocorrelation Sidelobe ⁵	Same	+1.1 dB
10 ⁻⁶ Probability Pilot Crosscorrelation Sidelobe ⁵	Same	+1.1 dB
Notes:		
1. ±12 MHz precorrelation bandwidth		
2. ±2 MHz precorrelation bandwidth		
3. Signal received at specified minimum levels		
4. Interference at spectral peak		
5. Combined even and odd correlations		

Therefore, the advantages of adding a signal in the L1 band are two fold:

- The measurements of one more signal add redundancy and therefore increase the reliability of the measurements
- The new modulation technique as well as the coding of the navigation message allows an improvement in terms of accuracy of the measurements especially in challenging environments.

Chapter Three: GALILEO L1 SIGNAL

This chapter begins with a brief overview of the history of the Galileo system as well as the forecast plan for the deployment of the full constellation. Then, since this thesis focuses on the signals in the L1 band, the structure of the Galileo L1 Open Service (OS) signal is presented in detail. A particular emphasis is given to the structure of this signal and its main properties and characteristics, including the properties common with the GPS L1 signal. Afterwards, the signal model used for Galileo L1 OS throughout this thesis is presented. Finally, the cross correlation properties of the signals are studied in detail and compared to those of the GPS L1 signal presented in the previous chapter.

3.1 Brief History of the Galileo System and Forecast Deployment of the Galileo Constellation

Nowadays, GPS in the United States and GLONASS in Russia are being modernized while, among others, COMPASS in China and Galileo in Europe are under development. In this section, the focus is on the history and the future development of Galileo. All the information concerning this section can be found on the ESA (European Space Agency) website¹.

Galileo provides a new GNSS with high accuracy and is controlled by civilians. The Galileo project is lead by the European Union (EU) – and more specifically the European Commission (EC) and the European Space Agency (ESA). Its design has been conceived

¹ <http://www.esa.int/esaNA/galileo.html>

in consultation with the United States and Russia to be interoperable with GPS and GLONASS. During its design, Galileo promised to be the only GNSS to deliver at that time a standalone position in real-time at the metre level. However, GPS and GLONASS current signals are now being modernized, new frequencies are added and the new generation should have the same level of performance as Galileo. One of the aims of this project is for the EU to have an independent GNSS. Indeed, there is no guarantee that both systems would stay uninterrupted in case of conflict (ESA website¹). Another reason for developing Galileo is the better coverage at high latitudes, especially useful for northern countries in Europe.

France, Germany, Italy and the United Kingdom created a team of engineers in 1999 to work on a European GNSS. The EU and the ESA originally agreed to the funding model in 2002. However, it was only in 2003 that the EU and the ESA officially agreed to the first stage of the Galileo program. Unlike GPS, the main use of Galileo is intended to be civilian and all the signals will be fully available for both civil and military use. At this point in time, the total cost of the project is estimated to 3.7 billion euro and the system is supposed to be operational by 2013 with a total of 30 satellites. Two-thirds of the satellites are supposed to be funded by industry and the remaining part by the EU and ESA.

¹ <http://www.esa.int/esaNA/galileo.html>

The US and the EU signed an agreement in June 2004 on a common design of the Open Service (OS) Galileo L1 signal and the future GPS L1C signal. Nevertheless, in 2007, only one test satellite had been launched and the problem of funds was still not completely resolved. By the end of 2007, the EU finally agreed to transfer a part of other funds to the Galileo project and try to attract more companies to finance the development.

The first Galileo satellite, a test satellite, GIOVE-A (Galileo In-Orbit Validation Element), was launched on 28 December 2005 and has been used to test the satellite equipment and to validate the signal properties as well as the satellite hardware such as the oscillator stability. It allowed the EU to secure the Galileo frequencies with the International Telecommunications Union. However, the GIOVE-A satellite does not transmit the signals as they will be in the future constellation (different modulation and ranging codes are used). Moreover, the GIOVE-A satellite can transmit only two frequencies at a time and regularly changes frequencies to secure them as mentioned earlier.

The second test satellite, GIOVE-B, was launched on 26 April 2008 and incorporates several improvements relative to the GIOVE-A satellite such as the CBOC modulation on the L1 OS signal and the hydrogen maser as oscillator. A picture of the GIOVE-B satellite in its test facility is shown in Figure 3-1. As for GIOVE-A, GIOVE-B has a forecast life expectancy of only two years. One of the technologies tested by GIOVE-B is the hydrogen maser with a theoretical stability of 1 ns per day. This clock is expected to be the most stable clock ever used in space. GIOVE-B does not use the ranging codes of

the future signals but the modulation used should be the same. This satellite is also used to secure the frequencies for the future signals.



Figure 3-1: GIOVE-B satellite in its test facility (from ESA website)

Four operational satellites will be launched and will be used to validate the Galileo system. Once validation is complete, the full constellation will be deployed. The constellation will contain 27 operational satellites plus 3 active spares. They are divided in three orbital planes and transmit on three frequencies including civilian and commercial signals (no military signal). The orbital planes are inclined 56 degrees relative to the equatorial plane. Due to the distribution of the satellites, Galileo will offer a slightly better coverage at high latitude which is very helpful for north Europe countries such as Norway (which recently entered the project). Indeed, it has been shown in

Lachapelle et al (2001) that the Galileo constellation performs better in terms of HDOP in most cases except when the masking angle is very high (in urban canyons for example). In case of a single satellite failure, an active spare will be used to replace it, and therefore the user will not experience a significant degradation in overall performance.

Once complete, Galileo will offer four services:

- Open Service (OS). This corresponds to the signals freely available which will be transmitted on two frequencies.
- Commercial Service (CS). This corresponds to the encrypted signal. It will be transmitted on three frequencies.
- Public Regulated Service (PRS) and Safety of Life (SoL). These two services will be used by the authorities for safety of life applications.

Moreover, the final system will offer a Search And Rescue (SAR) capability. To achieve this, on board each satellite a transponder will be installed in order to retransmit the signal and position from users to the rescue centre. Furthermore, the user will be informed that their message has been successfully transmitted (this is a main improvement of this service brought by Galileo compared to existing GNSSs or modernization plans of other GNSSs).

There will be two permanent ground operation centres, namely one in Italy and one in Germany. A scheme of the future constellation is shown in Figure 3-2. The system is supposed to be fully operational by 2013.

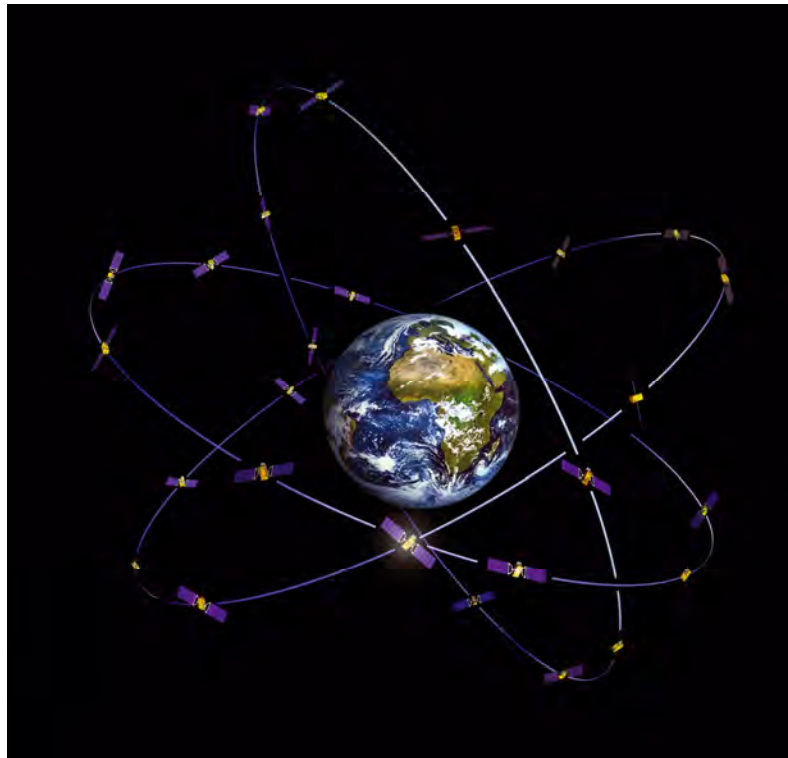


Figure 3-2: Galileo constellation (from ESA website)

As mentioned previously, Galileo will broadcast signals on three frequencies. The Galileo frequency plan presented in the Interface Control Document (OS SIS ICD 2008) is shown in Figure 3-3. The Galileo frequency bands used for navigation are shown in blue in the figure which also shows the GPS frequencies and the Galileo SAR frequencies. The three frequency bands for navigation are:

- the L1 band centered at 1575.42 MHz
- the E6 band centered at 1278.75 MHz
- the E5 band centered at 1191.795 MHz, which can be separated in two signals centered at 1176.45 MHz (E5a) and 1207.140 MHz (E5b)

As shown in Figure 3-3, some of the frequencies overlap with ARNS (Aeronautical Radio Navigation Services) and all of them with the RNSS (Radio Navigation Satellite Services) bands. In particular, the overlapping with ARNS band can become an issue in terms of interference. More specifically, ARNS includes signals employed by airports and airplanes for landing and positioning operations. DME (Distance Measuring Equipment) and TACAN (TACTical Air Navigation) systems are both part of the ARNS. The DME is a transponder-based radio navigation technology and an ICAO (International Civil Aviation Organization) standardized system. The DME is a civilian system used to compute the distances in measuring the propagation time of VHF or UHF (Ultra High Frequency) signals. The DME system is used by airplanes to determine the distance between the airplane and the land-based transponder. The TACAN system is another navigation system but military. It is employed by the USA (United States of America) and the other NATO (North Atlantic Treaty Organization) countries. It provides the same information than the DME system (bearing information) but with more accuracy. Due to their high power, these signals can be a threat for the Galileo signal. More information on ARNS signals can be found in Nava (2006).

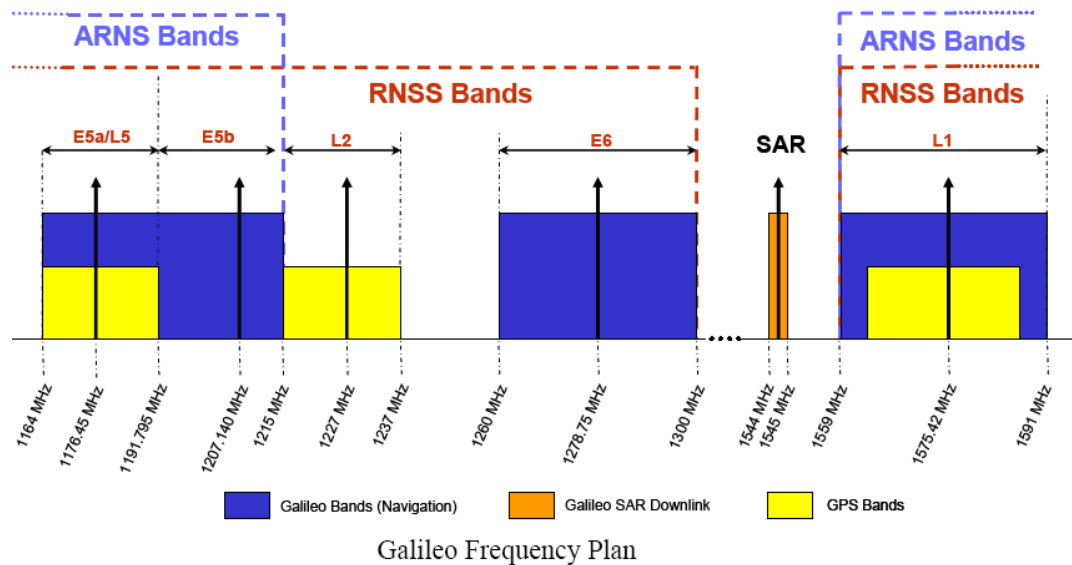


Figure 3-3: Galileo and GPS frequency plan (from OS SIS ICD 2008)

In Figure 3-4, the power spectral densities of the Galileo signals are shown. The E5 signal is modulated by an AltBOC (Alternative BOC) which can be considered as two separate QPSK signals transmitting both OS (Open Service) signals and commercial data. The E6 signal is modulated by a BPSK modulation and is for commercial use only.

The Galileo L1 signal can be divided into three channels: A, B and C. The A channel is a Public Regulated Service (PRS) signal and therefore has limited access. The A channel is modulated using a BOC(15,2.5). The B and C channels are OS channels. The information transmitted by these channels is available to all users. The B channel includes a navigation message and is called the data channel. The C channel does not carry any navigation message, only ranging codes are present, and is called the pilot channel. The total nominal received power of the B and C channels is 1.5 dB above GPS L1 C/A and is equal to -157 dBW. As mentioned previously, in this research, the signal of interest is Galileo L1, and since the A channel has a regulated access, only L1-B and L1-C

components will be considered herein. The main properties of these two channels are described in the next section.

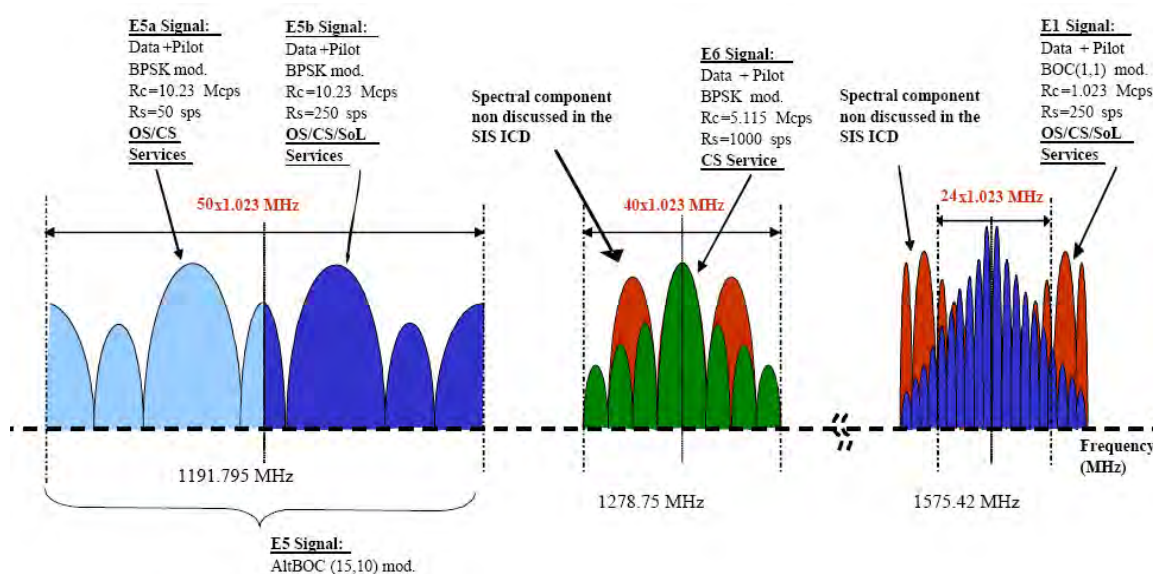


Figure 3-4: Power Spectral densities of the Galileo signals (from OS SIS ICD 2008)

3.2 Structure of the Open Service Galileo L1 Signal

In this section, the structure of the Galileo L1 OS signal is described in detail. The differences between the L1 OS signal broadcast by GIOVE-A and the future Galileo L1 OS signal are shown. In addition, part of the algorithms that have been tested using the GIOVE-A signal are presented. Unless otherwise specified, the following description of the signal is from the Galileo OS SIS ICD (2008) and the GIOVE-A SIS ICD (2007).

Some characteristics of the GIOVE-A signals differ from those of the future Galileo signals. Of particular concern is that, in the case of L1-C, the length of the primary code

has been doubled for the GIOVE-A signal compared to the future signals. A second concern is the modulation used: a BOC(1,1) modulation is used in the case of GIOVE-A whereas a CBOC (Composite BOC) modulation is used for the final signals. The other characteristics (except for the codes used) are the same.

The L1-B and L1-C channels are transmitted in the cosine part of the L1 signal. Both channels are transmitted at the same power and each approximately represents 22% of the total L1 signal power. On L1, 11% of the power is lost due to the CASM (Coherent Adaptive Subcarrier Modulation), which is used to have a constant transmitted power by the satellite (Borre et al 2007). On the data channel, L1-B, the I/NAV (Integrity NAVigation message type) navigation message is broadcast at 250 symbols/s and is encoded using a FEC (Forward Error Correction) technique.

In the final Galileo system, the L1 ranging codes will be memory codes. On the data and pilot channels, the spreading code will be composed of 4092 chips with a period of 4 ms. For the pilot channel, the primary code will be combined with a secondary code of 25 chips. The final (fully repeating) code of the pilot channel is called the tiered code and will be 100 ms long (4 ms x 25 secondary code chips). The principle of generation of this tiered code is shown in Figure 3-5 (GIOVE-A SIS ICD 2007). Relative to the final signal, the following differences are present in the GIOVE-A satellite:

- The primary codes can be generated using a LFSR (Linear Feedback Shift Register) instead of using memory codes.

- The length of the primary code on the pilot channel is twice as long. The primary code on the pilot channel therefore contains 8184 chips and lasts 8 ms, which gives a tiered code of 200 ms in total.

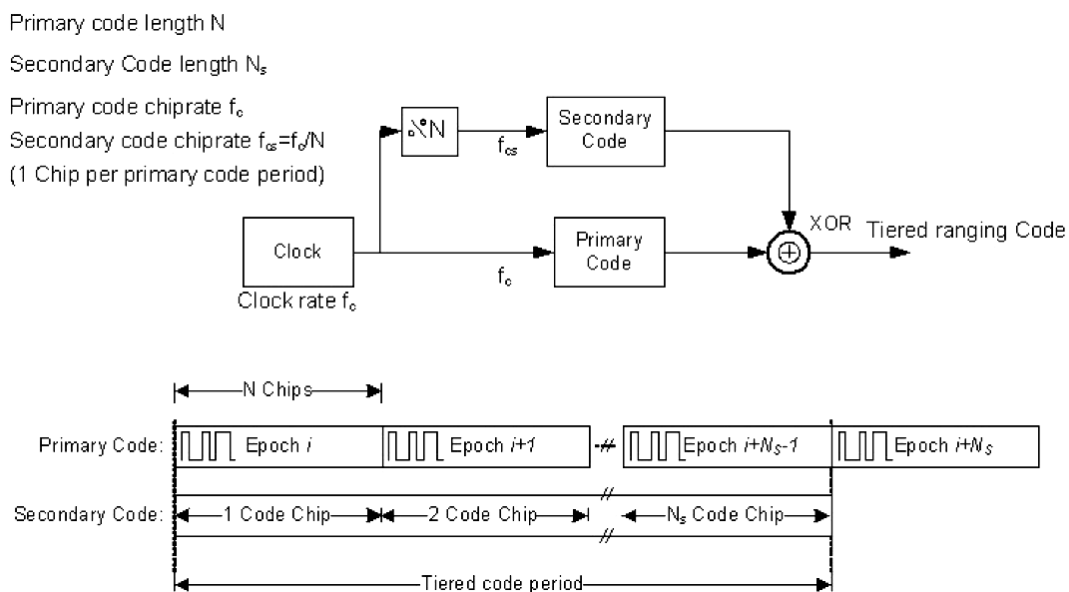


Figure 3-5: Tiered code generation (from GIOVE-A SIS ICD 2007)

On Galileo L1, the spreading codes are longer than on GPS L1 C/A. The increase in the length of the codes decreases the cross-correlation products. However, it increases the processing time if the acquisition is done on one ranging code period. On the pilot channel, the presence of a secondary code has several advantages (Julien 2005), namely it helps to achieve data synchronization on the data channel and it improves the resistance of the signal to narrow-band interference.

Another important difference between GPS L1 C/A and Galileo L1 is the ratio between the data rate and the length of one spreading code period. Indeed, in the case of Galileo L1 (and the same applies as mentioned earlier to GPS L1C), the sign of the data symbol /

secondary code can change every ranging code period. This property of the Galileo L1 signal is very important for the acquisition process as shown in Chapter 5.

Considering the modulation, the GIOVE-A L1 signal is modulated by a BOC(1,1) signal. The description of the BOC(1,1) modulation and its main properties are shown in Chapter 2.

Concerning the modulation of the Galileo L1 OS signal, as mentioned in the previous Chapter, the European Space Agency (ESA) and the Department of Defense (DoD) of the United States have been collaborating to come to an agreement on the design of the Galileo L1 signal and the future GPS L1C signal. In the first design of the Galileo L1 signal (OS SIS ICD 2006), the planned modulation was BOC(1,1). However, in order to improve the performance of the L1 signal, the modulation was changed in the last version of the ICD (OS SIS ICD 2008), opting for an MBOC (multiplexed BOC) modulation. For Galileo in particular, a CBOC (Composite BOC) modulation was adopted. The CBOC is a type of implementation of the MBOC. A CBOC modulation, is a combination of BOC(1,1) and BOC(6,1) modulations (a different implementation of MBOC than the TMBOC introduced in Chapter 2). The implementation of the CBOC is shown in Figure 3-6 (Floc'H & Soellner 2007). The subcarrier of the CBOC is generated as follows:

- For the data channel:

$$SC_{CBOC_Data}(t) = \sqrt{\frac{10}{11}} SC_{BOC(1,1)} + \sqrt{\frac{1}{11}} SC_{BOC(6,1)} \quad (3.1)$$

- For the pilot channel:

$$s_{CBOC_Pilot}(t) = \sqrt{\frac{10}{11}} s_{BOC(1,1)} - \sqrt{\frac{1}{11}} s_{BOC(6,1)} \quad (3.2)$$

where $s_{CBOC_Data}(t)$ and $s_{CBOC_Pilot}(t)$ are the CBOC subcarrier of the data and pilot channel respectively

$s_{BOC(1,1)}$ is the BOC(1,1) subcarrier

$s_{BOC(6,1)}$ is the BOC(6,1) subcarrier

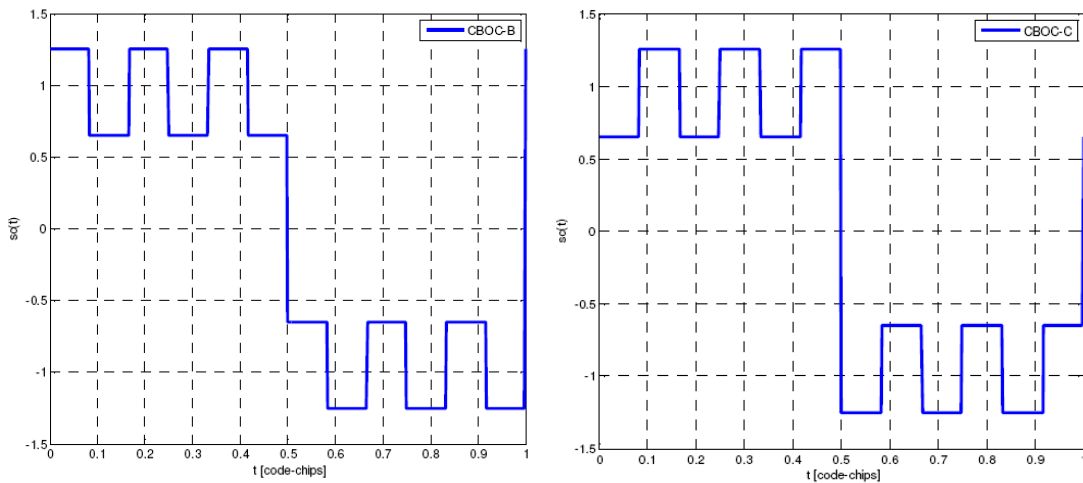


Figure 3-6: CBOC modulation on the data channel (on the left) and the pilot channel (on the right) (from Floc'H & Soellner 2007)

The Galileo L1 power spectrum (which is the same as GPS L1C for the OS part) is presented in Figure 3-7 (Avila-Rodriguez et al 2007). The equations of the PSD are the same as for the total GPS L1C signal (presented in the previous chapter) and are not reproduced here (Equation 2.12 in Chapter 2).

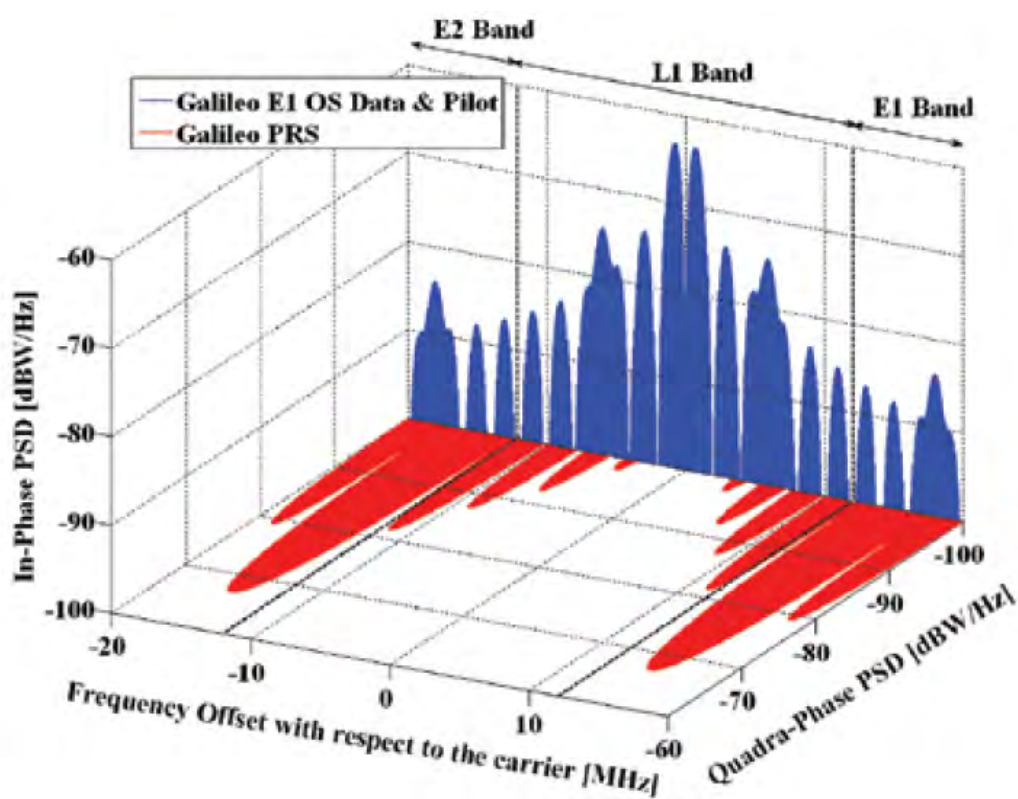


Figure 3-7: Galileo L1 power spectrum (from Avila-Rodriguez et al 2007)

The MBOC modulation has several advantages compared to the BOC(1,1) modulation:

- It helps to separate in frequency the new signals from the existing signals in the L1 band (intra-system and inter-system interference)
- Since the power spectrum is wider, the signal is more resistant to interference
- The main autocorrelation peak is narrower and therefore performs better in the presence of multipath

An example of the autocorrelation function of the GIOVE-A L1 codes is shown in Figure 3-8 with a code delay of 2500 chips for the data channel and 5500 for the pilot channel.

First, if one compares the overall shape of the autocorrelation of the data channel L1-B

and the pilot channel L1-C, one can see that the shape is the same except that the ratio between the peak and the noise level is double for the pilot channel. This result was theoretically expected since, in the case of GIOVE-A, the length of the code on the pilot channel is twice as long as on the data channel. Concerning the detail of the autocorrelation function, the shape is the same for the pilot and the data channel. Indeed, since the autocorrelations have been normalized, there is no difference in the amplitude of the main peak. This shape is typical of a BOC(1,1) modulation and is identical to the one of the data channel of GPS L1C as shown in the previous chapter.

The BOC(1,1) autocorrelation function can be approximated as (Julien 2005):

$$R_{N,BOC(1,1)} = \begin{cases} tri(x) - \frac{1}{2} \left(tri\left(\frac{x-\frac{1}{2}}{\frac{1}{2}}\right) + tri\left(\frac{x+\frac{1}{2}}{\frac{1}{2}}\right) \right) & \text{if } |x| < 1 \text{ chip} \\ 0 & \text{if } |x| > 1 \text{ chip} \end{cases} \quad (3.3)$$

where $tri\left(\frac{x}{y}\right)$ is the unit triangular function of width $2y$ centered at 0.

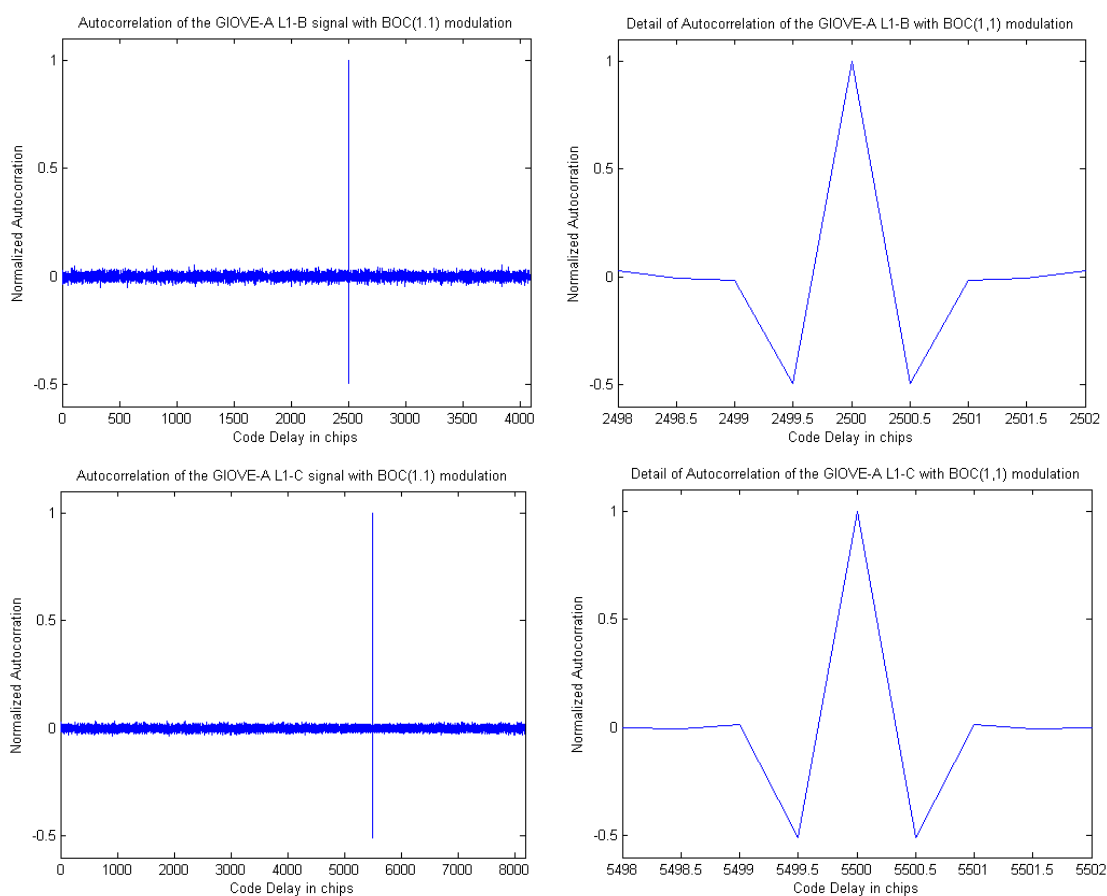


Figure 3-8: Example of autocorrelation of the GIOVE-A codes for the data channel (on top left) and for the pilot channel (on bottom left) and their detail (on the right)

In contrast to the GIOVE-A codes, an example of the autocorrelation of the future Galileo L1 OS codes is shown in Figure 3-9 with a code delay of 2416 chips. Only the data channel is shown here because the autocorrelations are the same on the data and pilot channel (same code properties for and same modulation). This autocorrelation has been generated using PRN 1 but the results are similar for other PRNs. Concerning the detail of the autocorrelation function, presented on the right of Figure 3-9, its general

shape is similar to the one of a BOC(1,1) with small deformations. This deformation is created by the BOC(6,1) component of the CBOC.

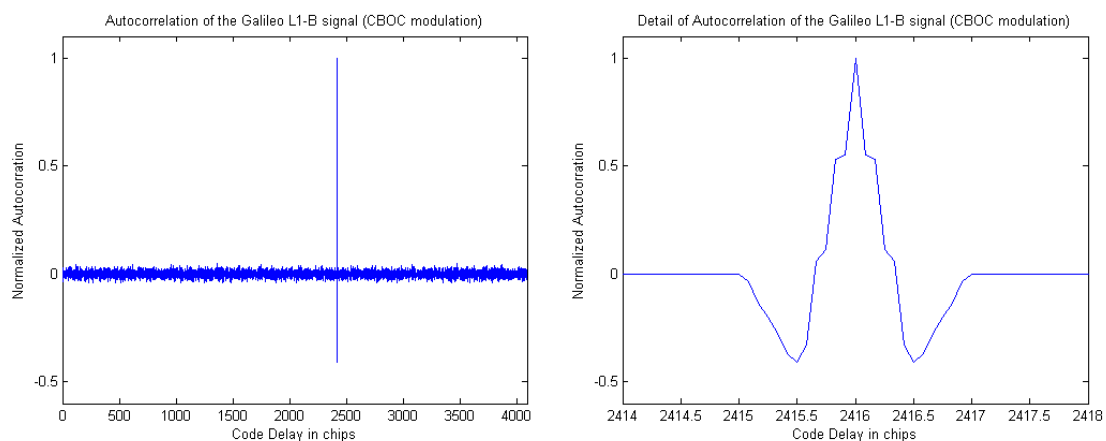


Figure 3-9: Example of autocorrelation of the Galileo codes for the data channel (on the left) and its detail (on the right)

3.3 Galileo L1 Signal Model

First, let us consider the signal model for the signal that will be broadcast by the future Galileo satellites on the L1 band. At the receiver level, and taking into account the propagation time, the Galileo Open Service L1 signal transmitted by one satellite can be expressed as follow:

$$s_{L1}(t_{Galileo}) = \frac{1}{\sqrt{2}} \left(\begin{array}{l} d_{L1-B}(t_{Galileo} - \tau_{L1}(t_{Galileo})) \cdot c_{L1-B}(t_{Galileo} - \tau_{L1}(t_{Galileo})) \cdot sc_{CBOC}(t_{Galileo} - \tau_{L1}(t_{Galileo})) \cdot \\ \cos(2 \cdot \pi \cdot (f_{L1} + f_{Dtotal}) \cdot t_{Galileo} + \phi_{L1}) \\ -c_{sec}(t_{Galileo} - \tau_{L1}(t_{Galileo})) \cdot c_{L1-C}(t_{Galileo} - \tau_{L1}(t_{Galileo})) \cdot sc_{CBOC}(t_{Galileo} - \tau_{L1}(t_{Galileo})) \cdot \\ \cos(2 \cdot \pi \cdot (f_{L1} + f_{Dtotal}) \cdot t_{Galileo} + \phi_{L1}) \end{array} \right) + w(t) \quad (3.4)$$

where s_{L1} is the L1 OS signal

$t_{Galileo}$ is the Galileo time

τ_{L1} is the time delay due to the propagation between the satellite and the receiver

including the delay induced by the atmospheric clock delays

d_{L1-B} is the data bit of the binary NRZ navigation message of the data channel

c_{L1-B} and c_{L1-C} are the L1 ranging code on the data and pilot channel respectively

sc_{CBOC} is the subcarrier CBOC modulation (see previous paragraph)

c_{sec} is the secondary code on the pilot channel

f_{L1} is the Galileo L1 central frequency (1575.42 MHz)

f_{Dtotal} is the Doppler frequency due to the satellite and user motion plus the

Doppler shift due to atmospheric and clock errors

ϕ_{L1} is the initial L1 phase in radians

$w(t)$ is the noise approximated as Gaussian with zero mean.

The carrier phase and code delay can be defined using a similar method as for GPS L1 C/A in Chapter 2 section 2.1.2.

Finally, concerning the signals broadcast by GIOVE-A on L1, the L1-B and L1-C signals can be expressed as follows (GIOVE-A SIS ICD 2007):

$$s_{L1-B}(t_{Galileo}) = \sum_{i=-\infty}^{+\infty} \left[\begin{array}{l} c_{L1-B,|i|_{L1-B}} \cdot d_{L1-B,[i]_{DC_{L1-B}}} \cdot \text{rect}_{T_{C,L1-B}}(t_{Galileo} - i \cdot T_{C,L1-B}) \cdot \\ \text{sign}[\sin(2\pi \cdot R_{S,L1-B} \cdot t_{Galileo})] \end{array} \right] \quad (3.5)$$

$$s_{L1-C}(t_{Galileo}) = \sum_{i=-\infty}^{+\infty} \left[\begin{array}{l} c_{L1-C,|i|_{L1-C}} \cdot \text{rect}_{T_{C,L1-C}}(t_{Galileo} - i \cdot T_{C,L1-C}) \cdot \\ \text{sign}[\sin(2\pi \cdot R_{S,L1-C} \cdot t_{Galileo})] \end{array} \right] \quad (3.6)$$

and the total baseband signal on L1 (without L1-A) can be written as:

$$s_{L1}(t_{Galileo}) = \frac{1}{\sqrt{2}} [s_{L1-B}(t_{Galileo}) - s_{L1-C}(t_{Galileo})] \quad (3.7)$$

using the following notations:

- s_{L1-B} and s_{L1-C} are the L1-B and L1-C signals, including the code, the subcarrier, the modulation and the data
- $c_{L1-B,|i|_{L1-B}}$ and $c_{L1-C,|i|_{L1-C}}$ are the ranging codes of the L1-B and L1-C components
- $d_{L1-B,[i]_{DC_{L1-B}}}$ is the navigation message
- $\text{rect}_{T_C}(t)$ is a “rectangle” function (defined to equal to one between 0 and T_C and 0 elsewhere)
- $R_{S,L1-B}$ and $R_{S,L1-C}$ are the subcarrier frequencies of L1-B and L1-C (used in the BOC modulation)

Here $R_{S,L1-B} = R_{S,L1-C} = 1.023\text{MHz}$

3.4 Cross Correlation Properties of the Galileo L1 Open Service Signal

As mentioned in the previous chapter, one of the important properties of the codes is their cross correlation performance. The same method as was used in the previous chapter for GPS L1 C/A and L1C is used here for Galileo L1-B and L1-C. First, the cross correlation protection of the Galileo L1 OS codes for the data and pilot channels (including the CBOC modulation) is computed. Then, the cross correlation performance is studied considering various Doppler offsets.

For the Galileo codes, the correlation protection in the absence of Doppler or sampling was found to be about 28 dB for both the data and pilot channels and about 28 dB as well for the cross correlation between the pilot and data channel.

More specifically, if one looks at the cross correlation of the PRN codes 1 and 2, in 50 % of the cases there is a protection of 45 dB or more for the L1 data and pilot channels or the cross correlation between the pilot and the data channel as shown in Figure 3-10. As can be seen in the figure, the pilot channel alone performs the same as the data channel alone and the data channel cross correlated with the pilot channel. For this figure, the PRN 1 has been chosen as an example to compute the cross correlation of the data and pilot channel. However, the performance is similar if other PRNs are considered. As mentioned, the data and pilot channels have the same performance, which was expected since they have the same modulation. Therefore, only the results for the data channel are shown here. Similar results can be found for all other cross correlation products.

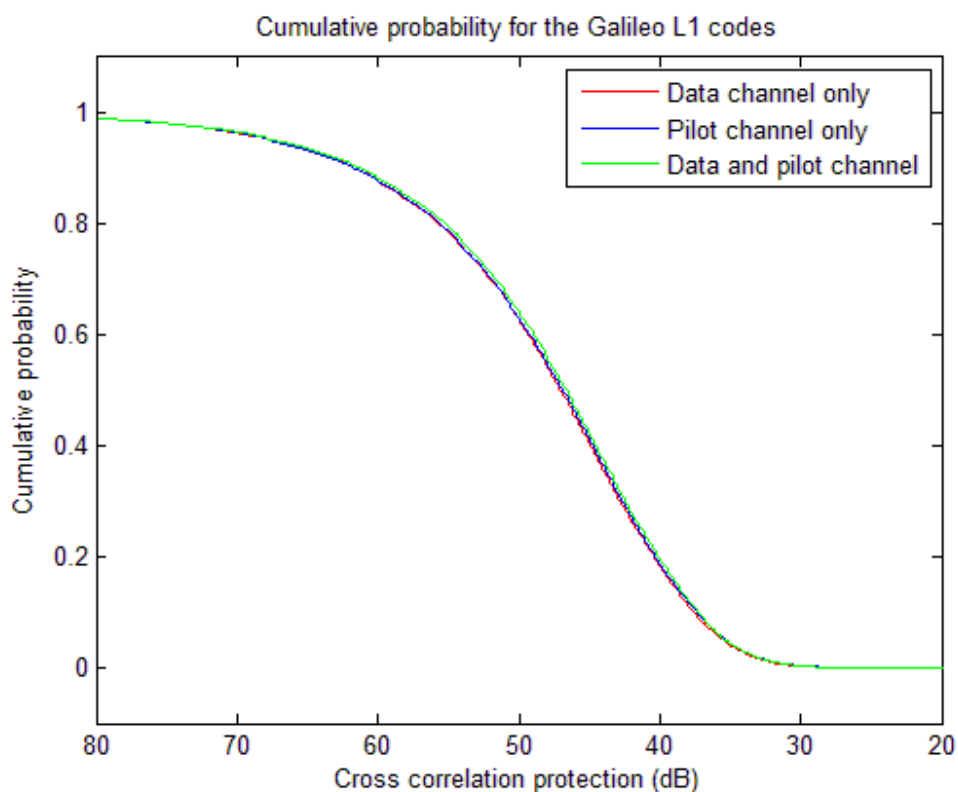


Figure 3-10: Cumulative probability for the pilot and data channels of Galileo L1 for PRN 1

The same process is now repeated but using a sampled code. Due to the CBOC modulation, a sampling rate of 15 MHz is chosen in order to keep most of the signal power. The results with sampling are presented in Figure 3-11. As can be seen, the results with and without sampling give almost the same performance. Indeed, due to the CBOC modulation, for each chip of the primary code, 12 chips of the subcarrier are created and therefore it is equivalent to scaling the chipping rate by 12. Thus, due to the high number of chips, the curve is already “smooth” to the naked eye. Therefore, sampling the code,

while sampling more the curve, does not significantly change the results as in the case of the TMBOC on GPS L1C.

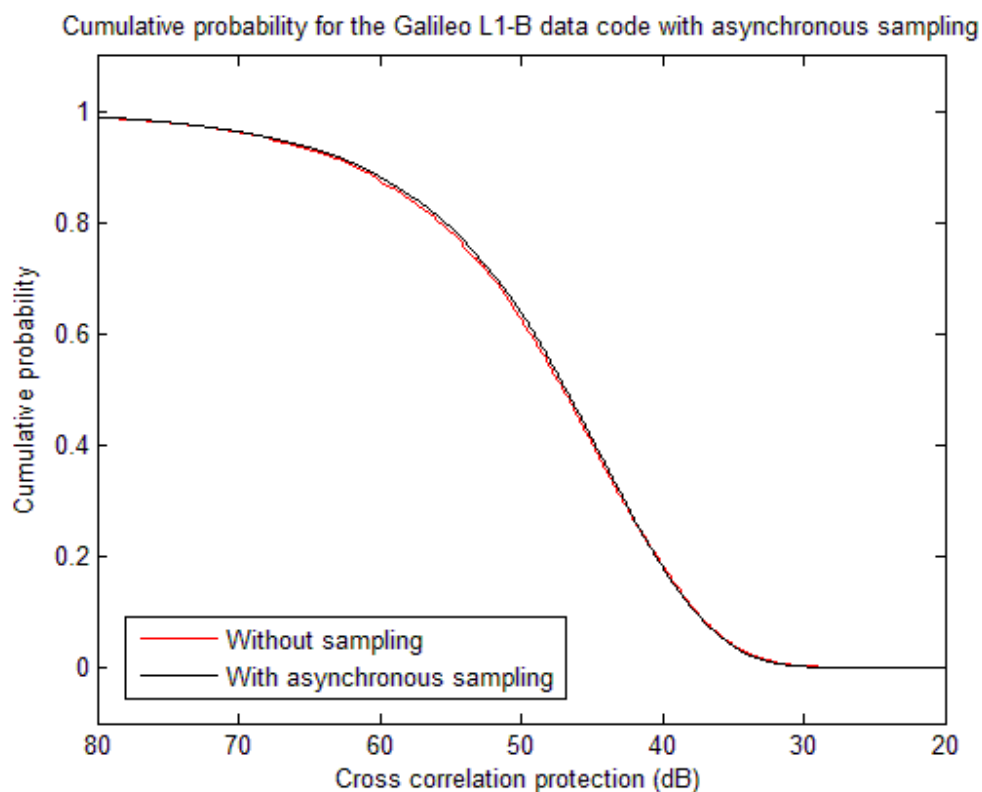


Figure 3-11: Cumulative probability for the Galileo L1-C pilot code with and without sampling

Finally, the impact of the Doppler offset between two codes being correlated is studied. The range of Doppler offsets considered is from 0 to 1000 Hz and the results for the data channel are shown in Figure 3-12. All these results have been obtained using 15 MHz sampling rate (for the reasons explained above). Finally, it is noted that both the code Doppler and carrier Doppler have been simulated.

First, the results obtained in the case of no Doppler offset are exactly the same as those in Figure 3-11. This was to be expected since for zero Doppler the carrier wave is completely removed before the correlation and therefore the results are the same as without a carrier. As seen in the figure, one experiences a small degradation due to a Doppler shift. The degradation increases with the Doppler offset. All these results have been obtained using the cross correlation of PRNs 1 and 2 but similar results would be obtain with other PRNs. All the simulations have been done using a simulation in Matlab.

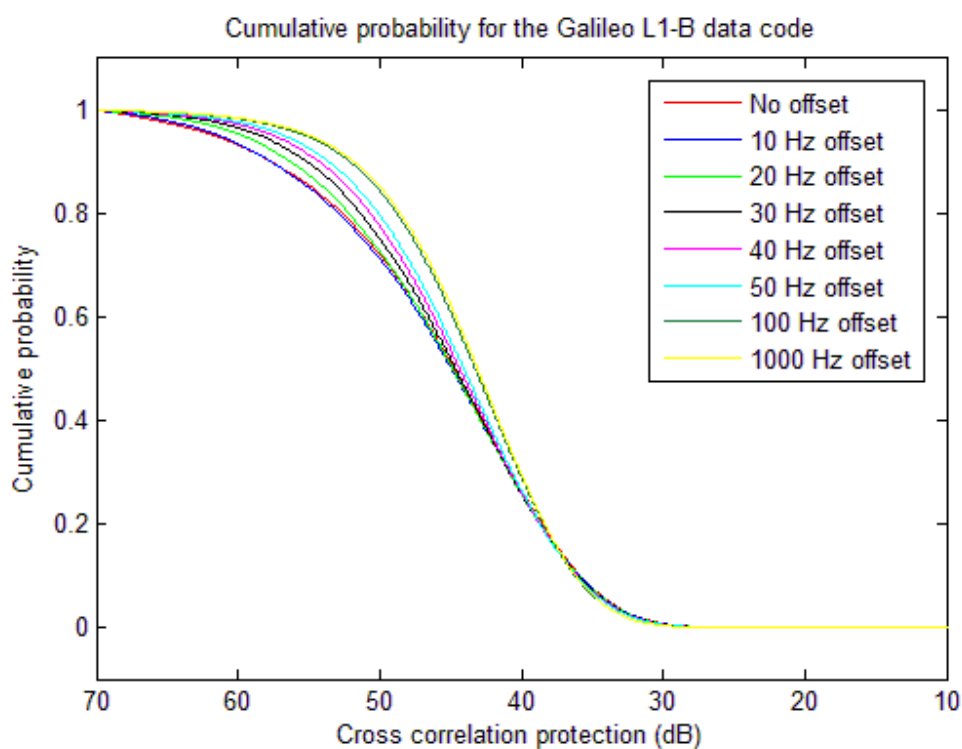


Figure 3-12: Cumulative probability for the Galileo L1-B channel for various Doppler offsets ranging from 0 to 1000 Hz

The Galileo L1 OS signal is very similar to the GPS L1C signal and the performance of each signal individually should be similar (the main difference being the sharing of the power between the data and the pilot channel). However, the combination at the position level of the two constellations would increase the reliability and accuracy of the solution in position.

Chapter Four: GPS AND GALILEO L1 SOFTWARE SIGNAL SIMULATOR

This chapter begins with a brief overview of the structure of the software signal simulator developed herein. Indeed, as mentioned in the previous chapters, since the GPS L1C and Galileo signals are not broadcast yet, a software signal simulator is needed in order to test the algorithms of acquisition and tracking developed in this thesis. A particular emphasis is given to the implementation of the main functions included in the software signal simulator. Then, the interference sources used in the next chapters are described and their implementation is explained. Finally, the derivation of the oscillator model developed in this thesis is described in detail and the Allan variance computed using samples generated by this method is compared to those of standard oscillators.

The software signal simulator is a “C”-based GNSS simulator software program and is an enhanced version of the IFG2Sim™ (Intermediate Frequency GPS and Galileo Simulator) developed by Macchi et al (2008) in the PLAN Group at the University of Calgary. This software is able to simulate raw samples of the L1 frequency of the OS (Open Service) signals of GPS and Galileo at an intermediate frequency (IF). The software generates IF samples for static or mobile users using one bit quantization. The software simulates the signal at the output of a front-end taking into account only white noise; possible interference sources and satellite clock errors, i.e. multipath, orbital, receiver clock errors and atmospheric errors are not simulated.

The signal software signal simulator is able to simulate IF samples at the output of a fictitious GNSS receiver front-end. The signals simulated are GPS L1 C/A, L1C (pilot and data channels) and the Galileo OS L1 signals (L1-B and L1-C) as described in each system's Interface Control Documents (IS-GPS-200D 2004 for GPS and OS SIS ICD Draft 1 2008 for Galileo). Two versions of the software signal simulator were developed for the Galileo signal: one with only a BOC(1,1) modulation and a second one with a CBOC modulation composed of a combination of BOC(1,1) and BOC(6,1) codes. The former version has been developed because it allows for a lower sampling rate (and thus bandwidth), which is of interest to many receiver developers and it is interesting to study the difference in performance between the two modulations as shown in the next chapters. The intermediate frequency is fixed to 1.25 MHz in the case of the BOC and 7.5 MHz in the case of the CBOC to avoid aliasing. The version with BOC has a fixed sampling frequency of 5 MHz (due to the necessary bandwidth to have the main lobe of the BOC(1,1)) and a fixed sampling frequency of 30 MHz for the CBOC version (due to the necessary bandwidth of the CBOC). Note that due to its smaller sampling rate, the version with the BOC(1,1) modulation is able to simulate samples in real time. Furthermore, in both versions, the modulated navigation message is as described in Draft 1 of the Galileo ICD.

The signal simulated by the software is presented in Figure 4-1. Please note that the orbital error, ionosphere and troposphere are not simulated here since the focus of this thesis is on signal acquisition and tracking and not the corresponding position domain solution. Multipath is not simulated either since it is not a focus of this thesis. However, it

is noted that extreme ionospheric conditions such as scintillation may also affect signal tracking, although not dealt with here.

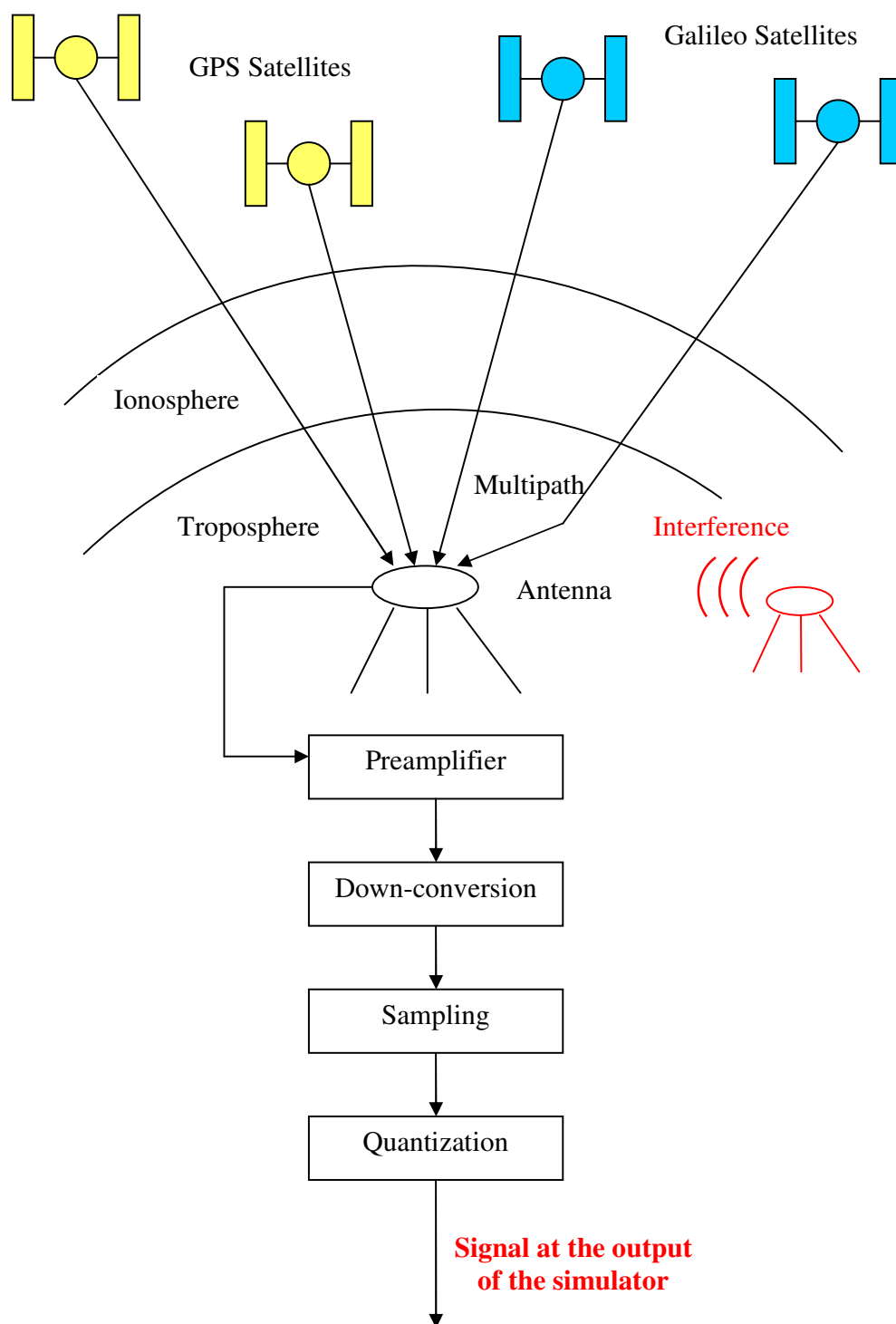


Figure 4-1: Signal simulated by the software signal simulator

4.1 Overview of the software signal simulator structure

The high level operation of the software signal simulator is presented in Figure 4-2. The software signal simulator needs the followings files as input:

- Trajectory Option File containing the parameters defining the motion of the user
- Option File containing all the options of the simulators (except the motion)
- Galileo Almanac File containing the almanac parameters for Galileo
- GPS almanac File containing the almanac parameters for GPS

The outputs of the software signal simulator are the following files:

- Signals Output File containing the samples of the signals simulated
- Trajectory File containing the trajectory of the user over time
- Oscillator error containing the error generated by the satellite oscillator at each sample
- True phase
- True Code delay

The advantage of a software signal simulator is the flexibility: the parameters can be changed easily and all the variables can be output if necessary.

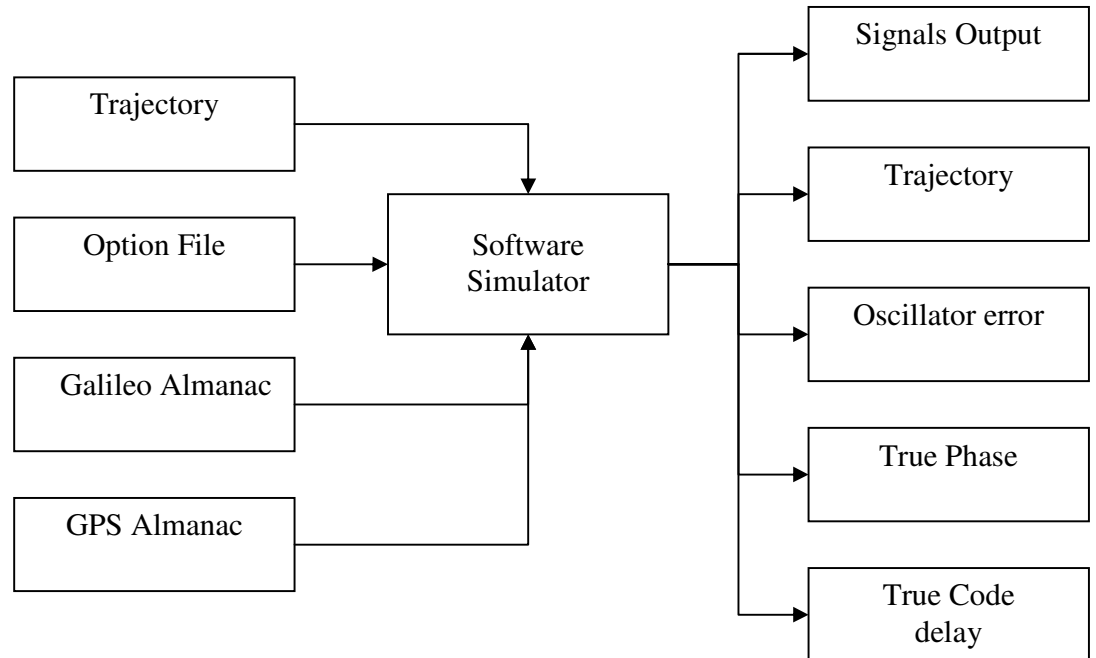


Figure 4-2: Top level architecture diagram of software signal simulator

The general structure of the simulator as well as the main functions and the links between them are presented in Figure 4-3. The main steps of the signal generation shown in the flow diagram are the following:

- Initialization including the initialization of the variables and the creation of the user motion
- A cubic spline interpolation is used to compute the position of the satellites over time. Every cubic spline interval (set at 60 s for all the results of this thesis as explained in Section 4.1.2) has the following functions:
 - Check the visible satellites and compute the cubic spline coefficients used to compute the position of the satellites

- If a satellite just became visible, create the corresponding navigation message (for GPS and Galileo)
 - Generate signal for all the channels (L1 C/A and L1C pilot and data for GPS and L1-B and L1-C for Galileo respectively) of one satellite
 - Repeat the previous step until all the satellites in view of the two constellations have been simulated
 - Add the signals from all the satellites of the two constellations (this step and the two previous ones are done every millisecond to save memory)
 - Write the generated samples to a file (includes quantization and the adding of the noise)
- Check if all the requested data have been simulated and exit the program

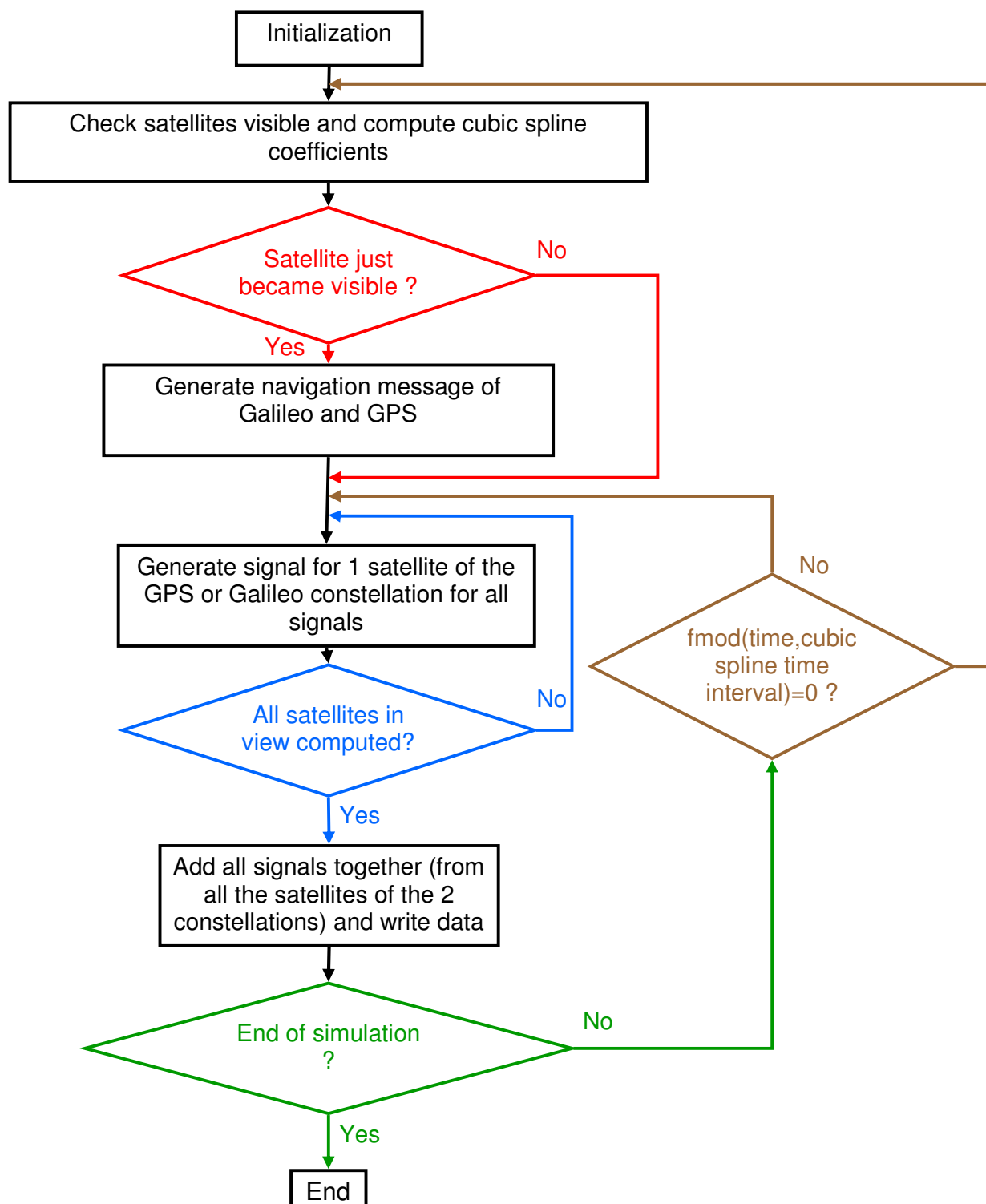


Figure 4-3: Flow Diagram of software signal simulator

All the steps of the flow diagram are presented into more detail in the following sections.

4.1.1 Initialization phase

The first step of the software signal simulator is the initialization phase. The initialization includes the following steps:

- Read the GPS and Galileo almanac files and store the parameters in memory
- Read the option file which contains the following values:
 - Signal over noise ratio C/N_0 (same for all the satellites)
 - Cut-off angle (angle under which the satellites are not considered visible anymore, a typical value is 5 degrees)
 - The start time (expressed in seconds since the beginning of the current GPS week) and the simulation time
 - The cubic spline interval which represents the interval over which the cubic spline coefficients used to compute the satellite position are computed (more details on this are given in the next paragraph)
 - The position of the user (at the beginning of the simulation)
 - Parameters for potential interference (see later in this chapter for details)
- Generate the user motion (the functions used to generate the user motion were provided by Professor M. Petovello). Combination of linear and circular motions with the choice of velocity and acceleration can be generated as follow:
 - Read the user motion file
 - Generate the user position over time until the end of the simulation

- Write the position and velocity of the user over time in a file
- Create a table of cosine values to speed up the processing time. There is no need to create a table of sine values since $\sin(x) = \cos\left(\frac{\pi}{2} - x\right)$
- Create a table of Gaussian noise to speed up the processing time. The table created contains 12 millions values to avoid correlation of the signal in case of long integration times in the acquisition process.
- Create a file to write the satellite clock error over time (see Section 4.3 of this chapter for more details)
- Generate the GPS PRN codes for L1 C/A and L1C (pilot and data channels)
- Generate Galileo L1B and L1C ranging codes
- Allocate all the necessary memory for the entire simulation

4.1.2 Cubic spline interpolation

Once the initialization phase is done, a cubic spline interpolation is used for each satellite in view in order to estimate its position over time. The position of the satellite is computed when the satellite sent the signal received at time t by the receiver.

The first step is to compute the position of each satellite in view at the time it sent the signal received at t by the receiver. To compute this position, an iterative process is used:

- 1) Compute the position of each satellite in turn, $P_{sat}(t)$, at t using the almanac parameters and applying the equations of the corresponding Interface Control Documents (IS-GPS-200D 2004 for GPS and OS SIS ICD Draft 1 2008 for

Galileo). Check if the satellite is visible (elevation higher than the elevation mask in the option file) and if it is, proceed to the next steps. If not, do the same computations for the next satellite.

- 2) Compute the transit time $t_{transit}$ using the following relation:

$$t_{transit} = \frac{|P_{sat}(t) - P_{rx}(t)|}{c} \quad (4.1)$$

where $P_{rx}(t)$ is the position of the receiver at t

- 3) Compute the position of the satellite at $t - t_{transit}$ using the almanac parameters
- 4) Rotate the position of the satellite from the ECEF frame at $t - t_{transit}$ to the frame at time t (this rotation accounts for the rotation of the Earth during the propagation of the signal from the satellite to the receiver):

$$P_{sat}(t) = \begin{bmatrix} \cos(\omega_e \cdot t_{transit}) & \sin(\omega_e \cdot t_{transit}) & 0 \\ -\sin(\omega_e \cdot t_{transit}) & \cos(\omega_e \cdot t_{transit}) & 0 \\ 0 & 0 & 1 \end{bmatrix} P_{sat}(t - t_{transit}) \quad (4.2)$$

where ω_e is the rotation rate of the Earth

- 5) Compute the new transit time $t_{transit2}$
- 6) If $|t_{transit2} - t_{transit}| \geq 1.10^{-11}$ then $t_{transit} = t_{transit2}$ and go back to the third step. If not, keep the last position of the satellite computed.
- 7) Proceed the same way for all satellites in view.

Compute the position of all the satellites in view at the time they sent the signal received at time $t + t_{CubicSpline}$ (where $t_{CubicSpline}$ is the cubic spline interval in the option file, fixed to 60 seconds through this thesis) using the same method as above. Note that the position of the receiver may not be the same at the beginning and the end of the cubic spline interval (due to possible motion). This is taken into account in the computation of the satellite position (step 2 above).

Compute the velocity of the satellites in view at the time it sent the signal received at times t and $t + t_{CubicSpline}$. The corresponding equations for compute the satellite velocity are shown in Appendix A.

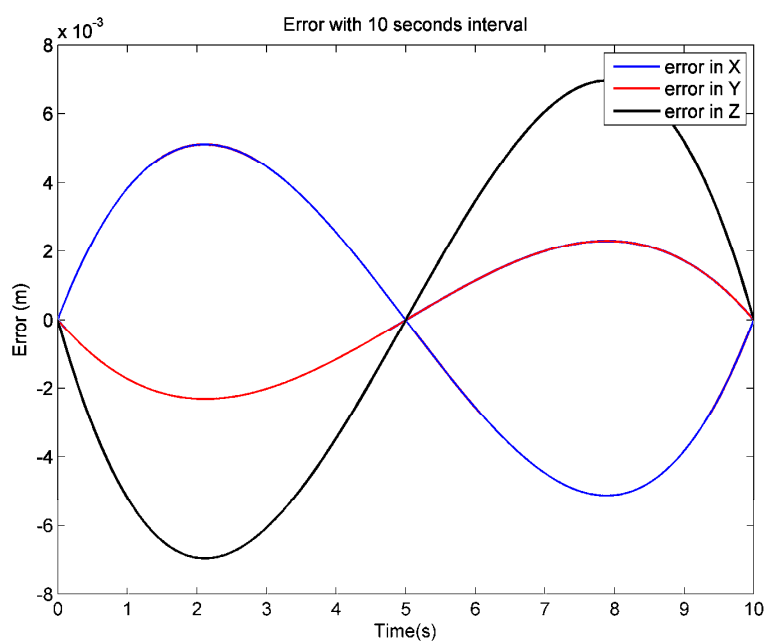
As stated above, a cubic spline interpolation is used to approximate the positions of the satellites over time. Specifically, each segment of the spline spans a time of $t_{CubicSpline}$ (60 s herein). A cubic spline is computed as

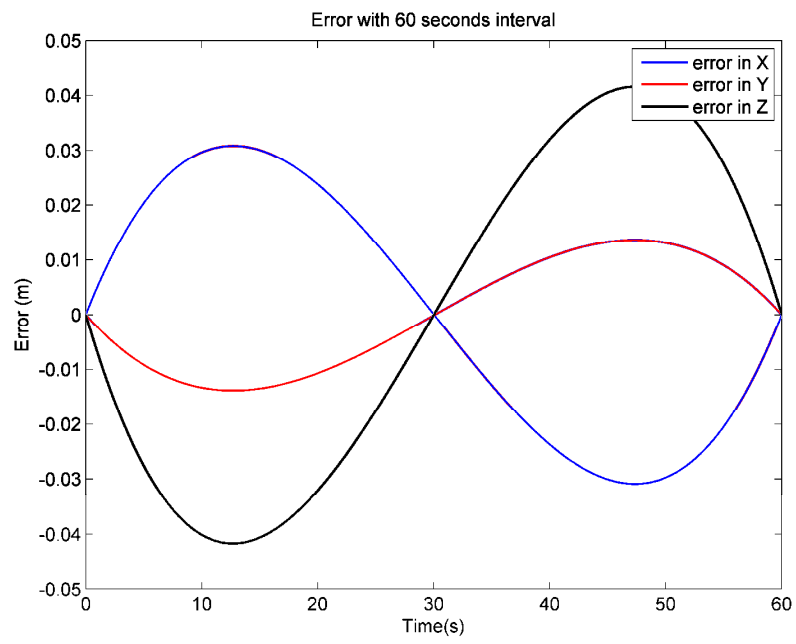
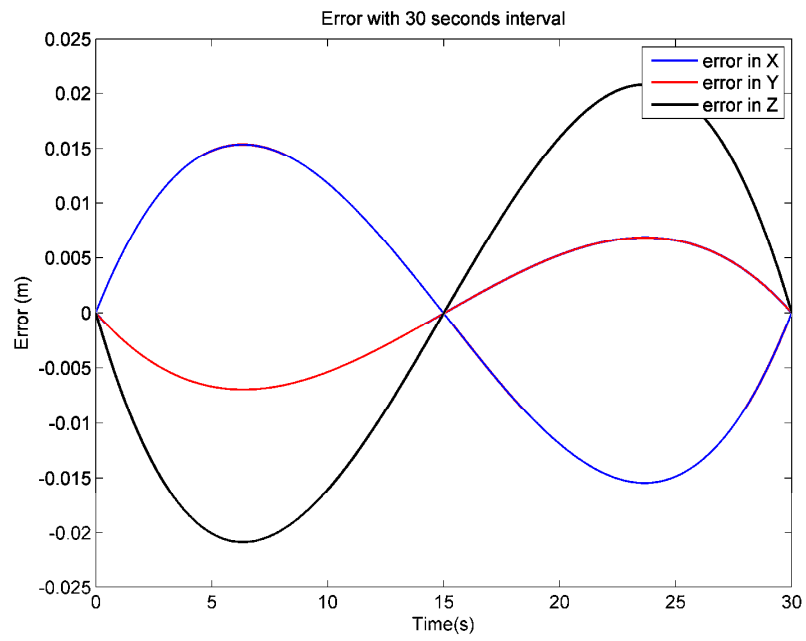
$$P_{sat}(t) = a + b \cdot t + c \cdot t^2 + d \cdot t^3 \quad (4.3)$$

where a , b , c and d are the spline coefficients. With this in mind, the cubic spline coefficients between the times t and $t + t_{CubicSpline}$ are computed using the position and velocity at the end points.

In order to validate this method and to choose the interval between two cubic spline interpolations, several tests were performed in static and dynamic mode with various

intervals and the error generated using the interpolation was computed. Here, only the results in static mode with intervals of 10, 30, 60 and 300 seconds are shown. The results with a moving receiver are very similar. The results are shown in Figure 4-4. As it can be seen and as expected, the error increases in the three axes with the length of the interval. A tradeoff between the magnitude of the error and the processing time (the process described above is time consuming due to the required iterations when computing the satellites) is therefore necessary and the interval is fixed at 60 seconds for all the tests of this thesis.





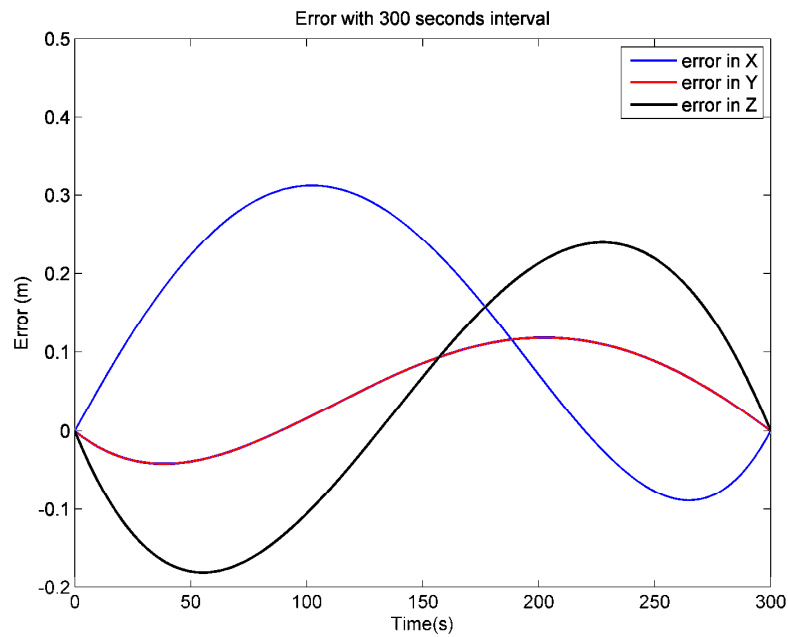


Figure 4-4: Error in the X, Y and Z axis for a static receiver using a cubic spline with an interval of 10, 30, 60 and 300 seconds

The error stays reasonable with an interval of 60 seconds without adding too much computation time. Therefore, the cubic spline interval is fixed at 60 seconds in all the following. A method to decrease the error without increasing the computation load significantly would be to increase the degree of the polynomial approximation.

4.1.3 Generation of the navigation message

For each cubic spline interval, the satellites in view are checked and the necessary navigation messages are created for new satellites. In order to generate the navigation message, the following steps are completed:

- Compute the number of frames to simulate: since only short simulations are considered in this thesis (a few minutes at the maximum), the navigation message can be created from the appearance of the satellite until the end of the simulation without experiencing any memory problems.
- Generate the navigation message frame by frame. However, only the first three frames of the navigation message are generated for L1 C/A, because these three frames contain all the necessary information to compute the position and velocity of the satellite at the user receiver. The subframes 4 and 5 contain information on other satellites and on the ionosphere, therefore there is no impact on the work of this thesis.
- Compute the bit of the navigation message to be transmitted when the satellite becomes visible (or at the beginning of the simulation depending on the case).
- Update the TOW (Time of Week) for each subframe (time at the beginning of the current subframe for Galileo and time at the beginning of the next subframe for GPS). The parity sequence (in the case of GPS C/A) and the CRC (Cyclic Redundancy Check) for Galileo are computed at each frame to take into account the change in TOW.

Since the Galileo system had not been deployed at the time of this thesis, some of the parameters of the Galileo navigation message are unknown and are set to zero in the simulated navigation message.

4.1.4 Generation of the signal broadcast by one satellite

One of the most important parts of the software simulator is the generation of the carrier frequency modulated by the ranging code and the data bits. In Figure 4-5, the flow diagram of the generation of the signal for one satellite for one millisecond is presented.

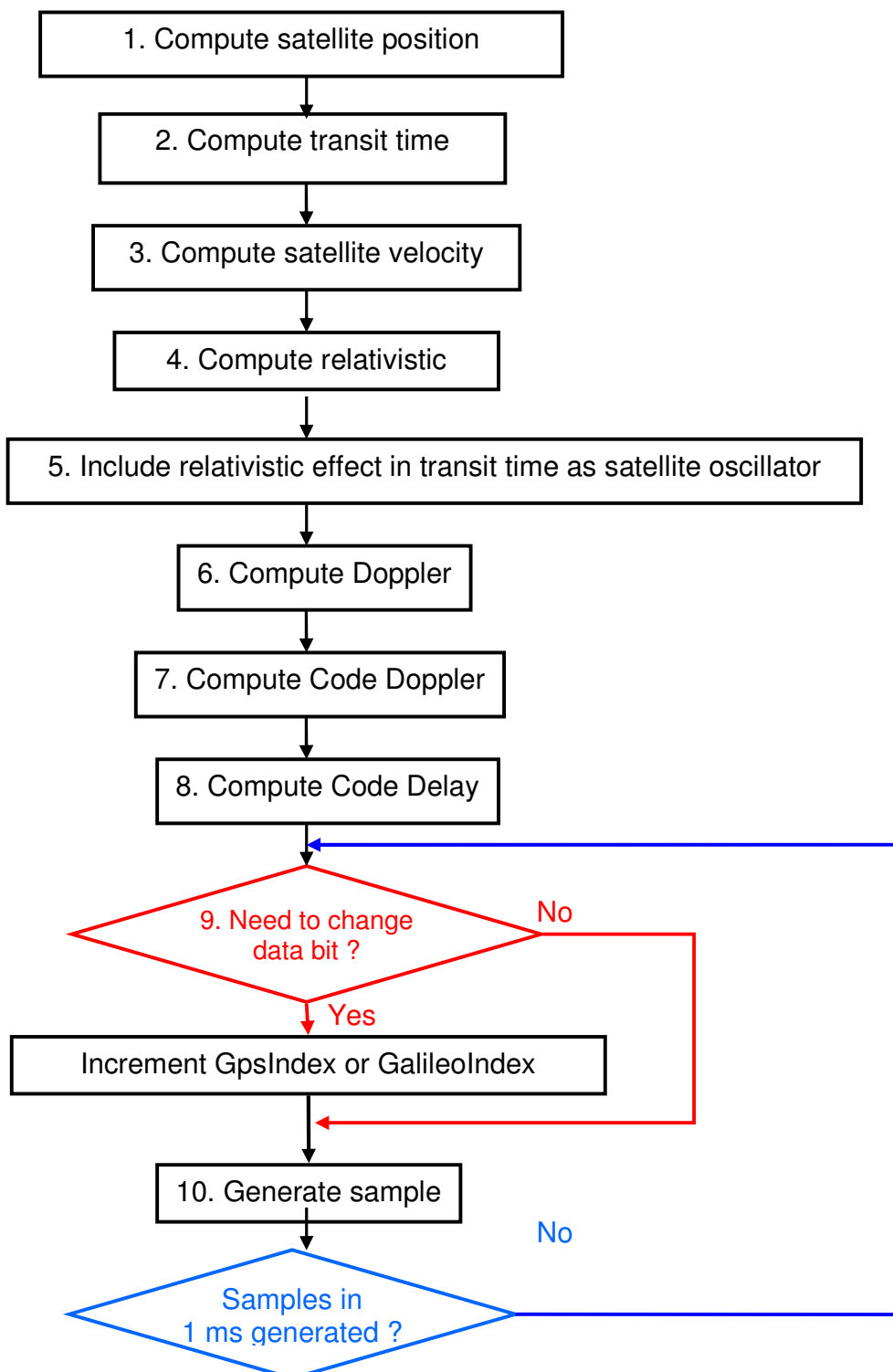


Figure 4-5: Flow chart of the signal generation

The signal generation for one satellite can be divided in several steps:

1. Computation of the satellite position: this is done using the cubic spline coefficients computed earlier. The position of the satellite is computed at the time the satellite sent the signal and not at the time the signal was received (see Section 4.1.2 on the cubic spline coefficients).
2. Computation of the transit time (namely the time needed for the signal to travel from the satellite to the receiver): the distance between the satellite and the receiver is computed and then divided by the speed of light to obtain the transit time.
3. Computation of the satellite velocity: this is also done using the cubic spline coefficients.
4. Computation of the relativistic effect: Due to the motion of the satellite relative to the user, the theory of Special Relativity states that the clock on board the satellite ticks slower than if there was no relative motion (Katz 1964). This effect is taken into account using the following (IS-GPS-200D 2004):

$$\text{Relativistic Effect} = \frac{-2 \cdot \vec{R} \cdot \vec{V}}{c^2} \quad (4.4)$$

where \vec{R} is the position of the satellite in the ECEF frame

\vec{V} is the velocity of the satellite in the ECEF frame

5. Include relativistic effect in transit time: the transit time needs to be recomputed in order to take into account the relativistic effect as satellite oscillator error.
6. Computation of the Doppler effect: the Doppler is computed using the velocity of the satellite relative to the receiver projected on the satellite-receiver vector:

$$f_D = \frac{v_r}{c} \cdot f \quad (4.5)$$

where f_D is the Doppler frequency

v_r is the relative velocity satellite-receiver projected on the satellite-receiver vector

f is the frequency of the GPS or Galileo signal

7. Computation of the code Doppler:

$$c_D = \frac{f_c}{f} \cdot f_D \quad (4.6)$$

where c_D is the code Doppler

f_c is the chipping rate

8. Computation of the code delay c_{delay} , for example in the case of L1 C/A:

$$c_{delay} = \text{fmod}(\text{transit time} \cdot 1.023 \cdot 10^6, 1023) \quad (4.7)$$

This is computed similarly for the other signals.

9. Check if the data bit needs to be changed each ranging code period. This will depend on the signal considered.

10. Generation of the signal itself according to the signal models presented in the previous chapters using the table of cosines created in the initialization phase to reduce the processing time.

4.1.5 Generation of the samples of the signal at the front-end level

Finally, once the signals for all the satellites in view for both constellations have been generated, a few steps remain:

- Add all the signals from both constellations for all the satellites in view taking into account the relative power between the different channels of the two constellations:
 - The signal over noise ratio for GPS L1 C/A can be expressed as:

$$\frac{C}{N_0} \Big|_{C/A} = \frac{A_{C/A}^2}{2} \cdot \frac{f_s}{2\sigma^2} \quad (4.8)$$

where $\frac{C}{N_0} \Big|_{C/A}$ is the signal over noise ratio for GPS L1 C/A

$A_{C/A}$ is the amplitude of the GPS L1 C/A signal

f_s is the sampling frequency

σ is the noise variance

- $\frac{C}{N_0} \Big|_{C/A}$ is known from the option file, $A_{C/A}$ is fixed to one and σ is computed accordingly
- Similar relation can be written for the other signals. The difference in power between the signals being known, the signal over noise ratio of the other signals is computed as a function of the one of GPS L1 C/A.

- Since the noise variance is the same for all the signals (noise is generated and added as explained below), the relative amplitude of each signals can be computed accordingly.
- Generate interference as specified in the option file and add it to the signal. Details regarding the generation of the interference signals are given in Section 4.2.
- Add the noise according to the C/N_0 using the table of Gaussian noise generated during the initialization to speed up the processing time.
- Quantize the samples (1-bit quantization) and write them into a file.

4.2 Generation of interference

In the later chapters, the MBOC modulation (implemented as a CBOC for Galileo and a TMBOC for GPS L1C) is approximated by a BOC(1,1) in the acquisition and tracking algorithms developed. Nevertheless, the effect on the acquisition and tracking sensitivity and accuracy generated by this approximation is first assessed. To do this, several tests are done in various conditions, including under the presence of interference sources. Therefore, two types of interference are simulated in the software signal simulator: continuous wave (CW) interference and narrowband interference. These two types of interference are presented in the following sections.

4.2.1 Continuous Wave (CW) Interference

The first type of interference considered is the CW (Continuous Wave) interference. The CW interference is an interference that can be represented by a pure sinusoid (Borio 2008). This interference can be generated from harmonics of various sources, as shown in Table 4-1 (Landry & Renard 1997).

Table 4-1: Sources and services of interference v/s harmonics (from Landry & Renard 1997)

ORDER	BAND (MHz)	USAGE
L1	1571.42 - 1579.42	C/A-GPS
2 th	785.71 - 788.71	UHF TV
3 th	523.807 - 526.473	UHF TV
4 th	392.855 - 394.855	Mobile/Station
5 th	314.284 - 315.884	Mobile/Station
6 th	261.903 - 263.237	Mobile/Station
7 th	224.488 - 225.631	Broadcasting
8 th	196.427 - 197.428	VHF TV
9 th	174.602 - 175.491	VHF TV
10 ^h	157.142 - 157.942	VHF Maritime
11 th	142.856 - 143.584	VHF Military
12 th	130.952 - 131.618	VHFCOM
13 th	120.878 - 121.494	VHFCOM
14 th	112.244 - 112.816	VOR/ILS
15 th	104.761 - 105.295	FM
16 th	98.214- 98.714	FM

The harmonics of TV emitters that can interfere with GNSS signals in the L1 band are presented in Figure 4-6 (Landry & Renard 1997).

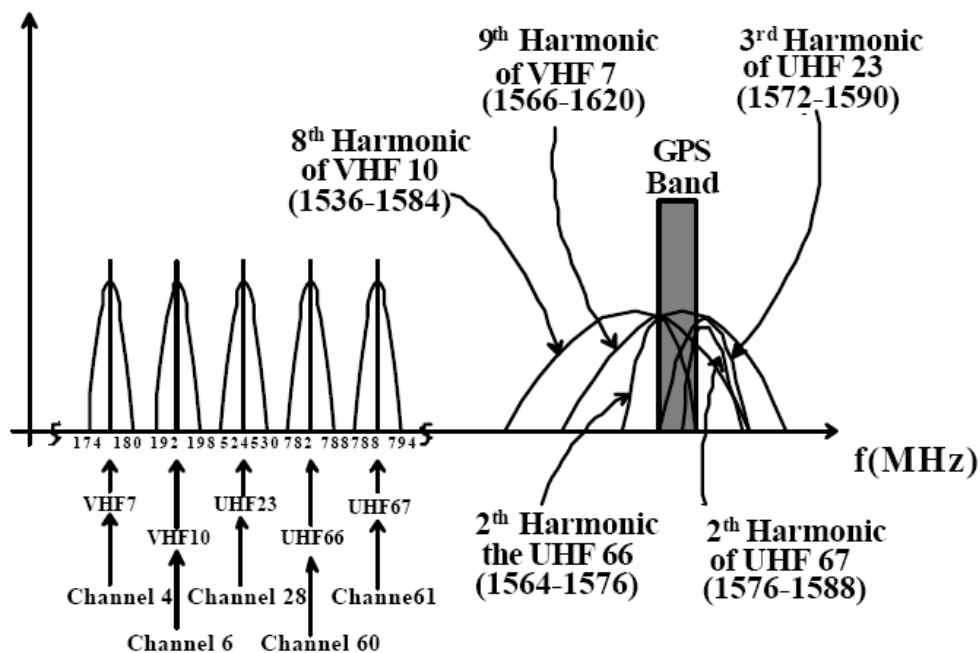


Figure 4-6: Potential TV interference (from Landry & Renard 1997)

The equation of a CW interference can be expressed as (Borio 2008):

$$i(t) = A \cdot \cos(2 \cdot \pi \cdot f \cdot t + \theta) \quad (4.9)$$

where i is the interference

A is the interference amplitude

f is the interference frequency

t is the time

4.2.2 Narrowband interference

The second type of interference considered is narrowband interference. Narrow refers here to a small bandwidth compared to the GPS frequency. Sources of narrow band interference in the L1 band include (Borio 2008):

- FM, VHF, UHF emitters (especially TV)
- Inter-system and intra-system GNSS interference
- Personal Electronic Devices

One way to generate narrowband interference is to generate white noise and to pass it through a band pass filter. More details on this and the type of filter used are presented in Appendix C. The variance of the Gaussian noise depends on the power of the interference and the bandpass filter used depends on the choice of the cut off frequency. The magnitude responses of two Butterworth band pass filters (one for each set of parameters) used in this thesis are shown in Appendix C.

4.3 Oscillator model

A Kalman filter for tracking is developed in Chapter 6 and among other parameters, the impact of different oscillators on the performance of the tracking is tested. Therefore, an oscillator model has been developed and implemented in the simulator. The development of the model and its validation is shown below.

4.3.1 Model in the Continuous Domain

The following model follows closely the model shown in Winkel (2003). However, an error has been found in the term concerning the Flicker noise in the aforementioned model. Therefore, a new model is shown here in order to solve for the Flicker noise using another method. The spectral density of the normalized frequency error of an oscillator can be expressed as a function of the oscillator's h parameters as follows (Winkel 2003):

$$S_y(f) = \sum_{\alpha=-2}^2 h_{\alpha} \cdot f^{\alpha} = \frac{h_{-2}}{f^2} + \frac{h_{-1}}{f} + h_0 + f \cdot h_1 + f^2 \cdot h_2 \quad (4.10)$$

or

$$S_y(w) = \frac{4\pi^2 h_{-2}}{w^2} + \frac{2\pi h_{-1}}{w} + h_0 + \frac{wh_1}{2\pi} + \frac{w^2 h_2}{4\pi^2} \quad (4.11)$$

where y is the ratio of the frequency errors δf normalized by the desired frequency,

$$\text{that is: } y \approx \frac{\delta f}{f_0}$$

$w = 2\pi f$ is the angular frequency and f is the frequency in Hz

S is the spectral density

h_i are the h parameters of the oscillator (see Table 4-2)

f_0 is the nominal frequency of the oscillator

Table 4-2 lists some sample h values for various oscillators.

Oscillator	White freq. noise (h_0)	Flicker (h_{-1})	Integrated freq. noise (h_{-2})
Standard quartz	$2 \cdot 10^{-19}$ s	$7 \cdot 10^{-21}$	$2 \cdot 10^{-20}$ Hz
TCXO	$1 \cdot 10^{-21}$ s	$1 \cdot 10^{-20}$	$2 \cdot 10^{-20}$ Hz
OCXO ¹	$8 \cdot 10^{-20}$ s	$2 \cdot 10^{-21}$	$4 \cdot 10^{-23}$ Hz
OCXO ²	$2.51 \cdot 10^{-26}$ s	$2.51 \cdot 10^{-23}$	$2.51 \cdot 10^{-22}$ Hz
Rubidium ¹	$2 \cdot 10^{-20}$ s	$7 \cdot 10^{-24}$	$4 \cdot 10^{-29}$ Hz
Rubidium ²	$1 \cdot 10^{-23}$ s	$1 \cdot 10^{-22}$	$1.3 \cdot 10^{-26}$ Hz
Cesium ¹	$1 \cdot 10^{-19}$ s	$1 \cdot 10^{-25}$	$2 \cdot 10^{-32}$ Hz
Cesium ²	$2 \cdot 10^{-20}$ s	$7 \cdot 10^{-23}$	$4 \cdot 10^{-29}$ Hz

Table 4-2: Parameters for the Allan variance of several oscillators (from Winkel 2003)

The normalized frequency error can also be expressed as $y(t) = \frac{\dot{\varphi}(t)}{2\pi f_0}$ where φ is the phase error of the oscillator as a function of time.

The phase variation $x(t)$ expressed in units of time can be written as $x(t) = \frac{\varphi(t)}{2\pi f_0}$.

Therefore, the spectral densities of y , $\dot{\varphi}$ and x can be related as follows:

$$\begin{aligned}
 S_y(\omega) &= \left| \frac{1}{\sqrt{2\pi}} \int_{-\infty}^{+\infty} y \cdot e^{-i\omega t} dt \right|^2 = \left| \frac{1}{\sqrt{2\pi}} \int_{-\infty}^{+\infty} \frac{\dot{\varphi}}{2\pi f_0} \cdot e^{-i\omega t} dt \right|^2 \\
 &= \left| \frac{1}{\sqrt{2\pi}} i\omega \int_{-\infty}^{+\infty} \frac{\varphi}{2\pi f_0} \cdot e^{-i\omega t} dt \right|^2 = \left| \frac{1}{\sqrt{2\pi}} i\omega \frac{1}{2\pi f_0} \int_{-\infty}^{+\infty} \varphi \cdot e^{-i\omega t} dt \right|^2 \quad (4.12) \\
 &= \left(\frac{2\pi f}{2\pi f_0} \right)^2 \left| \frac{1}{\sqrt{2\pi}} \int_{-\infty}^{+\infty} \varphi \cdot e^{-i\omega t} dt \right|^2 = \frac{f^2}{f_0} S_\varphi(\omega)
 \end{aligned}$$

$$\begin{aligned}
S_{\dot{\varphi}}(w) &= \left| \frac{1}{\sqrt{2\pi}} \int_{-\infty}^{+\infty} \dot{\varphi} \cdot e^{-iwt} dt \right|^2 = \left| \frac{1}{\sqrt{2\pi}} iw \int_{-\infty}^{+\infty} \varphi \cdot e^{-iwt} dt \right|^2 \\
&= w^2 \left| \frac{1}{\sqrt{2\pi}} \int_{-\infty}^{+\infty} \varphi \cdot e^{-iwt} dt \right|^2 = 4\pi^2 f^2 S_{\varphi}(w)
\end{aligned} \tag{4.13}$$

$$\begin{aligned}
S_x(w) &= \left| \frac{1}{\sqrt{2\pi}} \int_{-\infty}^{+\infty} x \cdot e^{-iwt} dt \right|^2 = \left| \frac{1}{\sqrt{2\pi}} \int_{-\infty}^{+\infty} \frac{\varphi}{2\pi f_0} \cdot e^{-iwt} dt \right|^2 \\
&= \left(\frac{1}{2\pi f_0} \right)^2 S_{\varphi}(w)
\end{aligned} \tag{4.14}$$

Therefore

$$S_x(w) = \frac{1}{w^2} S_y(w) \tag{4.15}$$

or

$$S_x(w) = \frac{4\pi^2 h_{-2}}{w^4} + \frac{2\pi h_{-1}}{w^3} + \frac{h_0}{w^2} + \frac{h_1}{2\pi w} + \frac{h_2}{4\pi^2} \tag{4.16}$$

However, only h_0 , h_{-1} and h_{-2} significantly affect the clock model's process noise elements (NovAtel 1997). Therefore, the following approximation is used:

$$S_x(w) \approx \frac{4\pi^2 h_{-2}}{w^4} + \frac{2\pi h_{-1}}{w^3} + \frac{h_0}{w^2}. \tag{4.17}$$

Let $X(p) = H(p) \cdot \mathcal{E}(p)$ with $S_x(w) \approx H(iw) \cdot H(-iw)$

where \mathcal{E} is a white noise of unit variance and zero mean

H is the transfer function to transform white noise into oscillator noise

p is the variable in Laplace domain

Now, let's consider separately the elements of $S_x(w)$:

$$S_x(w) = S_{-2}(w) + S_{-1}(w) + S_0(w) \quad (4.18)$$

with

$$S_{-2}(w) = \frac{4\pi^2 h_{-2}}{w^4} \quad (4.19)$$

$$S_{-1}(w) = \frac{2\pi h_{-1}}{w^3} \quad (4.20)$$

$$S_0(w) = \frac{h_0}{w^2} \quad (4.21)$$

- First, consider $S_{-2}(w) = \frac{4\pi^2 h_{-2}}{w^4}$. Converting this into the Laplace domain

gives $H_{-2}(p) = \frac{2\pi\sqrt{h_{-2}}}{p^2}$ which leads to $X_{-2}(p) = \frac{2\pi\sqrt{h_{-2}}}{p^2} \mathcal{E}(p)$ and

finally going back to the time domain leads to the differential equation:

$$\frac{d^2 X_{-2}(t)}{dt^2} = 2\pi\sqrt{h_{-2}} \mathcal{E}(t) \quad (4.22)$$

- Second, consider $S_{-1}(w) = \frac{2\pi h_{-1}}{w^3}$. Its Laplace domain equivalent is

$H_{-1}(p) = \frac{\sqrt{2\pi h_{-1}}}{p^{3/2}}$. However, $p^{3/2}$ cannot be converted directly from the

Laplace domain to the time domain. For this reason, one needs to find an approximation of w^3 which will lead to a transfer function which can be

transformed from the Laplace domain to the time domain easily. One solution is to approximate w^3 around the frequency where the Flicker noise is the most important w_0 . w_0 can be defined by the solution of the following equation:

$$\left. \frac{d}{dw} \left(\frac{2\pi h_{-1}}{S_y(w)} \right) \right|_{w=w_0} = \left. \frac{d}{dw} \left(\frac{S_{-1}(w)}{S_y(w)} \right) \right|_{w=w_0} = 0 \quad (4.23)$$

Evaluating this equation and solving for w_0 gives $w_0 = 2\pi \sqrt{\frac{h_{-2}}{h_0}}$.

Then, w^3 is approximated around w_0 as follows:

$$w^3 \Big|_{w \rightarrow w_0} = \left(a_0 + a_1(jw) + a_2(jw)^2 \right) \times \left(a_0 + a_1(-jw) + a_2(-jw)^2 \right) \quad (4.24)$$

To find the parameters a_0 , a_1 and a_2 a genetic algorithm is used. The definition of a genetic algorithm is given in Appendix B. A genetic algorithm has been used to solve non linear transfer functions (Loyka 1999). The principle of this genetic algorithm is to find parameters such that the approximation of w^3 is as close as possible to w^3 around w_0 . The genetic algorithm is implemented as follow:

- 1) Generate 100 sets of the parameters a_0 , a_1 and a_2 : each parameter is generated randomly inside an interval (depending on the value of w_0 and therefore on the h parameters). For the oscillators used in this thesis, the parameters were chosen in the interval $[-3;3]$. A larger interval can be chosen but the algorithm would take longer to converge. Each set of

parameters a_0 , a_1 and a_2 represent the chromosomes of one individual used in the genetic algorithm.

- 2) Choose the 30 best individuals according to a cost function. The cost function used in the genetic algorithm is the difference between the true w^3 and its approximation weighted as a function of the distance between w and w_0 :

$$F_C(i) = \sum_w (w^3 - \hat{w}_i^3)^2 \cdot W(w)$$

where

$$\hat{w}_i^3 = (a_0^i + a_1^i(jw) + a_2^i(jw)^2) \times (a_0^i + a_1^i(-jw) + a_2^i(-jw)^2)$$

a_0^i , a_1^i and a_2^i represent the chromosomes of the i^{th} individual

W is the weight function (shown in Figure 4-7)

F_C is the cost function

As such, the best individual is the one with the smallest cost.

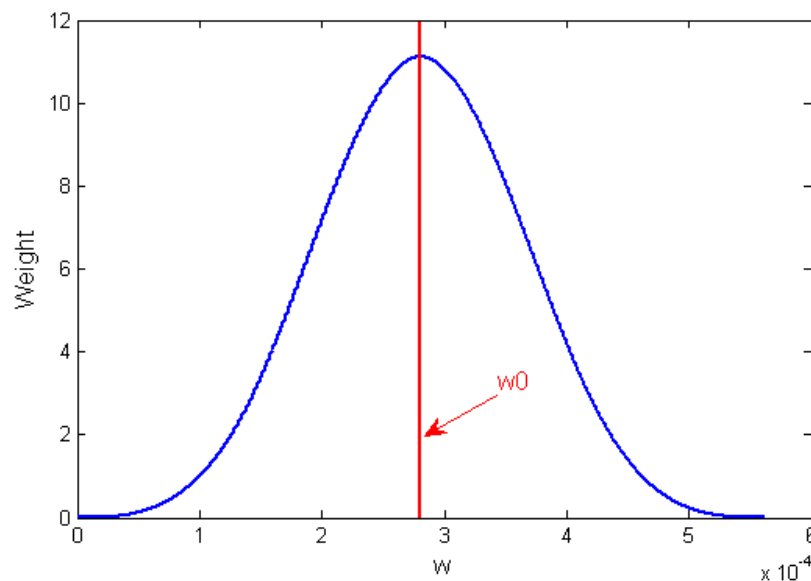


Figure 4-7: Weight function of the genetic algorithm

3) Breed: the 30 best individuals (chosen at the previous step) are kept and the other ones are killed. The 30 that remain are then coupled two by two to generate 70 new individuals (in order to retrieve the initial population of 100). Note that any individual can be paired with more than one other individual. For the generation of each new individual, the following steps are followed:

- The “mother” and “father” are chosen randomly among the 30 best individuals.
- A random weight w_k , uniformly distributed between 0 and 1, is chosen and applied to each chromosome of the “mother” and the weight $1-w_k$ is applied to the corresponding chromosome of the “father”.

- 4) Perform mutations:
 - Choose randomly 50 individuals in the population (while insuring that the best individual cannot be chosen for a mutation as one does not want to risk to degrade its best individual).
 - For each of the chosen 50 individuals, choose randomly one of the three chromosomes of this individual and mutate it (reinitialize this chromosome as it was done in step 1).
- 5) Go back to step 2 until a fixed number of generations has been done (trade off between processing time and accuracy of the approximation).
- 6) Recompute the cost function using the last population generated in order to choose the best individual defining the best set of parameters.

The inconvenience of such an algorithm is the long processing time. The advantage is that it always converges to the best solution if there are no local minima (Whitley 1993). An alternative approach would be a Chebyshev approximation but the results are not as good (Loyka 1999).

Once the parameters a_0 , a_1 and a_2 are computed, the transfer function to transform the noise into the Flicker noise (in the Laplace domain) can be expressed as:

$$H_{-1}(p) = \frac{\sqrt{2\pi h_{-1}}}{a_0 + a_1 p + a_2 p^2} \cdot \quad (4.25)$$

Therefore

$$X_{-1}(p) = \frac{\sqrt{2\pi h_{-1}}}{a_0 + a_1 p + a_2 p^2} \varepsilon(p) \quad (4.26)$$

which finally leads to the following differential equation:

$$a_0 X_{-1}(t) + a_1 \frac{dX_{-1}(t)}{dt} + a_2 \frac{d^2 X_{-1}(t)}{dt^2} = \sqrt{2\pi h_{-1}} \cdot \varepsilon(t). \quad (4.27)$$

This equation can also be written as:

$$\frac{d}{dt} \begin{bmatrix} \frac{dX_{-1}}{dt} \\ X_{-1} \end{bmatrix} = \begin{bmatrix} -\frac{a_1}{a_2} & -\frac{a_0}{a_2} \\ 1 & 0 \end{bmatrix} \cdot \begin{bmatrix} \frac{dX_{-1}}{dt} \\ X_{-1} \end{bmatrix} + \begin{bmatrix} \frac{\sqrt{2\pi h_{-1}}}{a_2} & 0 \\ 0 & 0 \end{bmatrix} \cdot \begin{bmatrix} \varepsilon_1 \\ 0 \end{bmatrix} \quad (4.28)$$

where ε_1 is a white noise of unit variance and zero mean

- Finally, let's consider $S_0(w) = \frac{h_0}{w^2}$. The associated transfer function is

$$H_0(p) = \frac{\sqrt{h_0}}{p} \text{ which in the Laplace domain leads to } X_0(p) = \frac{\sqrt{h_0}}{p} \varepsilon(p)$$

and finally leads to the following differential equation:

$$\frac{dX_0(t)}{dt} = \sqrt{h_0} \cdot \varepsilon(t) \quad (4.29)$$

To summarize the previous equations:

$$\frac{d}{dt} \begin{bmatrix} X_1 \\ X_2 \\ \dot{X}_{-1} \\ X_{-1} \end{bmatrix} = \begin{bmatrix} 0 & 1 & 0 & 0 \\ 0 & 0 & 0 & 0 \\ 0 & 0 & -\frac{a_1}{a_2} & -\frac{a_0}{a_2} \\ 0 & 0 & 1 & 0 \end{bmatrix} \cdot \begin{bmatrix} X_1 \\ X_2 \\ \dot{X}_{-1} \\ X_{-1} \end{bmatrix} + \begin{bmatrix} \sqrt{h_0} & 0 & 0 & 0 \\ 0 & 2\pi\sqrt{h_{-2}} & 0 & 0 \\ 0 & 0 & \frac{\sqrt{2\pi h_{-1}}}{a_2} & 0 \\ 0 & 0 & 0 & 0 \end{bmatrix} \cdot \begin{bmatrix} \varepsilon'_1 \\ \varepsilon'_2 \\ \varepsilon'_3 \\ 0 \end{bmatrix} \quad (4.30)$$

where ε'_i are independent white noise sequences of unit variance and zero mean. Note that $X_1 = X_0 + X_{-2}$ and $X_2 = \dot{X}_{-2}$. The total time error due to the oscillator is then given by $X_1 + X_{-1}$.

4.3.2 Transformation into the Discrete Domain

In order to implement the software signal simulator, the previous model needs to be transformed from the continuous model to the discrete domain. The previous system (Equation **Erreur ! Source du renvoi introuvable.**) can be rewritten as:

$$\dot{X} = F \cdot X + G \cdot W \quad (4.31)$$

with $X = \begin{bmatrix} X_1 \\ X_2 \\ \dot{X}_{-1} \\ X_{-1} \end{bmatrix}$

$$F = \begin{bmatrix} 0 & 1 & 0 & 0 \\ 0 & 0 & 0 & 0 \\ 0 & 0 & -\frac{a_1}{a_2} & -\frac{a_0}{a_2} \\ 0 & 0 & 1 & 0 \end{bmatrix}$$

$$G = \begin{bmatrix} \sqrt{h_0} & 0 & 0 & 0 \\ 0 & 2\pi\sqrt{h_{-2}} & 0 & 0 \\ 0 & 0 & \frac{\sqrt{2\pi h_{-1}}}{a_2} & 0 \\ 0 & 0 & 0 & 0 \end{bmatrix}$$

$$W = \begin{bmatrix} \mathcal{E}'_1 \\ \mathcal{E}'_2 \\ \mathcal{E}'_3 \\ \mathcal{E}'_4 \end{bmatrix}$$

and transformed in the discrete domain as follows (Grewal & Andrews 2001):

$$X_{k+1} = \phi_k X_k + W_k \quad (4.32)$$

where

$$\phi_k = e^{FT} \square I + FT + \frac{T^2}{2} F^2 = \begin{bmatrix} 1 & T & 0 & 0 \\ 0 & 1 & 0 & 0 \\ 0 & 0 & 1 - \frac{T \cdot a_1}{a_2} - \frac{T^2 \cdot \left(\frac{a_0}{a_2} - \frac{a_1^2}{a_2^2} \right)}{2} & \frac{T^2 \cdot a_0 \cdot a_1}{2 \cdot a_2^2} - \frac{T \cdot a_0}{a_2} \\ 0 & 0 & T - \frac{T^2 \cdot a_1}{2 \cdot a_2} & 1 - \frac{T^2 \cdot a_0}{2 \cdot a_2} \end{bmatrix}$$

$$Q_k = \int_t^{t+T} \phi_k G Q G^T \phi_k^T \quad \text{covariance matrix of the noise } W_k \text{ with } Q = I \text{ and}$$

$$G = \begin{bmatrix} \sqrt{h_0} & 0 & 0 & 0 \\ 0 & 2\pi\sqrt{h_{-2}} & 0 & 0 \\ 0 & 0 & \frac{\sqrt{2\pi h_{-1}}}{a_2} & 0 \\ 0 & 0 & 0 & 0 \end{bmatrix}.$$

A Choleski decomposition (Grewal & Andrews 2001) is finally used to simulate the noise according to the covariance matrix of the noise Q_k . The total time error due to the oscillator is then given by $X_1 + X_{-1}$ obtained by iterating X_k above. The system is initialized at zero for all the elements of X_k .

4.3.3 Simulation of the oscillator error

To validate the oscillator model developed, two oscillators are simulated using the model developed in Section 4.3.2. Then, the Allan standard deviation is computed from the samples generated. Finally, these Allan standard deviations are compared with the theoretical Allan standard deviations simulated using Equation 3.2 in Julien (2005). The sets of parameters used are the first OCXO (of two) and the first Rubidium (also of two) of Table 4-2. The same oscillators are used in the simulations later in this thesis. Figure 4-8 shows the theoretical and the simulated Allan standard deviations of these oscillators. The curves match well for both oscillators, except for a small bias. Therefore, the oscillator model developed above is validated.

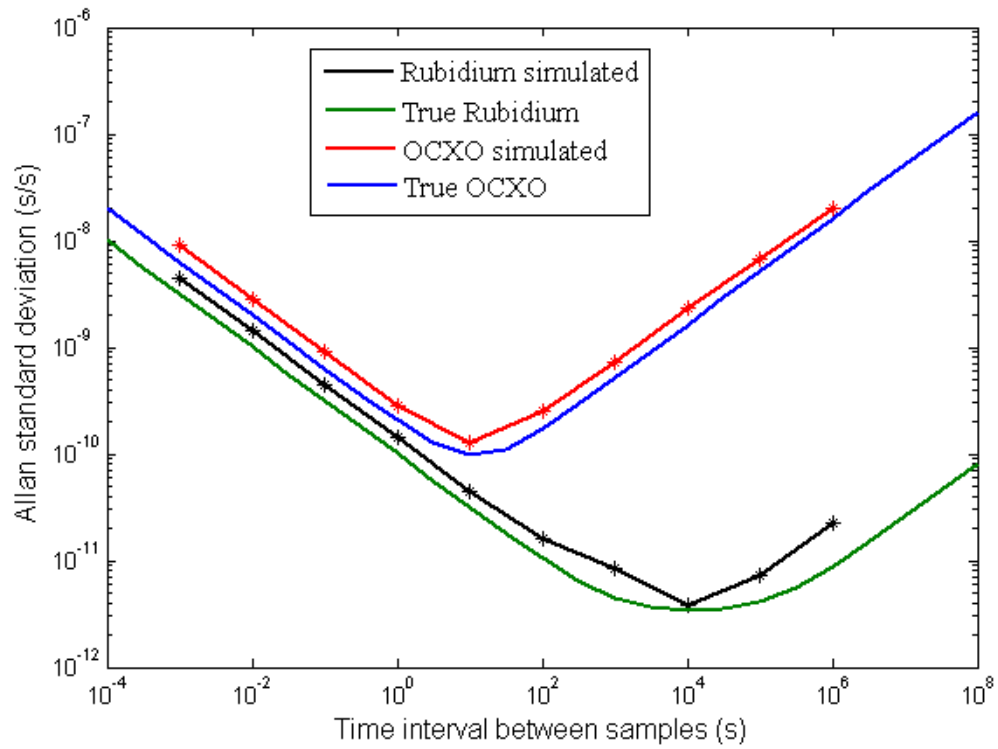


Figure 4-8: Theoretical Allan standard deviation and simulated Allan standard deviation for the OCXO and Rubidium oscillators

Chapter Five: DEVELOPMENT, TESTING AND STATISTICAL ANALYSIS OF INDEPENDENT GPS AND GALILEO L1 ACQUISITION ALGORITHMS

The goal of the acquisition process is to determine the code delay and the Doppler of the signal for each visible satellite in the sky. Once the signal is received, down converted and sampled by the front-end, a search is done on all PRNs to find the visible satellites and their corresponding code delay and Doppler shifts. To do so, the incoming signal is multiplied by a locally generated carrier corresponding to the intermediate frequency plus the Doppler and a local replica of the spreading code (Van Nee & Coenen 1991). This search is completed for all possible code Delays (e.g., 1023 chips in the case of GPS L1 C/A) and a range of expected Doppler shifts, typically between -5000 Hz and +5000 Hz for a static or slow moving receiver. In the case of a software receiver, these multiplications are in general realized in the frequency domain using an FFT (Fast Fourier Transform) (Akopian 2005). For a coherent acquisition, the size of the Doppler bin depends on the acquisition time: the longer the acquisition time, the smaller should the size of the frequency bins be (Raquet 2006). Thus, one has to keep in mind that in case of weak signals (indoor, urban canyon, foliage, etc.), the acquisition time needs to be increased in order to acquire the signal but this results in a rapidly increasing processing time due to the length of the vectors being correlated and the size of the frequency bins. However, it is possible to use a non coherent acquisition (addition of the squared correlator outputs) in order to acquire weak signals. This way, the size of the frequency bin does not need to be changed but the performance is not as good as in the previous

method due to the increase of the noise (since the correlations are squared before being added). However, it is possible to combine a non coherent or a differential technique with a coherent integration. These techniques permit to acquire signals attenuated by as much as 20 dB (e.g. MacGougan 2003, Shanmugam et al 2005).

This chapter begins with a description of several methods of acquisition based on a zero padding technique. These methods can be applied to Galileo or GPS L1C signals independently and the choice of the methods depends on the conditions. The methods are first presented, then their performance is assessed and compared using a statistical analysis and finally the methods are tested using real data from the GIOVE-A satellite. Finally, a method to combine the signals broadcast at the same frequency and from the same constellation is developed. This method can be used to combine GPS L1 C/A with L1C (data and pilot) or Galileo L1 data and pilot channels.

5.1 Acquisition methods for GPS L1C and Galileo L1

As explained in chapters 2 and 3, the Galileo L1 and GPS L1C signals have similar properties. Therefore, the same techniques of acquisition can be applied to these signals with similar performance. As such, in this section, the algorithms are developed and tested with Galileo L1 signals, and only the length of the ranging codes would change for GPS L1C. Moreover, as demonstrated in Appendix C, the MBOC modulation can be

approximated by a BOC(1,1) without a significant loss in acquisition sensitivity. Therefore, this approximation is used here.

The new techniques of acquisition for the Galileo L1 signal are developed below using the common zero padding technique (Yang et al 2004) as a basis. First, the test procedure used to test these algorithms using real data from the GIOVE-A satellite is presented. Then, the methods developed are introduced. Thereafter, their performance is compared using the deflection coefficient as a metric. Finally, the performance of each technique is fully assessed using a statistical analysis.

5.1.1 Test procedure

As mentioned before, there are only two Galileo test satellites in the sky, GIOVE-A and GIOVE-B. The GIOVE-A satellite has been used to test all the algorithms developed hereafter and to compare the performance of the data and pilot channel. There are a few differences between the properties of the L1 signal broadcast by GIOVE-A and the future signals, including the following properties of the GIOVE-A L1 OS signals:

- the modulation of the broadcast signals is a BOC(1,1) for both the pilot and data channel
- the length of the ranging code on the pilot channel is twice the one on the data channel (8184 chips instead of 4092).

However, the GIOVE-A satellite is able to transmit on only two frequencies at a time and therefore one should be careful when recording data from this satellite. The information

about the current Galileo frequencies transmitted can be found on the official GIOVE-A website: <http://www.giove.esa.int>.

The NASA overpass predictor was used to determine when the satellite was visible with a good elevation angle above Calgary. Since in this research the main goal was to develop and test new algorithms, the data were recorded only when the satellite was at a high elevation at a relatively high signal power. IF samples were recorded using a NovAtel L1 RF front-end (Euro3M Card). At the same time, the pseudorange, Doppler and C/N_0 measurements were recorded from a NovAtel 15a receiver for comparison purposes. Figure 5-1 shows the data collection setup.

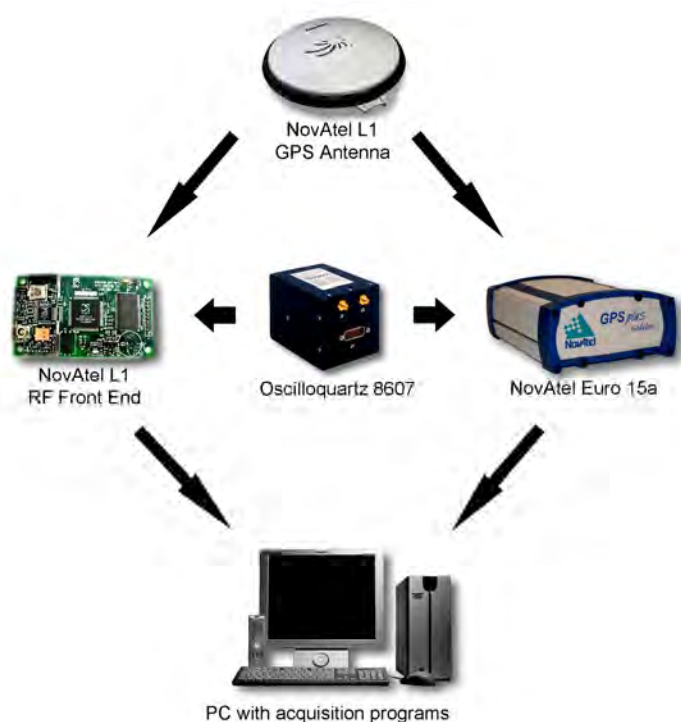


Figure 5-1: GIOVE-A data collection set-up

The Euro3M Card has the following characteristics:

- Records real samples at 40 MHz (equivalent to 20 MHz complex samples)
- Intermediate frequency is 70.42 MHz on L1
- Output used is one bit quantization on L1
- Front-end bandwidth of 16 MHz (two-sided)

An external rubidium oscillator (10 MHz) was used to drive the NovAtel Euro-3M. A rubidium oscillator was selected to remove any significant oscillator effects on signal tracking performance.

The NovAtel 15a receiver contains 16 channels capable of tracking and decoding GPS L1 and L5, Galileo L1 and E5a and SBAS signals. The receiver configuration used here was:

- 5 Galileo L1 channels
- 5 Galileo E5a channels
- 6 GPS L1 channels

The NovAtel 15a receiver is also connected to the external oscillator to have the same reference time as the NovAtel Euro-3M card.

5.1.2 Methods of acquisition of the Galileo L1 pilot and data channels

The acquisition scheme used for all the following acquisitions is the standard parallel code phase search acquisition presented in Figure 5-2. With this method, the correlation is computed in the frequency domain, which permits a reduction in the processing time compared to an acquisition in the time domain (Borre et al 2007).

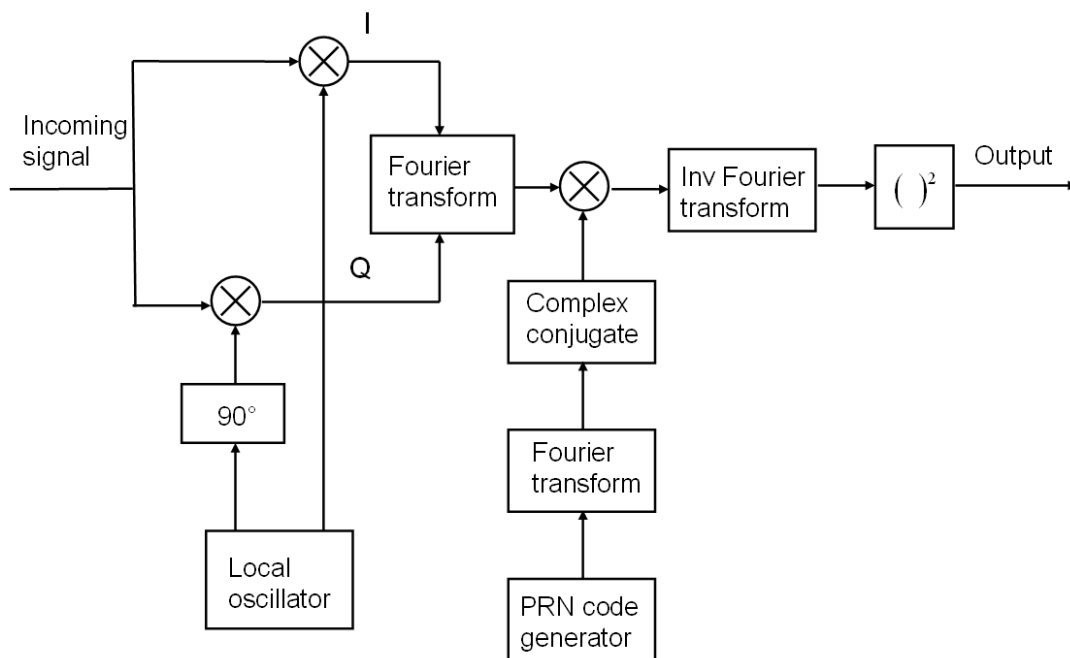


Figure 5-2: Parallel code phase search acquisition scheme

Since the first Galileo satellite has been launched, some research has been done about the acquisition and the tracking of the Galileo L1 signals. Nevertheless, few of the algorithms implemented have been tested with real data, but instead using signal simulators. Indeed, Marradi et al (2006), Spelat et al (2006), Botteron et al (2006) have developed Galileo receivers or algorithms of acquisition and tracking but tested them only through the use of signal simulators. A few researchers such as Ledvina et al (2006) have implemented algorithms and Galileo L1 receiver and have tested it using real data, but their main goal was to create it in real time and not to compare the performance of the signals using different algorithms. Finally, Psiaki et al (2006) have developed a statistical technique to decode the codes before their public release.

In this research, new methods of frequency-domain acquisition are proposed to acquire the pilot and data channel using different lengths of the incoming signal, adapted to the strength of the signal.

The acquisition is implemented to acquire the pilot channel using 16 ms of incoming signal and the data channel over 8 ms. This implementation uses the zero padding technique (Yang et al 2004) commonly used for L5 GPS (Mongrédién et al 2006). To compare the characteristics of the acquisition of the data and pilot channel, it is necessary to have the same length of incoming data. Thus, beginning with the zero padding technique, two new methods of acquisition are created and implemented to acquire the pilot channel using 16 ms of incoming signal and the pilot channel over 8 ms.

The usual techniques of acquisition for GPS L1 C/A cannot be applied to the Galileo L1 signals due to the properties of the signal. In particular, on L1-B, the sign of the bit of the navigation message can change each ranging code period, so if the integration is done over two (or more) ranging code periods a destructive combination can occur leading to degraded acquisition performance. The same problem is encountered in the case of L1-C even if there is no navigation message because the secondary code plays the same role: the sign of the secondary bit can change each time the ranging code repeats. The difference with L1-C however is that the structure of the secondary code is known, and once the receiver is synchronized with the secondary code, it can be effectively removed.

Four acquisition techniques are shown in this section, two for each of the pilot and data channels. The first two methods are implementations of the classic zero padding technique and are implemented for comparison with the new methods developed in this thesis (method 3 and 4). The third and fourth methods use combinations of the zero padding technique. The novelty stands in the way to scatter and combine acquisitions done using the zero padding technique. The algorithms are compared in terms of sensitivity and processing time, and finally using a statistical analysis.

5.1.2.1 First and second methods of acquisition

First, an acquisition strategy was implemented for the data channel L1-B using 8 ms of incoming signal. From now, this method is called D1 (D for data and 1 for method one). If the correlation is realized only over the length of one spreading code period (i.e. 4 ms), it is possible that no correlation peak will be visible if a change of sign happens in the incoming signal. Since the correlation is done in the frequency domain, a zero padding strategy is needed. This strategy has already been implemented in the case of GPS L5, for example in Mongrédien et al (2006) and is shown in Figure 5-3:

- Take 8 ms of incoming sample data.
- A local replica of the complete ranging code (4 ms for L1-B) is created and padded with 4 ms of zeros.
- The correlation is performed
- If the correlation is done on the 8 ms, one or two peaks will be generated depending on whether a change in the sign of the navigation message bits occurs,

and if so, where it occurs in the incoming data stream. However, a correlation peak will always be present in the first 4 ms of output, so only this part of the correlation result needs to be searched. Furthermore, the expected value of the first peak is always higher or of the same amplitude as the second peak because it always represents a correlation of the entire spreading code period, therefore the maximum needs to be searched only in the first 4 ms as stated above.

On the left side of Figure 5-3, an entire primary code in the middle of the 8 ms (in blue) correlates with the code replica and therefore generates a first peak corresponding to the coherent integration of the L1-B code over 4 ms. This yields a peak in the first 4 ms of output. For the second 4 ms of output, because the sign of the data bit (or bit of the secondary code) of the incoming signal is the same on the left and the right (in red; negative), the two portions of spreading code coherently add during correlation and a second peak of similar value as in the first 4 ms is produced.

On the right side of Figure 5-3, the first peak is also generated as explained above. However, in contrast to above, the sign of the data bit is not the same at the beginning and the end of the incoming signal (red and blue). Therefore, the integration will be destructive and only a small second peak will be visible. The size of this peak depends on the “size” of the destructive recombination: if the left and right parts are of the same size no second peak is visible, while if one is much smaller than the other a second peak almost as high as the first one will be visible.

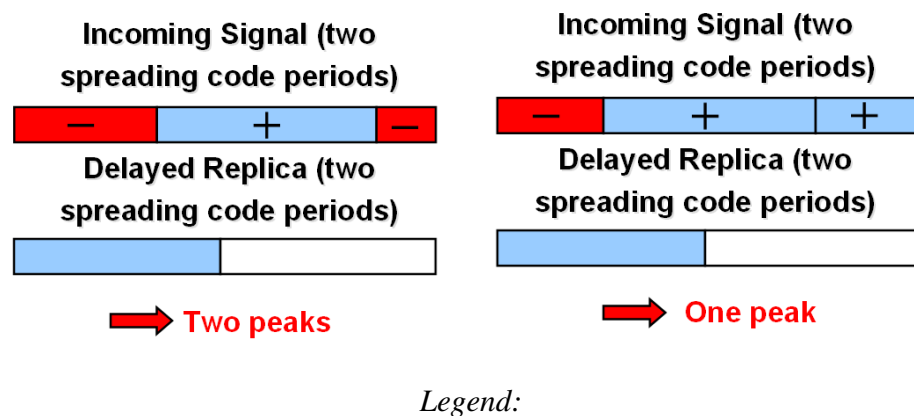


Figure 5-3: Illustration of the zero padding technique

The second method, hereafter called P1 (P for pilot, method 1) is the same as D1 but is implemented on 16 ms of incoming signal for the pilot channel. Since on the pilot channel the ranging code lasts 8 ms, it is possible to use a zero padding technique as well (similar to the one used to acquire the data channel using 8 ms of incoming signal) to acquire the signal using 16 ms of incoming data. The acquisition technique used on L1-C to acquire the signal on 16 ms is the following:

- 16 ms of incoming data are used
- A local replica of 8 ms of code is created (so one entire spreading code period) and is padded with 8 ms of zeros

- The two signals are correlated
- If the correlation is done on the 16 ms, one or two peaks will be generated depending on the sign change in the bit of the secondary code
- As before, a correlation peak will always be present in the first 8 ms and will always be the highest one, so the correlation peak need only to be searched in the first 8 ms of output.

5.1.2.2 Third method of acquisition

Comparing the performance of the pilot and data channel allows comparing the performance of the algorithms with different lengths of primary code (4 and 8 ms). To achieve this, the acquisition of the data channel is done as well using 16 ms of incoming data. This method is called D2 (Data channel, method 2). In this case, the zero padding technique presented above cannot be used. Indeed, in the case of the data channel, in 16 ms of data it is possible to have three changes in the sign of the data bit.

Thus, when the same zero padding technique as above is used:

- There will be no gain in using 16 ms of data instead of 8 ms if one spreading code period only is used and padded with 8 ms of zeros.
- A destructive combination can occur and the acquisition can be highly degraded if two or more spreading code periods are used and padded with zeros.

Therefore, an adaptation of the zero padding technique has been developed and implemented to realize an acquisition of the data channel using 16 ms of incoming signal. Specifically, the acquisition is realized using four different sub-groupings of the

incoming signal, each 8 ms long, as shown in Figure 5-4. In all cases, the local code consists of 4 ms of the ranging code (i.e., the full code) padded with 4 ms of zeros. The four sub-groupings of the incoming data are defined as follows:

1. The first 8 ms of incoming signal are considered.
2. The first and last 4 ms of incoming signal are not considered (only the 8 ms from the fifth to the twelfth millisecond are used).
3. The last 8 ms of incoming signal are considered.
4. The last 4 ms of incoming signal are combined with the first 4 ms of incoming signal.

The results of these four correlations are finally non-coherently added. The maximum value is searched in the first 4 ms for the same reasons as in the previous section: for each integration, the largest peak is always in the first 4 ms.

This method allows to acquire the signal using 16 ms of incoming signal, but it requires much more operations (and so more processing time) than the previous one. Consequently, this method should be used only in the case of weaker signals, where the first method does not provide a correlation peak strong enough to confidently identify the presence (or absence) of a signal. This method is equivalent in power to a non-coherent accumulation of four different 4-ms long coherent integration outputs. Nevertheless, if this method has to be implemented in a hardware receiver, the four correlations can be performed using four parallel correlators and in this case it will not require a longer processing time than the previous method, it will only use of more correlators in parallel.

However, these correlations may not necessarily be easy to perform in real time, and a solution using buffers may have to be explored using hardware.

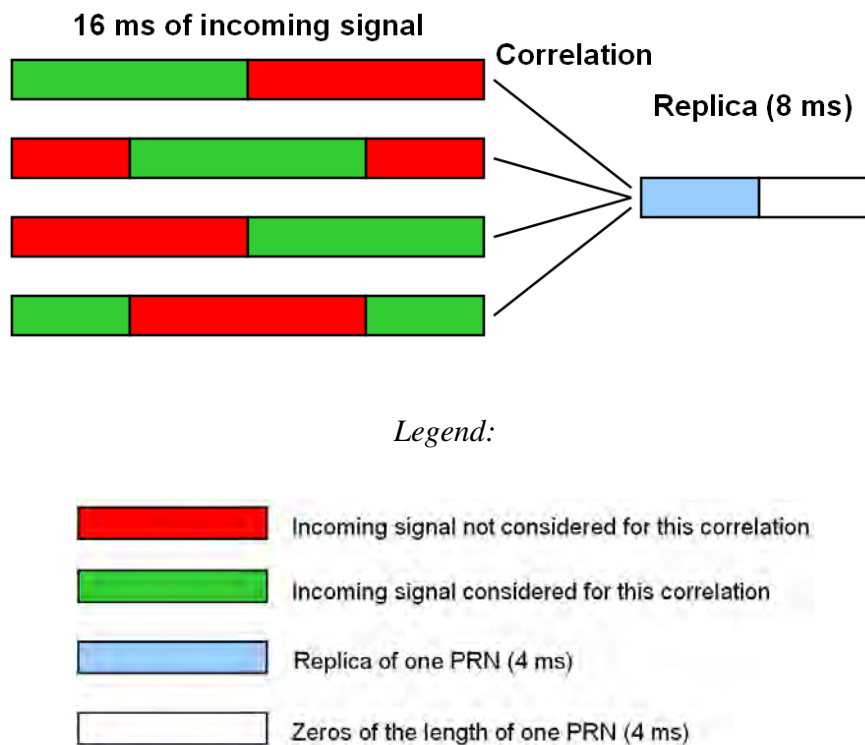


Figure 5-4: Illustration of the technique of correlation over 16 ms for the data channel (method D2)

5.1.2.3 Fourth method

Finally, another method of acquisition has been created to be able to acquire the pilot channel using 8 ms called P2 (Pilot channel, method 2). Indeed, if the acquisition is to be realized on the L1-C channel using only 8 ms of data (to compare with L1-B and to decrease the processing time) another problem is encountered: one entire primary code is

present in 8 ms of data but a change in the sign of the bit of the secondary code is possible (because the data samples are not likely to start and end on the code period boundaries). Thus, if the usual method of correlation is used directly with a replica of 8 ms of the code, it is possible to have no correlation at all or a very small peak.

Therefore, a new method has been created and implemented to avoid this problem. The acquisition is done in two integrations (see Figure 5-5):

- Generate the first half of the primary spreading code period (so 4 ms for L1-C) padded with 4 ms of zeros and correlate it with the 8 ms of incoming signal.
- Generate the second half of the primary spreading code period (so 4 ms) padded with 4 ms of zeros and correlate it with the same 8 ms of incoming signal. Note that the 4 ms of zeros are first and the code second in order for the peaks of the first and second integration to be aligned.
- Then the two correlation results are added non coherently over 8 ms (since the length of the primary code is 8 ms one needs to search for the maximum over 8 ms)

On the top scheme in Figure 5-5, the first half of the ranging code is correlated with the incoming signal. Due to the change in the sign of the bit of the secondary code, the reconstruction of the right part of the incoming signal (in blue) with the left end part (to form 4 ms of incoming signal) is destructive. Therefore, this first integration will generate, in this case, a small peak or no peak at all. Concerning the second integration (bottom scheme in Figure 5-5), the second part of the ranging code is correlated with the

remaining part (last 4 ms of the red part). Since there is no change of sign, a peak is generated and corresponds to the power of a coherent integration over 4 ms.

With this method, one peak is always present in the 8 ms of correlation. In the case of implementation in a software receiver, it increases the number of operations and processing time (compared to L1-B), but in the case of implementation in hardware, the two steps can be done simultaneously in parallel using two different correlators, and thus the time processing will not increase. Since there is 50% chance to have a data bit sign change in 8 ms, half of the time this method is equivalent in power to the non-coherent integration of two 4-ms integrations. In the case of a data bit sign change, one of the two 4-ms integrations will be maximized (for the given signal power) and the other 4-ms integration will be partially attenuated depending on the location of the data bit transition within the 4 ms. As the location of the data bit transition is uniformly distributed, the average of the second integration in a case of a data bit change will be 50% of the power of an integration over 4 ms. As such, the average of this method is equivalent to a non-coherent -summation of a 4-ms integration and a 2-ms integration.

This method decreases the cross correlation protection of the pilot ranging code since only half the code length is used for each integration.

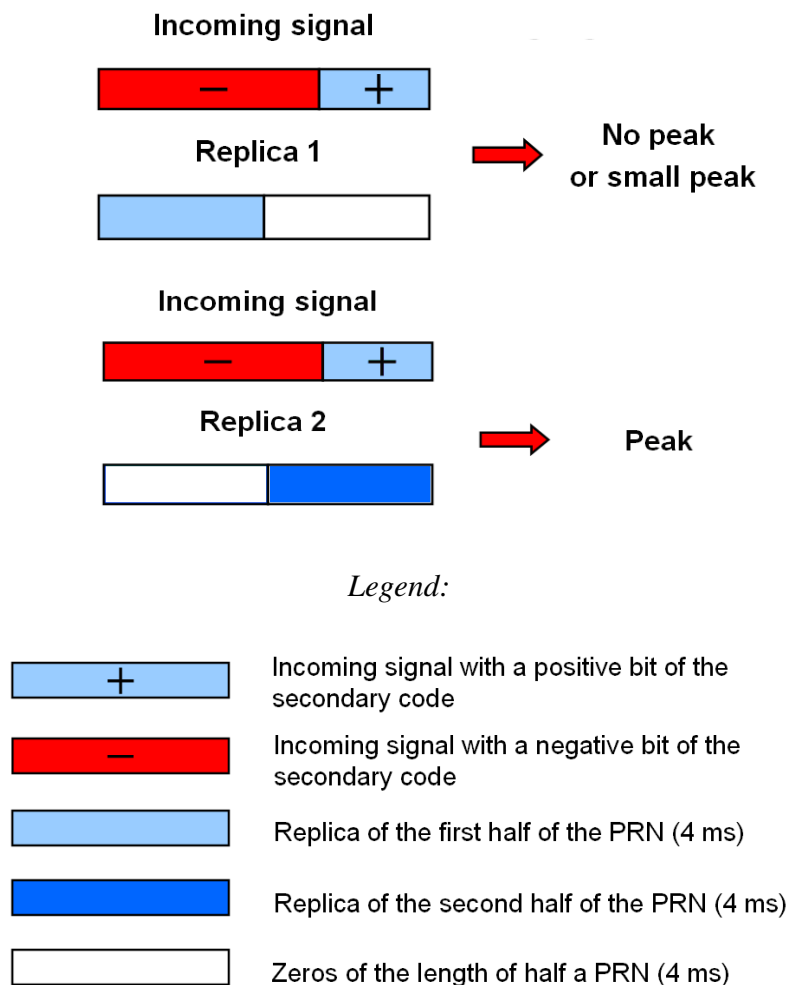


Figure 5-5: Illustration of the technique of correlation over 8 ms for the pilot channel (method P2)

The method P2 could be generalized in order to acquire long codes. Indeed, if one wants to acquire a code with a period of 1 s without computing only one integration (too much processing time), it is possible to “cut” the replica in 100 pieces of 10 ms each and realize 100 acquisitions added as above. This could be applied for example to long codes such as the pilot code on the GPS L2C signal.

5.1.3 Results of the acquisition methods using real data and comparison

The above acquisition algorithms were implemented in Matlab and were tested using data from the GIOVE-A satellite collected on April 16, 2007 during the day for 5 minutes. During data collection, the satellite had an elevation angle of about 65 degrees. The IF samples were used as input to the Matlab software. The results below compare the methods of acquisition presented in the previous section in terms of sensitivity.

In the case of the method D1, two main correlation peaks are observed, as illustrated in Figure 5-6. The first 4 ms (first ranging code period) corresponds to the code delays from 0 to 4091 and the second 4 ms (second ranging code period) corresponds to the code delays from 4092 to 8183. As explained in the previous section, the first (i.e., leftmost) peak is higher than the second one due to (potential) destructive combination in the second peak. For the data in Figure 5-6, the code delay between the incoming signal and the local replica is small (about 279.7 chips) thus if there is a destructive combination due to the change in the sign of the data bit, it is relatively small. As seen on the graph, the second peak is only slightly smaller than the first one. Two other important properties can be mentioned about this graph:

- There are exactly 4092 chips between the two peaks, which represents the length of the primary code on L1-B
- The two peaks are at exactly the same Doppler frequency

The previous observations are necessary properties of this acquisition but needed to be checked to validate the results.

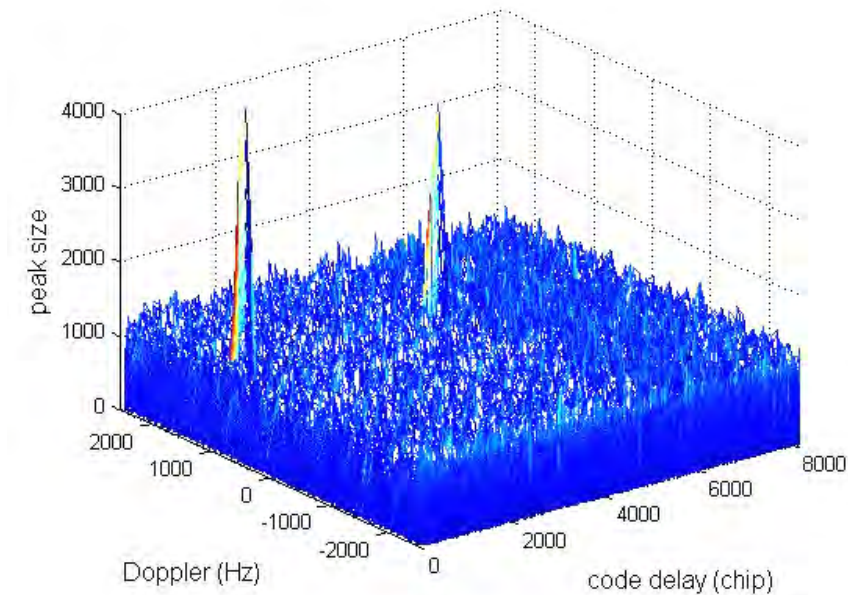


Figure 5-6: Acquisition of the data channel using 8 ms of incoming signal (method D1)

The above verification has been done on the all four methods of acquisition and the resulting Doppler frequencies are the same as the Doppler found with the NovAtel 15a receiver. The four following Figures (Figure 5-7 to Figure 5-10) show the outputs of the acquisition algorithms at the Doppler frequency where the maximum correlation occurs at -300 Hz. All the results are obtained using the same set of data.

Figure 5-7 and Figure 5-8 represent the acquisition results for the methods D1 and D2 respectively. Comparing the acquisition results of the methods D1 and D2 shows some differences but also the common points are clearly visible. In terms of similarities, both graphs show that the first peak (at around 638 chips) is higher than the second (at around 4730 chips) one due to destructive recombination (as explained before) and a difference of 4092 chips is observed between both peaks, as expected. The position of the peaks is

exactly the same for the two different integration times: same Doppler frequency and same code delay. Thus, these results show that the implementation of these two methods of acquisition are validated.

In terms of differences, the increase in the size of the peak for the method D2 (an analysis of the SNR is presented later) costs much processing time: it takes around four times longer to process the acquisition D2 than D1. Indeed, for D1 one coherent accumulation over 8 ms is computed whereas 4 non-coherent accumulations over 8 ms are computed for D2. Nevertheless, the acquisition method D2 has several advantages:

- It is possible to acquire weaker signals (such as indoors or in an urban environment).
- If developed in hardware, it could be the same as in the case of D1 as explained above.

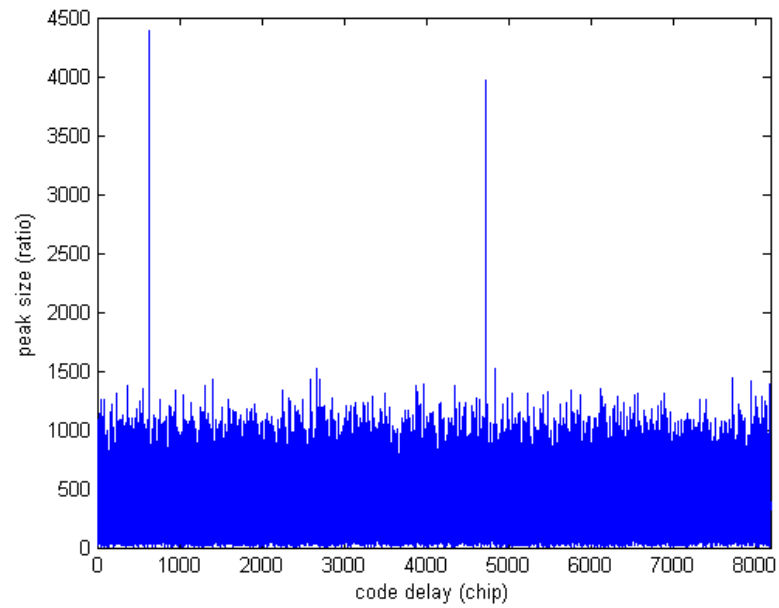


Figure 5-7: Results of the acquisition for the data channel using 8 ms of incoming signal (method D1)

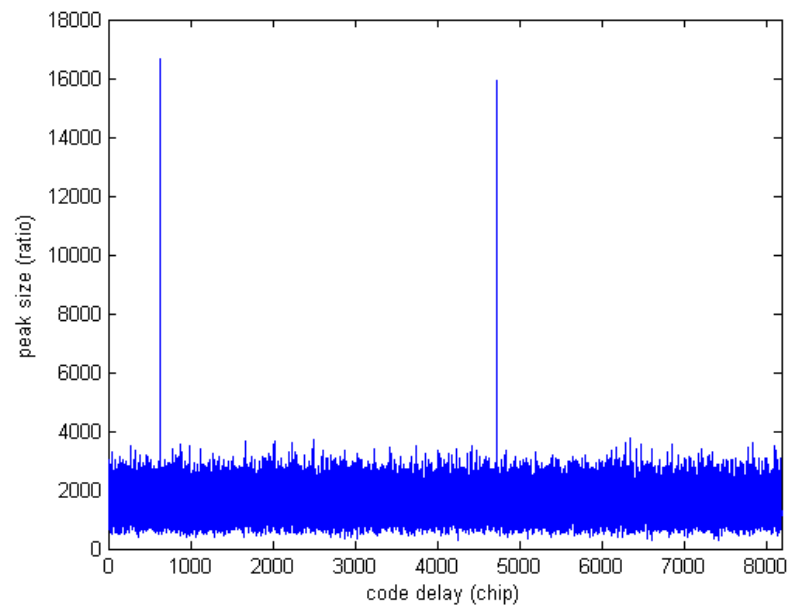


Figure 5-8: Results of the acquisition for the data channel using 16 ms of incoming signal (method D2)

Figure 5-9 and Figure 5-10 show the acquisition results for the methods P1 and P2. As before, comparing the acquisition results of the pilot channel over 8 ms and 16 ms shows some differences but also some similarities. In the first graph, there is only one peak since the length of the code is 8 ms and the acquisition is implemented on 8 ms (the length of spreading code period). The peak and thus the code delay are at the same place using both methods of acquisition. Moreover, these results are in accordance with those of the data channel: the determined code delay is exactly the same for the data and pilot channels.

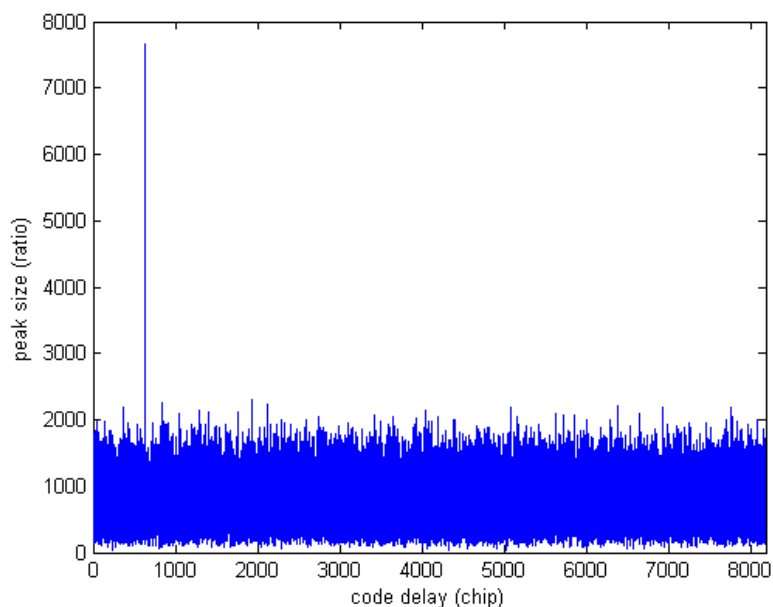


Figure 5-9: Results of the acquisition for the pilot channel using 8 ms of incoming signal (method P2)

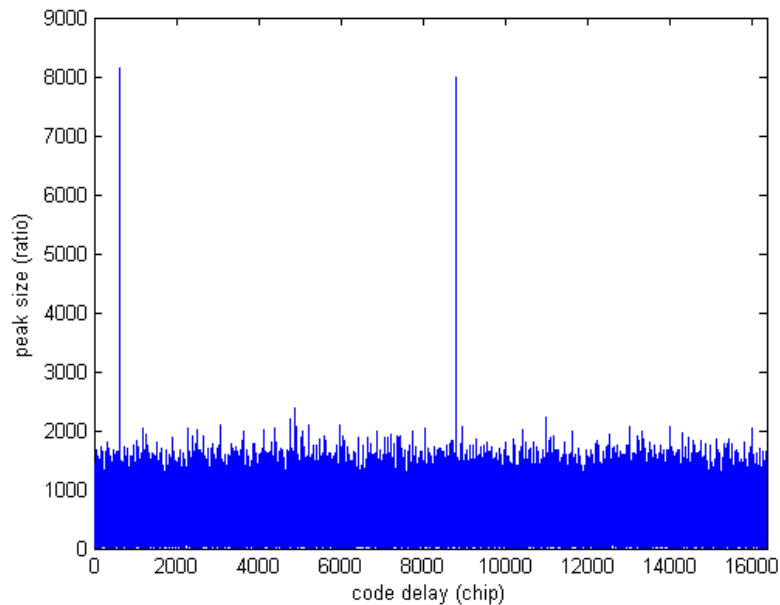


Figure 5-10: Results of the acquisition for the pilot channel using 16 ms of incoming signal (method P1)

On Figure 5-10, the first peak is almost the same size as the second one. This can have two explanations:

- The sign of the bit of the secondary code is the same over the 16 ms (so over the two spreading code periods) and thus there is no destructive combination
- Since the code delay is relatively small (only around 638 chips), the destructive combination between the parts of the spreading code at the beginning and at the end of the 16 ms is very small, therefore there is mainly one sign of bit of the secondary code

As before, the increase in the size of the peak for the method P1 costs much processing time: it is around two times longer for the method P2 than for P1. Indeed, for P1 one coherent accumulation over 8 ms is computed whereas 2 non-coherent accumulations over 4 ms are computed for P2. However, it is possible this way to acquire weaker signals than with P2. Nevertheless, if the method P2 was developed in hardware, it would be possible to use two correlators in parallel to do the two correlations (for the 8 ms of incoming data) and in this case the processing time for the method P2 would be reduced.

Since one of the main differences between GPS L1 and Galileo L1 is the modulation, it is interesting to look in more details at the correlation peak in these acquisitions. When the last acquisition (Figure 5-10) is investigated in more detail (pilot channel over 16 ms), the main peak is clearly visible as well as the two sided peaks at half a chip on each side of the main peak with half of the power of the main peak. As presented in Figure 5-11, the shape of correlator outputs is the same as for simulated data.

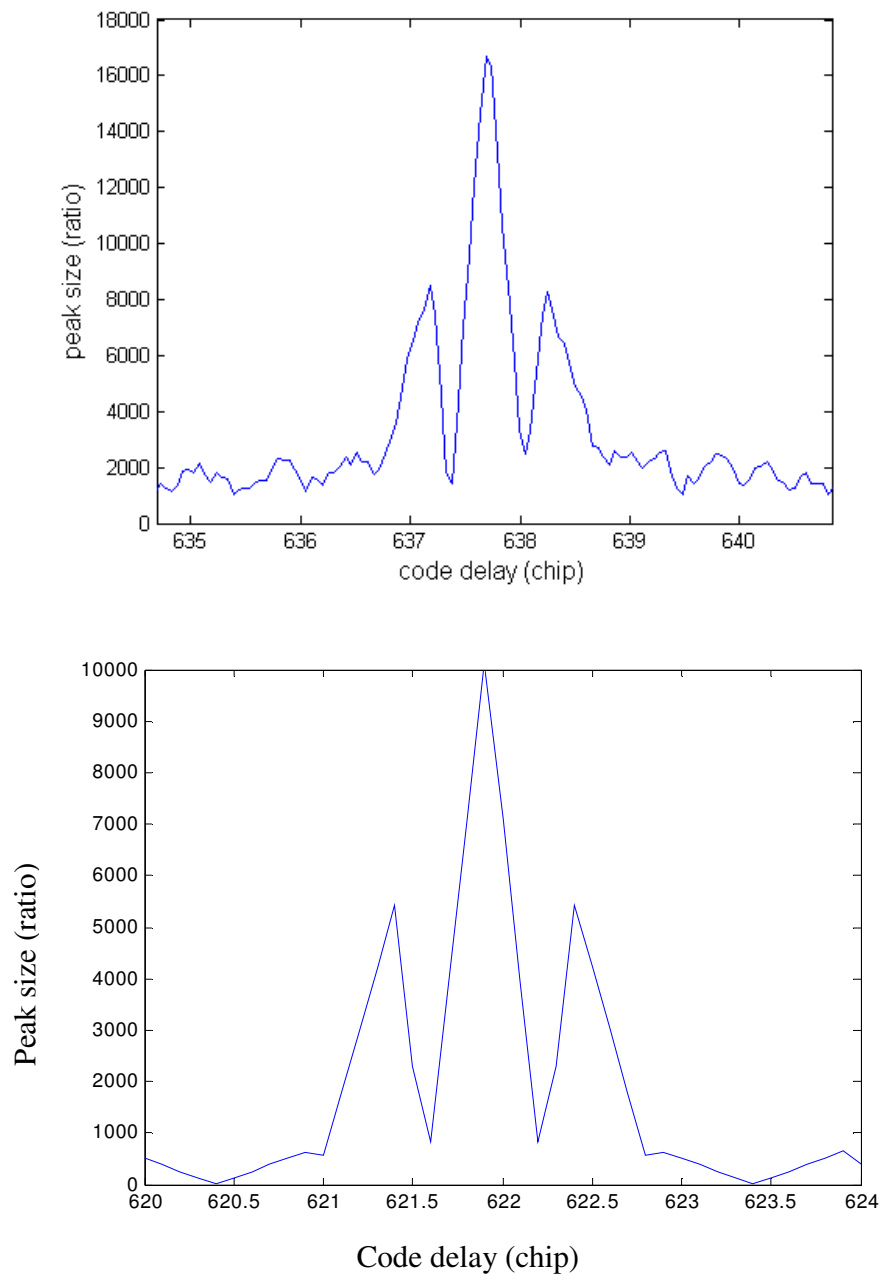


Figure 5-11: Detail of the BOC correlation for real data (on the top) and for simulated data (on the bottom)

To compare the four different acquisition strategies two parameters have been compared:

- The acquisition sensitivity

- The processing time

To compare the sensitivity of these four methods of acquisition, a deflection coefficient (which is a form of SNR) has been used:

$$d^2 = \frac{[E(T / H_1) - E(T / H_0)]^2}{\text{var}[T / H_0]} \quad (5.1)$$

where d is the deflection coefficient

$E(T / H_1)$ is the mean value of the main peak

$E(T / H_0)$ is the mean of the noise

$\text{var}(T / H_0)$ is the variance of the noise

This metric is not always a reliable one for comparing acquisition sensitivities (Borio et al 2008). Indeed, it is valid when the distributions at the output of the correlators are the same. However, in this case, only the family of the distributions is the same, not the degrees of freedom. Therefore, this metric is used as a first way of comparison but a statistical analysis is then performed to confirm the performance in the next section.

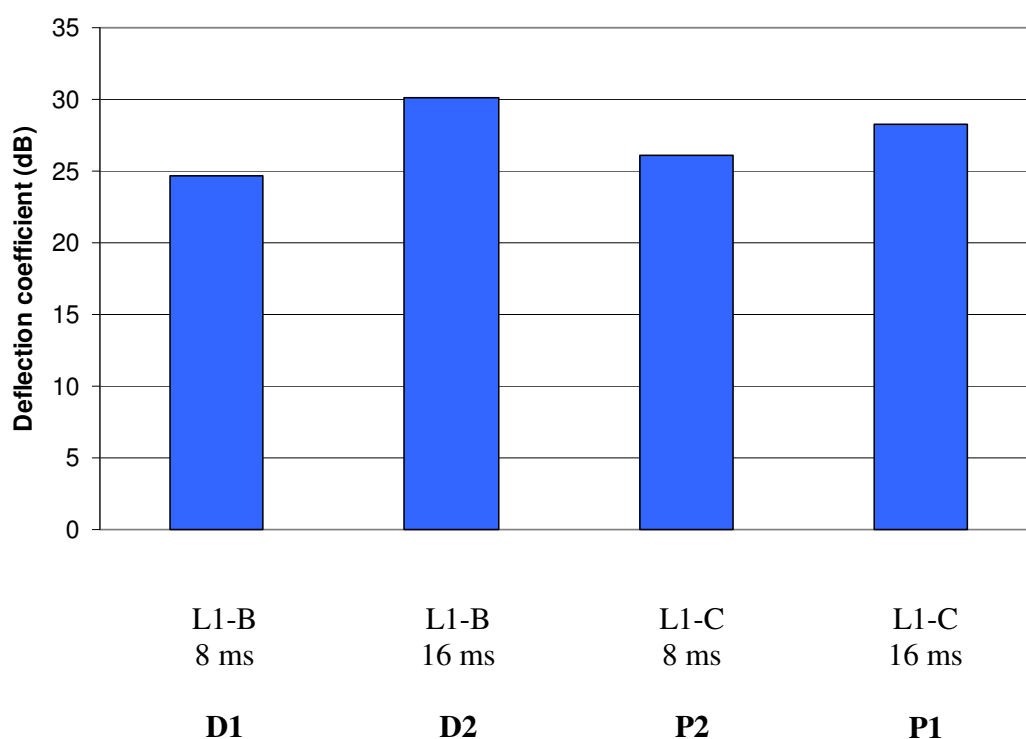


Figure 5-12: Comparison of the sensitivity of the four acquisition methods

To compute the deflection coefficients, thirty separate acquisitions have been performed for each acquisition method. The results are shown in

Figure 5-12 and can be summarized as follows:

- Indeed, there is an improvement of 5.5 dB for the method D2 compared to the method D1. In terms of power this method is equivalent to non-coherent accumulation of four different 4-ms long coherent integration outputs and therefore almost 6 dB improvement compared to one coherent accumulation over 4 ms (D1 case). However, the full 6 dB is not realized because of the non-coherent integration and therefore the noise is squared before being added (which

results in an increase of the noise). This effect is known as squaring loss (Lowe 1999).

- The result for the method P1 is 3 dB better than the method D1. This 3 dB increase was expected since the same method is used in both cases, but the length of the incoming signal in the L1-C case is double that for L1-B and thus the output power also doubles.
- The deflection coefficient for the method P2 is around 2 dB smaller than the method P1. Indeed, for P2 a coherent accumulation is computed over 8 ms whereas for P1 two coherent integrations over 4 ms (but one of them can be partially destructive as explained above in section 5.1.2.3) are computed.
- The deflection coefficient for the method P1 is around 1 dB higher than the method D1. In fact, for P1 two coherent integrations over 4 ms are computed (one of them being partially destructive) whereas for D1 only one coherent accumulation is computed.

The processing time is almost the same for the methods D1 and P2. Nevertheless, the acquisition method D2 takes four times more processing time than D1. The method P1 takes two times more processing time than the method P2. The methods D2 and P1 should be used only for weaker signals.

5.1.4 Statistical analysis of the proposed acquisition techniques

The objective of this section is to analyze the performance of the acquisition algorithms for Galileo L1 presented above. To analyze such performance, the probabilities of acquisition and false alarm are derived. In these algorithms, several code delays are searched in parallel using an FFT-based algorithm and the decision is made once all the correlations are evaluated. Thus, the final decision variable depends on all cells determined simultaneously. Moreover, the processing time of these algorithms is computed using the mean acquisition time.

5.1.4.1 Data channel over 8 ms (Method D1)

The acquisition method D1 is realized using zero padding and only one coherent integration interval. Therefore, the distribution at the output of the correlators is a Chi Square distribution with two degrees of freedom, χ_2^2 . Consequently, the probabilities of false alarm and detection for one cell can be expressed as (O'Driscoll 2007):

$$P_{fa}(\beta) = \exp\left(-\frac{\beta}{2 \cdot \sigma_n^2}\right) \quad (5.2)$$

$$P_{det}(\beta) = Q_1\left(\frac{\sqrt{\lambda}}{\sigma_n}; \frac{\sqrt{\beta}}{\sigma_n}\right) \quad (5.3)$$

where P_{fa} is the probability of false alarm for one cell

P_{det} is the probability of detection for one cell

β is the threshold

λ is a the non-centrality parameter depending on the size of the main peak and the noise variance

σ_n^2 is the noise variance at the correlator output

Q_K is the Marcum Q-function and can be expressed as (Marcum 1960, Shnidman 1989)

$$Q_K(a; b) = \frac{1}{a^{K-1}} \int_b^{\infty} x^K \cdot \exp\left(-\frac{x^2 + a^2}{2}\right) \cdot I_{K-1}(ax) dx \quad (5.4)$$

where I_0 is the modified Bessel function of the first kind. However, the probabilities of interest in our case are the global probabilities of false alarm and detection and not the ones over a single cell.

The global probability of false alarm (denoted with capitalized subscripts to distinguish it from (5.2)) is the probability that the maximum of search space cell is above a fixed threshold (in the proposed algorithms all the correlations are computed and then the maximum is chosen) and there is no signal present (Borio et al 2006):

$$P_{FA}(\beta) = P(\max > \beta) \quad (5.5)$$

which is the opposite of all the outputs being smaller than the threshold

$$P_{FA}(\beta) = 1 - P(\text{all cells} < \beta). \quad (5.6)$$

Moreover, beyond one chip spacing, the correlation is very small, therefore all the correlations can be approximated as independent and the global probability of false alarm can be approximated as:

$$P_{FA}(\beta) = 1 - \prod_{\text{all cells}} (1 - P_{fa}(\beta)) \quad (5.7)$$

All the correlation outputs are considered to have the same probability of false alarm, therefore:

$$P_{FA}(\beta) = 1 - (1 - P_{fa}(\beta))^{N \cdot L} \quad (5.8)$$

where N is the number of frequency bins and L the number of code delay bins in the 2D search space.

If the probability of false alarm for one cell is small (Taylor series of the first order), it can be approximated as:

$$P_{FA}(\beta) \approx 1 - (1 - N \cdot L \cdot P_{fa}(\beta)). \quad (5.9)$$

Finally, replacing the probability of false alarm over one cell by its expression (in (5.2)) yields

$$P_{FA}(\beta) = N \cdot L \cdot \exp\left(-\frac{\beta}{2 \cdot \sigma_n^2}\right) \quad (5.10)$$

The global probability of detection is the probability that the correct cell (i.e., the cell containing the signal) X_A is above the threshold and is the maximum amongst all cells:

$$P_{DET}(\beta) = P(X_A > X_i \ \& \ X_A > \beta) \quad (5.11)$$

where X_i are all the cells excluding the correct cell

which is equivalent to:

$$P_{DET}(\beta) = \int_{\beta}^{\infty} P(X_i < X_A | X_A = T) dP(X_A = T) \quad (5.12)$$

As before, the cells can be approximated as independent and

$$P_{DET}(\beta) = \int_{\beta}^{\infty} [P(X_i < T)]^{N \cdot L - 1} f_{det}(T) dT \quad (5.13)$$

where $f_{det}(T)$ is the density of probability of detection for one cell. Finally, one has:

$$P_{DET}(\beta) = \int_{\beta}^{\infty} [1 - P_{fa}(T)]^{N \cdot L - 1} f_{det}(T) dT \quad (5.14)$$

$$f_{det}(T) = -\frac{dP_{det}(T)}{dT} = -\frac{dP_{det}(b)}{db} \frac{db}{dT} = b \cdot \exp\left(-\frac{a^2 + b^2}{2}\right) \cdot I_0(ab) \frac{1}{2\sqrt{T}\sigma_n} \quad (5.15)$$

$$\text{with } a = \frac{\sqrt{\lambda}}{\sigma_n} \text{ and } b = \frac{\sqrt{\beta}}{\sigma_n}$$

The values of λ and σ_n^2 have been determined over 1000 acquisitions of real data from the GIOVE-A with a C/N_0 around 45 dB-Hz. Additional noise was added to the collected data in order to better study the acquisition performance under different conditions (see 5.1.4.5).

5.1.4.2 Data channel over 16 ms (Method D2)

The acquisition method D2 is realized using zero padding and four non-coherent integrations. Therefore, the distribution at the output of the correlators is a Chi Square

distribution with eight degrees of freedom, χ_8^2 . Consequently, in this case the probabilities of false alarm and detection for one cell can be expressed as (O'Driscoll 2007):

$$P_{fa}(\beta) = \exp\left(-\frac{\beta}{2 \cdot \sigma_n^2}\right) \sum_{i=0}^3 \left(\frac{\beta}{2 \cdot \sigma_n^2}\right)^i \quad (5.16)$$

$$P_{det}(\beta) = Q_4\left(\frac{\sqrt{\lambda}}{\sigma_n}; \frac{\sqrt{\beta}}{\sigma_n}\right) \quad (5.17)$$

Using a similar method as above, the global probabilities of false alarm and detection can be expressed as:

$$P_{FA}(\beta) = N \cdot L \cdot \exp\left(-\frac{\beta}{2 \cdot \sigma_n^2}\right) \times \left[1 + \frac{\beta}{2 \cdot \sigma_n^2} + \left(\frac{\beta}{2 \cdot \sigma_n^2}\right)^2 + \left(\frac{\beta}{2 \cdot \sigma_n^2}\right)^3\right] \quad (5.18)$$

and

$$P_{DET} = \int_{\beta}^{\infty} \left[1 - P_{fa}(T)\right]^{N \cdot L - 1} f_{det}(T) dT \quad (5.19)$$

$$f_{det}(T) = \frac{b^4}{a^3} \cdot \exp\left(-\frac{a^2 + b^2}{2}\right) \cdot I_3(ab) \frac{1}{2\sqrt{T}\sigma_n} \quad (5.20)$$

where I_3 is the Bessel function of third kind

5.1.4.3 Pilot channel over 16 ms (Method P1)

In the case of the method P1, it is the same method as for the method D1. Therefore, the global probabilities of detection and false alarm are the same, except that the value of L (number of code delay bins) has to be considered over 8 ms instead of 4 ms.

5.1.4.4 Pilot channel over 8 ms (Method P2)

The acquisition method P2 is realized using zero padding and two non-coherent integrations. Therefore, the distribution at the output of the correlators is a Chi Square distribution with four degrees of freedom, χ_4^2 . Consequently, in this case the probabilities of false alarm and detection for one cell can be expressed as (O'Driscoll 2007):

$$P_{fa}(\beta) = \exp\left(-\frac{\beta}{2 \cdot \sigma_n^2}\right) \sum_{i=0}^1 \left(\frac{\beta}{2 \cdot \sigma_n^2}\right)^i \quad (5.21)$$

$$P_{det}(\beta) = Q_2\left(\frac{\sqrt{\lambda}}{\sigma_n}; \frac{\sqrt{\beta}}{\sigma_n}\right) \quad (5.22)$$

Again, using a similar method as in the first case, the global probabilities of false alarm and detection can be expressed as

$$P_{FA}(\beta) = N \cdot L \cdot \exp\left(-\frac{\beta}{2 \cdot \sigma_n^2}\right) \cdot \left[1 + \frac{\beta}{2 \cdot \sigma_n^2}\right] \quad (5.23)$$

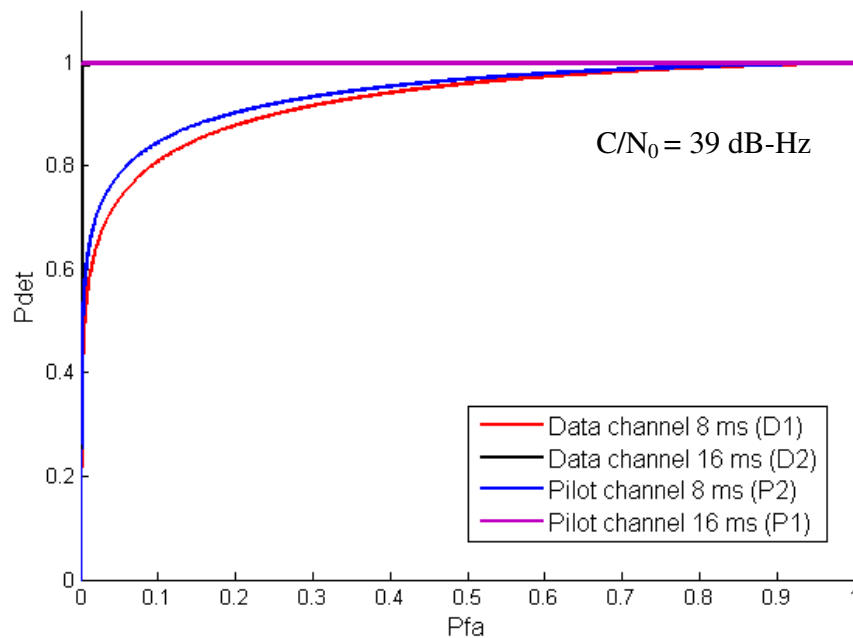
$$P_{DET} = \int_{\beta}^{\infty} \left[1 - P_{fa}(T)\right]^{N \cdot L - 1} f_{det}(T) dT \quad (5.24)$$

with

$$f_{\text{det}}(T) = \frac{b^2}{a} \cdot \exp\left(-\frac{a^2 + b^2}{2}\right) \cdot I_1(ab) \frac{1}{2\sqrt{T}\sigma_n} \quad (5.25)$$

5.1.4.5 ROC Curves

Using all the equations derived above, one can plot the Receiver Operating Characteristics (ROC) curves for all the acquisitions methods. The ROC curve represents the probability of detection as a function of the probability of false alarm. An “ideal” ROC curve would have a value of 1 for all the probabilities of false alarm. The results using a C/N_0 of 39 dB-Hz are shown in Figure 5-13.



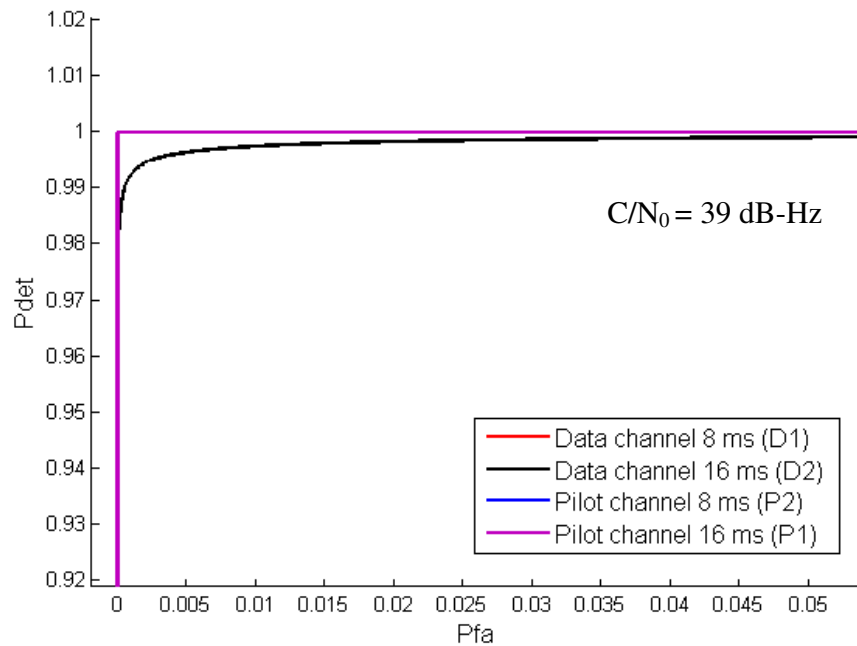


Figure 5-13: ROC Curves for the four acquisition methods. The lower plot shows the upper left portion of the top plot in more detail. Note that, on the top figure, the ROC curves corresponding to the methods D2 and P1 are overlaid.

As can be seen in Figure 5-13, the method D1 is the one with the poorest performance followed by the method P2. The best performance is found with the methods P1 and D2. However, for the methods P1 and D2, as mentioned earlier, the processing time is much higher than for the other two methods (four times longer for the data channel and two times longer for the pilot channel). Therefore, these acquisition methods should be used only when the other one does not succeed in acquiring the signal. These results are in accordance with the ones of the testing using real data (section 5.1.3).

5.1.4.6 Mean acquisition time of the proposed acquisition techniques

As mentioned at the beginning of section 5.1.4, another important parameter to determine the performance of an acquisition method is the mean acquisition time. The mean acquisition time represents the average computation load necessary to detect the correct cell in the acquisition process. The mean acquisition time is expressed in number of computer operations instead of time because the time depends on the processor speed. This is usually accomplished using a Markov chain. The Markov chain model applied to the methods above is shown in Figure 5-14.

In order to compute the acquisition time, the signal is supposed to be present and the final state should always be detection. At the end of the acquisition process, one can either have detection after time T_d (detection time) or a false alarm after time T_d . If the process is in the state of false alarm (signal detected in the wrong cell), it returns to the acquisition state after a penalty time T_p . T_p is left here as a parameter since it depends on the tracking algorithms used, i.e. of the necessary time to detect a false acquisition (but is on the order of a few seconds). Once back in the acquisition process, one again has the same possibilities as before.

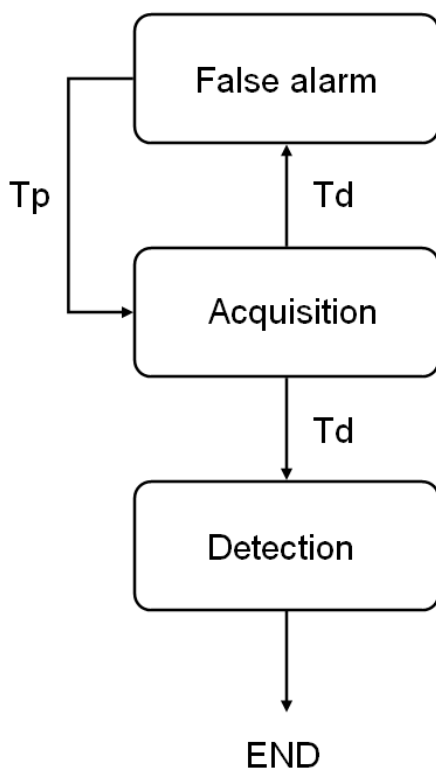


Figure 5-14: Acquisition bloc diagram

From Figure 5-14, one can deduce the expression of the mean acquisition time τ as a function of the global probabilities of false alarm and detection and the detection and penalty times. If the acquisition is successful at the first try, it takes the time T_d to acquire the signal and this event happens with a probability P_{DET} (Global probability of detection). If the acquisition is successful at the second try, it takes $T_d + T_p$ (false alarm and time to recover) plus T_d (time to detect on the second try). This event happens with a probability P_{fa}' (probability to detect the signal in the wrong cell when a signal is present

$P_{fa}' = 1 - P_{DET}$) and the probability to acquire successfully at the second try is P_{DET} . If one follows this reasoning for the third, fourth, etc., one has:

$$\tau = P_{DET} \cdot T_d + \left[P_{fa}' \cdot \left[(T_d + T_p) + P_{DET} \cdot T_d + \left[P_{fa}' \cdot \left[(T_d + T_p) + P_{DET} \cdot T_d + \left[P_{fa}' \cdot \left[(T_d + T_p) + P_{DET} \cdot T_d + \dots \right] \right] \right] \right] \right] \right]$$

← Successful acquisition at first try

← Successful acquisition at second try

← Successful acquisition at third try

← Successful acquisition at fourth try

← Successful acquisition at latter try

Finally, this leads to the following formula:

$$\tau = P_{DET} \cdot T_d + \sum_{i=1}^{\infty} P_{fa}'^i \left[(T_d + T_p) + P_{DET} \cdot T_d \right] \tag{5.26}$$

$$\tau = P_{DET} T_d + \frac{P_{fa}'}{1 - P_{fa}'} \left[(T_d + T_p) + P_{DET} \cdot T_d \right] \tag{5.27}$$

with $T_d = \alpha \cdot N \cdot L \cdot \log_2 N$, $N \cdot L \cdot \log_2 N$ being the number of multiplications in the FFT and α being a constant depending on the computer processor properties and representing the time taken to do one multiplication.

If one chooses a probability of false alarm (in case of no signal) of 10^{-3} and computes the probability of detection for each algorithm using the formulae derived in the previous section, one obtains the mean acquisition time values shown in Figure 5-15.

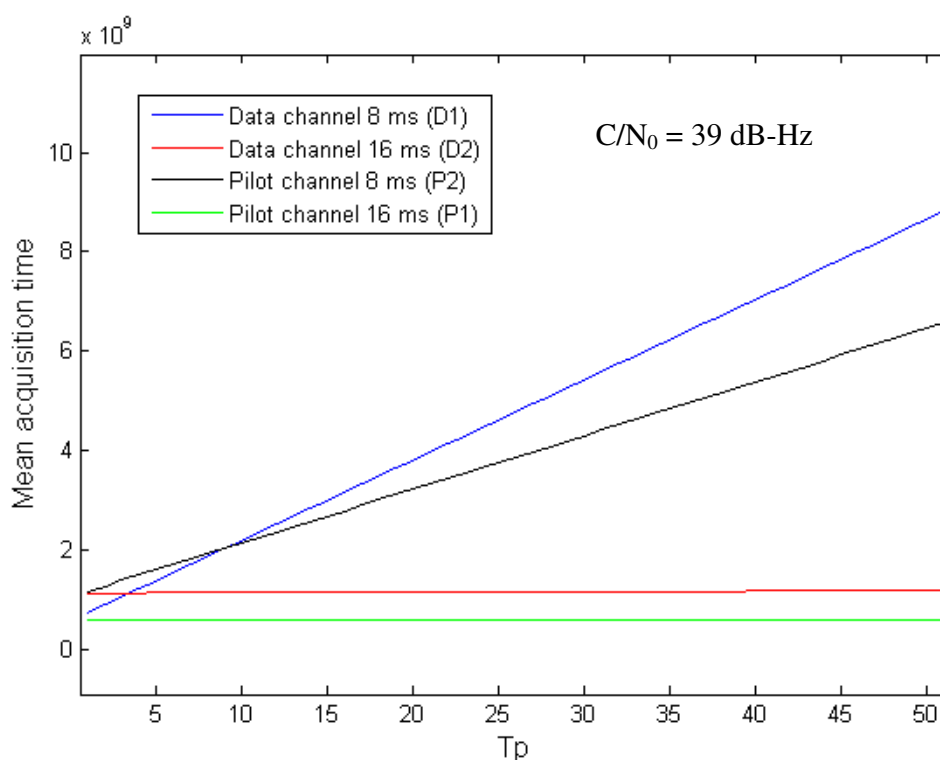


Figure 5-15: Theoretical mean acquisition time in function of the penalty time

As shown in Figure 5-15, even if the processing time for the method D1 is smaller than for D2, if a weak signal is considered, the probability of detection is small and therefore the mean acquisition time is higher relative to method D2 (except for very small T_p). Indeed, due to the higher probability of false alarm, one will have to do the acquisition process several times. Concerning P1 and D2, the probability of false alarm being very small, the penalty time has almost no impact on the mean acquisition time. In conclusion, in terms of mean acquisition time, it is better to use the acquisition algorithms using 16 ms of data in case of weak signals because the time lost to recover from several false alarms will increase the mean acquisition time.

5.2 Acquisition algorithm to combine GPS L1 C/A with GPS L1C (data and pilot channels)

A new method of acquisition is developed here to combine the GPS L1 C/A and L1C (data and pilot channels) signals inside the acquisition process. Note that a similar method can be applied to Galileo L1-B and L1-C channels. First, the method is explained in detail. Then, some results are shown using a signal generated by the software signal simulator described in Chapter 4.

5.2.1 Method of acquisition

The combined acquisition algorithm proposed herein is shown in Figure 5-16.

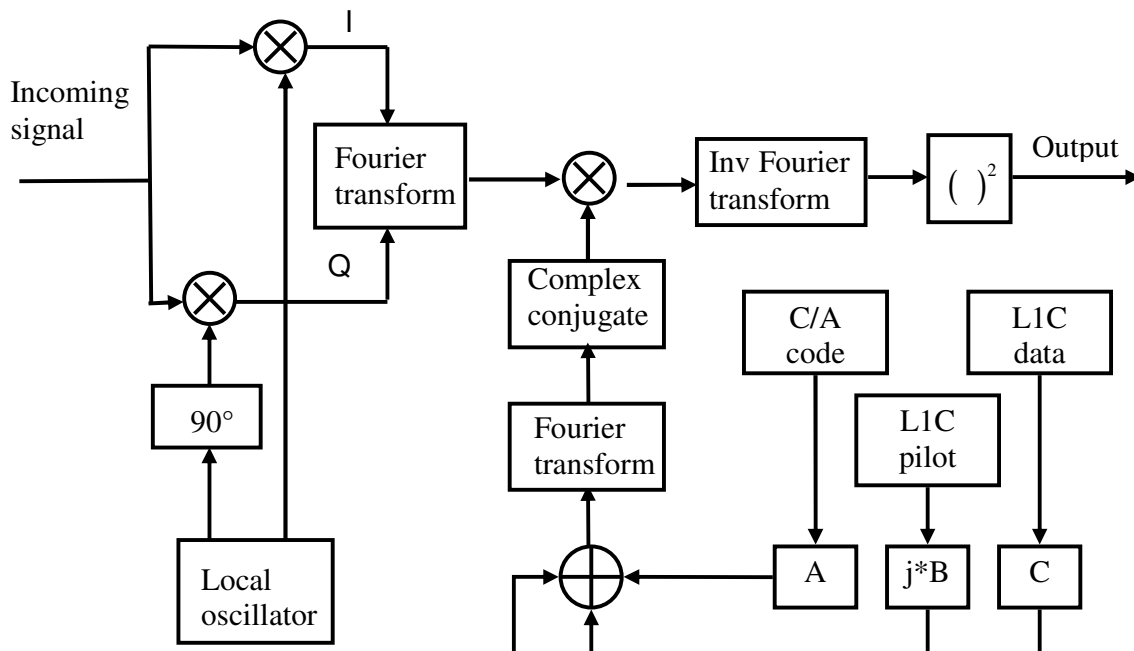


Figure 5-16: Combined GPS L1 C/A – L1C acquisition scheme

Most of the scheme in Figure 5-16 is similar to a classic parallel code phase search acquisition scheme as shown in Figure 5-2. However, there is an important difference in the generation of the local replica of the ranging code. Specifically, instead of generating only a single ranging code, the composite code is generated. The acquisition is realized as follows:

- 1) A carrier wave is generated at a fixed Doppler frequency f_D using a local oscillator.
- 2) The incoming signal is multiplied by the carrier wave generated in step 1 to generate the in phase component I .
- 3) The incoming signal is multiplied by the carrier wave generated in step 1 shifted by 90° to generate the in quadrature component Q .
- 4) The Fourier transform of the combination of the I and Q components is computed: $F(I + jQ)$ (where F represents the Fourier transform).
- 5) The local replica of the three ranging codes (GPS L1 C/A, L1C pilot and L1C data channels) are generated.
- 6) The three ranging codes generated in step 5 are multiplied respectively by A , $j*B$ and C and then added. The values of the scalars A , B and C are computed according to the relative power of the GPS L1 C/A and L1C signals. Details are shown later in this section. The L1C pilot channel is multiplied by j because the pilot channel is transmitted with a 90° shift compared to the L1 other channels.

- 7) The Fourier transform of the combination created in step 6 is computed and its complex conjugate is multiplied by the Fourier transform computed in step 4. The result is called *ConvCodeIQ*.
- 8) The inverse Fourier transform of the vector *ConvCodeIQ* computed in step 7 is computed and the results are squared.
- 9) Steps 1 through 8 are done for all Doppler shifts.

The *A*, *B* and *C* coefficients above are computed using the relative powers of the transmitted signals as follow:

- 1) If the correlations of the three signals were computed separately, before squaring the results (step 8 above), the distributions of the three correlator outputs in the presence of signal would be (O'Driscoll 2007):

$X_{C/A} \square N(\mu_{C/A}, \sigma_{C/A}^2)$ for the distribution of L1 C/A $X_{C/A}$

$X_{L1CD} \square N(\mu_{L1CD}, \sigma_{L1CD}^2)$ for the distribution of L1C data channel X_{L1CD}

$X_{L1CP} \square N(\mu_{L1CP}, \sigma_{L1CP}^2)$ for the distribution of L1D pilot channel X_{L1CP}

where $N(\mu, \sigma^2)$ represents the Gaussian of mean μ and variance σ^2

$\mu_{C/A}$, μ_{L1CD} and μ_{L1CP} are the size of the correlation peak of the L1 C/A,

L1C data and pilot channels respectively

$\sigma_{C/A}^2$, σ_{L1CD}^2 and σ_{L1CP}^2 are the variances of the noise associated with the

L1 C/A, L1C data and pilot channels respectively.

- 2) If the L1C data and pilot channels are combined into L1C as follows:

$$X_{L1C} = W_1 \cdot X_{L1CP} + (1 - W_1) \cdot X_{L1CD} \quad (5.28)$$

where X_{L1C} is the distribution of the combination

W_1 is a weight between 0 and 1

then the variance of L1C σ_{L1C}^2 can be expressed as:

$$\sigma_{L1C}^2 = W_1^2 \cdot \sigma_{L1CP}^2 + (1 - W_1)^2 \cdot \sigma_{L1CD}^2. \quad (5.29)$$

The combination is optimal when the variance σ_{L1C}^2 is minimal:

$$\begin{aligned} \min(\sigma_{L1C}^2) &= \frac{d\sigma_{L1C}^2}{dW_1} = 0 \\ \Rightarrow 2 \cdot W_1 \cdot \sigma_{L1CP}^2 - 2(1 - W_1) \cdot \sigma_{L1CD}^2 &= 0 \\ \Rightarrow W_1 &= \frac{\sigma_{L1CD}^2}{\sigma_{L1CD}^2 + \sigma_{L1CP}^2} \end{aligned} \quad (5.30)$$

3) Then, if the L1C and L1 C/A channels are combined into L1 as follows:

$$X_{L1} = W_2 \cdot X_{L1C} + (1 - W_2) \cdot X_{C/A} \quad (5.31)$$

where X_{L1} is the distribution of the combination

W_2 is a weight between 0 and 1,

the variance of X_{L1} , σ_{L1}^2 can be expressed as:

$$\sigma_{L1}^2 = W_2^2 \cdot \sigma_{L1C}^2 + (1 - W_2)^2 \cdot \sigma_{C/A}^2. \quad (5.32)$$

The combination is optimal when the variance σ_{L1}^2 is minimal:

$$\begin{aligned}
\min(\sigma_{L1C}^2) &= \frac{d\sigma_{L1C}^2}{dW_1} = 0 \\
\Rightarrow 2 \cdot W_1 \cdot \sigma_{L1CP}^2 - 2(1-W_1) \cdot \sigma_{L1CD}^2 &= 0. \quad (5.33) \\
\Rightarrow W_1 &= \frac{\sigma_{L1CD}^2}{\sigma_{L1CD}^2 + \sigma_{L1CP}^2}
\end{aligned}$$

4) Therefore, the optimal combination for the three channels is:

$$\begin{aligned}
X_{L1} = \frac{\sigma_{C/A}^2}{\sigma_{C/A}^2 + \sigma_{L1C}^2} \left[\frac{\sigma_{L1CD}^2}{\sigma_{L1CD}^2 + \sigma_{L1CP}^2} X_{L1CP} + \left(1 - \frac{\sigma_{L1CD}^2}{\sigma_{L1CD}^2 + \sigma_{L1CP}^2} \right) X_{L1CD} \right] \\
+ \left(1 - \frac{\sigma_{C/A}^2}{\sigma_{C/A}^2 + \sigma_{L1C}^2} \right) X_{C/A} \quad (5.34)
\end{aligned}$$

and

$$\begin{aligned}
A &= 1 - \frac{\sigma_{C/A}^2}{\sigma_{C/A}^2 + \sigma_{L1C}^2} = 0.4142 \\
B &= \frac{\sigma_{C/A}^2}{\sigma_{C/A}^2 + \sigma_{L1C}^2} \cdot \frac{\sigma_{L1CD}^2}{\sigma_{L1CD}^2 + \sigma_{L1CP}^2} = 0.4388 \quad . \quad (5.35) \\
C &= \frac{\sigma_{C/A}^2}{\sigma_{C/A}^2 + \sigma_{L1C}^2} \cdot \left(1 - \frac{\sigma_{L1CD}^2}{\sigma_{L1CD}^2 + \sigma_{L1CP}^2} \right) = 0.1470
\end{aligned}$$

Finally, the acquisition presented in Figure 5-16 needs to be done four times due to the relative signs between the L1 C/A and L1C pilot and data channels. Specifically, due to the different navigation messages on the L1 C/A and L1C data channels, and the secondary code on the L1C pilot channel, it is not possible to know (without aiding information) the relative sign between these signals. Therefore, a sign is applied in front of the A , B and C scalars to compute all the possible relative signs. The following possibilities are tested:

- $A + j * B + C$ called *Comb1*

- $A - j * B - C$ called *Comb2*
- $A + j * B - C$ called *Comb3*
- $A - j * B + C$ called *Comb4*

Since the results are squared at the end of the acquisition, the absolute sign of each scalar is not important but only the relative sign. The maximum of the four correlations is finally computed.

As mentioned earlier, a similar method can be applied to combine Galileo L1-B and L1-C. However, since the transmitted power of the signals is the same in this case, the coefficients applied to both ranging codes would be the same and equal to $\frac{1}{2}$. Moreover, concerning the sign only two possibilities would need to be tested: adding or subtracting the ranging codes.

5.2.2 Results using the software signal simulator

In order to test the method presented in the previous section, GPS L1 C/A and L1C data are simulated using the software signal simulator described in Chapter 4. Two different sets of data are simulated with the parameters shown in Table 5-1. Due to a possible change in the sign of the data bit or the secondary bit each ranging code period in the case of L1C, the correlation is done using 20 ms of incoming data using the zero padding technique explained in section 5.1.2.1.

Table 5-1: GPS L1 C/A – L1C Simulation parameters

Parameters	Values	
	First simulation	Second simulation
C/N ₀	45 dB-Hz	32 dB-Hz
Motion	No	No
Interference	None	None
Oscillator error	None	None

The result of the combined acquisition using the values of the first simulation is shown in Figure 5-17. During the first 10 ms, 10 peaks are visible for all combinations. These 10 peaks correspond to the correlation of GPS C/A each millisecond. The 4th peak (around the 3rd ms) is much higher than the other peaks for two of the combinations. One of these combinations corresponds to the acquisition of the three channels with the right sign. This is determined by the highest peak (blue curve). The other combination (green curve) corresponds to the combination with the right sign of L1 C/A with the pilot channel of L1C but a destructive combination (due to the wrong sign) with the data channel of L1C. Indeed, the broadcast power of the data channel of L1C is much smaller than for L1 C/A and the pilot channel of L1C. Therefore, a high peak is visible, but still smaller than when the three channels are combined with the right sign. Concerning the second 10 ms, there is again a peak every 10 ms for all the combinations corresponding to the correlation of

L1 C/A. One of the peaks is higher for one of the combinations (black curve) and this peak is located 10 ms after the highest peak mentioned above. This peak is smaller due to a destructive combination as explained in section 5.1.3.

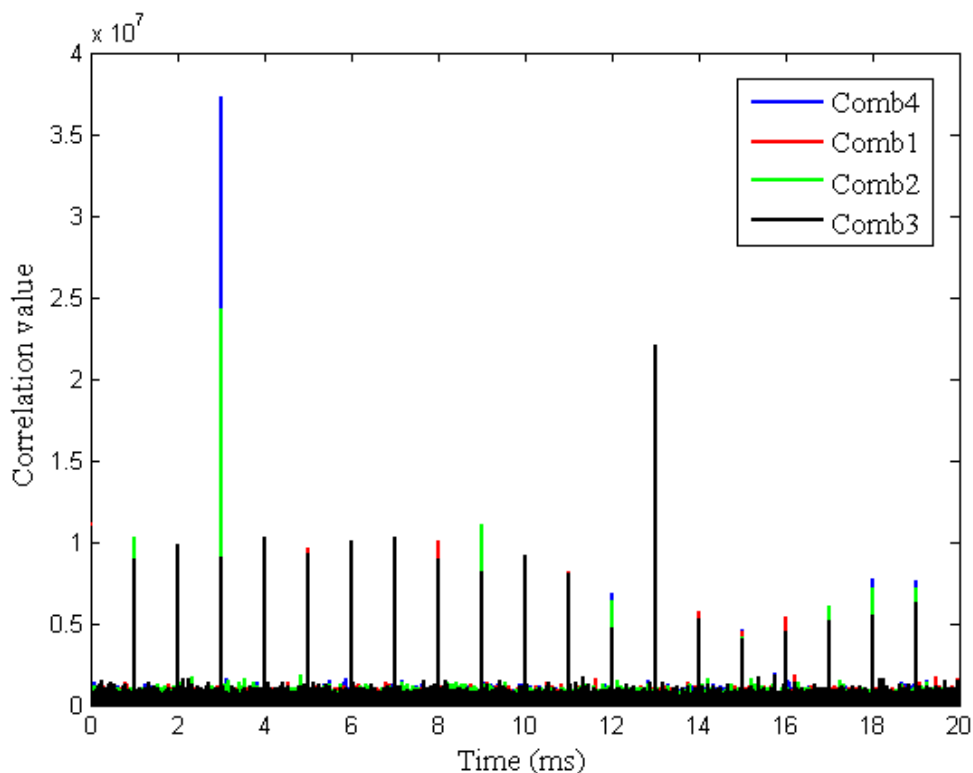


Figure 5-17: Results of the combined acquisition with a C/N_0 of 45 dB-Hz

The result of the combined acquisition using the values of the second simulation is shown in Figure 5-18. As with the first simulation, during the first 10 ms, 10 peaks corresponding to the correlation of GPS C/A each millisecond are visible. However, the ratio between the peaks and the noise level is much smaller than in the previous case due to the low C/N_0 . The 4th peak (around the 3rd ms) is again much higher than the other

peaks for two of the combinations. Overall, the same conclusions as above can be drawn, only the ratio between the peaks and the noise level changes. For comparison, Figure 5-19 shows the acquisition of the L1C data channel alone using the same data (second simulation). This acquisition is done using a zero padding technique with 20 ms of data. It is clearly visible that the acquisition of the L1C data channel alone fails whereas it succeeds in the case of the combined acquisition. However, the secondary peaks (appearing C/A ranging code period) can become an issue at low C/N_0 . Particularly, the probability of false alarm increases due to these peaks. The L1C data channel is chosen for this comparison because it is the signal transmitted with the lowest power.

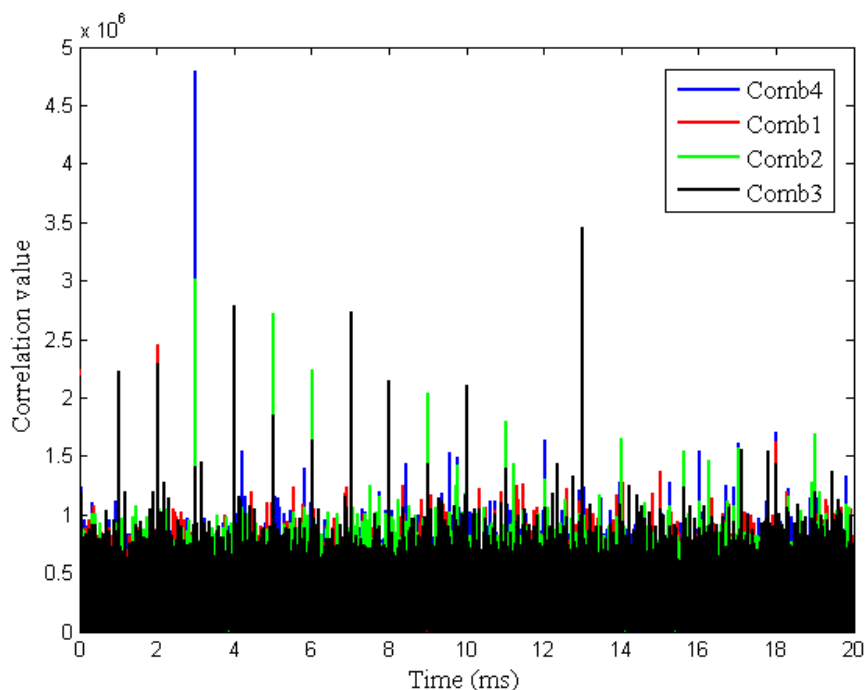


Figure 5-18: Results of the combined acquisition with a C/N_0 of 32 dB-Hz

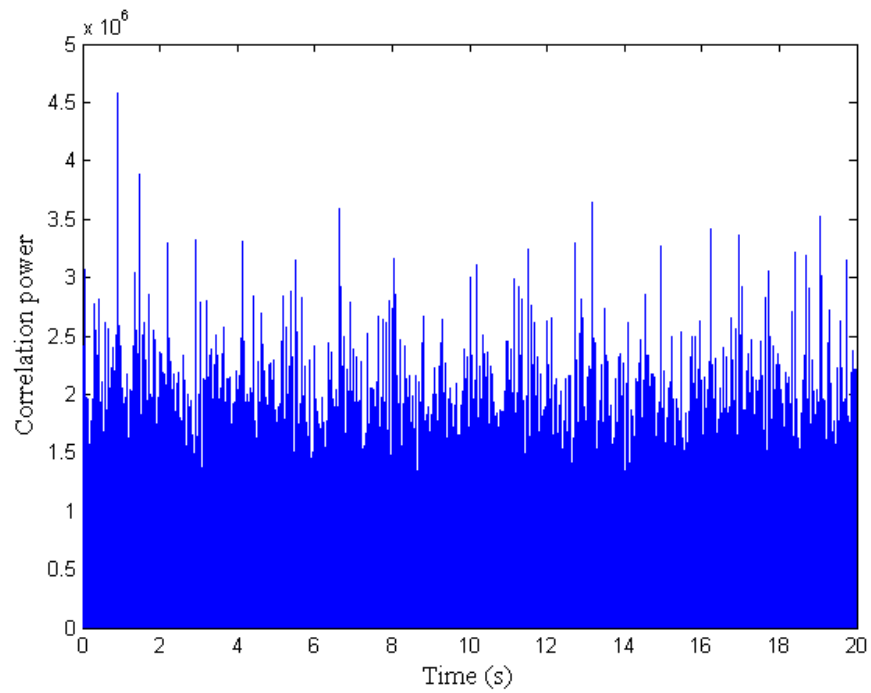


Figure 5-19: Acquisition of the LIC data channel alone for a C/N_0 of 32 dB-Hz

Chapter Six: DEVELOPMENT, IMPLEMENTATION AND TESTING OF COMBINED TRACKING FOR GPS AND GALILEO L1 SIGNALS

Once the signal is acquired, one needs to follow the Doppler and the code delay of the satellite over time; this is the objective of signal tracking. The goal of tracking is to keep all the power in the in-phase component, which allows the decoding of the bits of the navigation message.

This chapter begins with a brief overview of the traditional tracking methods. Then, a method to combine the signals broadcast at the same frequency and from the same constellation is developed. This method can be used to combine GPS L1 C/A with L1C (data and pilot) or Galileo L1 data and pilot channels. Afterwards, a Kalman filter able to track GPS L1 C/A alone developed in previous research (Petovello et al 2006) is implemented. Finally, a Kalman filter able to simultaneously combine GPS L1 C/A with L1C (data and pilot) or Galileo L1 data and pilot channels is developed, tested and finally compared to the performance of the Kalman filter for GPS L1 C/A alone.

6.1 Traditional tracking method

As mentioned before, the goal of tracking is to follow the Doppler, the code delay and the phase over time in order to compute pseudorange and phase measurements.

During traditional tracking, two loops are used in parallel to follow the carrier phase (or the frequency) and the code delay. A PLL (Phase Lock Loop) or FLL (Frequency Lock Loop) or a combination of both is used to follow the changes in the carrier part of the signal. The scheme of a traditional PLL is shown in Figure 6-1. A DLL (Delay Lock Loop) is used to follow the code delay. The scheme of a traditional DLL is shown in Figure 6-2. The incoming signal is multiplied by a locally generated carrier and spreading code, then discriminators are computed for both loops. The discriminator outputs are then filtered to deduce the correction to apply in code delay and Doppler (and code Doppler). Further details can be found in Van Dierendonck (1996), Kaplan (2006), Peterson et al (1995). With all the signals considered here, there is a sign ambiguity due to the navigation message or the secondary code. Due to this ambiguity, it is necessary to use a Costas loop (insensitive to 180° phase shift). Nevertheless, the secondary code is known, and once we know our position within it, it is possible to implement a pure phase lock loop on the pilot channel which allows a gain of up to 6 dB (Kaplan 2006, Tran & Hegarty 2002, Julien 2005).

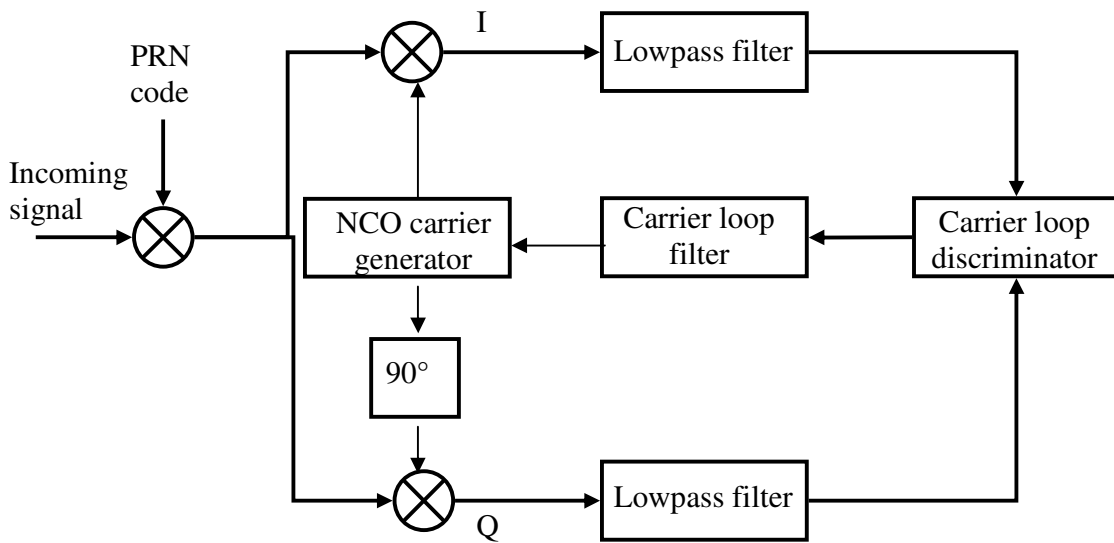


Figure 6-1: Scheme of a PLL (Phase Lock Loop)

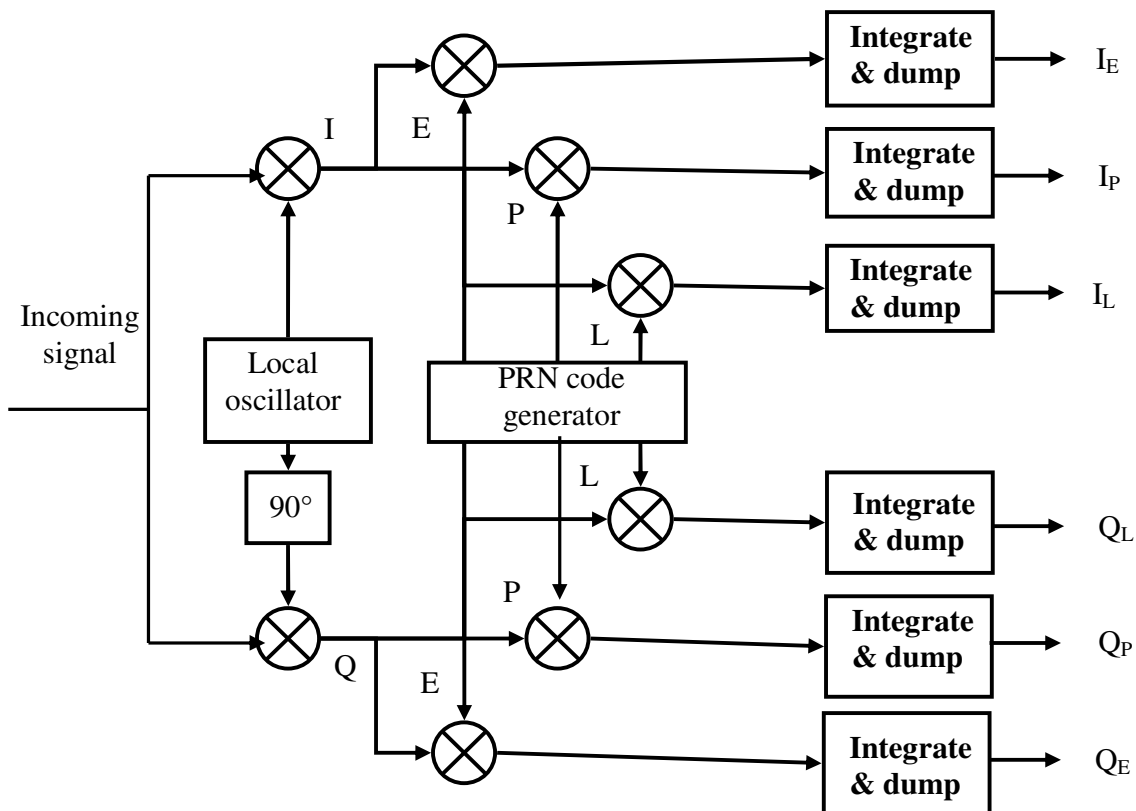


Figure 6-2: Scheme of a DLL (Delay Lock Loop)

The accuracy of a tracking loop depends on its ability to follow the errors, namely mainly thermal noise, multipath, interference and user dynamics. The DLL is more affected by noise and multipath than is the FLL or PLL, whereas interference can affect all the loops. The spreading code used to modulate the signal has a big influence on the impact of these errors on the tracking. For example, a higher chipping rate and a longer spreading code period can reduce the impact on the signal of these errors (Braasch 1997, Betz 2002, Tran 2004). From these observations, we can deduce that the L1C GPS and L1 Galileo signals should be less affected by these errors than L1 C/A due to the length of the spreading codes.

In the case of a BOC modulation, the autocorrelation function contains a main peak sharper than the one of a BPSK modulation which reduces the noise due to multipath (Betz 2002), but the side peaks can create an ambiguity and can be wrongly tracked instead of the main one, leading to degraded tracking performance. Some research has been done on the discriminators to avoid the tracking of these side peaks (Dovis et al 2005, Hegarty 1999, Julien 2005, Julien et al 2007, Macabiau et al 2003). One of the first commercial receivers able to track Galileo L1 and E5a has been developed by NovAtel (NovAtel 15a receiver) and its implementation is described in Gerein et al (2004). Some tracking techniques which can significantly simplify the receiver architecture of future GPS/Galileo L1 receivers have been developed in Julien et al (2007). These techniques take into consideration a pure BOC (1,1) instead of the complete CBOC modulation. However, these techniques are easily adaptable to full CBOC signals (consideration of

the BOC(6,1) as well). Indeed, depending on the tracking accuracy desired, the CBOC can be considered only as a BOC(1,1) for complexity reasons (see Appendix C).

Later in this chapter, the performance of a Kalman filter developed for tracking is compared to that of traditional tracking. The tracking parameters used in the software developed herein for this comparison are summarized in Table 6-1.

Table 6-1: Summary of Traditional Tracking Parameters

Receiver Parameter	Description
PLL Discriminator	$D_{PLL} = \tan^{-1} \frac{Q_p}{I_p}$
PLL Loop Order	Third order
PLL Loop Bandwidth	15 Hz
DLL Discriminator	$D_{DLL} = \frac{\sqrt{I_E^2 + Q_E^2} - \sqrt{I_L^2 + Q_L^2}}{\sqrt{I_E^2 + Q_E^2} + \sqrt{I_L^2 + Q_L^2}}$
DLL Loop Order	Second order
DLL Loop Bandwidth	2 Hz
PLL-Aided DLL	Yes
Correlation time	10 ms
Early-Late spacing	0.05 chip

6.2 Combined GPS L1 C/A and GPS L1C (data and pilot channels) tracking

A new method of tracking is developed here to combine the GPS L1 C/A and L1C (data and pilot channels) signals. Note that a similar method can be applied to Galileo L1-B and L1-C channels. First, the method is explained in detail then some results are shown using a signal generated by the software signal simulator described earlier.

6.2.1 Method of tracking

The combined tracking method developed is shown in Figure 6-3.

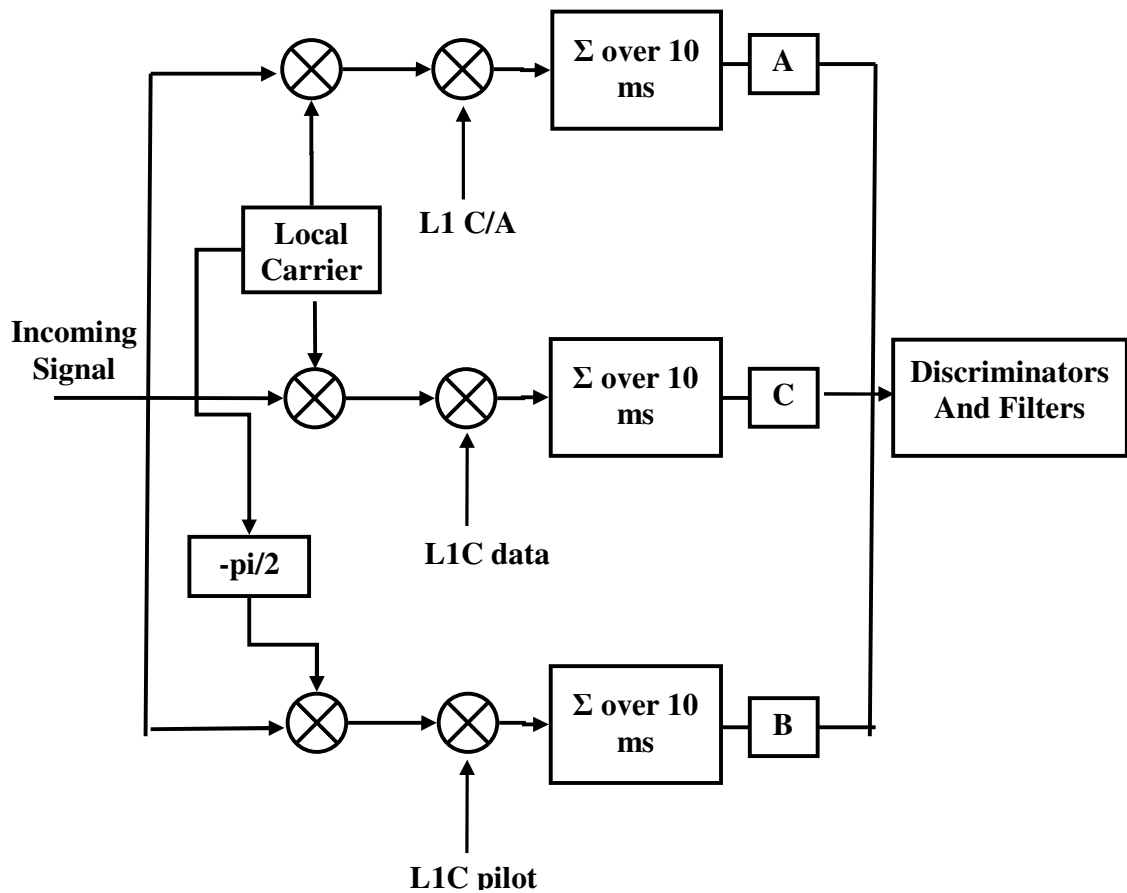


Figure 6-3: Scheme of the combined tracking method

With reference to Figure 6-3, the following steps are performed to realize the combined tracking:

1. Generate the local carrier (corresponding to the intermediate frequency plus Doppler).

2. Remove the carrier from the incoming signal. Note that a shift of $\frac{\pi}{2}$ is applied to the local carrier before multiplying it with the incoming signal in the case of the L1C pilot channel because the pilot channel is transmitted in quadrature.
3. Multiply separately by the L1 C/A, L1C data and pilot channels ranging codes. This correlation is computed for the prompt, early and late correlators for the inphase I and in quadrature Q components (see Figure 6-2). These correlations are computed over 10 ms for each ranging code.
4. The outputs of the previous correlators are then multiplied by the scalars A , B and C . These scalars have been computed in Chapter 5 (section 5.2.1) and are repeated here for convenience:

$$\begin{aligned}
 A &= 1 - \frac{\sigma_{C/A}^2}{\sigma_{C/A}^2 + \sigma_{L1C}^2} \\
 B &= \frac{\sigma_{C/A}^2}{\sigma_{C/A}^2 + \sigma_{L1C}^2} \cdot \frac{\sigma_{L1CD}^2}{\sigma_{L1CD}^2 + \sigma_{L1CP}^2} \\
 C &= \frac{\sigma_{C/A}^2}{\sigma_{C/A}^2 + \sigma_{L1C}^2} \cdot \left(1 - \frac{\sigma_{L1CD}^2}{\sigma_{L1CD}^2 + \sigma_{L1CP}^2} \right)
 \end{aligned} \tag{6.1}$$

5. Compute the following combinations (same as in Chapter 5 section 5.2.1 except the “j” is removed because the local carrier is already shifted by $\frac{\pi}{2}$ for the pilot channel):
 - $A + B + C$ called *Comb1*
 - $A - B - C$ called *Comb2*
 - $A + B - C$ called *Comb3*
 - $A - B + C$ called *Comb4*

6. Take the maximum of the four combinations in step 5.
7. Use the usual discriminators and filters of the DLL and PLL (see Figure 6-1 and Figure 6-2).

As mentioned earlier (and similar to the combined acquisition introduced in Chapter 4, Section 5.2.1), a similar method can be applied to combine Galileo L1-B and L1-C.

6.2.2 Results using the software signal simulator

In order to test the method presented in the previous section, data are simulated using the software signal simulator developed in Chapter 4. Three different sets of data are simulated with the parameters shown in Table 6-2. The C/N_0 indicated in the table is the C/N_0 of GPS L1 C/A. Concerning the third simulation, the motion is as follows:

- Static for 5 s
- Acceleration of 10 m/s^2 for 10 s
- Constant speed for 5 s
- Deceleration of 10 m/s^2 for 5 s
- Acceleration of 10 m/s^2 for 5 s

Table 6-2: Simulation parameters

Parameters	Values		
	First simulation	Second simulation	Third simulation
C/N ₀	45 dB-Hz	32 dB-Hz	45 dB-Hz
Motion	No	No	Yes
Interference	None	None	None
Oscillator error	None	None	None
Time of simulation	30 s	30 s	30 s

The simulated signals are tracked using the combined tracking method presented in the previous section as well as using a traditional tracking method able to track the GPS L1C data channel alone (lowest power of the three channels). One metric used to assess the performance of the method implemented and compare it to a traditional tracking method is the Phase Lock Indicator (PLI). The PLI can be defined as follows (Van Dierendonck 1996):

$$PLI(t) = \frac{\left(\sum_{i=1}^M I_p(t+i)\right)^2 - \left(\sum_{i=1}^M Q_p(t+i)\right)^2}{\left(\sum_{i=1}^M I_p(t+i)\right)^2 + \left(\sum_{i=1}^M Q_p(t+i)\right)^2} \quad (6.2)$$

where $PLI(t)$ is the PLI at time t

I_p is the in-phase prompt correlator

Q_p is the in-quadrature prompt correlator

M is fixed to 50 here

The results of the static tests (first and second simulation) are shown in Figure 6-4 and Figure 6-5. Note that the results of the first simulation for the combined method are reproduced in both figures for comparison purposes. As shown by the Doppler measurements and the PLI in these figures, the combined tracking is able to track the signals at 45 dB-Hz. The tracking using only the L1C data channel is able to track at 45 dB-Hz but its performance is not as good as that of the combined tracking, namely the Doppler measurements are noisier and the PLI is not as close to unity. Concerning the test at 32 dB-Hz, the Doppler measurements are noisier and the PLI is not as close to unity with the lower C/N_0 but the combined tracking is still able to track. However, the tracking using only the L1C data channel is not able to track when the signal is transmitted at 32 dB-Hz (C/N_0 of GPS L1 C/A). Concerning the test with motion (third simulation), the Doppler and PLI measurements for the combined tracking and the tracking using the L1C data channel only are shown in Figure 6-6. As for the static test, the Doppler measurements from the combined method are less noisy than the ones of the L1C data channel only. Concerning the PLI, again the L1C data channel only tracking is not as close to unity as the combined tracking but is affected by the user motion as much as the combined tracking.

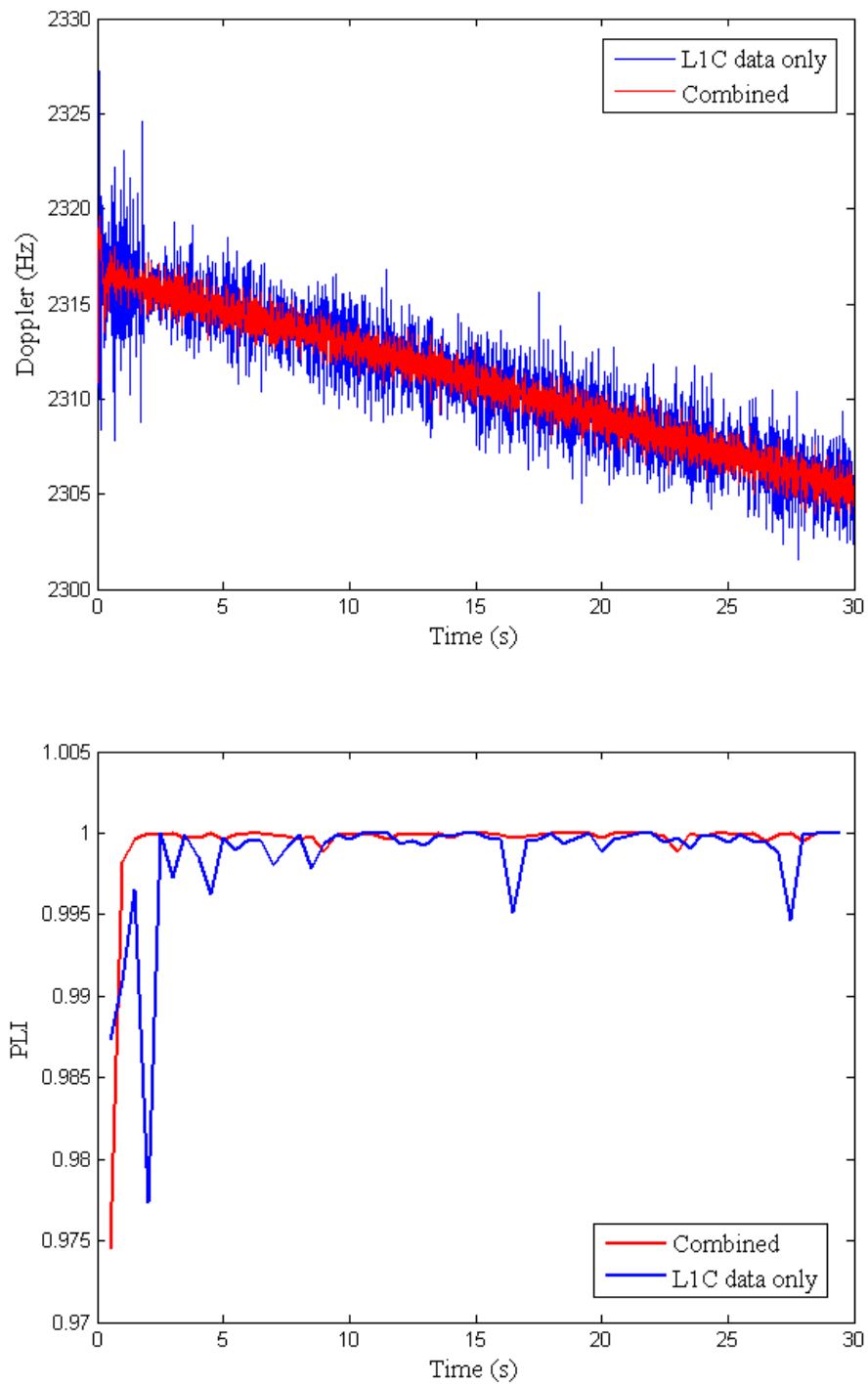


Figure 6-4: Doppler (on top) and PLI (on the bottom) for the combined tracking and the L1C data channel only tracking - First simulation

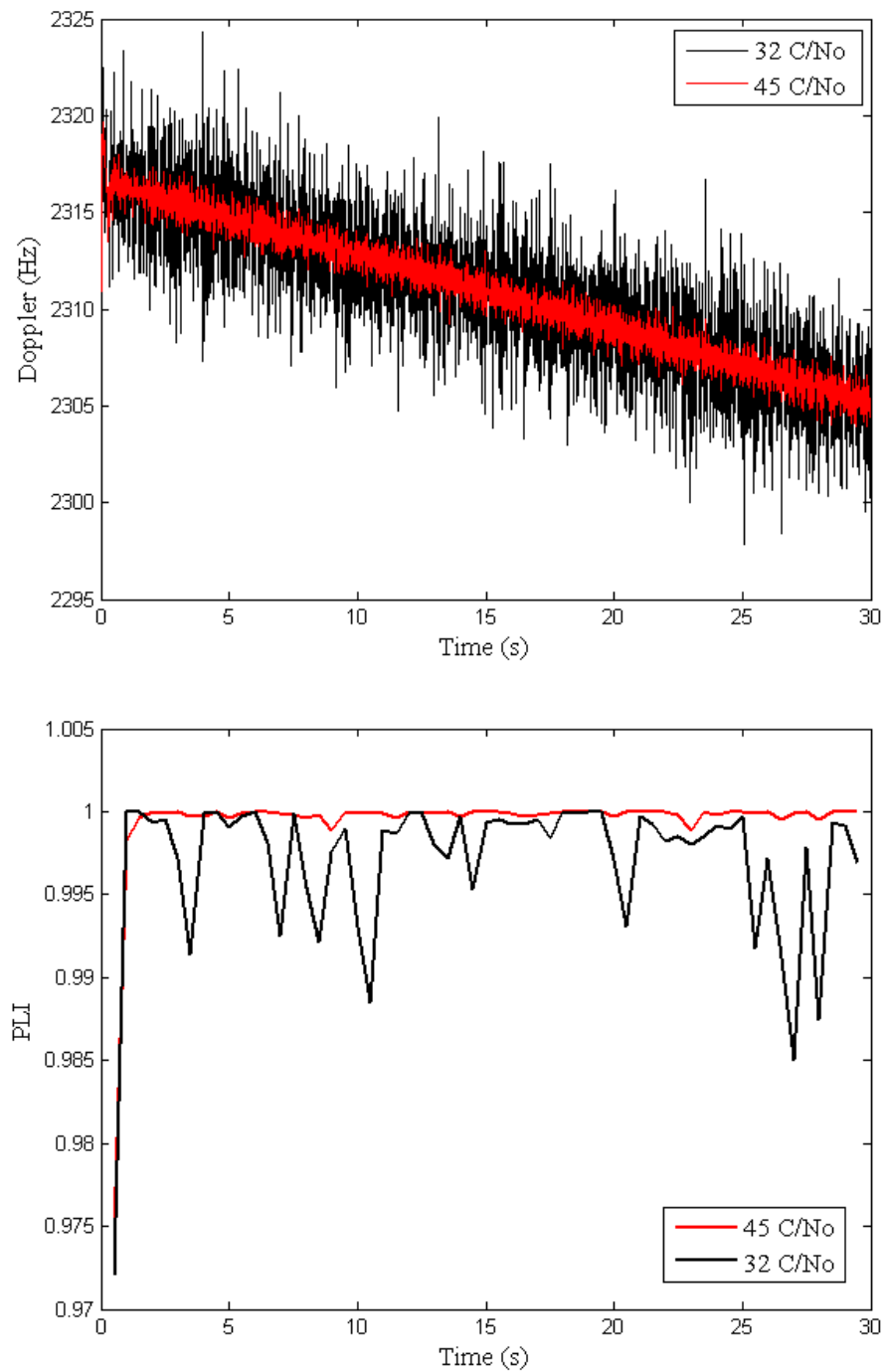


Figure 6-5: Doppler (on top) and PLI (on the bottom) for the combined tracking - First and second simulations

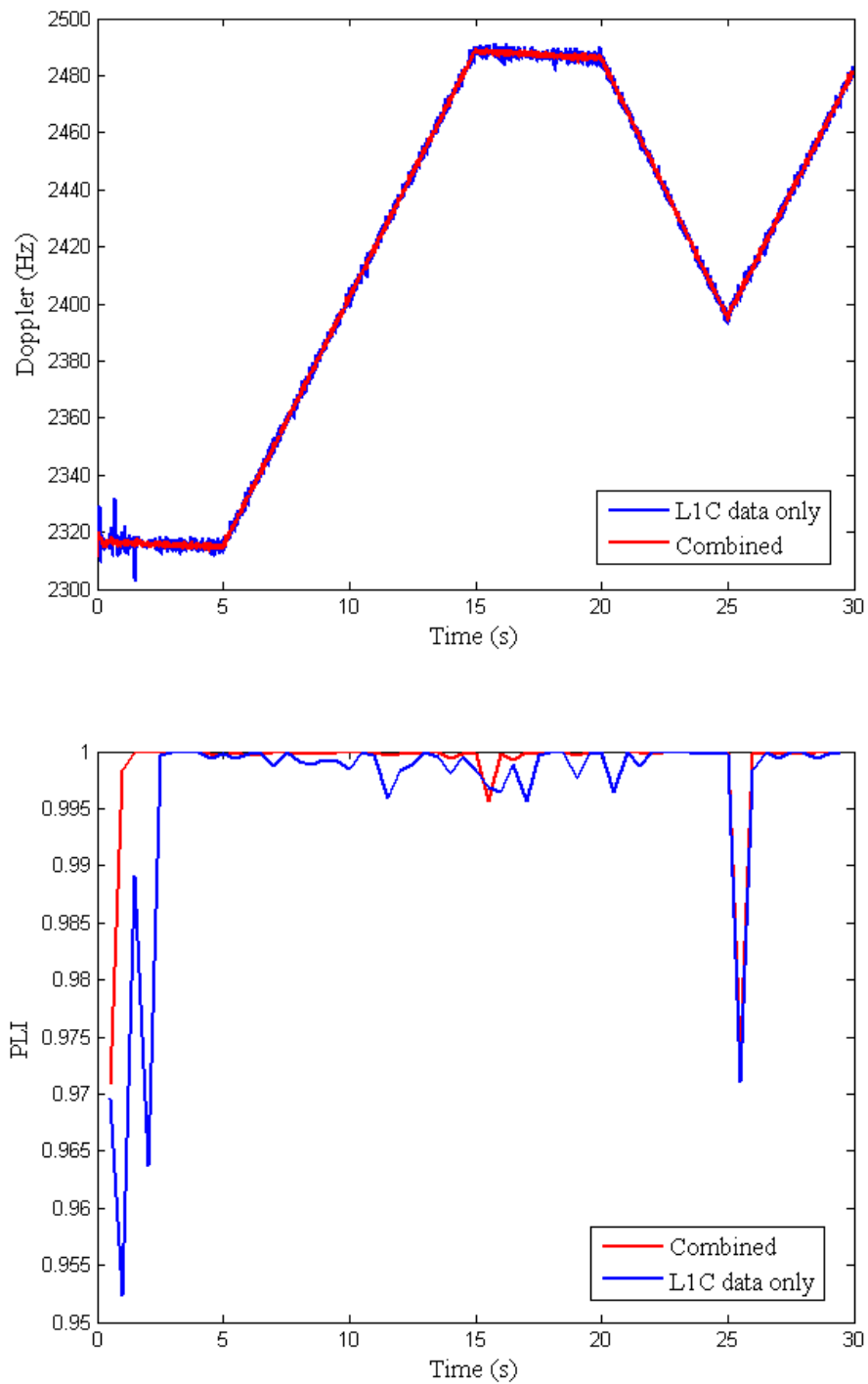


Figure 6-6: Doppler (on top) and PLI (on the bottom) for the combined tracking and the L1C data channel only tracking - Third simulation

From these tests, one can deduce that the combined tracking performs better than the traditional tracking but does not show a high improvement in case of dynamics. Indeed, since the same PLL bandwidth is used, the combined tracking is not able to perform better under dynamics. However, the increase in the number of observations increases the tracking accuracy and reliability.

6.3 Kalman filter for tracking

This section reviews the “traditional” Kalman filter which is then modified in the next section to track simultaneously several signals. The “traditional” KF is able to track GPS L1 C/A and the modified one combines the three GPS L1 channels. The comparison of the performance of the two Kalman filters with a traditional tracking method is also given in various conditions.

6.3.1 Traditional Kalman filter for GPS L1 C/A only tracking

The goal of a Kalman filter for tracking is to replace the discriminators as well as loop filters of the DLL and PLL by a Kalman filter to estimate the errors of frequency, code delay and code Doppler and to correct the code and carrier frequency generation. Concerning the Kalman filter for one channel only, the method presented here follows closely the methods presented in Petovello & Lachapelle (2006), Psiaki (2001) and Psiaki & Jung (2002). The novelty of this research is the creation of a method and its implementation to combine different signals in a single Kalman filter.

The observations used by the filter are the outputs of the six correlators (I and Q for early, prompt and late) and can be expressed as

$$\begin{cases} I = \tilde{A} \cdot \tilde{R}(\delta\tau - \Delta) \cdot \cos(\delta\varphi) + n_I & (6.3) \\ Q = \tilde{A} \cdot \tilde{R}(\delta\tau - \Delta) \cdot \sin(\delta\varphi) + n_Q & (6.4) \end{cases}$$

with
$$\tilde{A} = A \cdot \frac{\sin(\pi \cdot \delta f \cdot T)}{\pi \cdot \delta f \cdot T}$$

$$\delta\varphi = \delta\varphi_0 + \frac{T}{2} \cdot \delta f_0 + \frac{T^2}{6} \delta a_0$$

where A is the signal amplitude

\tilde{R} is the autocorrelation function

$\delta\tau$ is the error in the local code delay

Δ is the spacing between the prompt and the early/late correlators

$\delta\varphi$ is the average error in the local carrier phase over the integration interval

T is the coherent integration time interval

$\delta\varphi_0$ is the error in the local carrier phase at the beginning of the integration interval

δf_0 is the error in the local carrier frequency at the beginning of the integration interval

δa_0 is the phase acceleration error (frequency rate error) at the beginning of the integration interval

n is the noise (assumed as Gaussian).

In this expression, the amplitude has been combined with an attenuation factor that depends on the frequency error. Using this expression, the frequency error is only observed through the carrier phase error model.

In general, measurements to a Kalman filter must be expressed as a function of the state vector as follows:

$$\delta z_k = \left. \frac{\partial h(x_k, k)}{\partial x_k} \right|_{x_k = \hat{x}_k} \delta x_k + v_k = H_k \cdot \delta x_k + v_k \quad (6.5)$$

where $\delta z_k = z_k - \hat{z}_k$, $\delta x_k = x_k - \hat{x}_k$, z_k and x_k are the real values of the measurements and the state vector at time epoch k , \hat{z}_k and \hat{x}_k are the estimated values of the measurements and the state vector, δz_k is the measurement misclosure, δx_k is the perturbed state vector, H_k is the design matrix, $h(x, k)$ is the function which express z_k as function of x_k and v_k is the noise associated with the measurement model (assumed Gaussian with covariance matrix C_{v_k}).

Thus, the measurements misclosure represents the difference between the exact but unknown values of the measurements and the estimated measurements and can be expressed as follows:

$$\delta z_k = \begin{pmatrix} I_P \\ I_E \\ I_L \\ Q_P \\ Q_E \\ Q_L \end{pmatrix} - \tilde{A} \begin{pmatrix} R(\delta\tau) \cos(\delta\phi) \\ R(\delta\tau - \Delta) \cos(\delta\phi) \\ R(\delta\tau + \Delta) \cos(\delta\phi) \\ R(\delta\tau) \cos(\delta\phi) \\ R(\delta\tau - \Delta) \cos(\delta\phi) \\ R(\delta\tau + \Delta) \cos(\delta\phi) \end{pmatrix} \quad (6.6)$$

where I_P , I_E and I_L represent the outputs of the prompt, early and late correlators of the in-phase component, respectively, and Q_P , Q_E and Q_L represent the corresponding outputs of the quadrature component.

The dynamic model used can be expressed as follows:

$$\begin{pmatrix} \dot{A} \\ \delta\dot{\tau} \\ \delta\dot{\varphi}_0 \\ \delta\dot{f}_0 \\ \delta\dot{a}_0 \end{pmatrix} = \begin{pmatrix} 0 & 0 & 0 & 0 & 0 \\ 0 & 0 & 0 & \beta & 0 \\ 0 & 0 & 0 & 1 & 0 \\ 0 & 0 & 0 & 0 & 1 \\ 0 & 0 & 0 & 0 & 0 \end{pmatrix} \begin{pmatrix} A \\ \delta\tau \\ \delta\varphi_0 \\ \delta f_0 \\ \delta a_0 \end{pmatrix} + \begin{pmatrix} 1 & 0 & 0 & 0 & 0 \\ 0 & 1 & \beta & 0 & 0 \\ 0 & 0 & 1 & 0 & 0 \\ 0 & 0 & 0 & 1 & 0 \\ 0 & 0 & 0 & 0 & 1 \end{pmatrix} \begin{pmatrix} w_A \\ w_{code} \\ w_{clock} \\ w_{freq} \\ w_{acc} \end{pmatrix} \quad (6.7)$$

where β is used to convert carrier cycles to code chips and the w_i terms are the noise values associated with the i^{th} term.

To evaluate the covariance matrix of the process noise associated with the dynamic model, the main parameters taken into account are as follows:

- The ionospheric divergence effect (delay for the code and advance for the phase), which is represented by w_{code}
- The oscillator errors (clock drift and drift rate), which is represented by w_{clock} and w_{freq}
- Expected phase acceleration, which is represented by w_{acc}

One set of values used for the process noise covariance matrix are shown in Table 6-3 and depend on the type of oscillator and the level of dynamics. In terms of the receiver oscillator, the values shown correspond to an OCXO quality oscillator.

Table 6-3: Numerical values of the covariance matrix

Noise	Covariance
w_A	10^{-5} s^{-1}
w_{code}	$25 \cdot 10^{-6} \text{ m}^2 \cdot \text{s}^{-1}$
w_{clock}	$3.92 \text{ rad}^2 \cdot \text{s}^{-1}$ or $35.8 \text{ cm}^2 \cdot \text{s}^{-1}$
w_{freq}	$7.73 \cdot 10^{-2} \text{ rad}^2 \cdot \text{s}^{-3}$ or $0.707 \text{ cm}^2 \cdot \text{s}^{-3}$
w_{acc}	$0.5 \text{ rad}^2 \cdot \text{s}^{-5}$ or $4.75 \text{ cm}^2 \cdot \text{s}^{-5}$

In order to compute the design matrix H_k and the estimated measurement \hat{z}_k , one needs to estimate the values of the autocorrelation function as a function of the shift from the maximum correlation peak. For the simulated signals used herein, no front-end filter is simulated so the autocorrelation function is almost a perfect triangle. The derivative is estimated first, and then is integrated to obtain the autocorrelation function. The derivative is generated as piecewise-continuous as follows:

- $\frac{d\hat{R}(t)}{dt} = 1$ for $t = [-1 : -0.01]$
- $\frac{d\hat{R}(t)}{dt} = -100 \cdot t$ for $t = [-0.01 : 0.01]$
- $\frac{d\hat{R}(t)}{dt} = -1$ for $t = [0.01 : 1]$

Integrating the above using appropriate initial conditions gives:

- $\hat{R}(t) = t + 1$ for $t = [-1 : -0.01]$
- $\hat{R}(t) = -50t^2 + 0.995$ for $t = [-0.01 : 0.01]$
- $\hat{R}(t) = -t + 1$ for $t = [0.01 : 1]$.

Using the above, an extended Kalman filter has been implemented using the traditional Kalman filter equations, which are summarized briefly below (Gelb 1974):

$$x_k(-) = \Phi \cdot x_{k-1}(+) \quad (6.8)$$

$$P_k(-) = \Phi \cdot P_{k-1}(+) \cdot \Phi^T + Q_{k-1} \quad (6.9)$$

$$\bar{K}_k = P_k(-) \cdot H_k^T \left(H_k \cdot P_k(-) \cdot H_k^T + C_{v_k} \right)^{-1} \quad (6.10)$$

$$x_k(+) = x_k(-) + \bar{K}_k \cdot \delta z_k \quad (6.11)$$

$$P_k(+) = \left(I - \bar{K}_k \cdot H_k \right) P_k(-) \quad (6.12)$$

where x is the state vector

P is the covariance matrix of the state vector

Φ is the transition matrix

Q is the process noise covariance matrix

K is the Kalman gain matrix

H is the design matrix

C_v is the covariance matrix associated with the noise of the observation model

δz is the measurement misclosure.

The subscript denotes the time epoch and the (-) and (+) denotes if the corresponding quantity is considered before or after the measurement update, respectively.

At the end of each measurements update, the parameters of the NCO are corrected using the values of the state vector, and the corresponding values of the state vector used to update the NCO are set to zero for the next iteration. In other words, the state vector is reset to the following:

$$x_{k-1}(+) = \begin{bmatrix} \tilde{A} \\ 0 \\ 0 \\ 0 \\ \delta a_0 \end{bmatrix}_{k-1} . \quad (6.13)$$

The phase acceleration term is not reset because, for the receiver implemented herein, the carrier NCO assumes a constant frequency between updates.

6.3.2 Kalman filter to simultaneously combine GPS L1 C/A with GPS L1C (data and pilot channels)

This section describes a Kalman filter to simultaneously track the L1 C/A signal and the L1C (pilot and data channels) signal. In the following, the TMBOC modulation is considered as a BOC(1,1) modulation (i.e., the BOC(6,1) is ignored) since the loss created by this approximation is not consequential but results in a receiver that is easier to

implement (see Appendix C). The detail of the derivation of the model of the Kalman filter is shown in Appendix D.

One possible method to track all signals is to augment the state vector to include the L1C signal tracking errors. However, this approach implicitly considers the different signals as independent. Since the signals come from the same satellite and are time synchronized, one effectively loses information by doing so. Indeed, the amplitudes of the signals are related as a function of their transmitted power, but all the other states of the state vector are the same (i.e., code phase error, phase error, etc.). Therefore, this approach was not selected.

Another approach is to augment the measurement model using the outputs of the 18 correlators (6 correlators per signal/channel). The method developed here uses this approach. However, for the sake of efficiency, the Kalman filter is implemented using a sequential measurement processing method (Petovello 2003). The method is described below.

The measurements to the filter are the outputs of the 18 correlators, six for L1 C/A and six for each the pilot and data channels of L1C. The output of these correlators depends on the amplitude of the signal, the autocorrelation function, the error in code delay and the error in phase, as shown previously, namely:

$$\begin{cases} I = \tilde{A} \cdot \tilde{R}(\delta\tau - \Delta) \cdot \cos(\delta\varphi) + n_I \\ Q = \tilde{A} \cdot \tilde{R}(\delta\tau - \Delta) \cdot \sin(\delta\varphi) + n_Q \end{cases}$$

The difference from the Kalman filter in the previous section is that in this case, there are three measurement vectors, that is one for each channel. The state vector is the same as before since all the errors are the same between channels. Only the amplitude of the signal changes is due to the difference in the transmitted power. This is compensated by using a scale factor in the amplitude term (see later in this section for more detail). For each channel, all the outputs of the correlators are normalized by the square root of the sum of the square of the in-phase and in-quadrature prompt correlators in order to match them with the proposed model of the autocorrelation function. To take into account the different powers of the channels, the value of the C/N_0 in the matrix associated with the measurement model is changed accordingly for each channel (more details are shown in Appendix D).

Considering the autocorrelation function, two different models have to be derived here:

- One for the L1 C/A: the model shown above will be used
- One for L1C_D and L1C_P, due to the BOC modulation. This model is presented below.

To model the autocorrelation function of the BOC modulation, the derivative is estimated first, and then is integrated to obtain the autocorrelation function. The derivative is generated as piecewise-continuous over seven intervals. However, the model becomes complicated due to the inflexion points resulting from the side peaks (around 0.5 chips from the main peak) and since it does not have an impact on the performance, these areas are approximated by a constant over very small intervals and the derivative is modeled

without discontinuities (see Appendix D for more details). This model is presented in Figure 6-7.

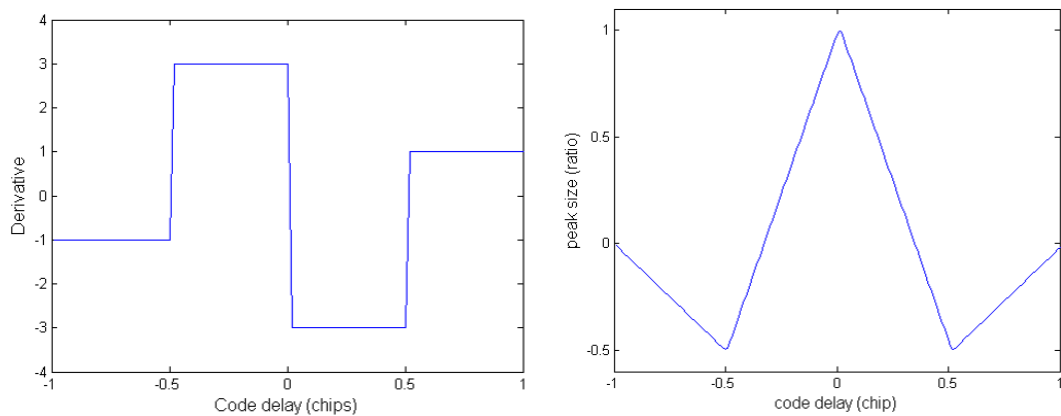


Figure 6-7: Model of the autocorrelation function of L1C (on the right) and its derivative (on the left)

The measurement vector is also the same as before, but is considered on a channel-by-channel basis. To make this distinction, the channel vector is now denoted as $Z_{channel,k}$, where “channel” is either L1C/A, L1CD or L1CP. Because the measurement vector is the same, we can use the same model as for L1 C/A, except apply it three times (in succession) per integration interval, using the measurements of the three channels. This is possible because the noise values are sufficiently uncorrelated between the three channels due to the orthogonality properties of the codes. With this in mind, the following paragraph describes the update process in more detail. Interested readers are also directed to Gelb (1974).

For the receiver implemented herein, the integration time chosen is 10 ms due to the ranging code period of the L1C codes. The equations used are similar to those for L1 C/A. The basic steps used to implement the filter are as follows:

- Predict the state vector and its covariance at the measurement time.
- Update the state vector using the L1 C/A measurements in the same way as for the traditional filter. The linearization point is the predicted state vector from the previous step.
- Update the state vector using the measurements of L1C data channel. In this case however, the linearization point is the state vector estimate from the previous step.
- Update the state vector using the L1C pilot channel. Again, the linearization point is the state vector estimate from the previous step.
- Correct the code and carrier NCOs using the state vector estimates and then reset it to zero, as discussed above.

In summary, after each iteration, one has a new estimate of the state vector using the measurements from all the signals processed up to that step. The signs of the outputs of the prompt correlators are used to determine the signs of the data bits on L1 C/A and L1C.

Using the above method, the sizes of the corresponding update matrices (i.e., H, R and K) are not increased compared to the traditional Kalman filter presented in the previous section, thus providing an efficiency gain. Moreover, using this method (with appropriate modifications), one can update the different channels asynchronously and, for example,

integrate longer on the pilot channel (no data bits) than on the data channels to track weaker signals.

For both Kalman filters, the effect of dynamics is taken into account by increasing the variance of the phase acceleration process noise (higher values means higher dynamics). Indeed, the motion of the user induces higher variations in the phase, the frequency, the phase acceleration and the code phase. In addition, increasing the variance of the process noise corresponding to phase acceleration increases as well the variances of the process noise corresponding to the frequency and the phase (since the frequency and phase are the first and second integrals of the phase acceleration). The variance of the process noise corresponding to the code phase is increased as well since $\delta\dot{t} = \beta \cdot \delta f_0 + w$ with

$$w = w_{code} + \beta \cdot w_{clock}.$$

6.3.3 Results and comparison of the performance of the Kalman filters with the traditional tracking

In order to analyze the performance of the Kalman filter using L1 C/A only and the combined Kalman filter and to compare them to the traditional tracking, results of several tests in static and dynamic mode are shown below.

6.3.3.1 Tests in static mode

To analyze the performance of the combined Kalman filter and compare it with the performance of the Kalman filter with C/A only and the traditional tracking, several tests in static mode were conducted. To do these tests, the software simulator developed in Chapter 4 is used. The parameters of the static tests are shown in Table 6-4. The oscillator used in this test is the same as that presented in Chapter 4.

For each test, the performance is assessed using the PLI and the Doppler values. Moreover, since all the results are generated using the software simulator, the true (simulated) Doppler and code delay are known. Therefore, these values are compared with the ones found by the Kalman filter with C/A only, the traditional tracking and the combined Kalman filter.

Table 6-4: Simulation parameters

Parameter	Value		
	Test 1	Test 2	Test 3
GPS L1 C/A C/N ₀	45 dB-Hz	30 dB-Hz	45 dB-Hz
Motion	No		
Simulation time	20 s		
Oscillator Error Model	None	None	OCXO ¹
Interference	No		

The Doppler and the Doppler error of the first test are shown in Figure 6-8. First, both Kalman filters are less noisy than the traditional tracking. Indeed, the noise associated with the traditional tracking is about 1 Hz around the true Doppler, whereas the noise associated with both Kalman filters is similar and almost null. Figure 6-9 represents the code delay error for the first test for the three tracking methods. First, all three methods converge to the true code delay. Secondly, the traditional tracking is much noisier than both Kalman filters: the error in code delay varies from about -2.5 m to +2.5 m in the case of traditional tracking and between -50 cm and +50 cm for both Kalman filters. The variance of code delay error of the combined Kalman is smaller than that for the Kalman filter with only L1 C/A.

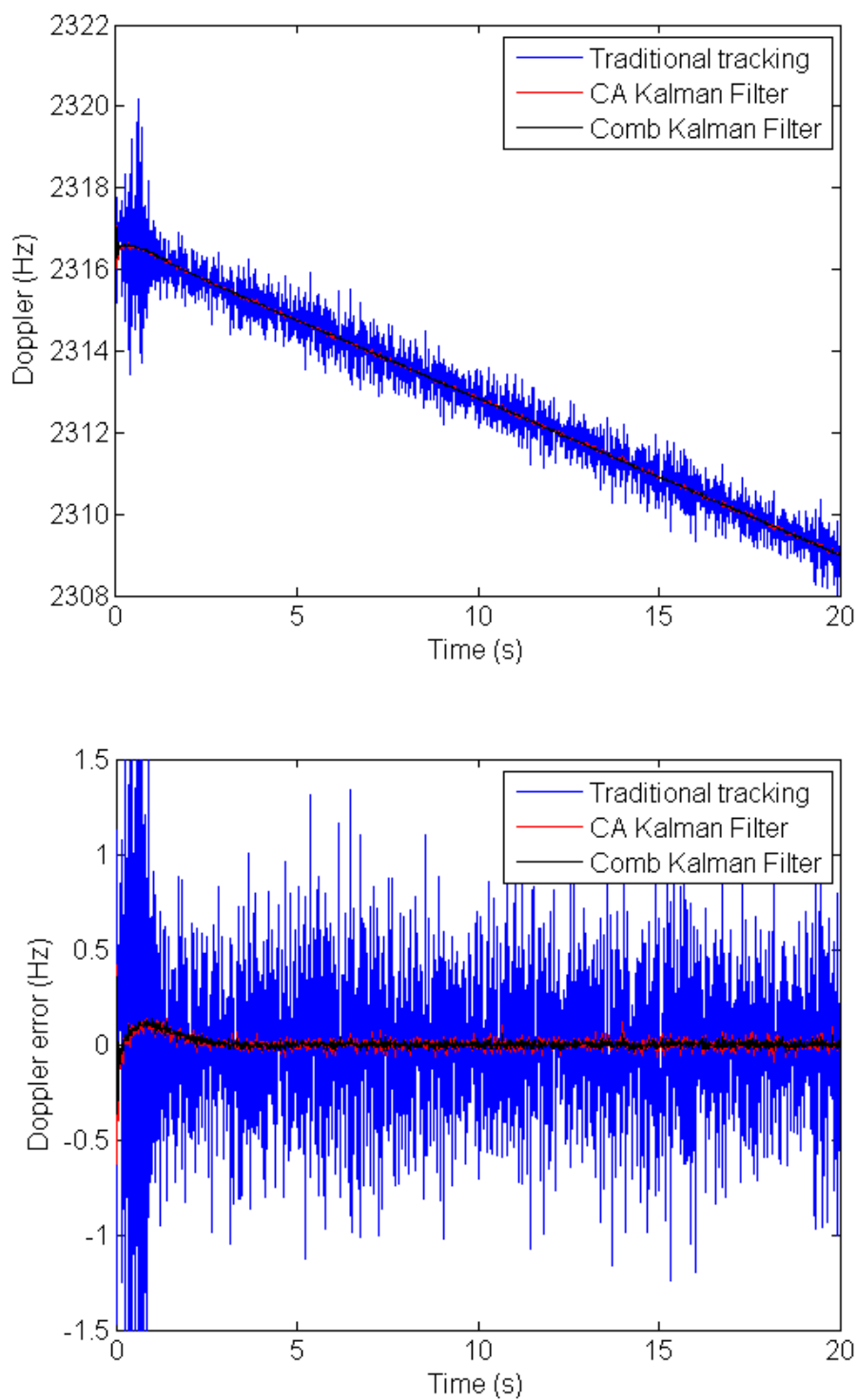


Figure 6-8: Doppler and error in Doppler for the first static test for the three tracking methods

Finally, Figure 6-10 shows the PLI (defined in Section 6.2.2) for the first test for the three tracking methods. All three PLI converge to approximately 1 which is the perfect value and the differences between the three approaches are not significant. Therefore, with a high C/N_0 and without any motion or error, the combined Kalman filter is able to track slightly better than the two other methods. Moreover, the three signals are tracked simultaneously using the combined Kalman filter. The performance does not change significantly compared to the Kalman filter with L1 C/A alone. However, this is not surprising because the results were already very good using only L1 C/A because of the strong signals considered, and it must be borne in mind that the simulator does not simulate any errors except white noise.

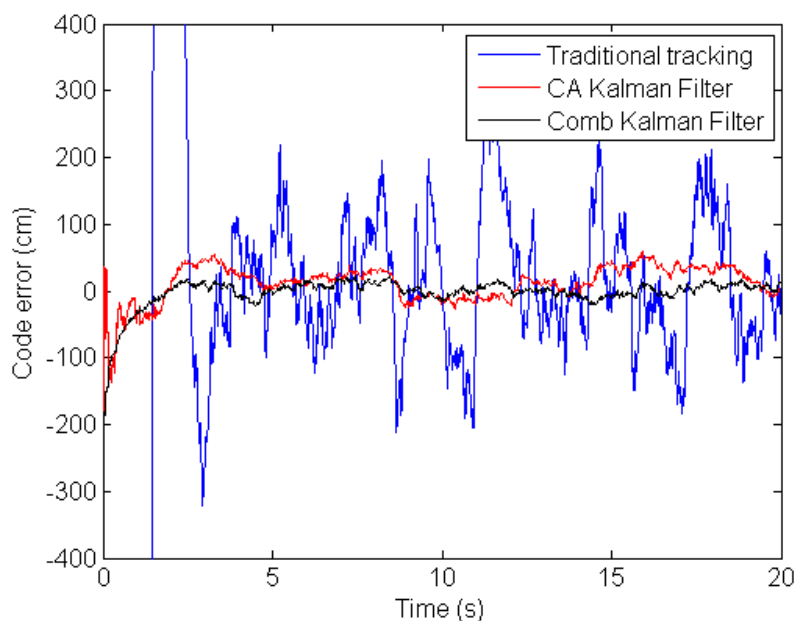


Figure 6-9: Code delay error for the first test for the three tracking methods

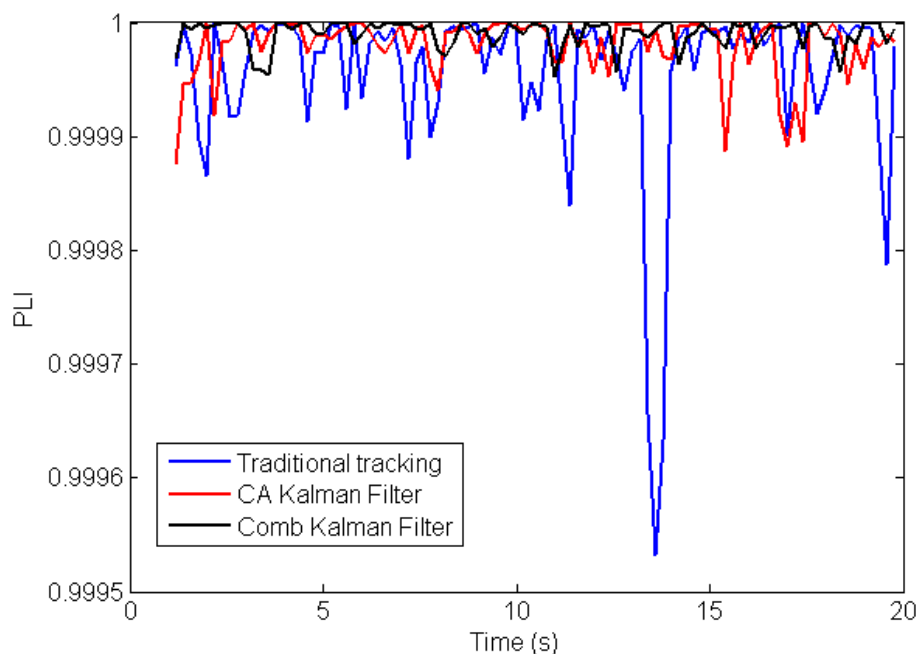


Figure 6-10: PLI for the first test for the three tracking methods

Concerning the second static test, the results are shown in Figure 6-11. Here, only the results for the combined Kalman filter and the Kalman filter for C/A only are shown. Indeed, the traditional filter was not able to track the signal in this case. As shown on the top figures (Doppler and Doppler error), both filters are able to track at low C/N_0 (30 dB-Hz), and the Kalman filter for C/A only is slightly noisier than the combined Kalman filter. The same conclusion can be drawn from the bottom left figure, showing the code delay error. The code delay error stays larger for the Kalman filter for C/A only than the combined Kalman filter. This is again confirmed by the PLI which experiences marginally lower values for the Kalman filter for C/A only than the combined Kalman filter, even if the PLI is still very close to one. Therefore, both Kalman filters are able to track at low C/N_0 values, whereas the traditional tracking method cannot, even if the error

increases compared to high C/N_0 . Moreover, the combined Kalman filter shows better performance than the Kalman filter for C/A only for all the parameters considered. Nevertheless, one has to keep in mind that these results have been generated using simulated data, thus only white noise is simulated. With real data, the difference is expected to be larger since other effects will be present. In particular, weak signals may also contain multipath, which can degrade the performance of the filter.

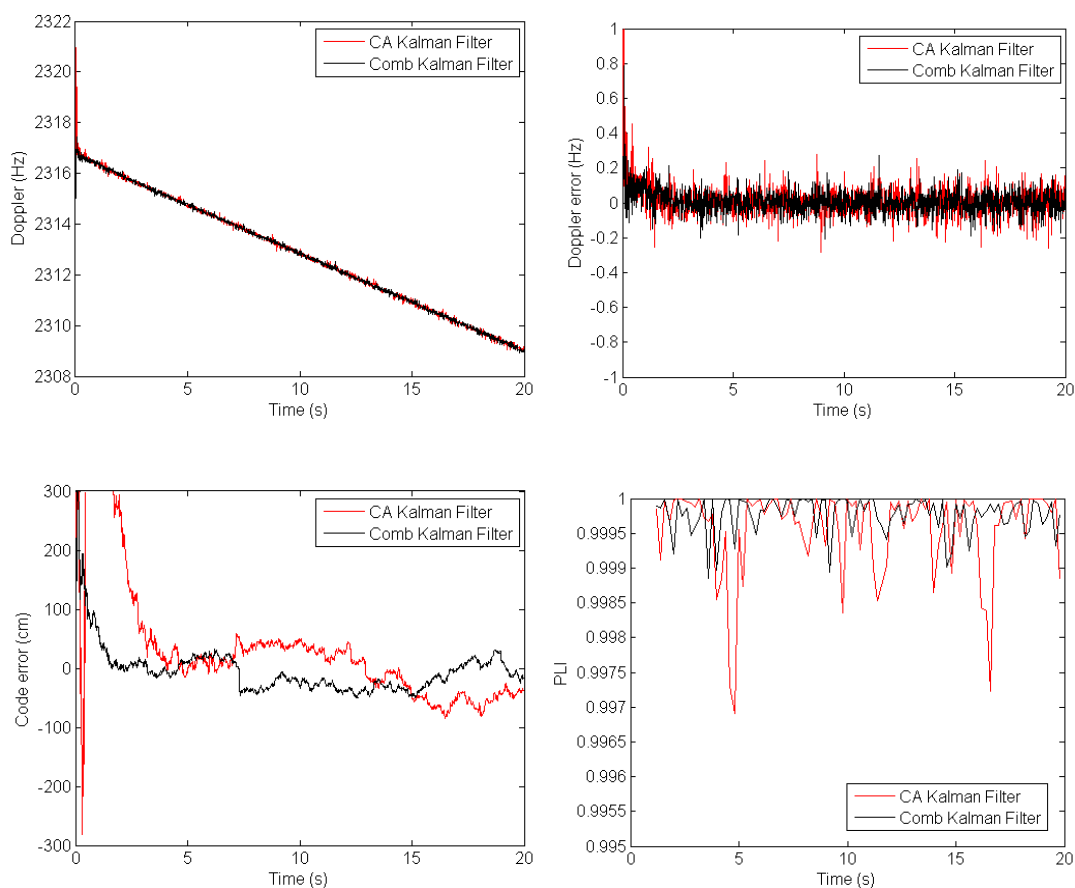


Figure 6-11: Doppler and Doppler error for the second static test (top figures), code delay error (bottom left figure) and PLI (bottom right figure)

Concerning the third static test (tests including oscillator error simulation), the results are shown in Figure 6-12. First, other tests have been run using other oscillators and the results are very similar and the same conclusions can be drawn. As can be seen in these figures, the convergence time of the combined Kalman filter is smaller than that for the C/A code Kalman filter. Moreover, the noise level is much smaller for the Doppler and for the code delay for both Kalman filters relative to the traditional tracking. Indeed, the Kalman filters use the a priori information on the oscillator model (through the noise covariance matrix associated to the dynamic model) whereas the traditional tracking does not have any information on the oscillator. In addition, the level of noise of the combined Kalman filter is again smaller than the one of the C/A code Kalman filter.

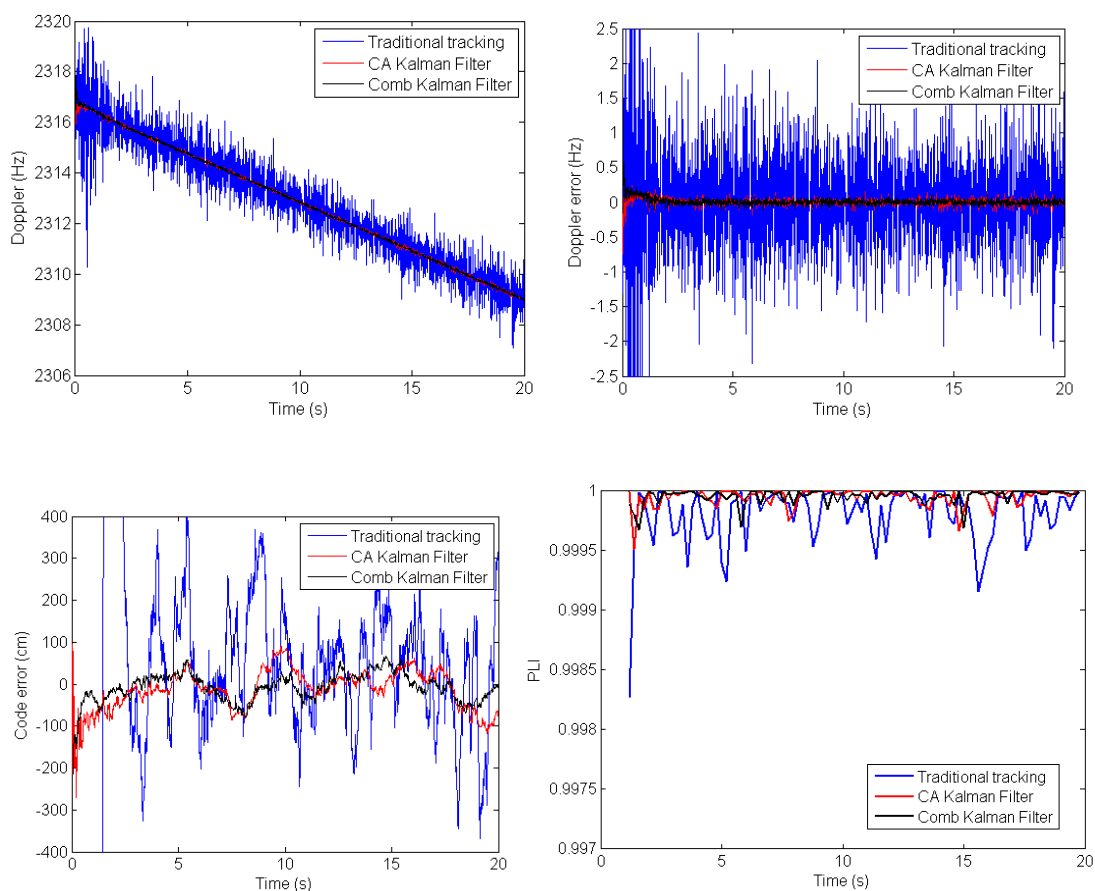


Figure 6-12: Doppler and Doppler error for the third static test (top figures), code delay error (bottom left figure) and PLI (bottom right figure)

The improvement brought by the Kalman filter (relative to the traditional tracking method) can be explained by the selection of the process noise parameters and by the fact that the code, frequency and phase are all tracked together, instead of in separate loop filters (linked only through the loop aiding). Note that in the case of varying C/N_0 , the Kalman filter can weigh measurements according to the C/N_0 (whereas a regular loop gives equal weights to all measurements) and therefore would show better results. Moreover, the use of the three channels inside the combined Kalman filter multiplies the

number of observations by three and therefore improves the tracking performance and is able to track better at high and low C/N_0 . Finally, the combined Kalman filter performs better as well when an oscillator error is simulated. The h parameters used in the Kalman filters to model the process noise associated with the dynamic model are the same as the ones used in the software signal simulator. This is justified because it is expected that the Kalman filter developers will know which oscillator is used.

6.3.3.2 Tests in dynamic mode

The performance of the combined Kalman filter is now compared with the performance of the L1 C/A code Kalman filter and the traditional Kalman filter in terms of tracking accuracy and the maximum level of dynamics supported. For all these tests, the variances of the noise associated with the dynamic model for the one signal Kalman filter and the combined Kalman filter are set to the same values in order to compare their performance with the same level of input noise. However, the value of the process noise corresponding to phase acceleration is increased depending on the dynamics as explained at the end of Section 6.3.2. Toward this goal, three simulations are realized with the parameters shown in Table 6-5. The values of the phase acceleration are the maximum acceleration values squared (for instance a maximum acceleration of 2 m/s^2 would give a phase acceleration value of $(2/\lambda)^2 \text{ cycles}^2/\text{s}^4$ with λ the wavelength).

Table 6-5: Simulation parameters

Parameter	Value		
	Test 1	Test 2	Test 3
C/N₀	45 dB-Hz	35 dB-Hz	45 dB-Hz
Motion	Motion 1	Motion 1	Motion 2
Simulation time	30 s	30 s	30 s
Oscillator Error Model	None	None	None
Interference	No		

The motion 1 is as follows:

- Static for 5 s
- Acceleration of 10 m/s² for 5 s
- Constant speed for 5 s
- Deceleration of 10 m/s² for 5 s
- Acceleration of 10 m/s² for 5 s
- Constant speed for 5 s.

The motion 2 is as follows:

- Static for 5 s
- Acceleration of 40 m/s² for 5 s

- Constant speed for 5 s
- Deceleration of 40 m/s^2 for 5 s
- Acceleration of 40 m/s^2 for 5 s
- Constant speed for 5 s.

The Doppler, Doppler error, code delay error and PLI over time for the first dynamic test are shown in Figure 6-13. In the case of the satellite used in this test, about one third of the user dynamics are projected on the axis satellite-receiver. As seen in this figure, the three tracking methods are able to track under the simulated dynamics at high C/N_0 . The variance of the Doppler error is much smaller in the case of the Kalman filters than for the traditional filter. Moreover, at each change in dynamics (every 5 s), the traditional tracking is clearly affected (as demonstrated by the PLI) whereas the two other methods are only slightly affected. Besides, on the figures showing the Doppler error and the PLI over time, we can see that the combined Kalman filter is less affected by the dynamic change than the C/A code Kalman filter. Concerning the code delay error, the noise of the combined Kalman filter is slightly smaller than for the C/A code Kalman filter which is already much smaller than the traditional tracking. Finally, on the plots of the PLI and the Doppler error over time, one can see that the biggest impact of the dynamics is around 20 s, which corresponds to a change of dynamics from -10 m/s^2 to $+10 \text{ m/s}^2$. Therefore, in presence of reasonable dynamics and at high C/N_0 , the combined Kalman filter performs best.

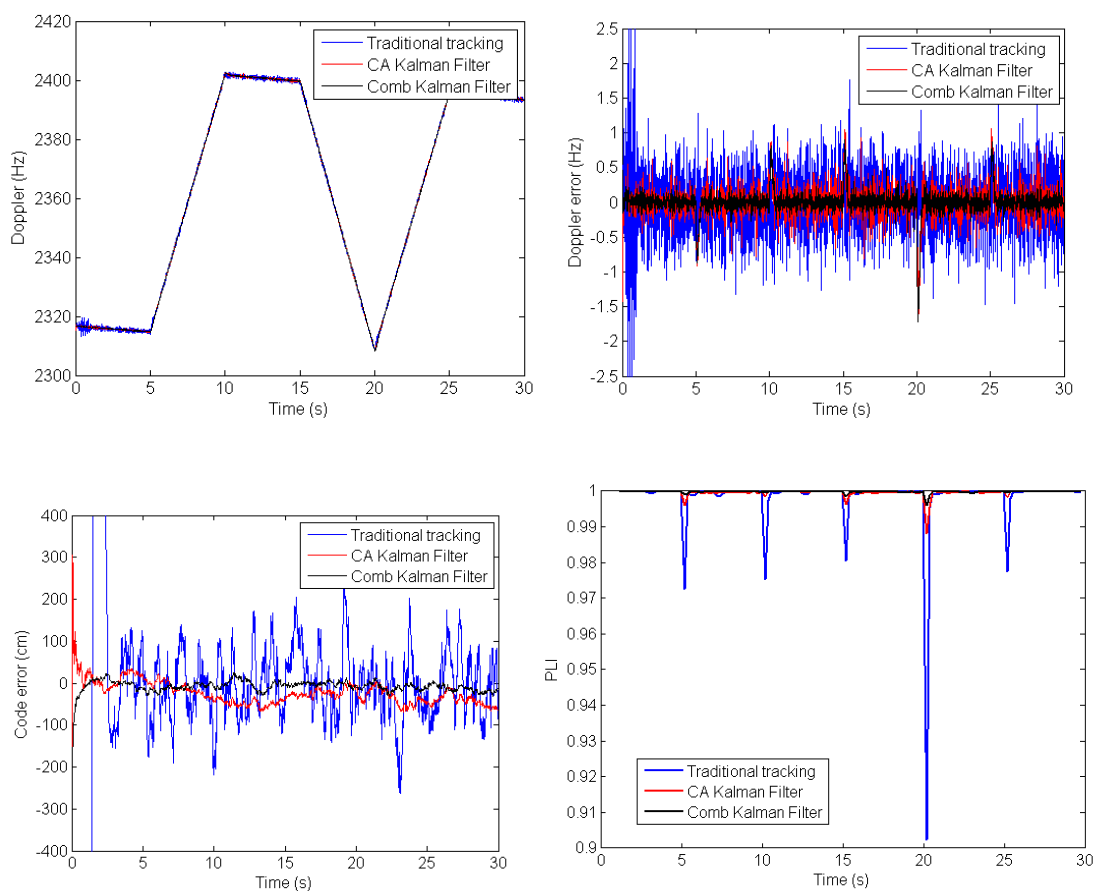


Figure 6-13: Doppler and Doppler error for the first dynamic test (top figures), code delay error (bottom left figure) and PLI (bottom right figure)

The Doppler, Doppler error, code delay error and PLI over time for the second dynamic test for the both Kalman filters are shown in Figure 6-14. The traditional method is not able to track at low C/N_0 . The combined Kalman filter is able to follow the medium dynamics at low C/N_0 . However, as it can be seen with the Doppler error, the code delay error and the PLI plots, the noise is higher at lower C/N_0 . Nevertheless, the combined Kalman filter is able to track medium dynamics at low C/N_0 better than the C/A code Kalman filter (which is affected by the dynamic changes every 5 s as shown by the PLI).

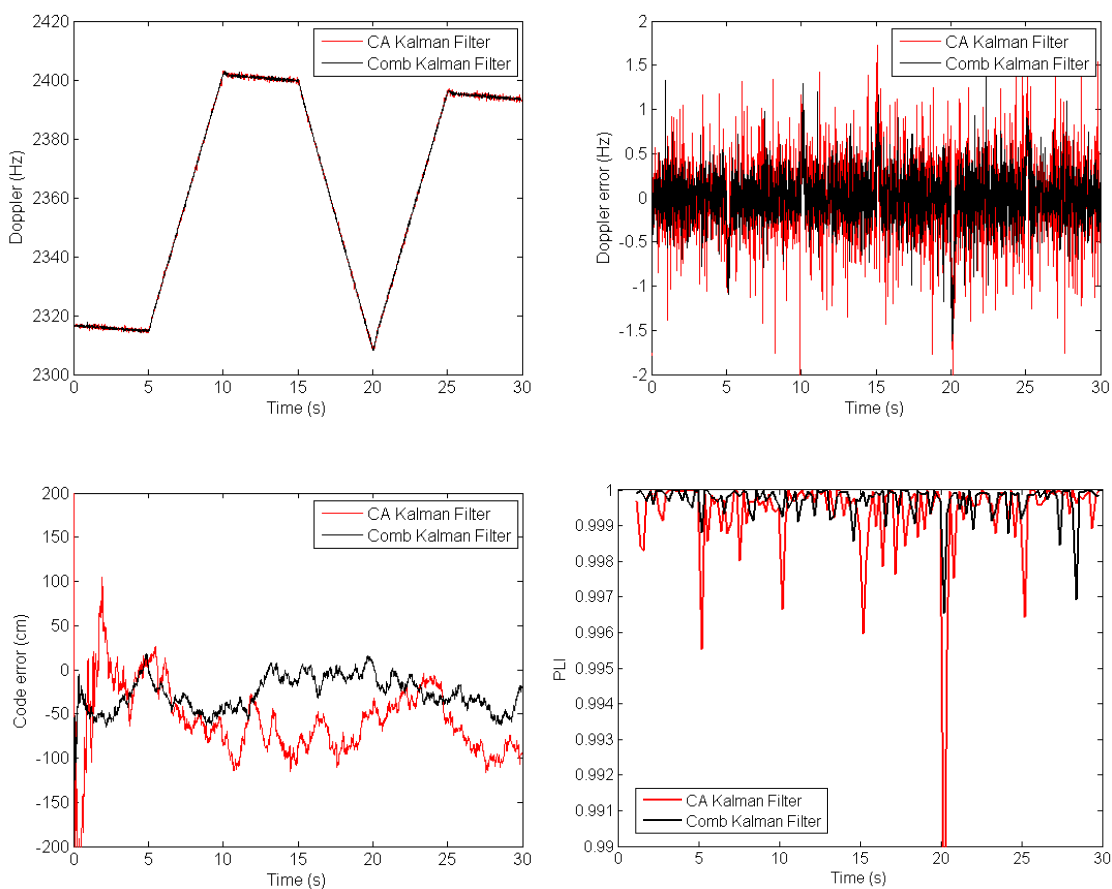
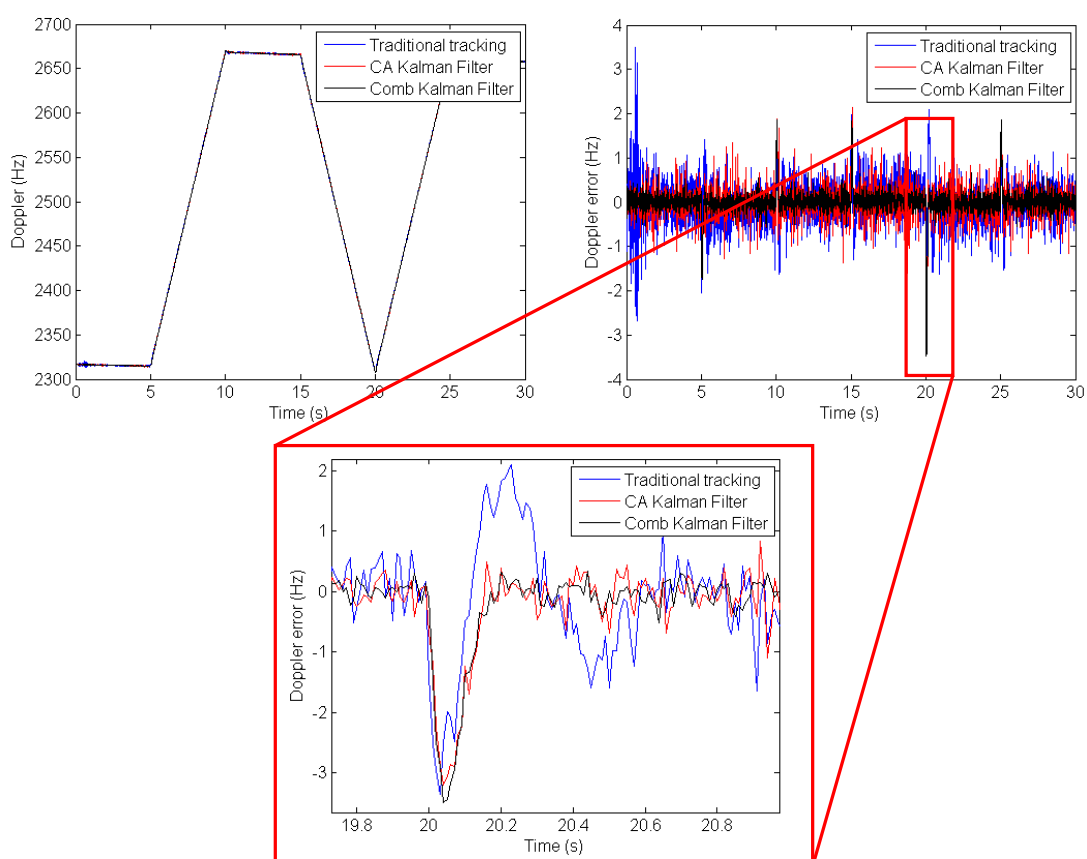


Figure 6-14: Doppler and Doppler error for the second dynamic test (top figures), code delay error (bottom left figure) and PLI (bottom right figure)

The Doppler, Doppler error, code delay error and PLI over time for the third dynamic test for the three methods are shown in Figure 6-15. Both Kalman filters are able to track the high dynamics for the length of the simulation with medium Doppler and code delay errors. Both Kalman filters experience a jump every change of dynamics (every 5 s) as visible on the plots of the Doppler error and the code delay error. However, both Kalman filters recover much faster than the traditional tracking (as evidenced by the Doppler error for the highest dynamic change). Moreover, as demonstrated by the PLI, the

traditional tracking experiences a lot of difficulties at each dynamic change. Besides, the Doppler noise and code delay error are smaller for the combined Kalman filter than for the C/A code Kalman filter. Therefore, the combined Kalman filter yields the best tracking and error performance in presence of high dynamics at high C/N_0 .



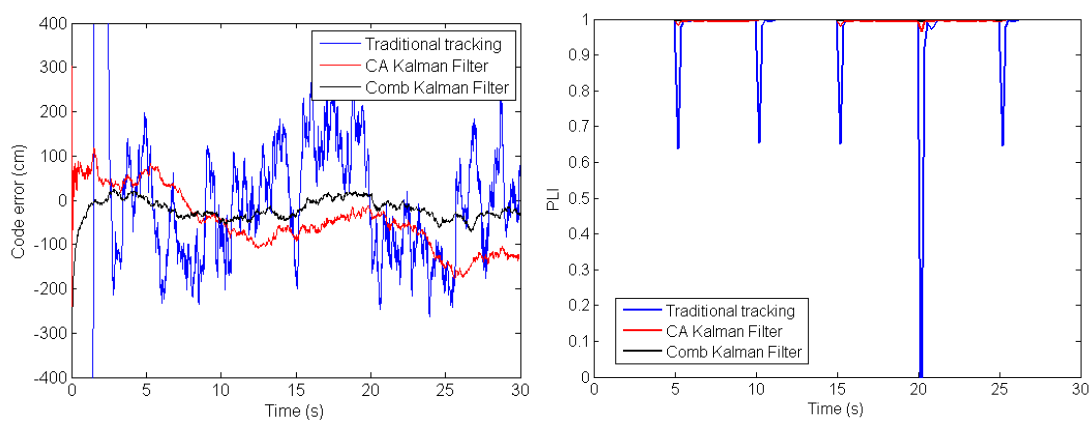


Figure 6-15: Doppler and Doppler error for the third dynamic test (top figures), detail of the Doppler error (middle figure) and code delay error (bottom left figure) and PLI (bottom right figure)

Chapter Seven: CONCLUSIONS AND RECOMMENDATIONS FOR FUTURE WORK

Methods to acquire the Galileo L1 and GPS L1 signals have been developed and tested in this thesis. Moreover, algorithms to combine these signals at the acquisition and tracking levels have been implemented and tested under various conditions. In order to test these algorithms, a complete software signal simulator able to simulate GPS L1 and Galileo L1 signals has been developed. This chapter summarizes the main conclusions of this thesis and gives some recommendations for future work.

7.1 Conclusions

The purpose of this thesis was to develop algorithms of acquisition and tracking adapted to the new GPS signal L1C and the Galileo L1 signal. Moreover, one of the goals was to improve acquisition and tracking performance using combined acquisition and tracking schemes. In the process of working towards these goals, a GPS and Galileo L1 signal software simulator was developed in order to test the algorithms. The major findings of this research are presented below.

7.1.1 Signal Software Simulator

Since the GPS L1C signal and the future Galileo L1 signals are not yet broadcast, a complete signal software simulator was developed as part of this thesis. The software

simulates IF samples at the output of a fictitious front-end taking into account only white noise, while possible interference sources and satellite clock errors, i.e. multipath, orbital, receiver clock errors and atmospheric errors are not simulated. Moreover, static as well as dynamic users can be simulated. The model for the satellite clock error was developed in this thesis and its Allan standard deviation compared with the corresponding theoretical Allan standard deviation. The Allan standard deviation computed using the new method matches well the theoretical one except for a small bias. Only the results for the OCXO and Rubidium oscillators were shown but similar results can be obtained for other oscillators.

7.1.2 Acquisition algorithms

Four acquisition techniques were shown for Galileo L1 (but the same methods can be applied to GPS L1C). The first two methods were implementations of the classic zero padding technique and were used for comparison with the new methods developed in this thesis. The third and fourth methods used combinations of the zero padding technique. These methods were tested using the GIOVE-A satellite and then their performance was statistically derived. For both the data and pilot channel, the methods using 16 ms of data performed better than the methods using only 8 ms, but required more processing time. Indeed, the method using 16 ms on the data channel showed an improvement of 5.5 dB compared to the 8 ms. Concerning the pilot channel, the method using 16 ms showed an improvement of 2 dB compared to the method on 8 ms. As explained in Chapter 4, the improvement on the data and pilot channel is not the same because the methods of

acquisition used are different. As demonstrated by the mean acquisition time, in case of weak signals, the acquisition using only 8 ms of incoming signal might fail and successive trials to acquire the signal might take longer than using directly the methods requiring 16 ms of data. Therefore, the optimal algorithm depends on the operational environment of the receiver (i.e., weak or strong signals).

Then, a method to combine the GPS L1 C/A and L1C (data and pilot channels) signals during the acquisition process was developed. This method was tested using the software signal simulator developed in this thesis at low and high C/N_0 values. At low C/N_0 (32 dB-Hz), the combined acquisition was able to acquire signals that could not be acquired using the L1C data channel alone using a coherent integration time of 10 ms in both cases. Moreover, the three channels (L1 C/A and L1C data and pilot channels) were acquired simultaneously. A similar method can be used to acquire the Galileo L1 pilot and data channel, changing the coefficients to take into account the broadcast power of these two channels.

7.1.3 Tracking algorithms

Considering the tracking, a new method was developed to combine the GPS L1 C/A and L1C (data and pilot channels) signals. This algorithm was tested using the signal software simulator at high (45 dB-Hz) and low C/N_0 (30 dB-Hz) and in static and dynamic modes (about 10 g). The combined tracking showed better performance than the traditional tracking of the L1C data channel. Indeed, at high C/N_0 , the Doppler measurements were

less noisy and the PLI was closer to unity. At low C/N_0 , only the combined tracking was able to track the signals. However, as expected, the combined tracking did not show a significant improvement compared to the traditional tracking in case of dynamics. A similar method could be applied to Galileo L1, changing the coefficients according to the broadcast powers.

From the traditional Kalman filter for one signal, a Kalman filter combining the GPS L1 C/A and L1C (pilot and data channels) channels was developed to track all three signals simultaneously. The combined Kalman filter was tested using the software signal simulator and its performance was compared with the single-signal Kalman filter and the traditional tracking under various conditions. Both Kalman filters showed better performance than the traditional tracking (more accurate tracking and far less noise) in all cases. Furthermore, the Kalman filters were able to track at low C/N_0 (30 dB-Hz) whereas the traditional tracking could not. Moreover, the combined Kalman filter showed better performance than the Kalman filter for one signal in static mode at low and high C/N_0 both with and without oscillator error. Finally, the combined Kalman filter also showed better performance in presence of reasonable dynamics as well as high dynamics.

7.2 Recommendations for future work

The main recommendations for future work are briefly described below.

7.2.1 Use of Real Data

The software signal simulator developed as part of this thesis has been validated using an independent software receiver developed by the PLAN Group. However, the use of real data would allow further tests on the algorithms developed here; for example, in presence of multipath such as would be encountered in urban canyons or indoors. The Galileo system should be fully operational by 2013 and the first GPS L1C should be launched in 2013.

7.2.2 Acquisition

In this thesis, methods to acquire the signal using half, one or two ranging code periods have been developed and tested. In case of very weak signals, an integration using two ranging code periods might not be sufficient to acquire the signal. Therefore, following the same idea as in this thesis, the acquisition algorithms could be extended to several ranging code periods.

7.2.3 Tracking

Discriminators have been developed elsewhere to avoid the tracking of the side peaks of the autocorrelation function of the BOC(1,1) and CBOC. These discriminators could be used with the techniques of tracking developed here in order to further improve the tracking performance. Moreover, the tracking performance of the GPS L1C and Galileo

L1 signals should be tested in the presence of multipath to assess their multipath mitigation capability. However, a realistic multipath model is very difficult to simulate. Therefore, this study should be done using real data if possible. Finally, the combined Kalman filter has been tested under various dynamics but only the effect of acceleration has been assessed. It would be interesting to assess the effect of higher dynamics such as jerk on the filter performance. Finally, the knowledge of the secondary code on the pilot channel (of GPS L1C or Galileo L1) can be used to integrate longer and asynchronously update the Kalman filter or the combined tracking.

7.2.4 Position solution

Finally, pseudorange measurements can be computed from the combined GPS L1 channels and the combined L1 channels separately. Then, these pseudorange measurements can be combined using least-squares or a Kalman filter to compute the position of the user. Using both constellations in order to compute the user position would improve the position accuracy and reliability.

References

Akopian, D. (2005) "Fast FFT based GPS satellite acquisition methods", IEE Proc. Radar Sonar Navig., vol. 152, no. 4, pp. 277- 286

Andrea Nava, S. (2006) *Analysis and Simulations of Mitigation Techniques for Pulsed Interferers on GNSS Signals*, MSc thesis, Politecnico di Torino, Italy

Avellone, G., M. Frazzetto, and E. Messina (2007) A New Waveform Family for Secondary Peaks Rejection in Code Tracking Discriminators for Galileo BOC(n,n) Modulated Signals, Proceedings of the 2007 National Technical Meeting of the Institute of Navigation, January 22 - 24, 2007, The Catamaran Resort Hotel, San Diego, California

Avila-Rodriguez, J., G.W. Hein, S. Wallner, J. Issler, L. Ries, L. Lestarquit, A. De Latour, J. Godet, F. Bastide, T. Pratt and J. Owen (2007) "The MBOC Modulation, A final touch for the Galileo frequency and signal plan", GNSS Inside, September-October 2007

Bastide F., O. Julien, C. Macabiau and B. Roturier (2002), *Analysis of E5/L5 Acquisition, Tracking and Data Demodulation Threshold*, Proceedings of 15th International Technical Meeting of the Satellite Division of the Institute of Navigation, ION GPS 2002, Portland, OR, Sept. 24-27 2002, pp.2196-2207

Benedicto, J., S.E.Dinwiddy, G. Gatti, R. Lucas and M. Lugert (2000) *GALILEO: Satellite System Design and Technology Developments*, ESA, November 2000

Betz J.W. (2002), *Binary Offset Carrier Modulations for Radionavigation*, Navigation, Journal of the Institute of Navigation, Winter 2001-2002, Volume 48, Number 4, pp.227-246

Betz, J.W., M.A. Blanco, C.R. Cahn, P.A. Dafesh, C.J. Hegarty, K.W. Hudnut, V. Kasemsri, R. Keegan, K. Kovach, Capt L.S. Lenahan, H.H. Ma, J.J. Rushanan, D. Sklar, T.A. Stansell, C.C. Wang and S.K. Yi (2006) *Description of the LIC Signal*, Proceedings of the ION GNSS 06, Fort Worth, TX, 26-29 Sept. 2006

Betz J.W. (2002), "Binary Offset Carrier Modulations for Radionavigation", Navigation, Journal of the Institute of Navigation, Winter 2001-2002, Volume 48, Number 4, pp.227-246

Borio, D. M. Fantino and L. Lo Presti (2006) *The Impact of the Galileo Signal in Space in the Acquisition System*, Tyrrhenian International Workshop on Digital Communications (TIWDC'06), Satellite Navigation and Communications Systems, Island of Ponza, Italy

Borio, D. M. Fantino, L. Lo Presti, and L. Camoriano (2006) *Acquisition analysis for Galileo BOC modulated signals: theory and simulation*, in Proc. European Navigation Conference ENC'06, Manchester, UK

Borio, D. (2008), *A Statistical Theory for GNSS Signal Acquisition*, Phd Thesis, Politecnico Di Torino, Italy, (Available at <http://plan.geomatics.ucalgary.ca>)

Borio, D., C. Gernot, F. Macchi and G. Lachapelle (2008) *The Output SNR and its Role in Quantifying GNSS Signal Acquisition Performance*, ENC GNSS 08, 23-25 April 2008, Toulouse, France

Borre, K., D.M. Akos, N. Bertelsen, P. Rinder and S. H. Jensen (2007), *A software-defined GPS and Galileo receiver A single frequency approach*, Birkhauser, Boston, Basel, Berlin

Bosser, P., Bock, O., Pelon, J. and Thom, C. (2006) "An Improved Mean-Gravity Model for GPS Hydrostatic Delay Calibration", IEEE Geoscience and Remote Sensing Letters, 4, 3-7, 2007

Botteron, C., G. Wälchli, G. Zamuner, M. Frei, D. Manetti, F. Chastellain, P.-A. Farine and P. Brault (2006) *A flexible Galileo E1 Receiver Platform for the Validation of Low Power and Rapid Acquisition Schemes*, Proceedings of the US Institute of Navigation GNSS (Forth Worth, Texas, USA, Sept. 26-29)

Braasch, M. (1997), "Multipath Effects in Global Positioning System: Theory and Applications" Volume I, Progress in Astronautics and Aeronautics Volume 164, AIAA, pp. 547-568

Brown, R.G. and P.Y.C. Hwang (1992), *Introduction to Random Signals and Applied Kalman Filtering*, John Wiley & Sons, Inc., USA

Cabler, H. (2003) *GPS Modernization, A Path Toward Improved Capabilities*, aICAO CAR/SAM ATN/GNSS Seminar

Cameron, A. (2007) *The GPS LIC and Galileo LIF signals of the future have been optimized to use a multiplexed binary offset carrier (MBOC) waveform*, GPS World Perspectives (July 2007), <http://sidt.gpsworld.com/gpssidt/article/articleDetail.jsp?id=444833>

Cannon, M.E. (2005), *Satellite Positioning*, ENGO 561 Lecture Notes, Department of Geomatics Engineering, the University of Calgary

Crews, C.L. (2008) *Long-Term Future of GPS*, Proceedings of ION NTM 2008, San Diego, CA

Dempster, A.G. (2006), "Correlators for L2C: Some Considerations", Inside GNSS, pp. 32-37

DiFranco, J.V. and W. L. Rubin (2004) *Radar Detection*, SciTech Publishing

Dovis, F. P. Mulassano and L. Lo Presti (2005) *A Novel Algorithm for the Code Tracking of BOC(n,n) Modulated Signals*, Proceedings of the ION GNSS 2005, Long Beach, California

Dovis, F., L. Lo Presti, M. Fantino, P. Mulassano and J. Godet (2008) "Comparison between Galileo CBOC Candidates and BOC(1,1) in Terms of Detection Performance", International Journal of Navigation and Observation

European Space Agency (ESA) website:
<http://www.esa.int/esaNA/galileo.html>, access date October 2007

Floc'H, JJ. and M. Soellner (2007) *Comparison Between BOC CBOC and TMBOC Tracking*, ION NTM 2007, San Diego, California

Galileo Open Service, Signal In Space Interface Control Document, OS SIS ICD (2006), Draft 0

Galileo Open Service, Signal In Space Interface Control Document, OS SIS ICD (2008), Draft 1

GIOVE-A Navigation Signal-In-Space Interface Control Document SIS ICD (2007), First Issue

Gelb, A. (1974) *Applied Optimal Estimation*. The M.I.T. Press

Gerein, N., M. Olynik and M. Clayton (2004) *Galileo BOC(1,1) Prototype Receiver Development*, Proceedings of the 17th International Technical Meeting of the Satellite Division of the Institute of Navigation ION GNSS 2004, September 21 - 24, 2004, Long Beach Convention Center Long Beach, California

Gerein, N., *The Revised IS-GPS-200D Specification New Spreading Codes + A Brief Introduction to IS-GPS-800 Spreading Codes* (2006), ION Alberta lunch meetings, december 2006

Grewal, M. S. and A. P. Andrews (2001) *Kalman Filtering: Theory and Practice using Matlab*, 2nd Edition, John Wiley & Sons, New York, Chichester

Hatch, R., (1995) "Relativity and GPS-I", Galilean Electrodynamics, vol. 6, no.3, pp. 52-57

Hegarty, C. (1999), *Evaluation of the Proposed Signal Structure for the New Civil GPS Signal at 1176.45 MHz*, WN99W0000034, The MITRE Corporation

Hegarty, C. J. (2006) *Optimal and near-optimal detector for acquisition of the GPS L5 signal*, in Proc. of ION NTM, National Technical Meeting, Monterey, CA, Jan. 2006, pp. 717 - 725.

Hegarty, C., M. Tran, and A. J. Van Dierendonck (2003) *Acquisition algorithms for the GPS L5 signal*, in Proc. of ION/GNSS, Portland, OR, Sept. 2003, pp. 165 – 177

Hein, G. W., J-A Avila-Rodriguez, L. Ries, L. Lestarquit, J-L Issler, J. Godet and T. Pratt (2005) *A candidate for the Galileo L1 OS Optimized Signal*, ION GNSS 2005, September 13-16 2005, Long Beach, California, USA

Hein, G.W. J. Avila-Rodriguez, S. Wallner, A.R. Pratt, J. Owen, J. Issler, J.W. Betz, C.J. Hegarty, S. Lenahan, JJ. Rushanan, A. L. Kraay and T.A. Stansell (2006) *MBOC: The New Optimized Spreading Modulation Recommended for GALILEO L1 OS and GPS L1C*, PLANS 2006

Holmes, J.K. (1982), *Coherent Spread Spectrum Systems*, John Wiley and Sons, New York

Hudnut, K. W. (2005) *Future Navigation Needs Your Input*, GPS World (November 2005), <http://www.gpsworld.com/gpsworld/Position/Future-Navigation-Needs-Your-Input/ArticleStandard/Article/detail/192974>

INTERFACE SPECIFICATION IS-GPS-200 Revision D (2004), Navstar GPS Space Segment/Navigation User Interfaces

INTERFACE SPECIFICATION IS-GPS-800 Draft (2007), Navstar GPS Space Segment/User Segment L1C Interfaces

Julien, O. (2005), *Design of Galileo L1F Tracking Loops*, PhD Thesis, Department of Geomatics Engineering, University of Calgary, UGCE Report 20227

Julien, O., C. Macabiau, J. Issler, and L. Ries (2007) *1-Bit Processing of Composite BOC (CBOC) Signals and Extension to Time-Multiplexed BOC (TMBOC) Signals*, Proceedings of the 2007 National Technical Meeting of the Institute of Navigation, January 22 - 24, 2007, The Catamaran Resort Hotel, San Diego, California

Julien, O. C. Macabiau, J.-A. Avila Rodriguez, S. Wallner, M. Paonni, G. W. Hein, J.-L. Issler, and L. Ries (2007) *On Potential CBOC/TMBOC Common Receiver Architectures*, Proceedings of the GNSS 2007, Forth Worth, TX

Julien, O. (2008) *GNSS Receiver Design*, ENGO 638 Lecture Notes, Department of Geomatics Engineering, The University of Calgary

Kaplan, E.D. (2006) *Understanding GPS Principles and applications*, second edition, Artech House Publishers, Norwood, MA

Katz, R. (1964) *An Introduction to the Special Theory of Relativity*, University of Nebraska

Kay, S. M. (1993) *Fundamentals of Statistical Signal Processing, Volume 2: Detection Theory*

Lachapelle, G., M.E. Cannon, K. O'Keefe, P. Alves (2001) *Technical Benefit Analysis of Galileo for Canada*, Contract Report Prepared for the Canadian Space Agency, Ottawa

Lachapelle, G. (2006), *GPS Theory and Applications*, ENGO 625 Lecture Notes, Department of Geomatics Engineering, The University of Calgary

Landry, R. and A. Renard (1997) *Analysis of potential interference sources and assessment of present solutions for GPS/GNSS receivers*

Ledvina, B.M., M.L. Psiaki, T.E. Humphreys, S.P. Powell and P.M. Kintner Jr. (2006) *A Real-Time Software Receiver for the GPS and Galileo L1 Signals*, Proceedings of the US Institute of Navigation GNSS (Forth Worth, Texas, USA, Sept. 26-29)

Lowe, S.T. (1999) *Voltage Signal-to-Noise Ratio (SNR) Nonlinearity Resulting From Incoherent Summations*, TMO Progress Report 42-137

Loyka, S.L. (1999) "Applying Genetic Algorithm to Modeling Nonlinear Transfer Functions", *IEEE Telecommunications in Modern Satellite, Cable and Broadcasting Services*, vol. 1, pp. 247-250

Macabiau, C., L. Ries, F. Bastide, J.-L. Issler (2003), *GPS L5 Receiver Implementaion Issues*, Proceedings of the US Institute of Navigation GPS/GNSS (Portland, OR, USA, Sept. 9-12), pp. 153-164

Macchi, F. and M.G. Petovello (2007) Development of a One Channel Galileo L1 Software Receiver and Testing Using Real Data, Proceedings of the US Institute of Navigation GNSS, Fort Worth, TX, USA, Sept. 25-28

MacGougan, G.D. (2003), *High Sensitivity GPS Performance Analysis in Degraded Signal Environment*, Master's Thesis, UCGE Report #20176, Departement of Geomatics Engineering, The University of Calgary

Marcum, J. A (1960) "Statistical theory of target detection by pulsed radar", IEEE Trans. Inform. Theory, vol. 6, pp. 59 – 267

Marradi, L., G. Franzoni, D. Fossati, L. Foglia and V. Gabaglio (2006) *Results of the GARDA Galileo Receiver Development and Evolution to Safety-Of-Life Receiver Applications*, Proceedings of the US Institute of Navigation GNSS (Forth Worth, Texas, USA, Sept. 26-29)

Mattos, P. G. (2005) *Acquisition of the Galileo OS L1b/c signal for the mass-market receiver*, in Proc. of ION GNSS, 18th International Technical Meeting, Long Beach, CA, Sept. 2005, pp. 1143 – 1152

Mattos, P. G. (2006) "Galileo L1c - acquisition complexity: Cross correlation benefits, sensitivity discussions on the choice of pure pilot, secondary code, or something different", Proc. of IEEE Position Location and Navigation Symposium (PLANS/ION), Apr. 2006, pp. 845 – 852

Misra, P. and P. Enge (2006), *Global Positioning System: Signals, Measurements and Performance*, Ganga-Jamuna Press

Mongredien, C., G. Lachapelle and M.E. Cannon (2006) *Testing GPS L5 Acquisition and Tracking Algorithms Using a Hardware Simulator*, Proceedings of the US Institute of Navigation GNSS (Fort Worth, TX, USA, Sept. 26-29)

Mongrédien, C., M.E. Cannon and G. Lachapelle (2007) *Performance Evaluation of Kalman Filter Based Tracking for the New GPS L5 Signal*, Proceedings of GNSS07, Forth Worth, 25-28 Sep

Mongrédien, C. (2008) *GPS L5 Software Receiver Development for High-Accuracy Applications*, PhD Thesis, Department of Geomatics Engineering, University of Calgary, UGCE Report 20268

Nunes, F., F. M. G. Sousa, J. M.N. Leitao (2005) *Improving Multipath Mitigation in GPS/Galileo BOC Signals with Gating Functions*, Proceedings of the 61st Annual Meeting, June 27 - 29, 2005, Royal Sonesta Hotel, Cambridge, Massachusetts

O'Driscoll, C. (2007) *Performance Analysis of the Parallel Acquisition of Weak GPS Signal*, PhD Thesis, Department of Electrical and Electronic Engineering, National University of Ireland, Cork, Ireland

Pany, T., M. Irsigler and B. Eissfeller (2005) *S-Curve Shaping: A New Method for Optimum Discriminator Based Code Multipath Mitigation*, Proceedings of the 18th International Technical Meeting of the Satellite Division of the Institute of Navigation ION GNSS 2005, September 13 - 16, 2005, Long Beach Convention Center, Long Beach, California

Parkinson, B.W. (1996), *Introduction and Heritage of NAVSTAR, the Global Positioning System in Global Positioning System: Theory and Applications Volume I*, Progress in Astronautics and Aeronautics Volume 164 AIAA, pp.3-28

Peterson, R.L., R.E. Ziemer and D.E. Borth (1995), *Introduction to Spread Spectrum Communications*, Prentice Hall

Petovello, M.G. (2003) *Real-time Integration of a Tactical-Grade IMU and GPS for High-Accuracy Positioning and Navigation*, Ph.D. thesis, UCGE Report No. 20173

Petovello, M.G. and G. Lachapelle (2006), *Comparison of Vector-Based Software Receiver Implementation with Applications to Ultra-Tight GPS/INS Integration*, Proceedings of ION GNSS 2006

Psiaki, M.L. (2001), *Smoother-Based GPS Signal Tracking in a Software Receiver*, Proceedings of ION GPS 2001, pp. 2900-2913

Psiaki, M.L. and H. Jung (2002), *Extended Kalman Filter Methods for Tracking Weak GPS Signals*, Proceedings of ION GPS 2002, pp. 2539-2553

Psiaki, M.L., T.E. Humphreys, S. Mohiuddin, S.P. Powell, A.P. Cerruti and P.M. Kintner, Jr. (2006) *Searching for Galileo*, Proceedings of the US Institute of Navigation GNSS (Forth Worth, Texas, USA, Sept. 26-29)

Qaisar, S.U. and A. G. Dempster (2007) *An Analysis of LI-C/A Cross Correlation & Acquisition Effort in Weak Signal*, Environments International Global Navigation Satellite Systems Society IGNSS Symposium 2007, Australia

Raquet, J. (2006), *GNSS Receiver Design*, Lecture Notes, Department of Geomatics Engineering, The University of Calgary

Ries, L., F. Legrand, L. Lestarquit, W. Vigneau, J-L. Issler (2003) *Tracking and Multipath Performance Assessments of BOC Signals Using a Bit-Level Signal Processing Simulator*, Proceedings of the 16th International Technical Meeting of the Satellite Division of the Institute of Navigation ION GPS/GNSS 2003, September 9 - 12, 2003, Oregon Convention Center, Portland, Oregon

Rushanan, J. (2007) *The Spreading and Overlay Codes for the GPS L1C Signal*, Proceedings of ION NTM 2007, San Diego, 22-24 Jan 2007

Shanmugam, S.K., R. Watson, J. Nielsen, and G. Lachapelle (2005), *Differential Signal Processing Schemes for Enhanced GPS Acquisition*, Proceedings of the US Institute of Navigation GNSS, Long Beach, CA, USA, 13-16 Sept. 2005

Shanmugam, S.K. (2008) *New Enhanced Sensitivity Detection Techniques for GPS L1 C/A and Modernized Signal Acquisition*, PhD's Thesis, UCGE Report #20264, Department of Geomatics Engineering, The University of Calgary

Shnidman, D. A. (1989) "The calculation of the probability of detection and the generalized Marcum Q-Function", IEEE Transactions on Information Theory, vol. 35, no. 2, pp. 389-400

Shnidman, D. A. (1995) "Radar detection probabilities and their calculation", IEEE Trans. Aerosp. Electron. Syst., vol. 31, no. 3, pp. 928 – 950

Skone, S. (2007), *Atmospheric Effects on Satellite Navigation Systems*, ENGO 633 Lectures Notes, Department of Geomatics Engineering, the University of Calgary

Spelat, M., M. Hollreiser, M. Crisici and M. Falcone (2006) *GIOVE-A Signal-In-Space Test Activity at ESTEC*, Proceedings of the US Institute of Navigation GNSS (Forth Worth, Texas, USA, Sept. 26-29)

Spilker, J.J. (1996), *GPS Signal Structure and Theoretical Performance* in Global Positioning System: Theory and Applications Volume I, AIAA, pp. 57-120

Tran, M. and C. Hegarty (2002), *Receiver Algorithms for the New Civil GPS Signals*, Proceedings of the US Institute of Navigation NTM, San Diego, CA, 28-30 Jan 2002

Tran, M. (2004), "Performance Evaluation of the New GPS L5 and L2 Civil (L2C) Signals", Navigation: Journal of the Institute of Navigation, Vol. 51, No. 3, Fall 2004

Tsui, J. B-Y (2005) *Fundamentals of GPS Receivers – 2nd Edition*, Wiley

University of Colorado website,
<http://www.colorado.edu/geography/gcraft/notes/gps/gif/cagenera.gif>, last access date 28 October 2008

US Coast Guards Navigation Center Website,
<http://www.navcen.uscg.gov/navinfo/Gps/ActiveNanu.aspx>, last access date 20 November 2008 and <http://www.navcen.uscg.gov/gps/geninfo/global.htm>, last access date 27 January 2009

Van Dierendonck A.J. (1996), *GPS Receivers*, in *Global Positioning System: Theory and Applications Volume I*, AIAA, pp.329-408

Van Nee, D. J. R. and A. J. R. M. Coenen (1991) "New fast GPS code-acquisition technique using FFT", *Electronics Letters*, vol. 27, no. 2, pp. 158–160

Wallner, S., J. Avila-Rodriguez, and G. W. Hein (2006) *Galileo E1 OS and GPS L1C pseudo random codes requirements, generation, optimization and comparison*, in *Proceedings of First CNES Workshop on Galileo Signals and Signal Processing*, Toulouse, France

Wallner, S., J.A. Avila-Rodriguez, G. W. Hein and J. J. Rushanan (2007) *Galileo E1 OS and GPS L1C Pseudo Random Noise Codes - Requirements, Generation, Optimization and Comparison -*, *Proceedings of GNSS07*, Forth Worth, 25-28 Sep 2007

Whitley, D. (1993) *A Genetic Algorithm Tutorial*, Colorado State University

Winkel, J.O. (2003), *Modelling and Simulating GNSS Signal Structures and Receivers*, Ph.D. Thesis, University FAF, Munich

Yang, C., C. Hegarty, and M. Tran (2004), *Acquisition of the GPS L5 Signal Using Coherent Combining of I5 and Q5*, *Proceedings of the US Institute of Navigation GNSS*, Long Beach, CA, USA, Sept. 21-24

Yang, C, M. Miller and T. Nguyen (2007), "Symmetric Phase-Only Matched Filter (SPOMF) for Frequency-Domain Software GPS Receivers", *Journal of the Institute of Navigation*, Spring 2007

Ziedan, N.I. and J.L. Garrison (2004), *Extended Kalman Filter-Based Tracking of Weak GPS Signals under High Dynamic Conditions*, *Proceedings of ION GNSS 2004*, pp. 20-31

Appendix A: Computation of the satellite velocity using the ephemeris parameters

The position, velocity and acceleration of a satellite at a time T_k can be determined using the broadcast ephemeris parameters. From the equations presented in Kaplan (2006) and in the Interface Control Documents (IS-GPS-200D) for the satellite position, one can derive the satellite velocity and acceleration as presented below.

The following notations are used through this Appendix:

M_0 is the mean anomaly at the reference time of the ephemeris

n is the corrected mean motion

T_k is the difference between the current time and the reference time of the ephemeris

e is the eccentricity

Ω is the argument of perigee at the reference time of the ephemeris

C_{uc} is the amplitude of cosine correction to argument of latitude

C_{us} is the amplitude of sine correction to argument of latitude

C_{rc} is the amplitude of cosine correction to orbital radius

C_{rs} is the amplitude of sine correction to orbital radius

C_{ic} is the amplitude of cosine correction to inclination angle

C_{is} is the amplitude of sine correction to inclination angle

i_0 is the inclination angle at the reference time of ephemeris

$\frac{di}{dt}$ is the rate of change of inclination angle

T_{oe} is the reference time of ephemeris

Ω_0 is the longitude of the ascending node (at weekly epoch)

Ω_e is the rate of Earth rotation

$\dot{\Omega}$ is the rate of change of longitude of the ascending node

- Mean anomaly M_k

$$M_k = M_0 + n \cdot T_k$$

$$\dot{M}_k = n$$

- Eccentric anomaly E_k

$$E_k = M_k + e \cdot \sin(E_k)$$

$$\dot{E}_k = \frac{\dot{M}_k}{1 - e \cdot \cos(E_k)}$$

- True anomaly v_k

$$\cos(v_k) = \frac{\cos(E_k) - e}{1 - e \cdot \cos(E_k)}$$

$$\Leftrightarrow \cos(E_k) = \frac{\cos(v_k) + e}{1 + e \cdot \cos(v_k)}$$

$$\dot{v}_k = \frac{\dot{E}_k \cdot \sin(E_k) \cdot (1 + e \cdot \cos(v_k))}{\sin(v_k) \cdot (1 - e \cdot \cos(E_k))}$$

- Argument of latitude ϕ_k

$$\phi_k = v_k + \Omega$$

$$\dot{\phi}_k = \dot{v}_k$$

- Argument of latitude correction $\delta\phi_k$

$$\delta\phi_k = C_{us} \cdot \sin(2 \cdot \phi_k) + C_{uc} \cdot \cos(2 \cdot \phi_k)$$

$$\delta\dot{\phi}_k = 2 \cdot \dot{\phi}_k \cdot (C_{us} \cdot \cos(2 \cdot \phi_k) - C_{uc} \cdot \sin(2 \cdot \phi_k))$$

- Radius correction δR_k

$$\delta R_k = C_{rs} \cdot \sin(2 \cdot \phi_k) + C_{rc} \cdot \cos(2 \cdot \phi_k)$$

$$\delta\dot{R}_k = 2 \cdot \dot{\phi}_k \cdot (C_{rs} \cdot \cos(2 \cdot \phi_k) - C_{rc} \cdot \sin(2 \cdot \phi_k))$$

- Inclination correction δi_k

$$\delta i_k = C_{is} \cdot \sin(2 \cdot \phi_k) + C_{ic} \cdot \cos(2 \cdot \phi_k)$$

$$\delta\dot{i}_k = 2 \cdot \dot{\phi}_k \cdot (C_{is} \cdot \cos(2 \cdot \phi_k) - C_{ic} \cdot \sin(2 \cdot \phi_k))$$

- Corrected argument of latitude u_k

$$u_k = \phi_k + \delta\phi_k$$

$$\dot{u}_k = \dot{\phi}_k + \delta\dot{\phi}_k$$

- Corrected radius i_k

$$i_k = i_0 + \frac{di}{dt} \cdot T_k + \delta i_k$$

$$\dot{i}_k = \frac{di}{dt} + \delta\dot{i}_k$$

- Corrected longitude of node Ω_k

$$\Omega_k = \Omega_0 + (\dot{\Omega} - \Omega_e) \cdot T_k + \Omega_e \cdot T_{oe}$$

$$\dot{\Omega}_k = \dot{\Omega} - \Omega_e$$

- In plane x position X_p and y position Y_p

$$X_p = R_k \cdot \cos(u_k)$$

$$Y_p = R_k \cdot \sin(u_k)$$

$$\dot{X}_p = \dot{R}_k \cdot \cos(u_k) - R_k \cdot \dot{u}_k \cdot \sin(u_k)$$

$$\Leftrightarrow \dot{X}_p = \dot{R}_k \cdot \cos(u_k) - \dot{u}_k \cdot Y_p$$

$$\dot{Y}_p = \dot{R}_k \cdot \sin(u_k) + R_k \cdot \dot{u}_k \cdot \cos(u_k)$$

$$\Leftrightarrow \dot{Y}_p = \dot{R}_k \cdot \sin(u_k) + \dot{u}_k \cdot X_p$$

- ECEF x-coordinate X_s , y-coordinate Y_s and z-coordinate Z_s

$$X_s = X_p \cdot \cos(\Omega_k) - Y_p \cdot \cos(i_k) \cdot \sin(\Omega_k)$$

$$Y_s = X_p \cdot \sin(\Omega_k) + Y_p \cdot \cos(i_k) \cdot \cos(\Omega_k)$$

$$Z_s = Y_p \cdot \sin(i_k)$$

$$\dot{X}_s = \dot{X}_p \cdot \cos(\Omega_k) - \dot{Y}_p \cdot \cos(i_k) \cdot \sin(\Omega_k) + \dot{i}_k \cdot Z_s \cdot \sin(\Omega_k) - Y_s \cdot \dot{\Omega}_k$$

$$\dot{Y}_s = \dot{X}_p \cdot \sin(\Omega_k) + \dot{Y}_p \cdot \cos(i_k) \cdot \cos(\Omega_k) - \dot{i}_k \cdot Z_s \cdot \cos(\Omega_k) + X_s \cdot \dot{\Omega}_k$$

Appendix B: Genetic algorithm principle

A Genetic Algorithm is a method used to find an approximation of to an expression according to constraints. More information on genetic algorithms can be found in Whitley (1993).

B.1) Methodology

A genetic algorithm is based on a population of individuals with chromosomes. The chromosomes represent the parameters to be estimated (one chromosome per parameter). Therefore, each individual represents one set of parameters as defined by its chromosomes. The chromosomes of each individual are initialized, then selected using a cost function defined according to constraints, and afterwards the best individuals of the population are bred and a mutation is realized on the population. The previous steps are repeated until the ending criterion is met.

B.1.a) Initialization

An initial population of N individuals is first created. The chromosomes of each individual are generated randomly to cover the range of possible solutions (called the search space). The size of the population depends on the problem considered. However, one needs to find a trade-off between the processing time and the population size.

B.1.b) Selection

A cost function is applied to all the individuals of the population. Then, a fixed number of the population n is selected according to the outputs of this cost function. The number of individuals selected depends on the problem (in the genetic algorithm developed in this thesis, 30 % of the population was selected). The cost function depends as well on the problem and represents the constraints of the approximation. A cost function can be for example the distance between the true value and its estimate. The individuals not selected in this process are “removed”.

B.1.c) Breeding

The n individuals identified in the selection step are then bred with each other. One method to breed them is:

- A “mother” is chosen randomly in the population
- A “father” is chosen randomly in the population
- A random weight w_k , uniformly distributed between 0 and 1, is chosen and applied to each chromosome of the “mother” and the weight $1-w_k$ is applied to the corresponding chromosome of the “father”.

Note that using this method, the same mother-father couple can be used several times.

$N-n$ individuals are generated in order to retrieve the initial population size N .

B.1.d) Mutation

First, the same cost function as in Section B.1.b) is applied and the best individual is put aside. Among the $N-1$ remaining individuals, m are chosen randomly. The m individuals selected are then mutated, meaning that one or several of their chromosomes are reinitialized using the same method as in section B.1.a). At the end of this step, the population size is N . The mutation is done to avoid the algorithm converging to a local minimum or maximum.

B.1.e) Ending

The steps 2 through 4 are repeated until the ending criterion is met. The best individual of the population is finally chosen using the cost function of section B.1.b). There can be different ending criterion: a fixed number of iterations, a minimum value of the cost function (or a maximum depending on the cases), or improvement of the value of the cost function from one step to another.

B.2) Advantages / Inconveniences

A genetic algorithm always converges to the best solution. However, it takes much processing time and might take significant time to converge to a good enough approximation.

Appendix C: Impact of the approximation of the MBOC by a BOC(1,1) on acquisition performance

The focus of this appendix is on the effect of approximating the MBOC modulation with a BOC(1,1) modulation in terms of acquisition and tracking performance. Indeed, the MBOC modulation generates a larger spectrum for the signal. This larger spectrum requires a higher sampling frequency and more importantly, a larger computational burden. This can be an issue for mass market receivers which have limited resources or for software receivers where processing requirements are already high. A solution is to approximate the MBOC by a BOC at the receiver level. In so doing however, part of the signal is ignored, which results in reduced performance (Dovis et al 2008).

The objectives of this appendix are to quantify the losses induced by this approximation, particularly in the presence of multipath and interference. To achieve this, a MBOC signal is simulated in software with interference and multipath derived using various parameters. The simulated signal is then acquired and tracked using both MBOC and BOC modulations. Concerning the interference, the results are compared in terms of C/N_0 (Carrier to noise ratio). In the case of multipath, the error is computed in terms of error envelope for early-late processing.

C.1) Overall methodology

The CBOC signal is simulated using the software signal simulator and then acquired and tracked for all the interference sources. The test procedure is shown in Figure 1-1. The acquisition module has been developed in software using Matlab. The general parameters used for the tracking are presented in Table C-1.

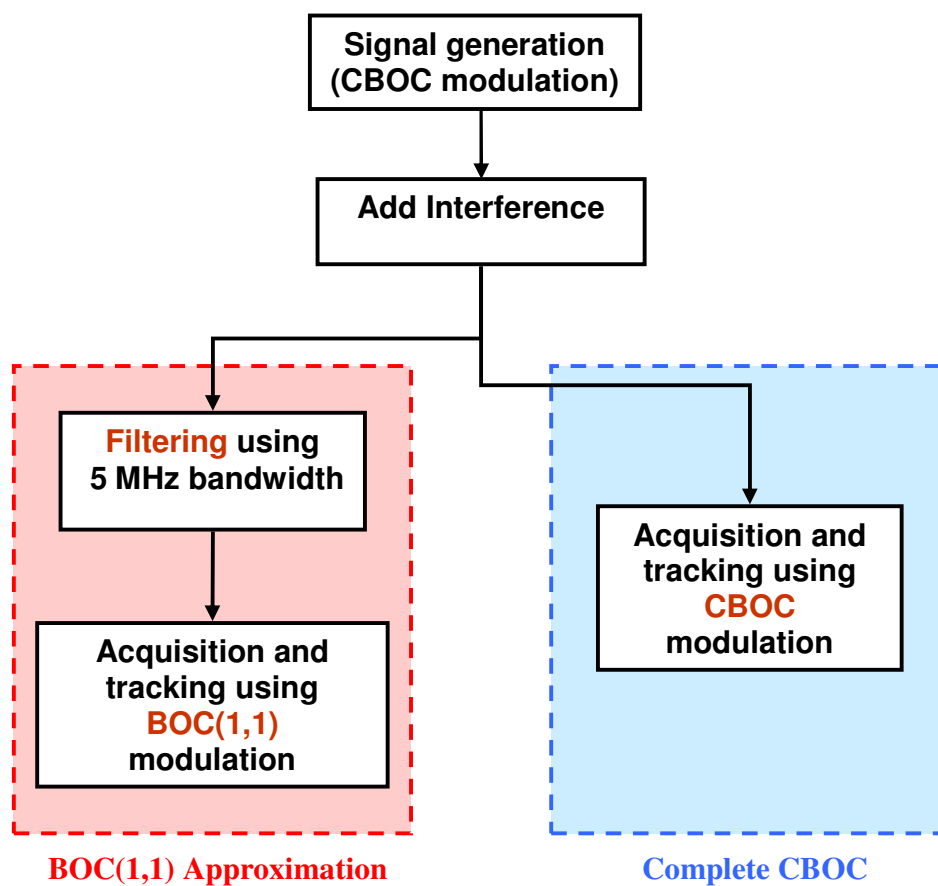


Figure C-1: Test procedure

Table C-1: Tracking parameters

Receiver Parameter	Description
PLL Discriminator	$D_{PLL} = \tan^{-1} \frac{Q_P}{I_P}$
PLL Loop Order	Third order
PLL Loop Bandwidth	10 Hz
DLL Discriminator	$D_{DLL} = \frac{\sqrt{I_E^2 + Q_E^2} - \sqrt{I_L^2 + Q_L^2}}{\sqrt{I_E^2 + Q_E^2} + \sqrt{I_L^2 + Q_L^2}}$
DLL Loop Order	Second order
DLL Loop Bandwidth	0.5 Hz
PLL aided DLL	Yes
Integration time	One ranging code period
Early-Late spacing	0.05 chip

C.2) CW Interference

C.2.a) Simulation parameters

The analysis of the CW interference on receiver performance is done using two tests: one for the acquisition process and the other for tracking. The parameters of the simulation are presented in Table C-2. The interference power is expressed in dB relative to the desired nominal GNSS signal power. The interference frequency is given relative to the IF (Intermediate Frequency) plus the Doppler frequency of the satellite considered (i.e., a frequency of zero occurs at the centre of the Doppler shifted IF signal). The interference

amplitude is incremented every 100 ranging code periods thus allowing 100 values to compute the deflection coefficient for the acquisition.

The interference frequency is chosen to be 1.023 MHz such that it is centered on one of the two main lobes of the BOC(1,1) modulation. The interference power for the acquisition and tracking is increased until the receiver cannot acquire or track the signal. The final values are given in Table C-2,

Table C-2: CW interference simulation parameters

Parameter	Value	
	Acquisition	Tracking
Signal power	45 dB-Hz	45 dB-Hz
Interference power (beginning)	-6 dB	0 dB
Interference power (end)	25 dB	35 dB
Interference frequency	1.023 MHz	1.023 MHz
Simulation time	15 s	20 s

C.2.b) Acquisition results

The acquisition process was repeated continuously throughout the test, over 100 code periods for each interference power, even if the acquisition were successful. This was done in order to obtain a sufficient sample size from which to draw meaningful statistical

results. Concerning the acquisition, the results are compared in terms of a deflection coefficient which can be expressed as follows:

$$d^2 = \frac{[E(T/H_1) - E(T/H_0)]^2}{\text{var}(T/H_0)}$$

where d is the deflection coefficient

$E(T/H_1)$ is the mean value of the main peak

$E(T/H_0)$ is the mean of the noise

$\text{var}(T/H_0)$ is the variance of the noise

In general, the deflection coefficient is not a reliable metric to compare different acquisition algorithms (Borio et al 2008). However, in this case, the same acquisition method is used and only the signals to be acquired change. Therefore, the deflection coefficient can be used to compare relative performance.

As shown in Figure C-2, the CBOC has better performance in terms of deflection coefficient for all levels of interference power. Indeed, the difference between the CBOC and the BOC(1,1) is around 1 dB for all interference powers considered. In other words, the CBOC is more resistant to interference than BOC(1,1).

This result was to be expected. Indeed, as shown in Chapter 2, the differences between the CBOC and the BOC(1,1) in terms of spectrum are the side lobes located at around +/- 6 MHz from the L1 central frequency. The CW interference is located at 1.023 MHz from the L1 central frequency, that is to say in the middle of one of the main lobes of the

BOC(1,1). Therefore, this interference has a direct impact on the BOC(1,1) part of the CBOC but minimal impact on the BOC(6,1) part of the CBOC.

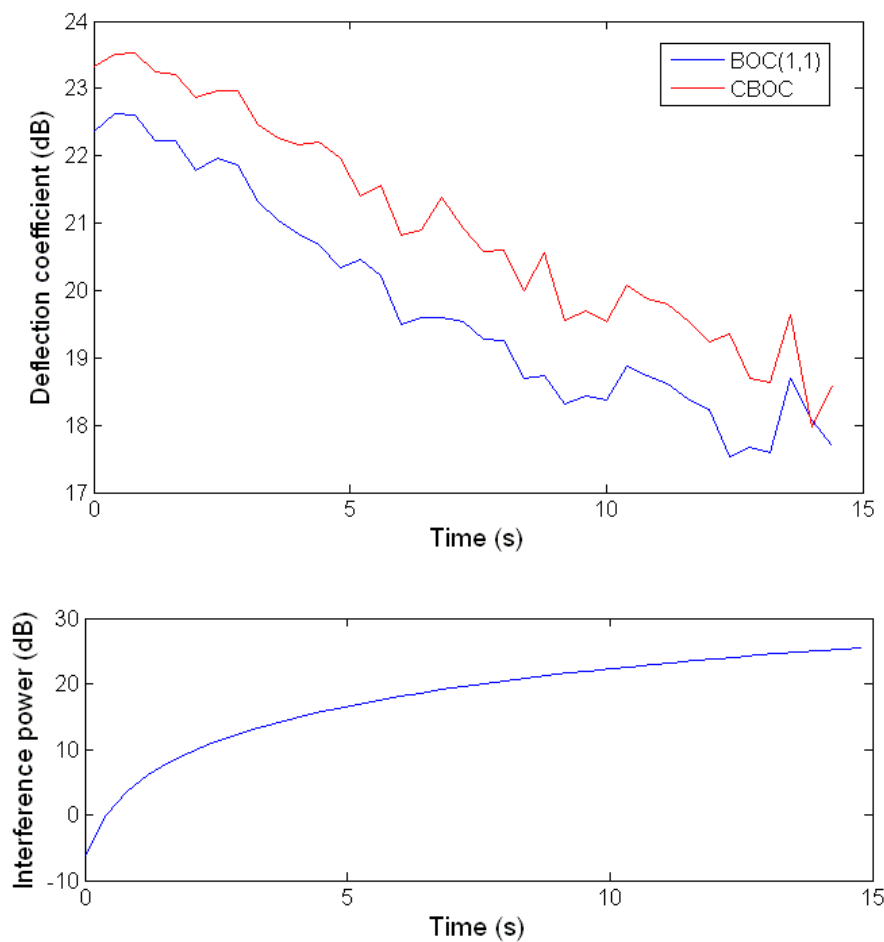


Figure C-2: Deflection coefficient as a function of the interference power for a CW interference (on top) and Power of the CW interference over time (at the bottom)

C.2.c) Tracking results

Concerning the tracking, the results are compared in terms of the computed C/N_0 . First, one can notice in Figure C-2 and Figure C-3 that the effect of the interference is smaller on tracking than on acquisition. Indeed, in the case of acquisition, after around 14 s of

simulation, the acquisition process fails. However, in the case of tracking, after 7 s (at which point the power of the interference is the same as after 14 s for the acquisition test), the C/N_0 is still above 35 dB, which is high enough to maintain lock on the signal. It was predictable that the effect of the interference on tracking would be smaller than on acquisition. Specifically, in the case of the tracking one already knows where the signal is (Doppler, code delay), so one just has to follow the changes in Doppler and code delay over time. However, in the case of acquisition, no information is available regarding the Doppler nor the code delay.

The PLI (Phase Lock Indicator) is used to know when the receiver loses lock. The description of the PLI can be found in Van Dierendonck (1996). The PLI can be expressed as:

$$PLI_k = \frac{NBD_k}{NBP_k}$$

$$\text{where } NBD_k = \left(\sum_{i=1}^M I_i \right)_k^2 - \left(\sum_{i=1}^M Q_i \right)_k^2$$

$$NBP_k = \left(\sum_{i=1}^M I_i \right)_k^2 + \left(\sum_{i=1}^M Q_i \right)_k^2$$

Finally, as shown in Figure C-3, Figure C-4 and Figure C-5, the CBOC has again better performance than the BOC(1,1) for all the interference powers. Moreover, and as shown in Figure C-4 and Figure C-5, the BOC(1,1) loses lock after 18 s whereas the CBOC keeps lock until the end of the test. The reasons for this are the same as discussed in the context of acquisition.

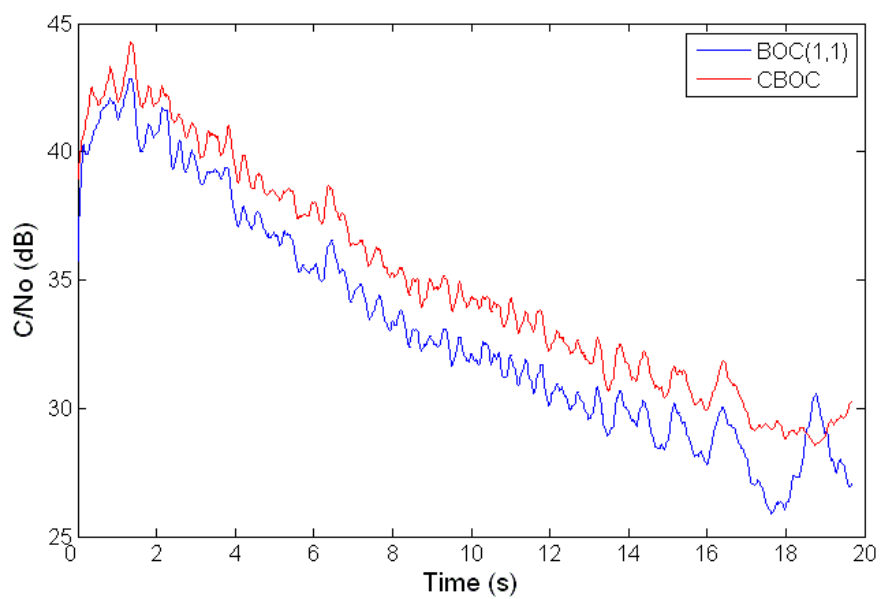


Figure C-3: C/N_0 as a function of the interference power for CW interference

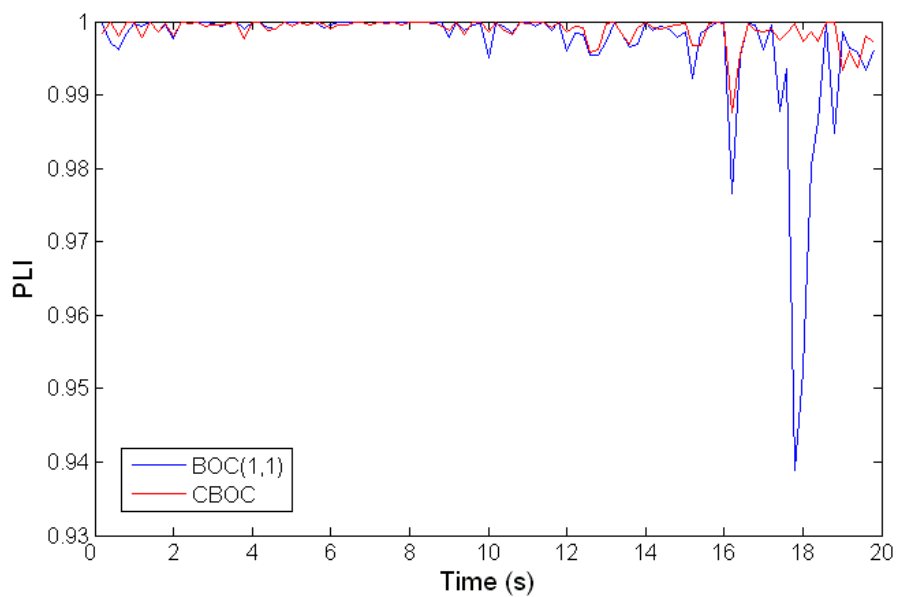


Figure C-4: Phase lock indicator (PLI) for CBOC and BOC for CW interference

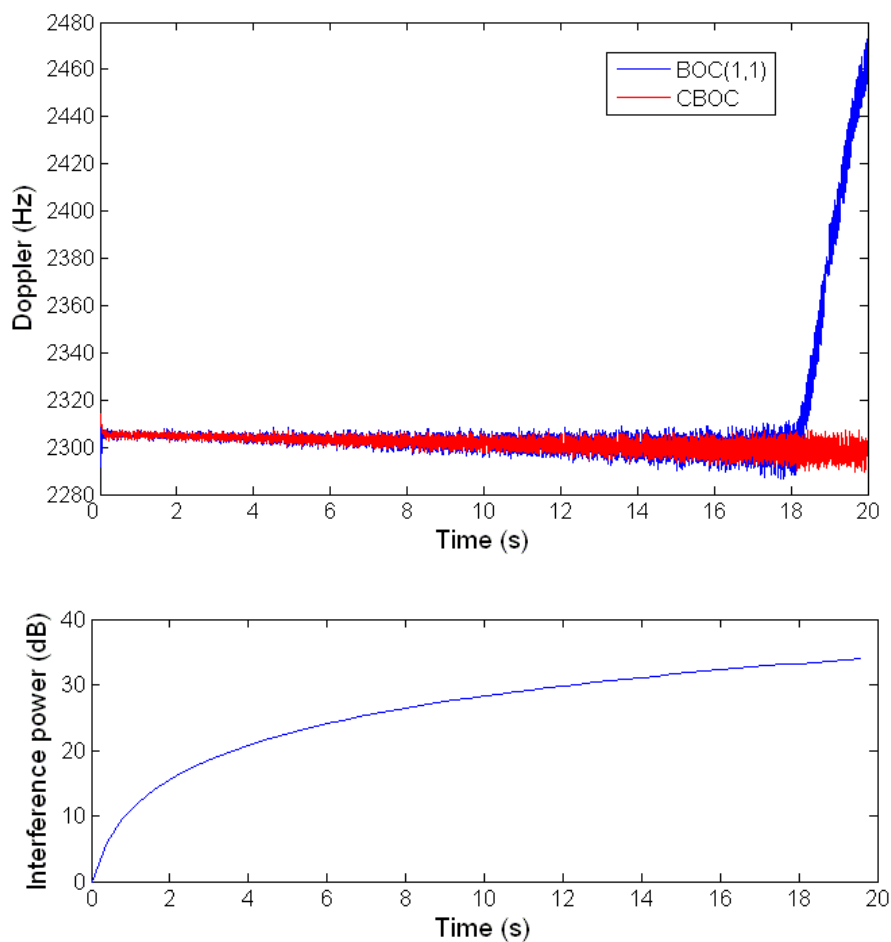


Figure C-5: Doppler in function of time for CBOC and BOC modulations in presence of CW interference (on top) and Power of the CW interference over time (at the bottom)

C.3) Narrowband interference

The second type of interference considered is narrowband interference. Narrow refers here to a small bandwidth compared to the GPS frequency.

C.3.a) Simulation parameters

The analysis of the narrowband interference on acquisition and tracking performance is done using four tests: two for the acquisition process and two for tracking. The two tests on acquisition and tracking differ in terms of the central frequency of the band pass filter (the filters are presented below and more details are given in Chapter 4). In one case, the central frequency is in the middle of the main lobe of the BOC(1,1), i.e. 1.023 MHz and in the other case in the middle of the BOC(6,1) main lobe, namely 6 MHz.

The parameters of the all tests are presented in Table C-3 and Table C-4. The interference power is given relative to the nominal signal level (difference in dB). The central frequency of the interference is the difference relative to the IF plus Doppler.

Table C-3: Simulation parameters for narrowband interference at 1 MHz

Parameter	Value	
	Acquisition	Tracking
Signal power	45 dB-Hz	45 dB-Hz
Interference power (beginning)	-5 dB	-5 dB
Interference power (end)	4 dB	30 dB
Interference central frequency	1.023 MHz	1.023 MHz
Interference bandwidth	1 MHz	1 MHz
Simulation time	15 s	14 s

Table C-4: Simulation parameters for narrow band interference at 6 MHz

Parameter	Value	
	Acquisition	Tracking
Signal power	45 dB-Hz	45 dB-Hz
Interference power (beginning)	-5 dB	-5 dB
Interference power (end)	13.5 dB	32 dB
Interference central frequency	6.138 MHz	6.138 MHz
Interference bandwidth	1 MHz	1 MHz
Simulation time	15 s	15 s

The magnitude responses of the two band pass filters centered on 1 MHz and 6.138 MHz are presented in Figure C-6 and Figure C-7, respectively. The Butterworth band pass filters implemented are of order six.

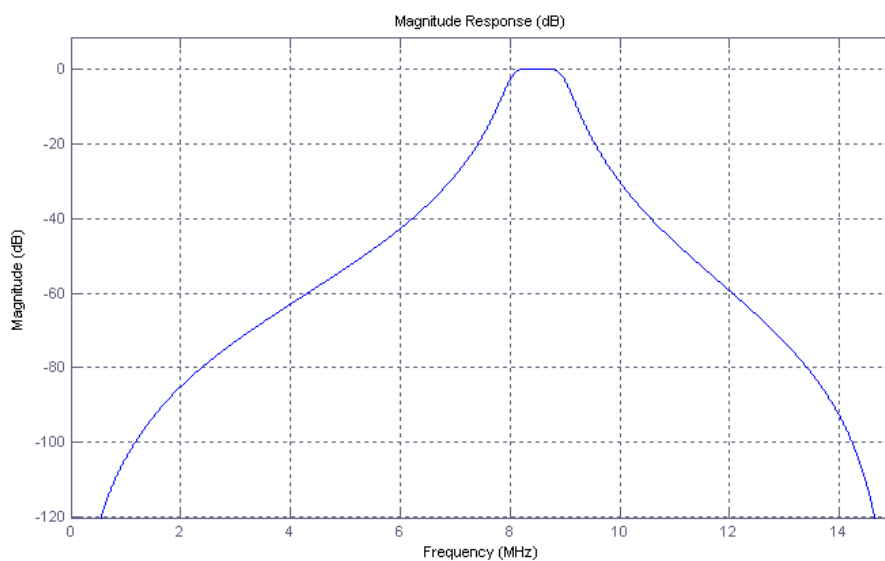


Figure C-6: Magnitude response of the band pass filter centered at 1 MHz from the IF

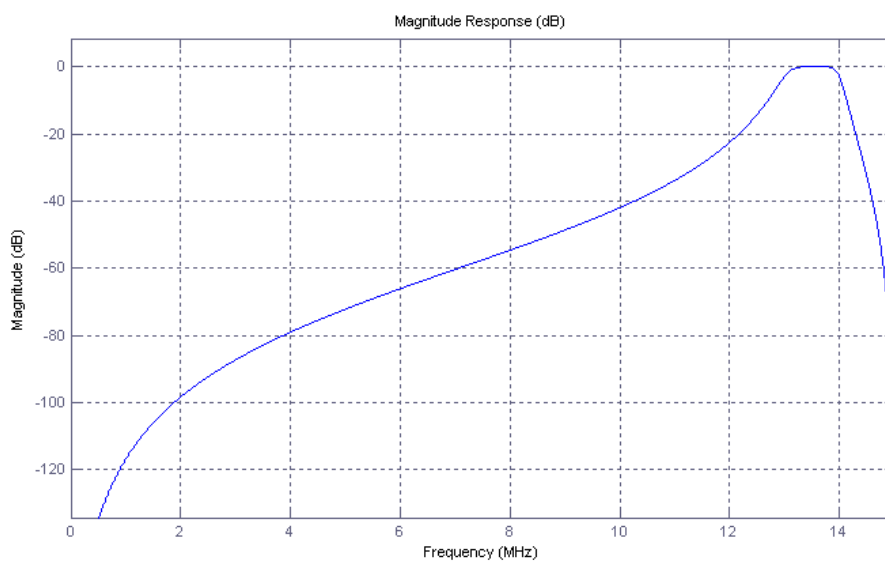


Figure C-7: Magnitude response of the band pass filter centered at 6 MHz from the IF

C.3.b) Acquisition and tracking results

The same metrics as with the CW interference are also used here, namely the deflection coefficient to assess the performance of the acquisition and C/N_0 for the tracking.

First, in the case of an interference at 1 MHz from the IF, the central frequency of the interference is located in the middle of one of the main lobes of the BOC(1,1) signal. Moreover, since the bandwidth of the band pass filter has been fixed to 1 MHz, almost an entire lobe of the two main lobes of the BOC(1,1) signal is affected by the interference. Therefore, and as demonstrated in Figure C-8 and Figure C-9, the deflection coefficient of the BOC(1,1) is more affected than the deflection coefficient of the CBOC for all the interference power considered. Moreover, the performance of the CBOC degrades less than the performance of the BOC(1,1) when the power of the interference increases as shown by Figure C-9.

Concerning the tracking, as shown in Figure C-10 and Figure C-11, the CBOC performs better than the BOC(1,1) by 1.5 dB. For the same reasons as for CW interference, the tracking is less affected than acquisition. Moreover, as for CW interference, the BOC(1,1) approximation loses lock before the CBOC.

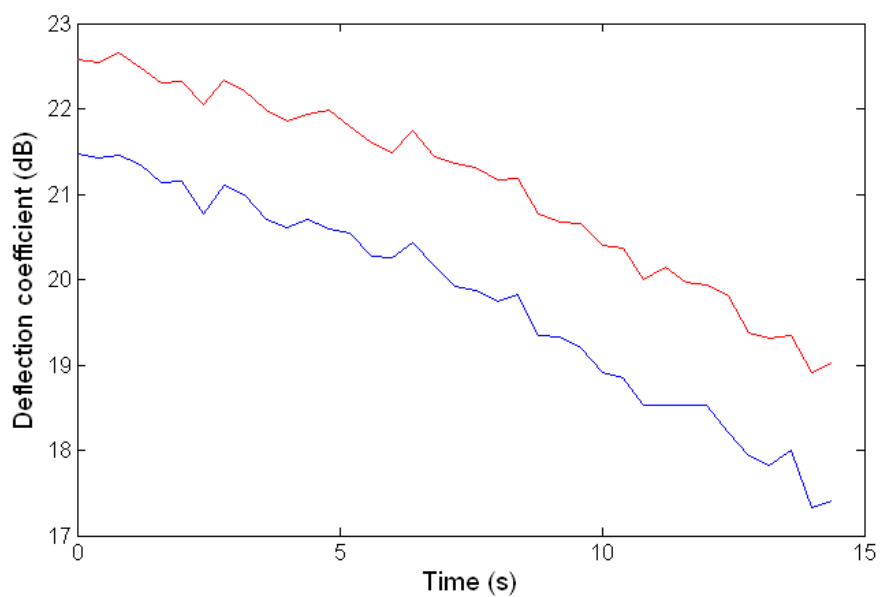
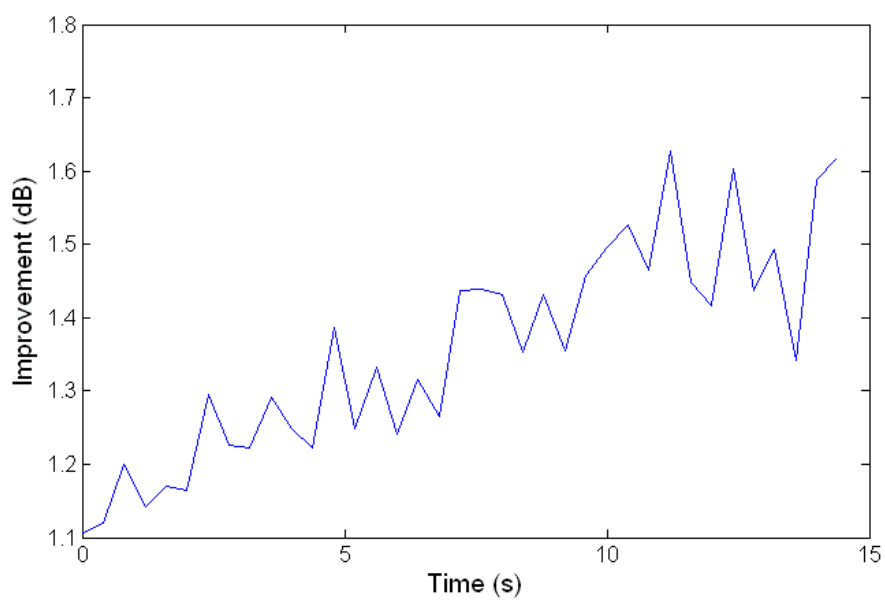


Figure C-8: Deflection coefficient as a function of the interference power for a narrow band interference at 1 MHz



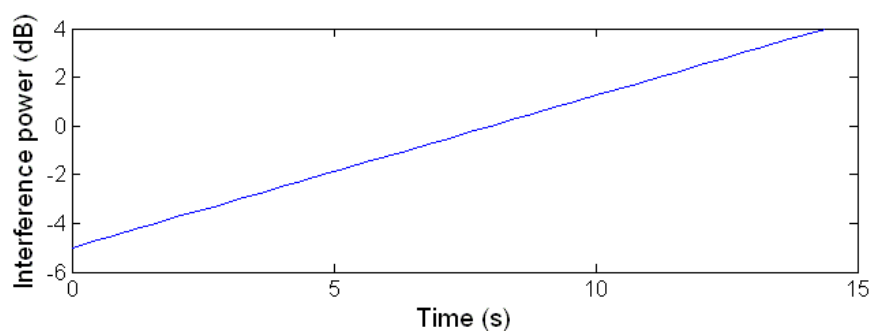


Figure C-9: Improvement in the deflection coefficient of the CBOC compared to the BOC for a narrowband interference at 1 MHz (on top) and interference power over time (at the bottom)

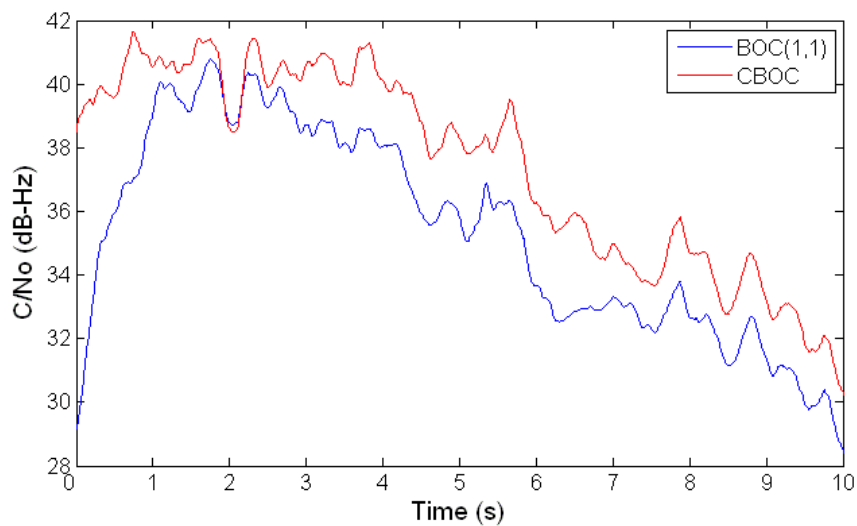


Figure C-10: C/N_0 as a function of the interference power for narrowband interference centered at 1 MHz

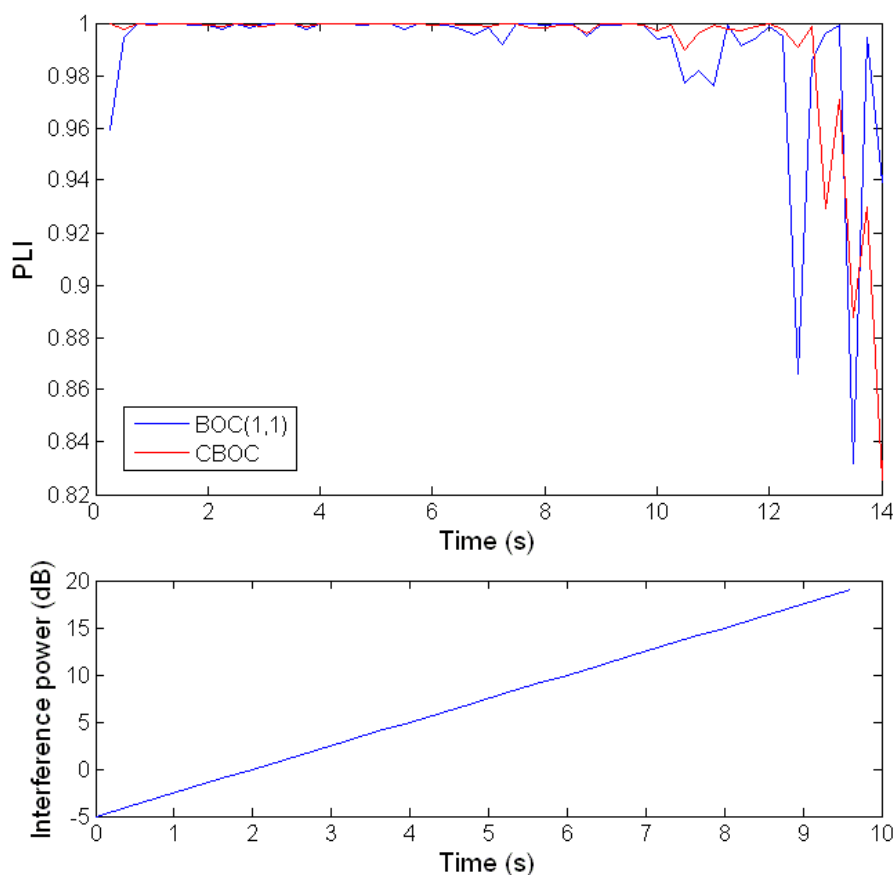


Figure C-11: Phase lock indicator for the BOC(1,1) and CBOC in the presence of narrowband interference at 1 MHz (on top) and Interference power over time (at the bottom)

Concerning the narrow band interference centered at 6 MHz from the IF, the central frequency of the interference is now located in one of the two main lobes of the BOC(6,1). Since the bandwidth of the interference has been fixed at 1 MHz, almost an entire lobe of the two main lobes of the BOC(6,1) signal is affected by interference. Therefore, in this case, the spectrum of the BOC(1,1) is not affected by interference. Indeed, the interference is filtered out since the bandwidth of the BOC(1,1) signal is 5 MHz. However, the spectrum of the CBOC is affected due to the BOC(6,1) part of the

CBOC. This is the worst case scenario for CBOC modulation. As shown in Figure C-12 and Figure C-13, when the interference power is low, the CBOC still has better performance than BOC(1,1). However, when the power of the interference increases, CBOC is affected by the interference but not BOC(1,1) and therefore the performance of CBOC becomes worse than that of BOC(1,1). The same results hold for tracking as shown in Figure C-14 and Figure C-15; when the power of the interference increases, CBOC has worse performance than BOC(1,1). Nevertheless, it is important to note that the interference power is higher in this case than in the previous one (the increase from beginning to the end is about double). Therefore, the interference has to be comparatively stronger to have an impact on acquisition and tracking performance.

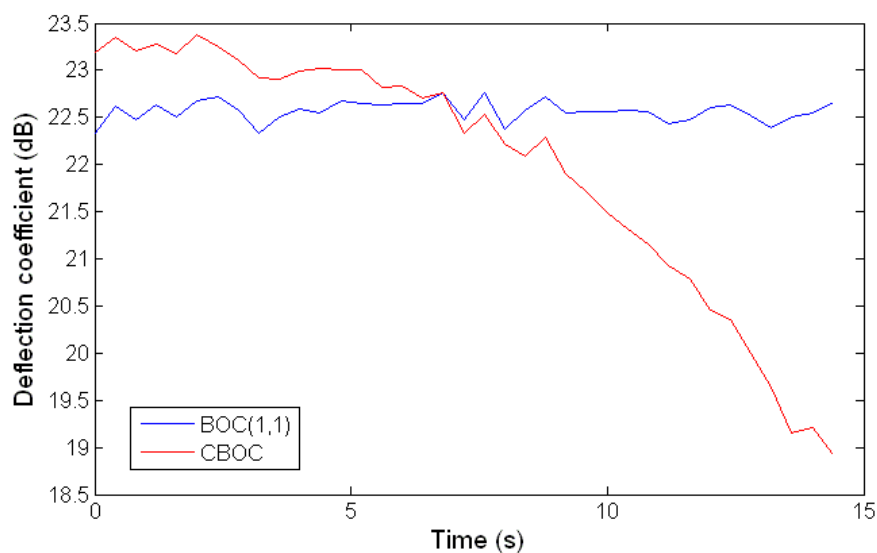


Figure C-12: Deflection coefficient as a function of the interference power for a narrowband interference at 6 MHz

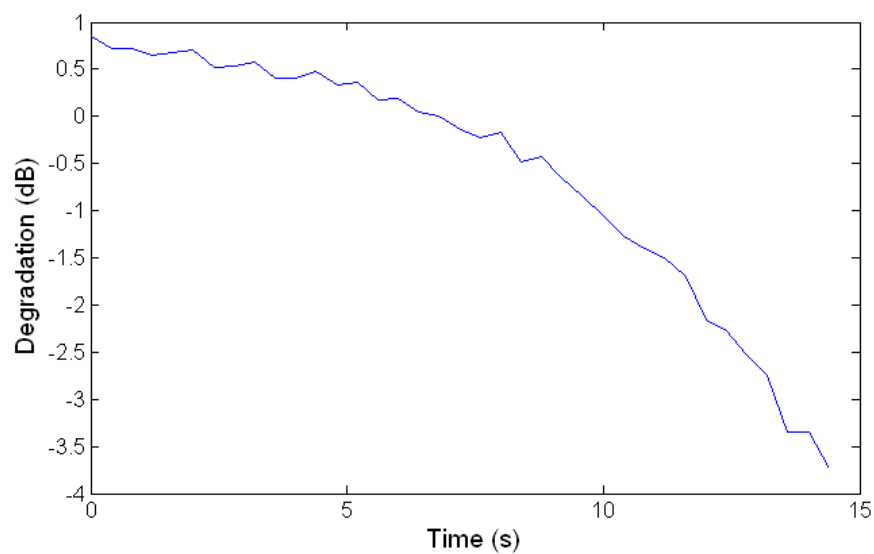


Figure C-13: Difference between the deflection coefficients of the CBOC and BOC for narrowband interference at 6 MHz

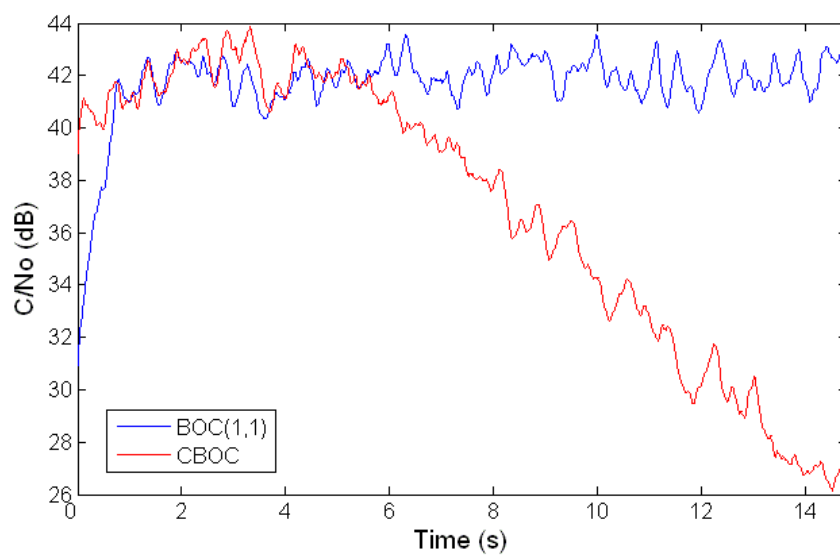


Figure C-14: C/N_0 as a function of the interference power for narrowband interference centered at 6 MHz

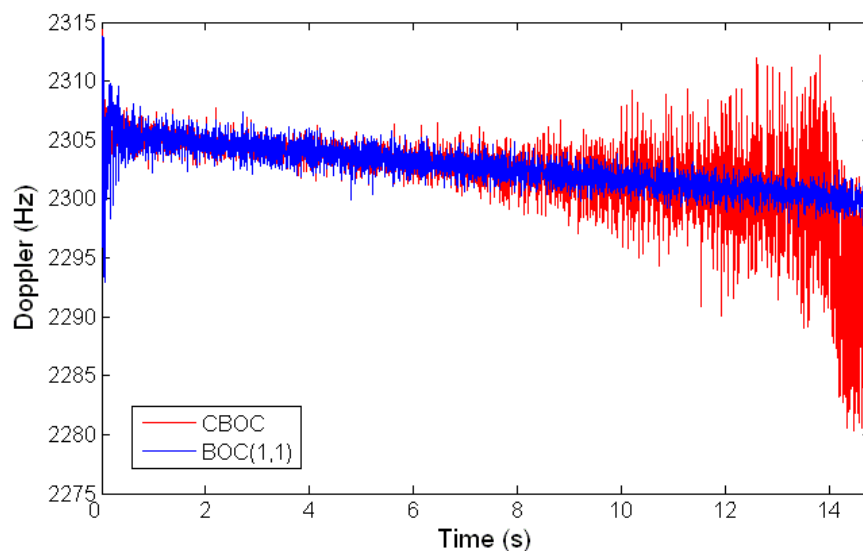


Figure C-15: Doppler as a function of the interference power for narrow band interference centered at 6 MHz

Therefore, for both the acquisition and tracking stages of the receiver:

- If the narrowband interference is centered at 1 MHz from the IF, CBOC has better performance than BOC(1,1) for all the interference powers considered.
- If the narrowband interference is centered at 6 MHz from the IF, when the power of the interference increases, the performance of CBOC becomes worse than that for BOC(1,1) approximation.
- A narrowband interference with the same power has less effect centered at 6 MHz than at 1 MHz.

C.4) Approximation in the presence of multipath

C.4.a) Description

The objective here is to study the impact of multipath on CBOC modulation, and on the approximation of the CBOC by a BOC(1,1). Therefore, a simple model of multipath is simulated here, with variable delay compared to the direct signal. Then the multipath is added to the direct signal and the error is computed using either a BOC(1,1) or a CBOC modulation.

C.4.b) Results

The multipath envelope is computed using noncoherent early-late processing (NELP) with an early-late spacing of 0.05 chips and an infinite bandwidth in order to study only the effect of modulation without filtering effects.

The results are shown in Figure C-16. The results for the CBOC are similar to the ones of Hein (2006) except that here the bandwidth is not limited. The corresponding results with limited bandwidth are shown in Figure C-17. The multipath envelope of a CBOC signal tracked using a BOC(1,1), is the same as the one of BOC(1,1) tracked by a BOC(1,1). However, the multipath envelope of the CBOC (tracked using a CBOC) is better than the one of the CBOC tracked using a BOC(1,1) as shown in Figure C-16 for

all multipath delays. Therefore, even if the performance of the BOC(1,1) is not as good as for the CBOC, they are still equal to a pure BOC(1,1) signal.

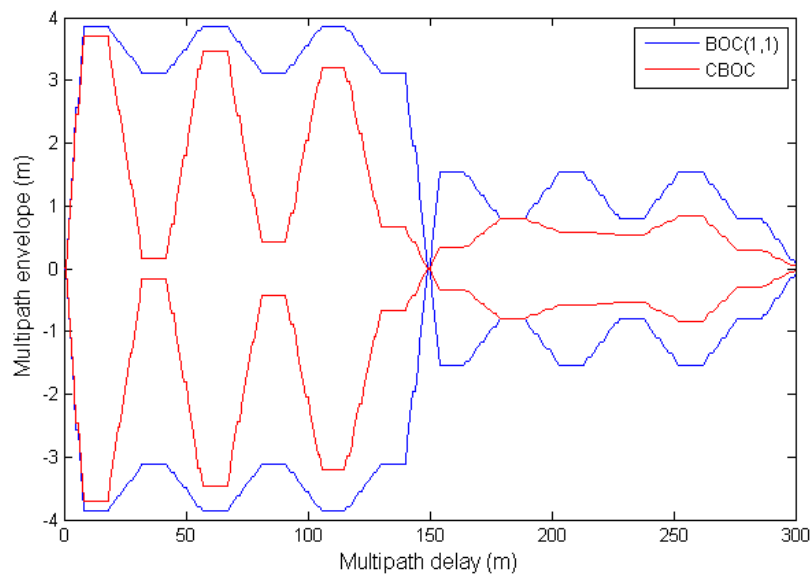


Figure C-16: Multipath envelope for BOC(1,1) in blue and CBOC in red

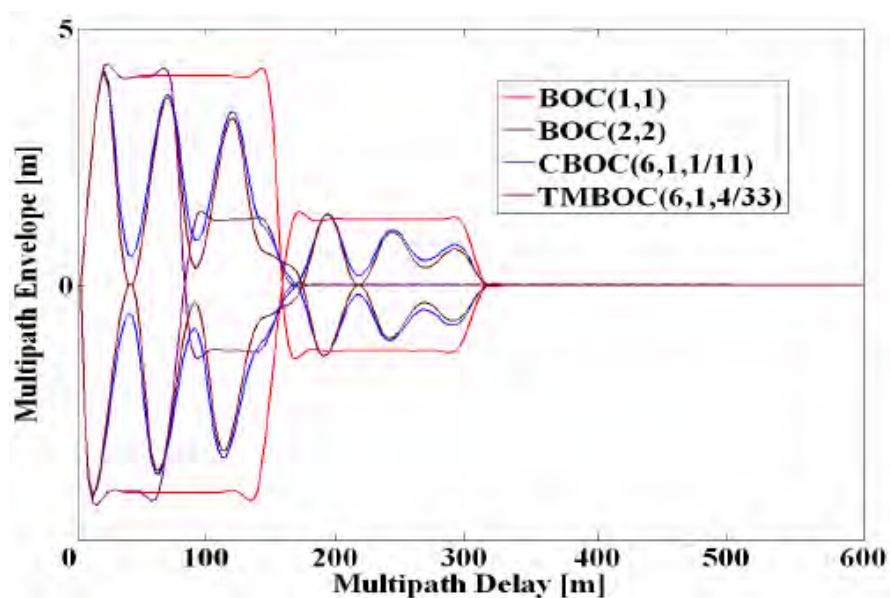


Figure C-17: Multipath envelope for NELP processing, 24 MHz bandwidth and 0.05 chip early-late spacing (from Hein 2006)

Appendix D: Implementation of a Kalman filter for GPS L1 C/A and L1C (data and pilot) signal tracking

In the context of this work, the goal of a Kalman filter for tracking is to combine the outputs of the correlators for the L1 C/A and L1C (data and pilot) signals to increase observability to get better estimates of the state vector, and thus improve tracking.

Derivation of the observation model

The output of the correlators for L1 C/A and L1C are almost the same except for the amplitude of the signal (since these signals do not all have the same transmitted power).

The observables are the outputs of the 18 correlators (3 for each signal) and can be expressed as follows:

➤ For L1 C/A:

- In phase prompt correlator: $I_{-P_{C/A}} = \tilde{A} \cdot \tilde{R}_1(\delta\tau) \cdot \cos(\delta\phi) + n_{IP_{C/A}}$
- In phase early correlator: $I_{-E_{C/A}} = \tilde{A} \cdot \tilde{R}_1(\delta\tau - \Delta) \cdot \cos(\delta\phi) + n_{IE_{C/A}}$
- In phase late correlator: $I_{-L_{C/A}} = \tilde{A} \cdot \tilde{R}_1(\delta\tau + \Delta) \cdot \cos(\delta\phi) + n_{IL_{C/A}}$
- In quadrature prompt correlator: $Q_{-P_{C/A}} = \tilde{A} \cdot \tilde{R}_1(\delta\tau) \cdot \sin(\delta\phi) + n_{QP_{C/A}}$
- In quadrature early correlator: $Q_{-E_{C/A}} = \tilde{A} \cdot \tilde{R}_1(\delta\tau - \Delta) \cdot \sin(\delta\phi) + n_{QE_{C/A}}$

- In quadrature late correlator: $Q_{-L_{C/A}} = \tilde{A} \cdot \tilde{R}_1(\delta\tau + \Delta) \cdot \sin(\delta\phi) + n_{QL_{C/A}}$

➤ For L1C Data:

- In phase prompt correlator: $I_{-P_{L1CD}} = \alpha_D \cdot \tilde{A} \cdot \tilde{R}_2(\delta\tau) \cdot \cos(\delta\phi) + n_{IP_{L1CD}}$
- In phase early correlator: $I_{-E_{L1CD}} = \alpha_D \cdot \tilde{A} \cdot \tilde{R}_2(\delta\tau - \Delta) \cdot \cos(\delta\phi) + n_{IE_{L1CD}}$
- In phase late correlator: $I_{-L_{L1CD}} = \alpha_D \cdot \tilde{A} \cdot \tilde{R}_2(\delta\tau + \Delta) \cdot \cos(\delta\phi) + n_{IL_{L1CD}}$
- In quadrature prompt correlator: $Q_{-P_{L1CD}} = \alpha_D \cdot \tilde{A} \cdot \tilde{R}_2(\delta\tau) \cdot \sin(\delta\phi) + n_{QP_{L1CD}}$
- In quadrature early correlator:
 $Q_{-E_{L1CD}} = \alpha_D \cdot \tilde{A} \cdot \tilde{R}_2(\delta\tau - \Delta) \cdot \sin(\delta\phi) + n_{QE_{L1CD}}$
- In quadrature late correlator: $Q_{-L_{L1CD}} = \alpha_D \cdot \tilde{A} \cdot \tilde{R}_2(\delta\tau + \Delta) \cdot \sin(\delta\phi) + n_{QL_{L1CD}}$

➤ For L1C Pilot:

- In phase prompt correlator: $I_{-P_{L1CP}} = \alpha_P \cdot \tilde{A} \cdot \tilde{R}_2(\delta\tau) \cdot \cos(\delta\phi) + n_{IP_{L1CP}}$
- In phase early correlator: $I_{-E_{L1CP}} = \alpha_P \cdot \tilde{A} \cdot \tilde{R}_2(\delta\tau - \Delta) \cdot \cos(\delta\phi) + n_{IE_{L1CP}}$
- In phase late correlator: $I_{-L_{L1CP}} = \alpha_P \cdot \tilde{A} \cdot \tilde{R}_2(\delta\tau + \Delta) \cdot \cos(\delta\phi) + n_{IL_{L1CP}}$
- In quadrature prompt correlator: $Q_{-P_{L1CP}} = \alpha_P \cdot \tilde{A} \cdot \tilde{R}_2(\delta\tau) \cdot \sin(\delta\phi) + n_{QP_{L1CP}}$
- In quadrature early correlator:
 $Q_{-E_{L1CP}} = \alpha_P \cdot \tilde{A} \cdot \tilde{R}_2(\delta\tau - \Delta) \cdot \sin(\delta\phi) + n_{QE_{L1CP}}$
- In quadrature late correlator: $Q_{-L_{L1CP}} = \alpha_P \cdot \tilde{A} \cdot \tilde{R}_2(\delta\tau + \Delta) \cdot \sin(\delta\phi) + n_{QL_{L1CP}}$

with $\tilde{A} = A \cdot \frac{\sin(\pi \cdot \delta f \cdot T)}{\pi \cdot \delta f \cdot T}$

$$\delta\phi = \delta\phi_0 + \frac{T}{2} \cdot \delta f_0 + \frac{T^2}{6} \delta\alpha_0$$

using the following notations:

- A signal amplitude
- α_D and α_P the scale factors to account for the difference in transmitted power of the L1C data and pilot channels (known)
- \tilde{R}_1 autocorrelation function of the C/A signal (taken into account the number of code periods considered for each coherent integration)
- \tilde{R}_2 autocorrelation function of the L1C signal, thus a BOC(1,1) (taken into account the number of code periods considered for each coherent integration)
- $\delta\tau$ error in the local code delay
- Δ spacing between the prompt and the early/late correlators
- $\delta\phi$ average error in the local carrier phase over the integration interval
- T coherent integration time interval
- $\delta\phi_0$ error in the local carrier phase at the beginning of the integration interval
- δf_0 error in the local carrier frequency at the beginning of the integration interval
- $\delta\alpha_0$ phase acceleration error (frequency rate error) the beginning of the integration interval
- n_l are the noise values in the in phase correlator (Gaussian)

- n_Q are the noise values in the in quadrature correlator (Gaussian)

Two things are also worth noting:

- In this model the TMBOC of the pilot channel is not considered, but only the BOC(1,1) part. Therefore, the model of the autocorrelation function is considered the same for the pilot and data channels.
- The noise values between C/A, L1C_D and L1C_P are assumed uncorrelated due to the code orthogonality .

From the above equations, one can deduce the necessary elements of the state vector X to completely describe the system (using this modeling):

$$X_k = \begin{pmatrix} \tilde{A} \\ \delta\tau \\ \delta\phi_0 \\ \delta f_0 \\ \delta a_0 \end{pmatrix}_k$$

There is no need to increase the state vector compared to the model for L1 C/A because, as shown in the equations for the correlator outputs (above), the elements of the state vector are the same for GPS L1 C/A, L1C_D and L1C_P.

Since the noise values are independent between the three signals considered, it is possible to use a sequential Kalman filter, and thus do not increase the size of the matrices considered compared to the one channel Kalman filter. However, the number of steps to compute the update is increased.

The measurement vectors are as follow:

$$Z_{C/A,k} = \begin{pmatrix} I_P \\ I_E \\ I_L \\ Q_P \\ Q_E \\ Q_L \end{pmatrix}_{C/A,k}, \quad Z_{L1CD,k} = \begin{pmatrix} I_P \\ I_E \\ I_L \\ Q_P \\ Q_E \\ Q_L \end{pmatrix}_{L1CD,k} \quad \text{and} \quad Z_{L1CP,k} = \begin{pmatrix} I_P \\ I_E \\ I_L \\ Q_P \\ Q_E \\ Q_L \end{pmatrix}_{L1CP,k}$$

containing the output of the 3x6 correlators for L1 C/A, L1C_D and L1C_P described above.

As in the model for one channel only, the measurement model has to be linearized as follows:

$$\delta z_{C/A,k} = \left. \frac{\partial h_{C/A}(x_k, k)}{\partial x_k} \right|_{x_k = \hat{x}_k} \delta x_k + v_k = H_{C/A,k} \cdot \delta x_k + v_k$$

$$\delta z_{L1CD,k} = \left. \frac{\partial h_{L1CD}(x_k, k)}{\partial x_k} \right|_{x_k = \hat{x}_k} \delta x_k + v_k = H_{L1CD,k} \cdot \delta x_k + v_k$$

$$\delta z_{L1CP,k} = \left. \frac{\partial h_{L1CP}(x_k, k)}{\partial x_k} \right|_{x_k = \hat{x}_k} \delta x_k + v_k = H_{L1CP,k} \cdot \delta x_k + v_k$$

where:

- z_k and x_k are the real values of the measurements and the state vector
- \hat{z}_k and \hat{x}_k are the estimated values of the measurements and the state vector
- δz_k are the measurement misclosures
- δx_k is the perturbed state vector
- H_k is the design matrix and is detailed in the following

- v_k is the noise associated with the measurement model (Gaussian with covariance matrix C_{v_k} detailed in the following)

Then, different measurement misclosures are computed sequentially:

- First the measurement misclosure of L1 C/A is computed as follows

$$\delta z_{C/A,k} = \begin{pmatrix} I - P_{C/A} \\ I - E_{C/A} \\ I - L_{C/A} \\ Q - P_{C/A} \\ Q - E_{C/A} \\ Q - L_{C/A} \end{pmatrix} - \tilde{A} \begin{pmatrix} R_1(\delta\tau_1).\cos(\delta\phi_1) \\ R_1(\delta\tau_1 - \Delta).\cos(\delta\phi_1) \\ R_1(\delta\tau_1 + \Delta).\cos(\delta\phi_1) \\ R_1(\delta\tau_1).\sin(\delta\phi_1) \\ R_1(\delta\tau_1 - \Delta).\sin(\delta\phi_1) \\ R_1(\delta\tau_1 + \Delta).\sin(\delta\phi_1) \end{pmatrix}$$

using the last estimate available (i.e. the predicted one).

- Then, the measurement misclosure of L1C_D is computed as follows

$$\delta z_{L1CD,k} = \begin{pmatrix} I - P_{L1CD} \\ I - E_{L1CD} \\ I - L_{L1CD} \\ Q - P_{L1CD} \\ Q - E_{L1CD} \\ Q - L_{L1CD} \end{pmatrix} - \alpha_D \cdot \tilde{A} \begin{pmatrix} R_2(\delta\tau_2).\cos(\delta\phi_2) \\ R_2(\delta\tau_2 - \Delta).\cos(\delta\phi_2) \\ R_2(\delta\tau_2 + \Delta).\cos(\delta\phi_2) \\ R_2(\delta\tau_2).\sin(\delta\phi_2) \\ R_2(\delta\tau_2 - \Delta).\sin(\delta\phi_2) \\ R_2(\delta\tau_2 + \Delta).\sin(\delta\phi_2) \end{pmatrix} \quad \text{using the last estimate}$$

available (i.e. the one estimated with L1 C/A).

- Finally, the measurement misclosure of L1C_P is computed as follows

$$\delta_{L1CP,k} = \begin{pmatrix} I - P_{L1CP} \\ I - E_{L1CP} \\ I - L_{L1CP} \\ Q - P_{L1CP} \\ Q - E_{L1CP} \\ Q - L_{L1CP} \end{pmatrix} - \alpha_P \cdot \tilde{A} \begin{pmatrix} R_2(\delta\tau_3) \cdot \cos(\delta\phi_3) \\ R_2(\delta\tau_3 - \Delta) \cdot \cos(\delta\phi_3) \\ R_2(\delta\tau_3 + \Delta) \cdot \cos(\delta\phi_3) \\ R_2(\delta\tau_3) \cdot \sin(\delta\phi_3) \\ R_2(\delta\tau_3 - \Delta) \cdot \sin(\delta\phi_3) \\ R_2(\delta\tau_3 + \Delta) \cdot \sin(\delta\phi_3) \end{pmatrix} \quad \text{using the last estimate}$$

available (i.e. the one estimated with L1C_D).

The design matrix $H_{C/A,k}$ is computed as follows. $H_{L1CD,k}$ and $H_{L1CP,k}$ are computed similarly.

$$H_{C/A,k} = \begin{bmatrix} \frac{\partial I - P_{C/A}}{\partial \tilde{A}} & \frac{\partial I - P_{C/A}}{\partial \delta\tau} & \frac{\partial I - P_{C/A}}{\partial \delta\phi_0} & \frac{\partial I - P_{C/A}}{\partial \delta\mathcal{F}_0} & \frac{\partial I - P_{C/A}}{\partial \delta\alpha_0} \\ \frac{\partial I - E_{C/A}}{\partial \tilde{A}} & \frac{\partial I - E_{C/A}}{\partial \delta\tau} & \frac{\partial I - E_{C/A}}{\partial \delta\phi_0} & \frac{\partial I - E_{C/A}}{\partial \delta\mathcal{F}_0} & \frac{\partial I - E_{C/A}}{\partial \delta\alpha_0} \\ \frac{\partial I - L_{C/A}}{\partial \tilde{A}} & \frac{\partial I - L_{C/A}}{\partial \delta\tau} & \frac{\partial I - L_{C/A}}{\partial \delta\phi_0} & \frac{\partial I - L_{C/A}}{\partial \delta\mathcal{F}_0} & \frac{\partial I - L_{C/A}}{\partial \delta\alpha_0} \\ \frac{\partial Q - P_{C/A}}{\partial \tilde{A}} & \frac{\partial Q - P_{C/A}}{\partial \delta\tau} & \frac{\partial Q - P_{C/A}}{\partial \delta\phi_0} & \frac{\partial Q - P_{C/A}}{\partial \delta\mathcal{F}_0} & \frac{\partial Q - P_{C/A}}{\partial \delta\alpha_0} \\ \frac{\partial Q - E_{C/A}}{\partial \tilde{A}} & \frac{\partial Q - E_{C/A}}{\partial \delta\tau} & \frac{\partial Q - E_{C/A}}{\partial \delta\phi_0} & \frac{\partial Q - E_{C/A}}{\partial \delta\mathcal{F}_0} & \frac{\partial Q - E_{C/A}}{\partial \delta\alpha_0} \\ \frac{\partial Q - L_{C/A}}{\partial \tilde{A}} & \frac{\partial Q - L_{C/A}}{\partial \delta\tau} & \frac{\partial Q - L_{C/A}}{\partial \delta\phi_0} & \frac{\partial Q - L_{C/A}}{\partial \delta\mathcal{F}_0} & \frac{\partial Q - L_{C/A}}{\partial \delta\alpha_0} \end{bmatrix}$$

The covariance matrix associated with the measurements C_{v_k} is the same for all the measurements and can be expressed as follows (Van Dierendonck et al 1992):

$$C_{v_k} = \begin{pmatrix} \sigma_n^2 \cdot \tilde{R}(0) & \sigma_n^2 \cdot \tilde{R}(\Delta) & \sigma_n^2 \cdot \tilde{R}(\Delta) & 0 & 0 & 0 \\ \sigma_n^2 \cdot \tilde{R}(\Delta) & \sigma_n^2 \cdot \tilde{R}(0) & \sigma_n^2 \cdot \tilde{R}(2\Delta) & 0 & 0 & 0 \\ \sigma_n^2 \cdot \tilde{R}(\Delta) & \sigma_n^2 \cdot \tilde{R}(2\Delta) & \sigma_n^2 \cdot \tilde{R}(0) & 0 & 0 & 0 \\ 0 & 0 & 0 & \sigma_n^2 \cdot \tilde{R}(0) & \sigma_n^2 \cdot \tilde{R}(\Delta) & \sigma_n^2 \cdot \tilde{R}(\Delta) \\ 0 & 0 & 0 & \sigma_n^2 \cdot \tilde{R}(\Delta) & \sigma_n^2 \cdot \tilde{R}(0) & \sigma_n^2 \cdot \tilde{R}(2\Delta) \\ 0 & 0 & 0 & \sigma_n^2 \cdot \tilde{R}(\Delta) & \sigma_n^2 \cdot \tilde{R}(2\Delta) & \sigma_n^2 \cdot \tilde{R}(0) \end{pmatrix}$$

where σ_n^2 is the variance of the noise and \tilde{R} is the known autocorrelation function.

Derivation of the dynamic model

The goal is to find a matrix F such as:

$$\dot{X} = F \cdot X + G \cdot W$$

Derivation of the expression of the transition matrix F :

- The amplitude can be considered as almost constant over time

$$\dot{A} = 0 + w_A$$

- The variation of code Doppler is proportional to the variation of carrier frequency

$$\delta\dot{\tau} = \beta \cdot \delta\dot{f}_0 + w \quad \text{with } w = w_{code} + \beta \cdot w_{clock}$$

- Since $\delta\phi = \delta\phi_0 + \frac{T}{2} \cdot \delta\dot{f}_0 + \frac{T^2}{6} \delta\ddot{\alpha}_0$, one can write

$$\delta\dot{\phi}_0 = \delta\dot{f}_0 + w_{clock}$$

- For the same reason, one can write

$$\dot{\delta f}_0 = \delta a_0 + w_{freq}$$

- Finally, the effects of higher order are not considered, thus

$$\delta \dot{a}_0 = 0 + w_{acc}$$

Finally, one can write

$$\begin{pmatrix} \dot{A} \\ \delta \dot{\tau} \\ \delta \dot{\phi}_0 \\ \dot{\delta f}_0 \\ \delta \dot{a}_0 \end{pmatrix} = \begin{pmatrix} 0 & 0 & 0 & 0 & 0 \\ 0 & 0 & 0 & \beta & 0 \\ 0 & 0 & 0 & 1 & 0 \\ 0 & 0 & 0 & 0 & 1 \\ 0 & 0 & 0 & 0 & 0 \end{pmatrix} \begin{pmatrix} A \\ \delta \tau \\ \delta \phi_0 \\ \delta f_0 \\ \delta a_0 \end{pmatrix} + \begin{pmatrix} 1 & 0 & 0 & 0 & 0 \\ 0 & 1 & \beta & 0 & 0 \\ 0 & 0 & 1 & 0 & 0 \\ 0 & 0 & 0 & 1 & 0 \\ 0 & 0 & 0 & 0 & 1 \end{pmatrix} \begin{pmatrix} w_A \\ w_{code} \\ w_{clock} \\ w_{freq} \\ w_{acc} \end{pmatrix}$$

where β is used to convert from units of chips to units of cycles ($\frac{1}{1540}$ for GPS L1).

Thus the transition matrix can be expressed as

$$F = \begin{bmatrix} 0 & 0 & 0 & 0 & 0 \\ 0 & 0 & 0 & \beta & 0 \\ 0 & 0 & 0 & 1 & 0 \\ 0 & 0 & 0 & 0 & 1 \\ 0 & 0 & 0 & 0 & 0 \end{bmatrix}$$

However, the Kalman filter needs to be implemented in the discrete domain (one has samples and not continuous measurements), thus the dynamic model can be expressed as

$$x_{k+1} = \Phi_k \cdot x_k + w_k$$

$$\Phi_k = I + F \cdot T + \frac{T^2}{2!} \cdot F^2 + \dots$$

$$\text{Thus } \Phi_k = \Phi = \begin{pmatrix} 1 & 0 & 0 & 0 & 0 \\ 0 & 1 & 0 & \beta T & \frac{\beta T^2}{2} \\ 0 & 0 & 1 & T & \frac{T^2}{2} \\ 0 & 0 & 0 & 1 & T \\ 0 & 0 & 0 & 0 & 1 \end{pmatrix}$$

Concerning the noise associated with the dynamic model, in the continuous domain, its covariance matrix can be written as

$$Q = \begin{bmatrix} S_A & 0 & 0 & 0 & 0 \\ 0 & S_{code} & 0 & 0 & 0 \\ 0 & 0 & S_{clock} & 0 & 0 \\ 0 & 0 & 0 & S_{freq} & 0 \\ 0 & 0 & 0 & 0 & S_{acc} \end{bmatrix}$$

The values on this matrix are computed later on.

The matrix Q needs to be transformed in the discrete domain to have an expression of Q_k

(covariance matrix of w_k):

$$Q_k = \int_t^{t+T} \Phi(T) \cdot G \cdot Q \cdot G^T \cdot \Phi(T)^T$$

After computation, one finds:

$$Q_k = \begin{pmatrix} S_A \cdot T & 0 & 0 \\ 0 & S_{code} \cdot T + \beta^2 \cdot S_{clock} \cdot T + \beta^2 \cdot \frac{T^3}{3} \cdot S_{freq} + \frac{\beta^2 \cdot T^5}{20} \cdot S_{acc} & \beta \cdot S_{clock} \cdot T + \beta \cdot \frac{T^3}{3} \cdot S_{freq} + \frac{\beta \cdot T^5}{20} \cdot S_{acc} \\ 0 & \beta \cdot S_{clock} \cdot T + \beta \cdot \frac{T^3}{3} \cdot S_{freq} + \frac{\beta \cdot T^5}{20} \cdot S_{acc} & S_{clock} \cdot T + \frac{T^3}{3} \cdot S_{freq} + \frac{T^5}{20} \cdot S_{acc} \\ 0 & \beta \cdot \frac{T^2}{2} \cdot S_{freq} + \frac{\beta \cdot T^4}{8} \cdot S_{acc} & \frac{T^2}{2} \cdot S_{freq} + \frac{T^4}{8} \cdot S_{acc} \\ 0 & \frac{\beta T^3}{6} \cdot S_{acc} & \frac{T^3}{6} \cdot S_{acc} \\ \beta \cdot \frac{T^2}{2} \cdot S_{freq} + \frac{\beta T^4}{8} \cdot S_{acc} & \frac{\beta T^3}{6} \cdot S_{acc} & \\ \frac{T^2}{2} \cdot S_{freq} + \frac{T^4}{8} \cdot S_{acc} & \frac{T^3}{6} \cdot S_{acc} & \\ S_{freq} \cdot T + \frac{T^3}{3} \cdot S_{acc} & \frac{T^2}{2} \cdot S_{acc} & \\ \frac{T^2}{2} \cdot S_{acc} & T \cdot S_{acc} & \end{pmatrix}$$

Derivation of the variances of the noises associated to the dynamic model:

- S_A : the amplitude is almost constant over time (open sky conditions are considered here, i.e. no sudden change in signal power), so one can choose a variance of the noise very small, here $S_A = 10^{-5}$ has been chosen experimentally.
- S_{code} : This corresponds to the difference between the divergence of the ionospheric delay for the code and the phase over time. At the horizon, one can evaluate a code delay of 30 m, and 10 m at the zenith (Skone 2007). The time needed for the satellite to travel from the horizon to the zenith is 2 h 30 min (note that the case of a satellite going from 0° to 90° elevation angle is considered). Therefore, the variation is 20 m in 9000 s, thus around $2.5 \cdot 10^{-3}$ m in 1 s. Finally $S_{code} = 25 \cdot 10^{-6}$ (the previous result has to be multiplied by two to take into account for the divergence between the code and carrier phase and then squared).

- S_{clock} and S_{freq} : Depends on the oscillator parameters

$$S_{clock} = \frac{h_0}{2} \cdot w_{L1}^2 \text{ and } S_{freq} = 2 \cdot \pi^2 \cdot h_{-2} \cdot w_{L1}^2$$

where the parameters h_0 and h_{-2} are shown for some oscillators in Chapter 4 and

w_{L1} is the frequency of L1 in rad/s

- S_{acc} : Depends on the rate of change of the LOS range variation, so the change in Doppler. At the horizon, the Doppler is 5000 Hz, and 0 Hz at zenith. Thus, the average variation is 0.5 Hz/s. Thus, $S_{acc} = 0.25$ is chosen if there is no user motion. In the case of user dynamics, this value is set to the square of the acceleration on the axis receiver-satellite converted in cycles.

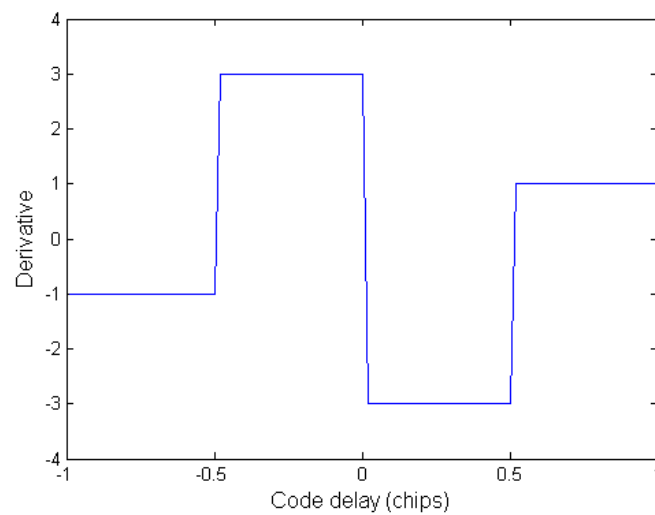
Model of the autocorrelation function

Considering the autocorrelation function, two different models have to be derived here:

- One for the L1 C/A: in this case the model developed for the Kalman filter for C/A only is used
- One for L1C_D and L1C_P due to the BOC modulation: this model is detailed below (the plot are shown in chapter 4 and the equations are shown here)

In this method, the derivative is estimated first, and then is integrated to obtain the autocorrelation function. The derivative is generated continuous but in seven parts:

- $\frac{d\hat{R}(t)}{dt} = -1$ for $t = [-1: -0.51]$
- $\frac{d\hat{R}(t)}{dt} = 200 \cdot t + 101$ for $t = [-0.51: -0.49]$
- $\frac{d\hat{R}(t)}{dt} = 3$ for $t = [-0.49: -0.01]$
- $\frac{d\hat{R}(t)}{dt} = -300t$ for $t = [-0.01: 0.01]$
- $\frac{d\hat{R}(t)}{dt} = -3$ for $t = [0.01: 0.49]$
- $\frac{d\hat{R}(t)}{dt} = 200t - 101$ for $t = [0.49: 0.51]$
- $\frac{d\hat{R}(t)}{dt} = 1$ for $t = [0.51: 1]$

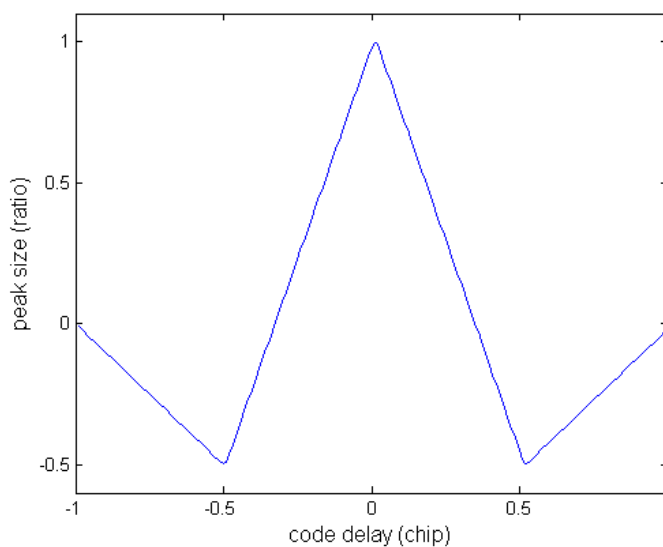


Now, one just has to integrate this function in seven different parts, using as initial conditions:

- $R(-1) = 0$
- $R(-0.51) = -0.49$
- $R(-0.01) = 0.995$
- $R(0.01) = 0.995$
- $R(0.51) = 0.49$
- $R(1) = 0$

However, since the model becomes pretty complicated around the inflection points, since it does not have an impact on the performance, the following approximation is implemented instead:

- $\hat{R}(t) = -t - 1$ for $t = [-1 : -0.51]$
- $\hat{R}(t) = -0.49$ for $t = [-0.51 : -0.49]$
- $\hat{R}(t) = 3t + 1$ for $t = [-0.49 : -0.01]$
- $\hat{R}(t) = 0.99$ for $t = [-0.01 : 0.01]$
- $\hat{R}(t) = -3t + 1$ for $t = [0.01 : 0.49]$
- $\hat{R}(t) = -0.49$ for $t = [0.49 : 0.51]$
- $\hat{R}(t) = t - 1$ for $t = [0.51 : 1]$



Initialization of the Kalman filter

The two parameters needed to be initialized are the state vector and the covariance matrix of the state vector. Using similar considerations than for the Kalman filter for one channel to determine the noise covariance matrix, the following parameters have been chosen:

$$x_0 = \begin{bmatrix} 1 \\ 0 \\ 0 \\ 0 \\ 0 \end{bmatrix} \text{ and } P_0 = \begin{bmatrix} 10^{-4} & 0 & 0 & 0 & 0 \\ 0 & 5 \cdot 10^{-5} & 0 & 0 & 0 \\ 0 & 0 & \pi^2 & 0 & 0 \\ 0 & 0 & 0 & 40^2 & 0 \\ 0 & 0 & 0 & 0 & 1 \end{bmatrix}$$